Epigenetic determinants of optimal skin response to UV radiation

---

A thesis submitted to The University of Manchester for the degree of

Doctor of Philosophy

in the Faculty of Biology, Medicine and Health

2019

Bethany M Barnes

School of Biological Sciences

Division of Musculoskeletal and Dermatological Sciences

Contents

Word count=42,941.

List of Figures

List of Tables

List of Abbreviations

5caC	5-carboxylcytosine
5fC	5-formylcytosine
5hmC	5-hydroxymethylcytosine
5mC	5-methylcytosine
5mC	5-methylcytosine
8-OHdG	8-hydroxydeoxyguanosine
A	Adenine
AP	Apurinic/apyrimidinic
AP-1	Activator protein 1
BER	Base excision repair
BSA	Bovine serum albumin
C	Cytosine
Ca^{2+}	Calcium
cDNA	Complimentary DNA
CGI	Cytosine-phosphate-guanine island
CPD	Cyclobutane pyrimidine dimers
CpG	Cytosine-phosphate-guanine
DAPI	4’,6-diamidino-2-phenylindole
DEG	Differentially expressed gene
DEJ	Dermo-epidermal junction
DMP	Differentially methylated probe
DMR	Differentially methylated region
DNA	Deoxyribonucleic acid
DNAm	DNA methylation
DNMT	DNA methyltransferase
ECM	Extracellular matrix
FPKM	Fragments per kilobase of transcript per million mapped reads
G	Guanine
GEO	Gene expression omnibus
GO	Gene ontology

H	Histone
KEGG	Kyoto Encyclopaedia of Genes and Genomes
MED	Minimal erythema dose
MMP	Matrix metalloproteinase
MSHB	Manchester Skin Health Biobank
NHEK	Normal human epidermal keratinocyte
NHS	Normal horse serum
PBS	Phosphate buffered saline
PMD	Partially methylated domain
POMC	Proopiomelanocortin
PPIA	Peptidylprolyl isomerase A
SD	Standard deviation
SED	Standard erythemal dose (10 mJ cm^{-1})
SEM	Standard error of the mean
SPF	Sun protective factor
SSR	Solar-simulating radiation
T	Thymine
TBS	Tris-buffered saline
TDG	Thymine DNA glycosylase
TET	Ten-eleven translocation
U	Uracil
UV	Ultraviolet
UVR	Ultraviolet radiation

Abstract

Genome-wide changes in DNA methylation (DNAm) are thought to contribute to ageing phenotypes by alteration of gene expression and genomic stability. The skin, by virtue of its direct exposure to the environment, also ages via extrinsic factors such as ultraviolet radiation (UVR). Chronically UVR exposed skin has been shown to harbour its own pattern of aberrant DNAm pattern. However, the interaction of the intrinsically-aged DNA methylome and the ability of the skin to respond optimally to UVR exposure has not thus far been delineated.

DNA methyltransferases (DNMTs) orchestrate the establishment and maintenance of DNAm, together with the ten-eleven-translocation (TET) proteins that facilitate its removal by oxidation. This study showed that the expression of DNMTs decreases upon traversing through the terminally differentiated layers of the epidermis, whereas the TETs appear inversely upregulated. This suggests that DNAm and the enzymes that control it are fundamentally important to epidermal homeostasis.

To investigate the contribution of DNAm to the pathogenesis of photodamage, sub-erythemal doses of UVR were applied to young and aged skin to recapitulate the early DNAm changes in chronically photoexposed skin. Substantial losses of DNAm in the aged but not young epidermis were observed. Aged epidermis also showed a dampened transcriptional response following UVR challenge, characterised by failure to activate key UVR-responsive pathways.

Finally, this study investigated the differences in DNAm due to intrinsic ageing. Changes in DNAm were significantly correlated with the expression of 651 genes, enriched in pathways related to: metabolism, pluripotency of stem cells and cancer. Additionally, a significant proportion of the genes showing a dampened response in aged epidermis following UVR challenge were those found to be differentially methylated between the young and aged epidermis prior to UVR challenge. This suggests that DNAm changes that occur in the skin with increasing age impair phenotypic plasticity, disposing the skin to respond poorly to UVR exposure.

Declaration

No portion of the work referred to in the thesis has been submitted in support of an application for another degree or qualification of this or any other university or other institute of learning.

Copyright

Acknowledgements

I would like to express my sincerest thanks to my supervisory team, Prof Rachel Watson, Prof Chris Griffiths and Dr David Gunn, for the opportunity to embark on this PhD project. I am especially indebted to my primary supervisor, Prof Rachel Watson, for the guidance and for your “door’s always open!” policy. All the gin didn’t go amiss either! I have worked alongside amazing colleagues in the Centre for Dermatology Research— thank you all for the support, good times and never failing to get the tequilas in (scorpions, maggots and all)! I am especially grateful to Dr Eleanor Smart and Dr Kieran Mellody for lending an ear, or a shoulder, when one was needed, and for patiently proof-reading this thesis. Thank you also to colleagues at the Dermatopharmacology Unit at Salford Royal NHS Foundation Trust, especially Susan Hawksworth and Gill Aarons, for help in volunteer recruitment and the taking of biopsies. A huge thank you to Dr David Gunn of Unilever R&D for supervision and guidance on the epigenetic aspects of this project, for all of the stimulating epigenetics talks and for hearing out every tenuous hypothesis with consideration! Thank you also to everyone at Unilever that made me feel so welcome while on placement, with special thanks to Magdalena Sawicka and Duncan Talbot for lending their expertise in molecular biology techniques. I would also like to thank my family and friends for supporting me throughout this PhD project. It would not have been possible without you. Finally, I would like to thank Unilever R&D and the BBSRC for funding this Industrial CASE studentship.

Chapter 1: Introduction

1.1 Overview

The skin ages through parallel intrinsic and extrinsic processes that culminate in a deterioration of cutaneous function, with significant associated morbidity (Farage et al., 2013). Excessive exposure to ultraviolet radiation (UVR) elicits photoageing, characterised by wrinkling, altered pigmentation and a reduction in elasticity and recoil (Gunn et al., 2009; Langton et al., 2010). The desire to maintain a youthful appearance has fuelled a global anti-ageing market estimated to be worth 216.5 billion U.S. dollars by 2021 (Statista, 2019). Furthermore, UVR is a complete carcinogen, defined by its ability to both initiate and promote cancer (Basu, 2018). Despite the known dangers of UVR exposure, however, the popularity of holidays to sunny destinations has led to a surge in skin cancer incidence. For example, between 1979 and 2015, the age-standardised incidence rate of malignant melanoma rose from 5.75 to 30.44 per 100,000 people, projected to increase a further seven percent by 2035 (Smittenaar et al., 2016).

Emerging evidence advocates an epigenetic aspect of the skin's response to photoexposure. 'Epi'— from the Greek επί, meaning over, outside of or around — relates to the chemical modifications that occur on top of the DNA sequence (for example, DNA methylation [DNAm]) and its associated proteins (for example, histone modifications, including methylation, acetylation and phosphorylation). These epigenetic processes, collectively called the 'epigenome' dictate the three-dimensional conformation of DNA, thus impacting upon gene expression and genomic stability. Exposure of the skin to UVR has been associated with perturbations to the epigenome at multiple levels (Vandiver et al., 2015; Rodríguez-Paredes et al., 2018; Bormann et al., 2016; Shen et al., 2017; Grönniger et al., 2010; Gu et al., 2015). Epigenetic changes are mitotically heritable (Kim & Costello, 2017) and therefore, it is likely that an accumulation of epigenetic changes, as a consequence of UVR exposure, will play a role in photoageing and increased risk of skin cancer.

The natural intrinsic ageing of the skin that occurs over time, is accompanied by its own pattern of epigenetic alterations that may impact upon its functionality and appearance. These epigenetic changes may determine how the skin further responds to photoexposure. No study has thus far examined, *in vivo,* or between different aged cohorts, the effects of low doses of UVR delivered in a controlled manner over a fixed length of time.

This thesis describes the DNAm changes in skin that occur over time and in response to UVR exposure. Thus it is important to first consider the structure and function of the skin and provide an understanding of the phenotypic changes that occur due to these aforementioned factors. Finally, DNA methylations and the modification of histone proteins are outlined, followed by a critical analysis of studies performed to date, which have identified changes ascribed to these factors.

1.2 Skin Structure and Function

The skin forms the first line of defence against a daily onslaught of environmental stressors, protecting against physical, chemical and radiation damage. Its ability to erect an effective barrier is dependent upon the architecture of its two main layers: the epidermis, a highly self-renewing epithelium that forms the outer layer of the skin (Sotiropoulou & Blanpain, 2012); and the underlying dermis, which consists of a rich extracellular matrix (ECM) (Prost-Squarcioni et al., 2008). At the interface of these two layers is a highly undulating dermo-epidermal junction (DEJ) (Ciarletta & Ben Amar, 2012). Subcutaneous to these layers is the *panniculus adiposus* (also called hypodermis), consisting of mature adipose tissue divided into lobules by fibrous septae, which functions as padding, an energy reserve, and as insulation (Busam, 2010) (Figure 1.1).

Not merely a physical barrier to the outside world, the skin is capable of diverse physiological functions. The skin actively excludes microbial pathogens by secretion of antimicrobials, including the cathelicidins and β-defensins (Murakami et al., 2002; Schauber & Gallo, 2008), and maintains an acidic pH between 4.0 and 6.0 that limits outgrowth of pathogenic microorganisms (Lambers et al., 2006; Chikakane & Takahashi, 1995). The eccrine sweat glands, a skin appendage, play an important role in thermoregulation, cooling the body through the evaporative heat loss of secreted sweat (Cui & Schlessinger, 2015). The skin is also densely innervated, allowing sensation of pain, temperature and other sensory inputs (Laverdet et al., 2015). Finally, exposure of the skin to UVR is the major source of vitamin D, which promotes dietary calcium (Ca^{2+}) absorption and bone mineralisation (DeLuca, 2004).

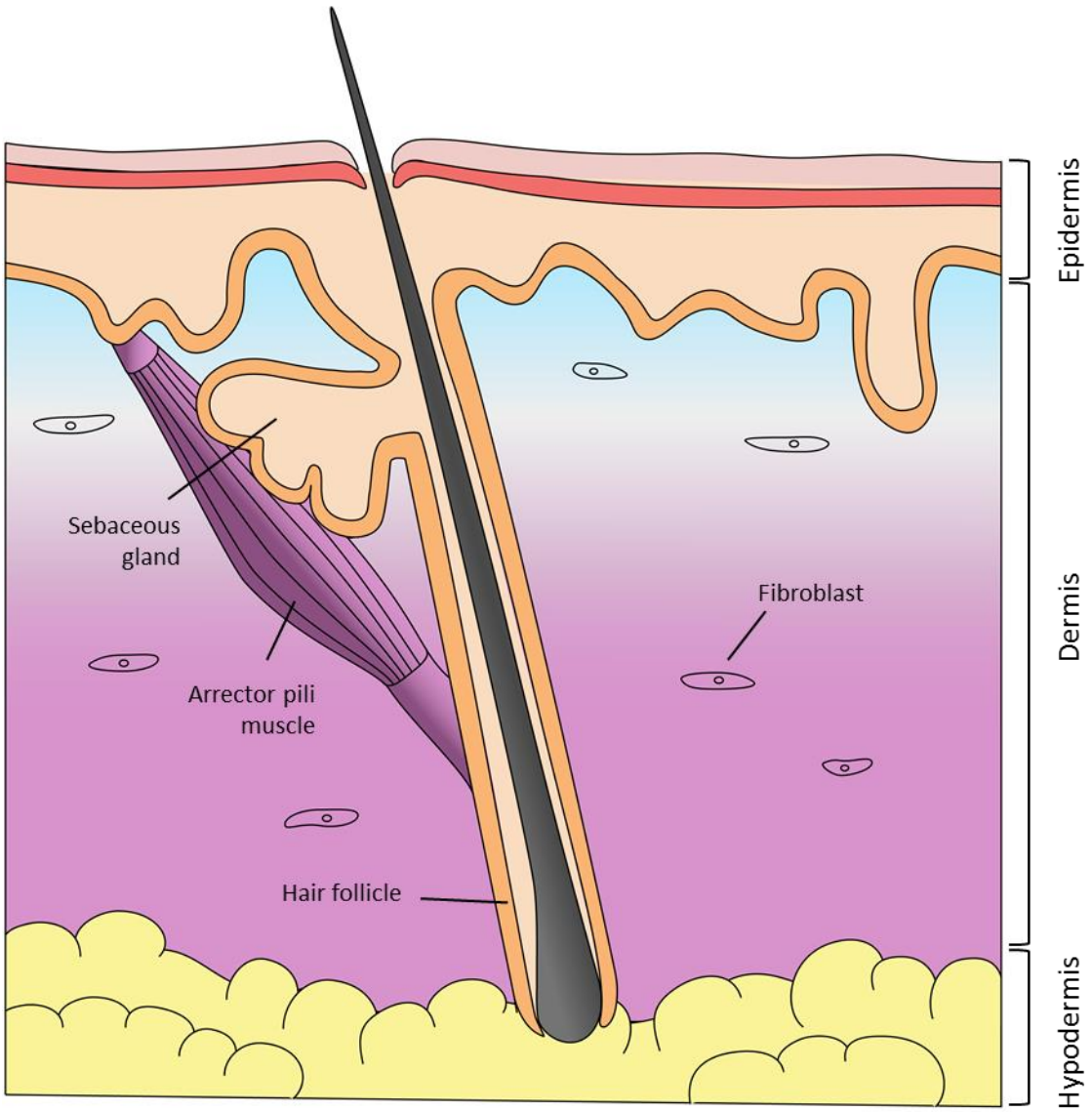

Figure 1.1: The anatomy of human skin.

The skin is composed of two main tissues: the epidermis and the dermis. The epidermis is an avascular stratified epithelium consisting of four distinct layers in most body sites. The outer root sheath of the hair follicle is contiguous with the innermost layer of the epidermis. The dermis underlies the epidermis, separated by a complex basement membrane termed the dermo-epidermal junction (DEJ).

1.2.1 The epidermis

The avascular epidermis, a stratified epithelium, continuously self-renews throughout life. Typically, the epidermis has numerous downward projections, called the rete ridges, which maximise the surface area between the epidermis and dermis. Due to its avascular nature, the epidermis is reliant entirely on the vasculature of the underlying dermis for nutrient exchange via diffusion across the DEJ (Lawlor & Kaur, 2015).

The keratinocyte is the most abundant cell type of the epidermis, representing approximately 90 to 95% of the cell population (Zhang & Michniak-Kohn, 2012). Keratinocytes originate in the innermost layer of the epidermis (the *stratum basale*). The keratinocytes of this layer can be divided into three functionally discrete compartments: stem cells, transit amplifying cells and post-mitotic differentiating cells. Transit amplifying cells act to amplify the number of cell progeny resulting from a single stem cell division (Rangel-Huerta & Maldonado, 2017). Upon detachment from the basement membrane, keratinocytes enter the *stratum spinosum*, exit the cell cycle, grow larger and execute a terminal differentiation programme (Adams & Watt, 1989; Watt, 2002). In the *spinosum* and *granulosum* strata, the cells remain transcriptionally active (Fuchs, 2016). However, differentiation culminates in the production of the annucleated, flattened cells (corneocytes) of the *stratum corneum* that complete the cutaneous barrier (Simpson et al., 2011). Corneocytes are continuously shed at the skin-to-air interface in a process called desquamation, and replaced by terminally differentiating cells from below (Has, 2018).

Variations in epidermal thickness are found between different anatomical sites; the thinnest is seen on the eyelids (50 μm), and thickest on the soles of the feet and palms of the hands (800 μm to 1.5 mm). An additional layer is found in so-called 'thick skin,' the *stratum lucidum*, representing an additional layer of dead cells between the *granulosum* and *corneum* strata (Gilaberte et al., 2016).

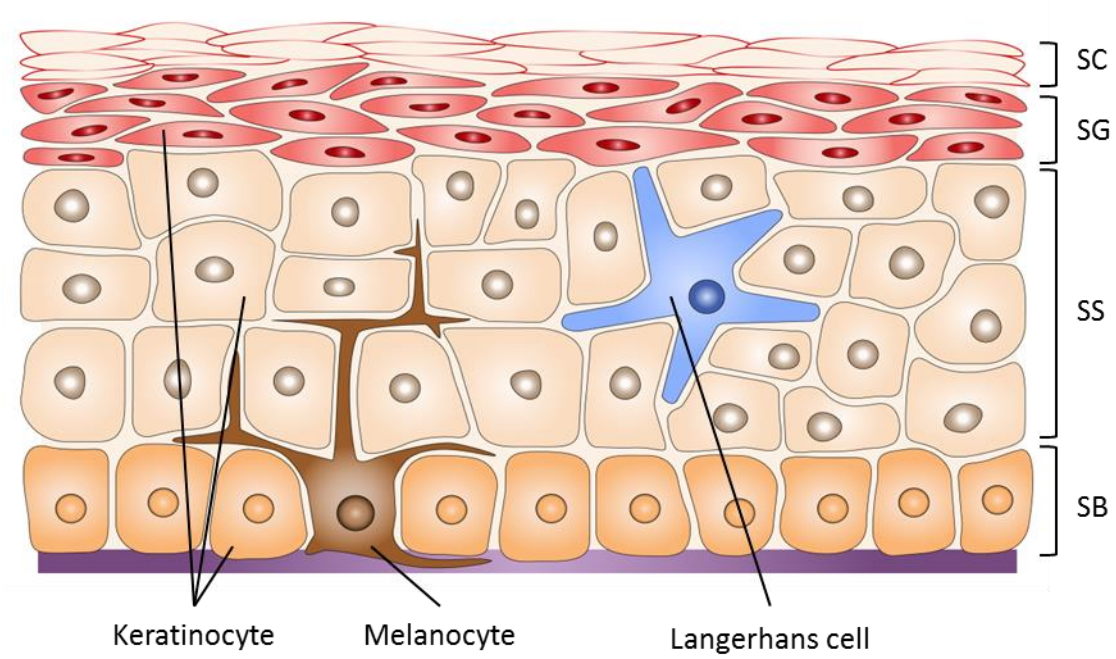

Figure 1.2: The layers of the epidermis

The epidermis is constituted of 90 to 95% keratinocytes, forming four main layers: the *stratum corneum* (SC), *stratum granulosum* (SG), *stratum spinosum* (SS) and *stratum basale* (SB). Other epidermal cell types include the melanocytes, which are found interspersed along the *stratum basale,* and the Langerhans cells, found throughout the epidermis.

1.2.1.1 Other epidermal cell types

While other cell types contribute minimally to the total number of cells residing in the epidermis, they nevertheless fulfil important roles. Melanocytes are interspersed along the *stratum basale*, with approximately one melanocyte for every 30 to 40 keratinocytes of the living cell layers (Fitzpatrick & Breathnach, 1963). Melanocytes possess melanosomes, specialised organelles filled with the enzymatic machinery to synthesise the pigment melanin (D'Alba & Shawkey, 2019). The melanosomes are translocated into neighbouring keratinocytes via dendritic processes of the melanocytes (Van Den Bossche et al., 2006). Differences in pigmentation between light

and dark-skinned individuals is due to the amount of melanogenesis (and the relative amounts of eumelanin and pheomelanin), rather than differences in the number of melanocytes present (Lin & Fisher, 2007). Langerhans cells are also present in the epidermis. These cells conduct immune surveillance, and present antigens to naive T cells in local lymph nodes following cutaneous infection, thereby initiating adaptive immune responses (Romani et al., 2012). Also present are the mechano-sensitive Merkel cells, which are found clustered in touch-sensitive sites such as the finger tips (Woo et al., 2015).

1.2.2 The dermis

The dermis is subdivided into two layers with no discrete border: the papillary (*stratum papillare*) and reticular dermis (*stratum reticulare*). The fibroblast is the principal cell type, which synthesises all of the major ECM components, including collagen, elastic fibres and glycosaminoglycans (Naylor et al., 2011). The dermal regions differ both in the composition and organisation of the ECM (Figure 1.3). The papillary dermis is generally 300 to 400 µm in thickness with a loose ECM, and contains a relatively high density of cells in comparison to the reticular layer. Projecting upwards between the epidermal rete ridges are the dermal papillae, which are rich in microvascular structures that supply nutrients to the epidermis (Lawlor & Kaur, 2015). The reticular dermis is the deeper and larger of the dermal compartments. The collagen and elastic fibres are arranged into thick, well-organised bundles (Figure 1.3), providing tensile strength and elasticity. The ECM of the dermis demonstrates a variety of functions not limited to its mechanical properties, but as a substrate for cell adhesion that mediates cell proliferation, migration, differentiation and gene expression of fibroblasts and other dermal resident cell types (Zeyer et al., 2019).

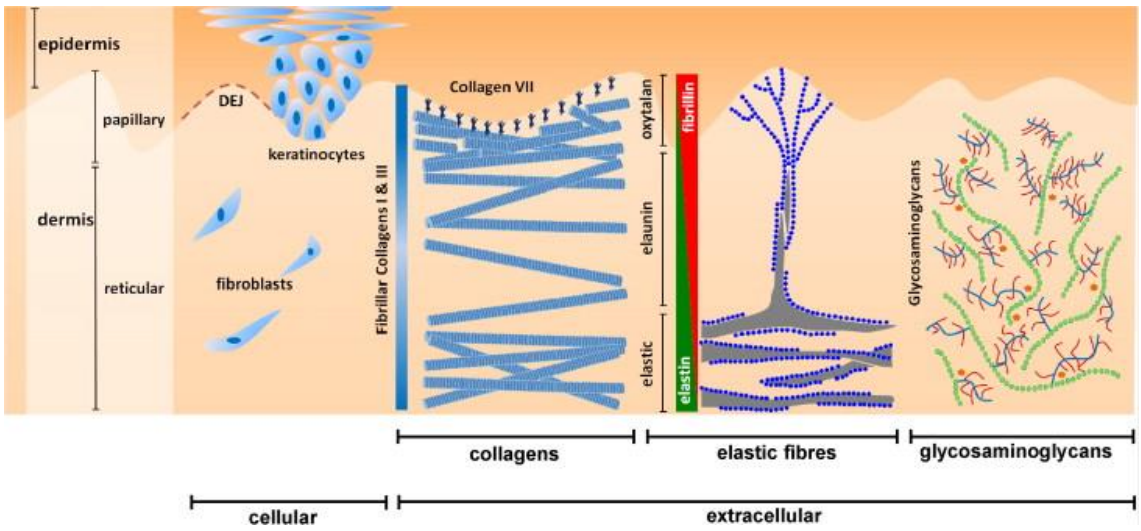

Figure 1.3: Extracellular matrix composition of the papillary and reticular dermis

Sparsely distributed fibroblasts are predominantly responsible for synthesising an extracellular matrix (ECM) constituted of collagens, elastic fibres and proteoglycans. The fibrillar collagens (I and III) are widely distributed in the papillary and reticular dermis. By contrast, collagen VII forms anchoring fibrils that ensure the tight connection of the epidermal basement membrane with the dermal ECM. The elastic fibre network consists of elastin and fibrillin. In the papillary dermis, fibrillin-rich microfibrillar bundles, called oxytalan fibres, form candelabra-like structures descending from the DEJ. Within the reticular dermis, the elastic fibre network comprises thick elastin-rich fibres. Glycosaminoglycans are abundant in the dermis: their crosslinking to other matrix proteins, such as the collagen network, forms supermolecular structures, which increase tissue stiffness. Abbreviaitons: DEJ, dermo-epidermal junction. Figure from Naylor et al. (2011).

1.2.3 Cutaneous ageing

The skin ages through parallel intrinsic and extrinsic processes, which culminate in a deterioration of cutaneous function, with significant associated morbidity. This includes dryness (xerosis) and itch (pruritus), increased susceptibility to infections, autoimmune disease, vascular complications and cutaneous malignancy (Farage et al., 2008). An individual's genetics, cellular metabolism and hormonal levels are thought to influence the progression of intrinsic skin ageing. As a result of its direct exposure with the external environment, including UVR, tobacco smoke and air pollution, the skin also undergoes extrinsic ageing. Chronic exposure to UVR is arguably the greatest driver of premature skin ageing (also called photoageing), estimated to account for up to 90% of the visible signs of skin ageing (Figure 1.4) (Südel et al., 2005). Photoageing is further discussed in subsequent sections (section 1.3.3), following a discussion of the ultraviolet (UV) magnetic spectrum and its effects on the skin (section 1.3).

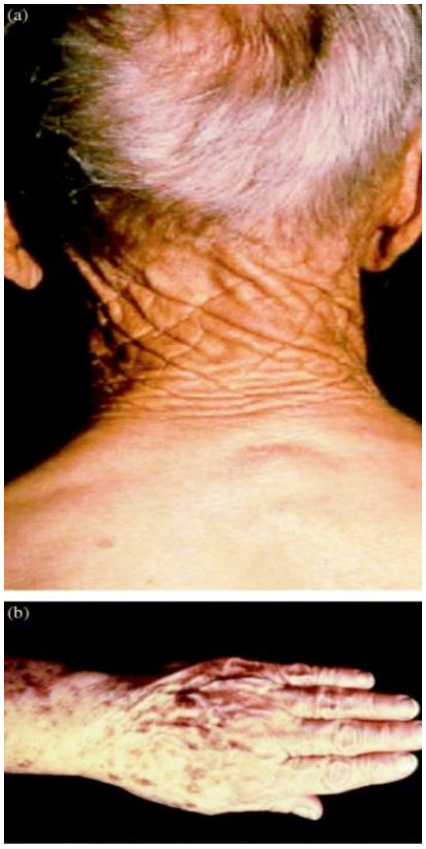

Figure 1.4: Extrinsic and intrinsic ageing of the skin.

(A) Intrinsic skin ageing is exemplified by uniformly pigmented, smooth skin below the collar line. The nape of the neck above the collar line shows classic characteristics of chronic sun exposure, including coarse wrinkling (cutis rhomboidalis nuchae). (B) The hands are also a major site of photoageing, exemplifying the wrinkling, laxity, and pigmentary changes that occur. Figure from Watson and Griffiths (2005).

1.2.3.1 Epidermal changes of intrinsically-aged skin

In ageing skin, the epidermis thins at an approximate rate of six percent per decade (Branchet et al., 1990), as a result of decreased epidermal turnover (Grove & Kligman, 1983). One of the most striking features of intrinsically-aged skin is flattening of the DEJ by approximately a third (Neerken et al., 2004; Lavker et al., 1987; Langton et al., 2016). The smaller contiguous surface means the skin is more susceptible to shearing forces. Furthermore, coupled with a decrease in vascularisation, this leads to a reduction in nutrient and oxygen delivery to the epidermis (Farage et al., 2013).

Functional studies have shown that the aged epidermis is more susceptible to chemically- and mechanically-induced damage (Ghadially et al., 1995). This has been attributed to an overall decrease in key *stratum corneum* lipids, including ceramides. Diminishing activity of key lipid producing enzymes, such as sphingomyelinase and ceramide synthase, has been shown in hairless mouse skin with age (Jensen et al., 2005). Alterations in lipid processing may also be exacerbated by the rising pH of ageing skin (Choi et al., 2007). Furthermore, following mechanically-induced damage by tape stripping, repair of the aged epidermis is significantly delayed as compared to young skin, with differences seen even after 6 days of recovery (Ghadially et al., 1995).

The number of melanocytes also decreases with increasing age, at a rate of 10 to 20% per decade after 30 years of age (Ortonne, 1990). Consequently, aged skin is less pigmented, and this correlates with an increase in UVR sensitivity, especially after 60 years of age (Amblard et al., 1982). The number of Langerhans cells is also decreased in aged skin by approximately 20%. The migratory capacity of the remaining Langerhans cells following *ex vivo* trauma is also impaired, from 15% migration as observed in young skin to only four percent in aged skin, possibly due to impaired expression of IL-1β in ageing Langerhans cells (Pilkington et al., 2018). These changes may contribute to increased skin infections and skin cancer through failure to conduct adequate immunesurveillance (Pera et al., 2015).

1.2.3.2 Dermal changes of intrinsically-aged skin

The dermis also becomes thinner in aged skin, by approximately 20% (Farage et al., 2013). There is a decrease in the number and proliferative capacity of fibroblasts, which, together with a decrease in ECM protein synthesis and an increase in matrix-degrading matrix metalloproteinases (MMPs), leads to large-scale alterations in dermal architecture (Gunin et al., 2011; Cole et al., 2018). This is associated with a gradual loss of elasticity and recoil in aged skin (Daly & Odland, 1979; Langton et al., 2019b).

1.2.3.3 Reactive oxygen species in the ageing process

Reactive oxygen species (ROS) are a type of unstable molecule that contains oxygen, including superoxide anion (O_2^-), hydrogen peroxide (H_2O_2), and hydroxyl radical (HO•) (Ray et al., 2012). They are a by-product of mitochondrial metabolism and are generated in the cellular response to, for example, xenobiotics, cytokines, and bacterial invasion (Zhang et al., 2016). At normal concentrations, ROS are considered important signalling molecules, affecting an array of cellular processes, such as proliferation, metabolism, differentiation, and cell survival (reviewed in Ray et al., 2012). Oxidative stress occurs when ROS are in excess, overwhelming the cell's ability to mount an effective antioxidant response. The free radical theory of ageing was originally described in the 1950s (Harman, 1956). It proposes that organisms age due to an accumulation of oxidatively-damaged macromolecular structures. However, interventions to reduce ROS burden have had mixed results; some studies have indicated that signalling effects of ROS activate cellular stress pathways, which may actually promote healthy ageing (Ristow & Schmeisser, 2011).

Well-recognised in the damage of DNA, ROS induce double strand breaks (Srinivas et al., 2019) and oxidative attack on nucleoside bases (Cadet & Richard Wagner, 2013). Oxidised bases, such as 8-hydroxydeoxyguanosine (8-OHdG), can lead to guanine (G) to thymine (T) or G to adenine (A) transversions if unrepaired. Base excision repair (BER) handles small, non-distorting but frequent lesions in the DNA, such as most of those generated by oxygen radicals. It is initiated by one of at least 11 different DNA glycosylases, which recognise and remove damaged or inappropriate bases, leaving an

abasic site in place (also called an apurinic/apyrimidinic [AP] site). An AP-endonuclease then cleaves the DNA strand 5' of the AP site, allowing the repair DNA polymerase to insert the correct nucleotide base. The ends are then processed, and ligated to complete the BER process (Cadet & Davies, 2017). A multitude of other proteins play roles in BER, including those involved in damage signalling and chromatin remodelling (Hinz & Czaja, 2015).

1.2.3.4 Telomere shortening in the ageing process

Telomeres are DNA-protein structures found at the ends of the chromosomes, pivotal to the preservation of genetic information. In mammals, the telomere repeat is TTAGGG, reiterated thousands of times (Moyzis et al., 1988). Telomere shortening occurs with each cell division due to incomplete replication of the 5' ends of newly synthesised DNA by DNA polymerase (Levy et al., 1992). This acts as a barrier to aberrant proliferation, as when telomere length reaches a critical limit, the cell undergoes senescence and/or apoptosis (Buckingham & Klingelhutz, 2011). Telomeres can be maintained by the enzyme complex telomerase, consisting of a reverse transcriptase component (TERT) and an RNA component (TERC), which is utilised by TERT in the addition of telomere repeats (Greider & Blackburn, 1989). Telomerase activity is present in the germline and some highly proliferative tissues. In the skin, telomerase is active in the epidermis, but is almost undetectable in the dermis (Bickenbach et al., 1998). Exposure of the skin to UVR, and other sources of inflammation, upregulate telomerase activity, suggesting that telomerase may be activated in the epidermis as is required, for example during cell proliferation and repair of damage (Taylor et al., 1996). *In vitro* studies have implicated ROS in accelerating telomere shortening, which may be especially sensitive to oxidative stress as they are G-rich. Thus, some of the effects of ROS may be mediated through telomere-associated cell senescence (Buckingham & Klingelhutz, 2011).

1.3 UV radiation

UV radiation represents wavebands of the electromagnetic spectrum that fall between that of ionising radiation (X-rays) and visible light. Three subdivisions of UVR are recommended by The Commission Internationale de l'Eclairage (CIE): UVC, 100 to 280 nm; UVB, 280 to 315 nm; and UVA, 315 to 400 nm. The CIE nomenclature is not always followed rigorously, with many using a cut-off between UVA and UVB of 320 nm, which creates significant variance in the calculation of UVR dose in experimental studies (Lerche et al., 2017). Atmospheric ozone blocks a large proportion of the Sun's UVR output in a wavelength-dependent manner, whereby shorter wavelengths are more highly absorbed. The UVR component of midday sun reaching the Earth's surface is approximately 95% UVA and five percent UVB radiation. There is essentially no UVC present at ground level (Lerche et al., 2017). Due to depletion of the ozone, catalysed by free chlorine released from man-made chlorofluorocarbons, it is predicted that the amount of UVR at ground level will increase, with associated adverse health effects (Eklund et al., 2013).

The depth of skin penetrance of UVR is also wavelength-dependent. The energy of a UV ray is transferred to an atom or molecule, raising one of its electrons to an excited state. This excitation energy must then be dissipated, which may occur via heat; light; loss of an electron, forming a free radical or ion; reaction with another molecule; or by fragmentation of the molecule. For an atom or molecule to absorb the energy of a UV ray, it must have electrons in the appropriate energy levels to do so, meaning not all molecules absorb all UV wavelengths. A molecule that absorbs a given UV wavelength is said to be a "chromophore" for that wavelength. The skin contains a number of endogenous chromophores within the UVR range, including DNA, urocanic acid, aromatic amino acids, melanins and their precursors (Young, 1997). Due to differences in absorbance of different UV wavelengths, the more energetic UVB is completely blocked by the epidermis, while UVA can penetrate into the dermis (Bruls et al., 1984) (Figure 1.5).

Exposure of the skin to UVR is associated with a number of injurious effects, occurring both in the acute (erythema, commonly referred to as a 'sunburn') and chronic phases

(for example, photoageing [section 1.3.3] and skin carcinogenesis). However, low levels of exposure pose beneficial effects (section 1.3.1).

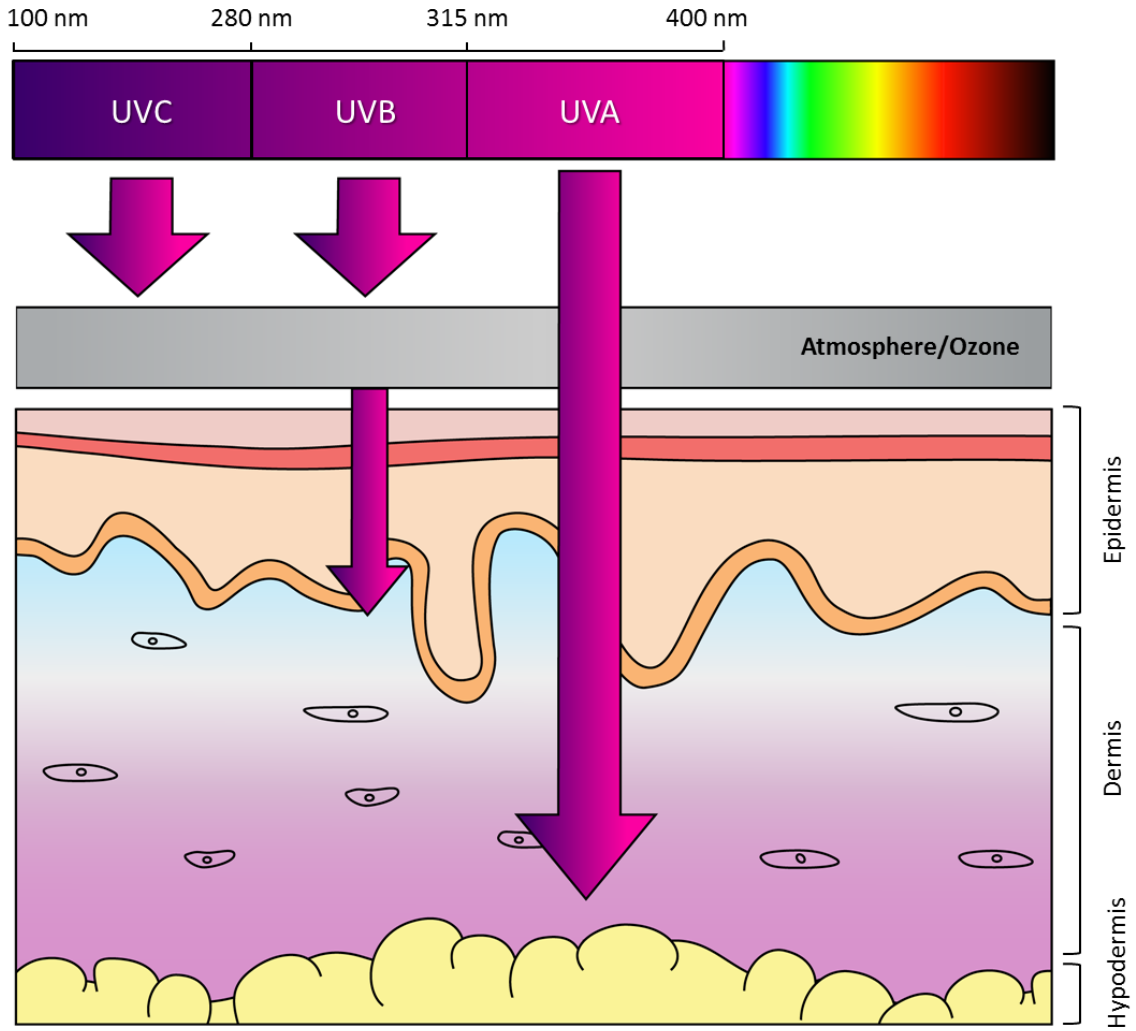

Figure 1.5: Skin penetrance of UV radiation.

UV radiation (UVR) is subdivided into UVA, UVB and UVC. A large proportion of UVR is blocked from reaching the Earth's surface by atmospheric ozone, with absorption increasing at shorter wavelengths of UVR. Of the terrestrial UVR, only approximately five percent is within the UVB waveband, the remaining 95% being UVA. There is essentially no UVC. The skin penetrance of UVR is also wavelength-dependent, with longer wavelengths penetrating as deep as the reticular dermis. UVB is blocked by the epidermis, preventing penetration to the deeper tissue layers.

1.3.1 Beneficial effects of UV radiation

While overexposure of the skin to UVR is of major detriment to human health, small levels of exposure pose beneficial effects. The major source of vitamin D in humans is exposure of the skin to UVB radiation. Specifically, UVR is absorbed by 7-dehydrocholesterol in the plasma membrane of epidermal cells and is converted to previtamin D3. Following further reactions that occur mainly in the liver and kidney, 1,25-dihydroxyvitamin D is formed, the principal hormonal form of vitamin D, responsible for most of its biological functions (Holick, 2017). Exposure of the skin to UVR also leads to an increase in β-endorphin via a p53-mediated mechanism (section 1.3.4). β-endorphin is an endogenous opioid that creates a feeling of well-being, and may contribute to sun-seeking behaviours (Cui et al., 2007).

UVR is also used in phototherapy regimens, for the management of dermatoses including psoriasis, atopic dermatitis, cutaneous T-cell lymphomas, morphea and vitiligo (Situm et al., 2014). This therapy is thought to work through immune suppression, alteration in cytokine expression and cell cycle arrest, which suppresses the disease activity (Bulat et al., 2011).

1.3.2 DNA Damage

Exposure to UVR may induce genomic lesions in the nuclear and mitochondrial DNA directly, as well as indirectly through the generation of ROS (section 1.2.3.3) (Cadet & Douki, 2018). The degree and type of UVR-induced DNA damage depends heavily on the wavelength. UVR from 245 to 290 nm is absorbed maximally by DNA, implicating UVB as a primary mutagen (Brenner & Hearing, 2008). The spectrum of DNA damage includes cyclobutane pyrimidine dimers (CPDs) and (6-4) photoproducts formed between adjacent pyrimidine bases. Less energetic, but 20-times more intense, UVA also induces the formation of CPDs, together with a wide variety of oxidatively generated lesions as a result of ROS production, such as single strand DNA breaks and oxidised bases (especially 8-OHdG) (Ikenhata & Ono, 2011).

DNA damage induced by UVR represent potentially mutagenic DNA lesions, which have been shown to have a direct correlation with cancer development, most commonly occurring within: proto-oncogenes, tumor suppressor genes, or DNA repair genes (Benjamin & Ananthaswamy, 2007). The p53 gene is involved in cell cycle arrest and activation of programmed cell death, with mutations detected in approximately 50% of all human cancers and in almost all of those occurring in the skin (Basset-Seguin et al., 1994). Mutational hotspots occur preferentially at trinucleotide sequences that incorporate a cytosine-phosphate-guanine (CpG) dinucleotide, the main methyl group acceptor site in the genome (section 1.4.3) (Tommasi et al., 1997). This is thought to owe to several phenomena: a red-shift in the absorbance spectra of methylated C versus unmethylated C (Martinez-Fernandez et al., 2017) and the enhanced deamination of C to T, when C is methylated (Lee & Pfeifer, 2003). If a cell replicates before the mismatch can be repaired, this results in the UVR signature C to T transition mutation (Ikenhata & Ono, 2011).

1.3.3 Photoageing

Chronically photoexposed skin displays severe wrinkling, extensive sagging, mottled pigmentation, telangiectasia (threadlike red lines due to broken or widened blood vessels) and various neoplasms (Orentreich et al., 2001). Histologically, photoageing is superimposed onto a background of intrinsically-aged skin. The additional effects of photoageing are characterised by an acceleration of epidermal thinning and deconvolution of the DEJ (Naylor et al., 2011; Montagna & Carlisle, 1979). While there are aberrations to the elastic fibre network in intrinsically-aged skin, a characteristic of photodamage is solar elastosis—tangled masses of dystrophic elastotic material (Sellheyer, 2003). The oxytalan fibres of the papillary dermis, which are gradually lost with increasing age, are greatly accelerated in their loss, even in minimally photodamaged skin (Watson et al., 1999).

Studies have shown that UVR activates many cytokine and growth factor receptors, in a ligand-mimicking manner. These signalling pathways increase the expression of c-Jun, which together with c-Fos, represents an integral part of the activator protein 1

(AP-1) transcription factor complex (Rittié & Fisher, 2002). AP-1 stimulates the transcription of MMPs, a large family of endoproteases that, collectively, have the capacity to degrade the components of the dermal ECM (Cole et al., 2018). Briefly, some of the MMPs upregulated by AP-1 include MMP-1, which initiates degradation of types I and III fibrillar collagens, and MMP-3 and MMP-9, which further degrade the collagen fragments generated (Fisher et al., 1996). Additionally, MMP-2, MMP-9, and MMP-12 degrade type IV collagen of the DEJ (Monaco et al., 2006; Gioia et al., 2009; Chandler et al., 1996). Type IV collagen is thought to play an important role in wrinkle formation, as it is reduced at the base of wrinkles as compared to the flanking region, highlighting the importance of the DEJ-related molecules in the structural integrity of the skin (Contet-Audonneau et al., 1999).

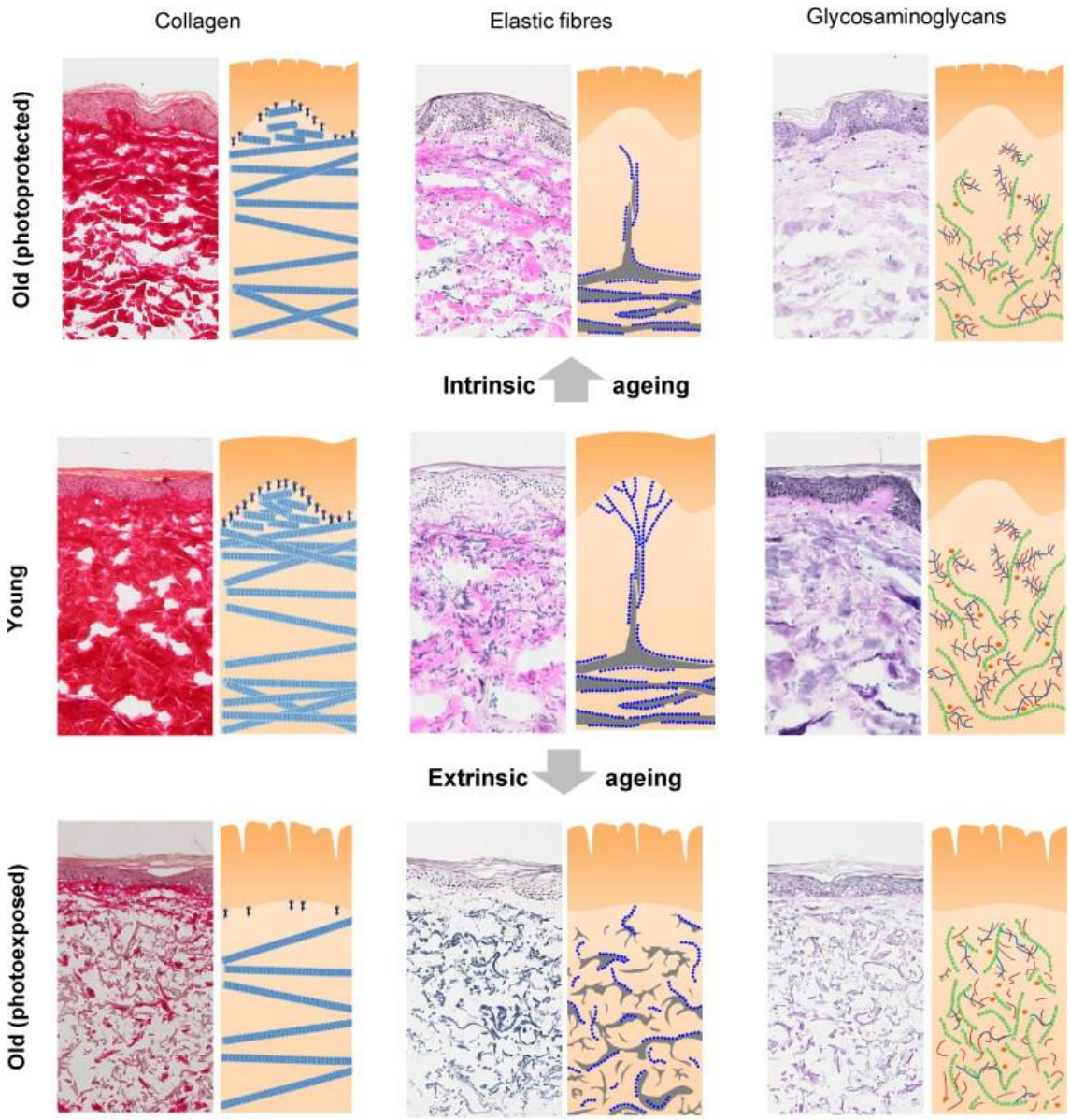

Figure 1.6: Alterations of dermal extracellular matrix architecture in intrinsically and photoaged skin.

The amount of glycosaminoglycans, collagen and elastic fibres is decreased in aged skin, due to a decrease in fibroblast numbers and reduced biosynthetic activity. The normal pattern of elastic fibres, called oxytalan fibres, located in the papillary dermis, gradually disappears. Figure taken from Naylor et al. (2011).

1.3.4 Photoprotection by melanin

Melanin is an excellent photoprotectant that absorbs both UVB and UVA radiation and dissipates the energy as heat. Differences in human skin pigmentation are a product of natural selection to adjust levels of constitutive pigmentation in the skin to levels of UVR (Jablonski and Chaplin, 2010). High UVR near the equator was a powerful selective pressure for the evolution of dark and highly photoprotective pigmentation, while the requirement for UVB photons to sustain cutaneous photosynthesis of vitamin D in low-UVB environments led to the evolution of less pigmented skin types. Skin colour can be graded by the Fitzpatrick scale (Fitzpatrick, 1988), based on self-reported tanning and sunburn susceptibility that categorises individuals into six skin phototypes (I to VI; table 1-1). Studies comparing the different Fitzpatrick phototypes found that melanin had an average sun protective factor (SPF) of between 2 and 10 in type VI individuals as compared to type I (Fajuyigbe & Young, 2016; Kaidbey et al., 1979). Thus, many aspects of photoageing are delayed in their acquisition in individuals with more pigmented skin types, by as much as 40 to 50 years (Langton et al., 2019a, 2017). The eventual deterioration of skin architecture in these individuals may coincide with reduced pigmentation that is seen with increasing age, which would be more permissive to UVR-induced damage (Chien et al., 2016).

Upon UVR exposure, keratinocytes produce proopiomelanocortin (POMC) via a p53-mediated response to DNA damage. POMC is post-translationally cleaved into biologically active peptides, including α-melanocyte stimulating hormone (MSH), adrenocorticotropic hormone (ACTH) and β-endorphin (section 1.3.1) (Cui et al., 2007). The melanotropic α-MSH mediates the tanning process by stimulating adjacent melanocytes to produce eumelanin (D'Orazio et al., 2006). A tan is estimated to have an SPF of 3 to 4, preventing further damage to subsequent UVR exposure (Nonaka et al., 1984).

Table 1.1: Fitzpatrick scale for classification of skin phototype adapted from Fajuyigbe & Young, 2016 (Fajuyigbe & Young, 2016)

Skin type	Phenotype	Sensitivity to sunburn	1 MED (as SED)	Tanning ability	Susceptibility to skin cancer
I	White (very fair)	Always burns	2–3	Never tans	High
II	White (fair)	Burns easily	2.50–3	Tans minimally	High
III	Cream white	Burns mildly	3–5	Tans gradually	High
IV	Light Brown	Burns slightly	4–7	Tans well	Moderate
V	Brown	Burns rarely	6–20	Tans profusely	Low
VI	Black/dark brown	Never/rarely burns	6–20	Always tans	Low

Abbreviations: MED, minimal erthythema dose; SED, standard erythema dose (1 mJ cm^{-2})

1.4 Epigenetic modifications

The term “epigenetics” by its most literal definition describes phenomena that exist outside of the concept of conventional genetic inheritance (epi; from the Greek επί, meaning over, outside of or around) (Brait & Sidransky, 2011). Waddington (2012) is attributed with its coining in a founding paper of the field, which he therein used to describe the control mechanisms exerted between the genotype and phenotype. In later work, Waddington suggested the concept of the epigenetic landscape, likening development to a marble rolling down a hill (Waddington, 1957) (Figure 1.7). Drivers of cell-fate commitment, including cell positioning and presence of signalling molecules, are illustrated by the furrows of the hill, and the accompanying epigenetic programme that reinforces commitment decisions by the unidirectionality of the marble’s movement (Mohammad & Baylin, 2010).

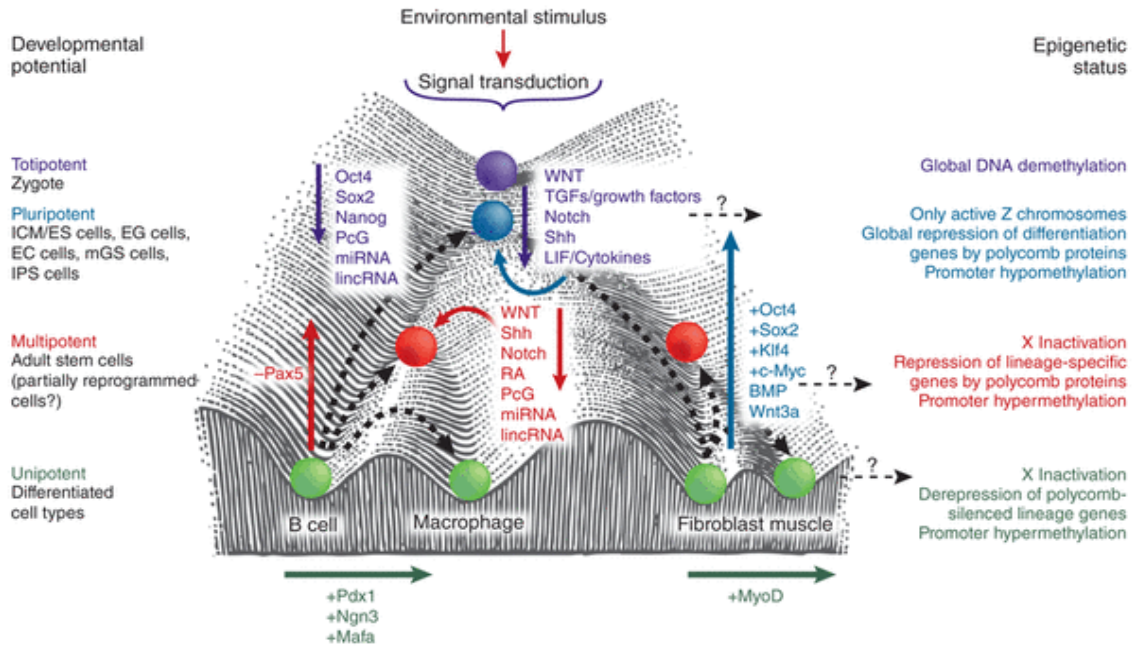

Figure 1.7: Waddington’s concept of an epigenetic landscape.

The marble (purple) is characteristic of the totipotent zygotic cell before a signal triggers differentiation. The furrows of the hill dictate divergent paths through the pluripotency, multipotency, adult stem cells and terminally differentiated state. Arrows represent directionality of factor influence ('+' indicating addition and '–' indicating removal). Downward arrows reflect the direction of normal development,

while the upward blue arrow at the bottom right of the hill depicts generation of induced pluripotent stem cells (iPSCs). Figure from Mohammad and Baylin (2010).

The epigenetic landscape has since been vastly elaborated, encompassing DNAm and histone modifications, nucleosome positioning and modification of gene expression by non-coding RNAs (ncRNAs) (Allis & Jenuwein, 2016). Whether all so-called epigenetic modifications satisfy the criterion of heritability remains unclear, but the boundaries that separate these mechanisms are blurring, with the synergy between epigenetic processes often an essential feature of their activity (Böhmdorfer & Wierzbicki, 2015; Jobe et al., 2012). Discussion of what constitutes an epigenetic mechanism will therefore likely continue for many years.

1.4.1 Overview of the structure of chromatin

Chromatin describes the structure of DNA and proteins, consisting of repeating units, called nucleosomes. These are octameric cylindrical structures consisting of two copies of each of the four core histone proteins (H2A, H2B, H3 and H4) that winds approximately 147 base pairs (bp) of DNA in 1.7 superhelical turns (Andrews & Luger, 2011). Stretches of DNA, 10 to 80 bp in length, connect the nucleosomes, bound at the entry and exit site of the core histone particle, by the linker histone (H1), which facilitates inter-nucleosomal interactions (Hergeth & Schneider, 2015).

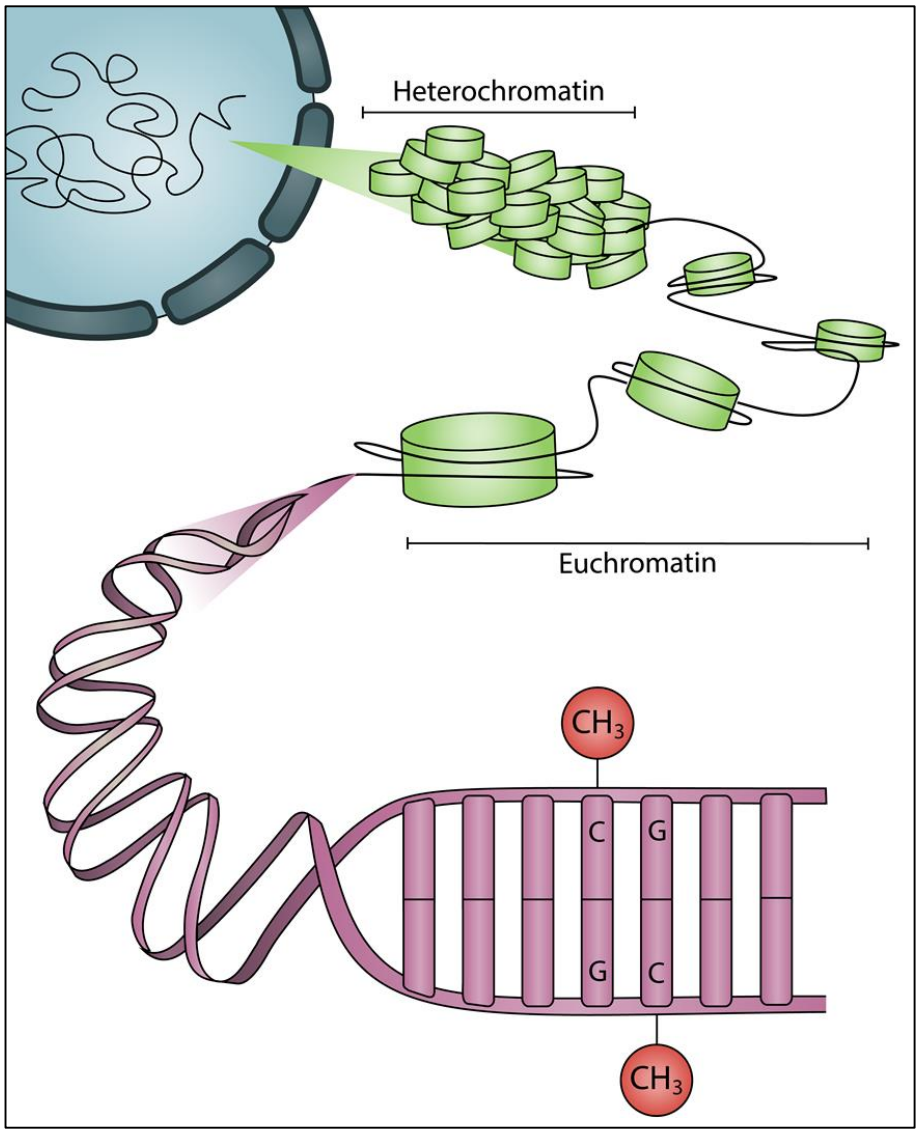

Figure 1.8: Hierarchy of genomic organisation

The nucleosome is considered the first level of chromatin folding, consisting of 147 base pairs of DNA wrapped around a histone octamer (green). The DNA can be methylated at palindromic cytosine-phosphate-guanine sites (red). Heterochromatin is a form of chromatin that is densely packed—as opposed to euchromatin, which is loosely packaged.

1.4.2 Histone Modifications

In the early 1960s, Allfrey et al. (1964) performed pioneering studies that demonstrated the post-translational modification of histone proteins. An

understanding of how changes to chromatin structure could arise was shown by the solving of the high-resolution X-ray structure of the nucleosome, evidencing inter-nucleosomal interactions of the protruding N-terminal tails (Luger et al., 1997). It is now well-established that these N-terminal tails perform multiple roles in nucleosomal array condensation (Fletcher & Hansen, 1995; Allan et al., 1982; Garcia-Ramirez et al., 1992). Histone modifications, such as acetylation, methylation and phosphorylation (Figure 1.9), among other modifications, act as a histone code, and affect diverse downstream chromatin-based processes (Taverna et al., 2007). Large families of proteins recognise the different PTMs, the residue to which they are attached and its quantity (Bannister & Kouzarides, 2011).

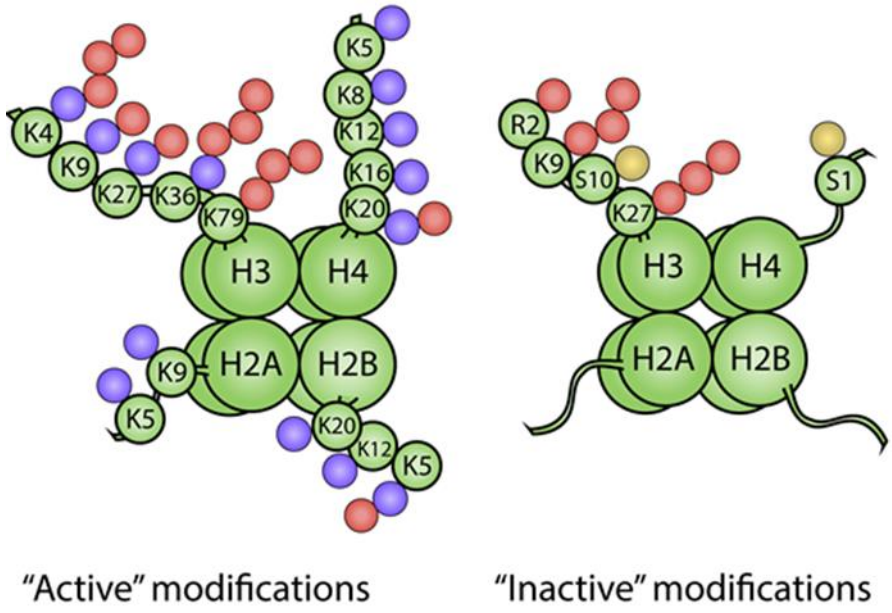

Figure 1.9: Examples of common histone modifications.

Histone (H) modifications predominantly occur on the N-terminal tails, consisting of methylation (red), acetylation (blue) and phosphorylation (yellow), among other modifications. Traditionally-associated 'active' and inactive' modifications are indicated.

1.4.2.1 Histone acetylation

Histone acetylation is controlled by enzymes that catalyse the addition of an acetyl group to the ε-amino group of a lysine (symbol: K) side chain (histone acetyl transferases [HATs]), and those that remove it (histone deacetylases [HDACs]) (Yang & Seto, 2007). Lysine residues possess a positive charge, which is neutralised upon addition of an acetyl group. This may prevent tight folding of nucleosomal arrays and increases accessibility of the DNA, as demonstrated by increased sensitivity to DNase I treatment (Hebbes et al., 1994). Accordingly, broad acetylation is known to mark domains permissive to gene transcription (Figure 1.9).

1.4.2.2 Histone methylation

Histone methylation occurs on the three basic residues: lysine (Murray, 1964), arginine (symbol: R) (Byvoet et al., 1972) and, less frequently, histidine (symbol: H) (Gershey et al., 1969; Greer & Shi, 2012). Enzymes that catalyse the addition of a methyl group are the histone methyltransferases, divided into three families: the SET (Su(var)3-9, Enhancer of Zeste, Trithorax) domain-containing proteins and DOT1-like proteins catalyse the transfer of a methyl group from the methyl group donor, S-adenosyl-L-methionine (SAM), to a lysine's ε-amino group, and the protein arginine N-methyltransferases (PRMTs) that catalyse the transfer of a methyl group from SAM to the ω-guanidino group of arginines (Greer & Shi, 2012). While acetylation occurs only singly, lysine may be modified by mono-, di- or tri-methylation. Similarly, arginines may be modified by mono- and symmetric or asymmetric di-methylation (Greer & Shi, 2012). Histone methylation can be a marker of both active and inactive regions of chromatin (Figure 1.9). For example, methylation of histone 3 at lysine 9 (H3K9me) occurs widely throughout the inactivated female X chromosome. Methylation of K4 on the same histone, however, is a marker for actively transcribed genes (Egger et al., 2004).

1.4.3 DNA methylation

Chemically, DNAm involves the covalent addition of a methyl group at the fifth carbon position of C, forming 5-methylcytosine (5mC). In mammals, DNAm occurs almost exclusively at symmetric CpG dinucleotides, catalysed by a family of DNA methyltransferases (DNMTs) (Jin & Robertson, 2013). The biological role of DNAm was predicted independently by Holliday and Pugh (1975) and Riggs (1975). In particular, they recognised the preference of a DNA methyltranferases for hemimethylated substrates, where the parental DNA strand is methylated and the daughter DNA strand requires methylation, was highly befitting of an enzyme involved in the maintenance of cell-type specific gene expression through meiotic and/ or mitotic division. Later, McGhee and Ginder (1979) examined DNAm at the single gene resolution using methylation-specific bacterial restriction endonucleases. They demonstrated that the methylation status of the beta-globin locus in different cell types of chickens correlated with expression of beta-globin. The role of DNAm in numerous phenomena is now well-recognised, including X-inactivation, asymmetric expression of imprinted genes, maintenance of cell type-specific gene expression and suppression of transposable elements (Moore et al., 2013).

Targeted mutation of DNMT1 in mice results in a global loss of DNA methylation and embryonic lethality (Li et al., 1992). Similarly, deletion of DNMT3B is also embryonic lethal. Loss of DNMT3A, which has been shown to be more lowly expressed than DNMT3b in the developing embryo, did not affect mice being carried to term. However, most homozygous mutant mice became runted and within weeks of birth (Okano et al., 1999). These findings established that DNMTs have important functions throughout development. During development, DNAm is established by the *de novo* methyltransferases DNMT3A and DNMT3B. DNMT3L possesses no catalytic activity itself, but stimulates the activity of the *de novo* methyltransferases by increasing their affinity for the methyl group donor, SAM (Kareta et al., 2006). By contrast, DNMT1 displays a preference for hemimethylated substrates, and is therefore the proposed maintenance methyltransferase that copies methylation patterns onto newly synthesised DNA, making DNAm a long-term and mitotically heritable mark. In support of this, DNMT1 is known to localise to replication foci during S phase of the cell cycle

(Probst et al., 2009). Numerous isoforms of all of the DNMTs have been demonstrated and are discussed in-depth later in this thesis (section 3.4).

DNAm in different genomic regions has different functional consequences (Figure 1.10). The CpG-poor genomic landscape is punctuated by CpG islands (CGIs) frequently found free of methylation within the proximal promoters of approximately 50% of mammalian gene promoters. This includes virtually all housekeeping genes, as well as a proportion of tissue-specific genes and developmental regulator genes (Deaton & Bird, 2011). CGIs are attributed with three main features: i) a length of more than 200 bp; ii) have over 50% GC composition, and; iii) retain an observed/expected ratio of CpG dinucleotides greater than 0.6 (Ioshikhes & Zhang, 2000). Regions with lower CpG density that lie within the 2 kb up- and downstream of a CGI are defined as CpG shores, while the 2 to 4 kb from a CpG island is the CpG shelf. The rest of the genome, not within these regions, is often termed open sea, especially in the context of DNAm microarray data annotation (Moran et al., 2016). Within CpG islands and shores, methylation obscures the cognate DNA sequence, interfering with binding of the transcriptional machinery that, in most cases, prevents expression of the nearby gene (Moore et al., 2013). On the other hand, gene-body methylation has been observed to be positively correlated with gene expression levels. Repression of spurious transcription within genes is one possible explanation for the prevalence of gene-body methylation (Jjingo et al., 2012). More than 90% of methylated CpGs are found in repetitive DNA elements, suggesting that cytosine methylation evolved as a defence against transposons and other parasitic elements, including Alu and LINE-1 sequences, which are the most common and well-characterised in the genome (Portela & Esteller, 2010).

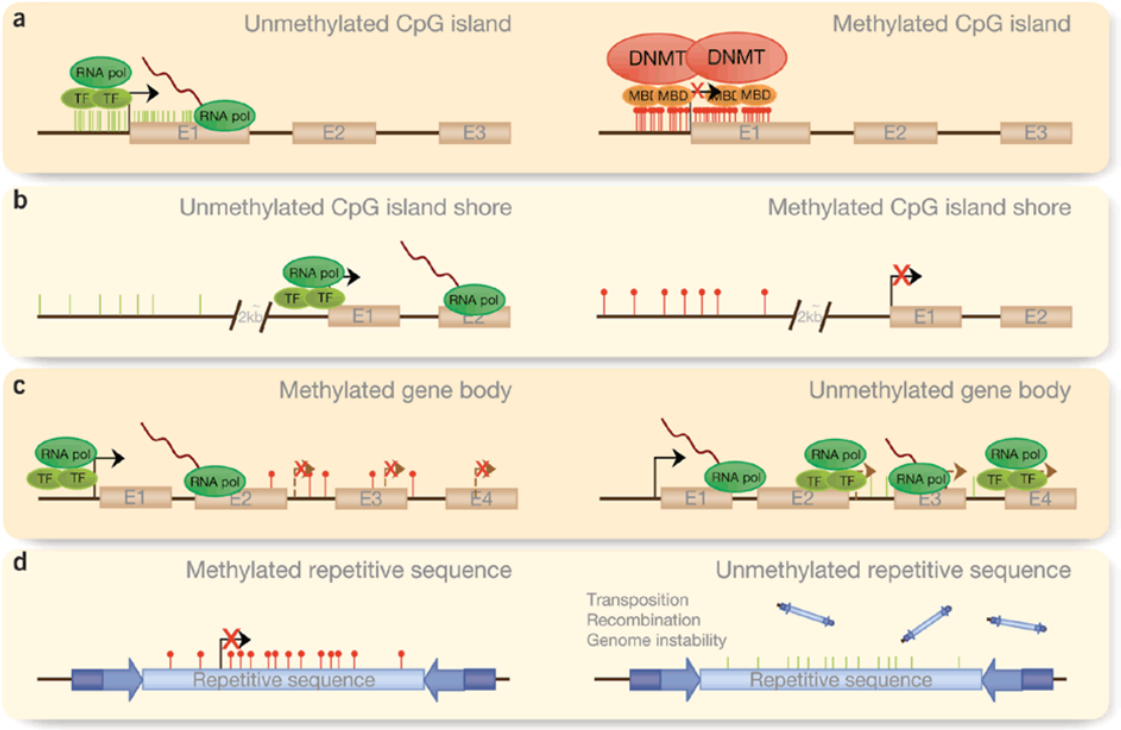

Figure 1.10: The functional effects of DNA methylation in discrete regions of the genome.

In the left column the normal scenario is depicted, with aberrations to normal DNA methylation (DNAm) patterns shown in the right column. (a) Unmethylated cytosine-phosphate-guanine (CpG) islands at promoters of genes are typically permissive to transcription. Hypermethylation suppresses transcription of the associated gene. (b) The same pattern is observed in island shores, which are located up to 2 kb upstream of the CpG island. (c) DNAm within the gene body facilitates transcription, preventing spurious transcription initiation. In disease, the gene body can be hypomethylated, allowing transcription to be initiated at several incorrect sites. (d) Repetitive sequences appear hypermethylated to prevent chromosomal instability, translocations and gene disruption. Portela and Esteller (2010).

1.4.3.1 DNA demethylation

While 5mC is recognised as the canonical mark of DNAm, additional modifications have recently come to light. Among them is the hydroxylation of 5mC to 5-hydroxymethylcytosine (5hmC) catalysed by the ten-eleven translocation (TET) family

of proteins (Figure 1.11) (Koivunen & Laukka, 2018). There are three TET paralogues, TET1, TET2 and TET3 (Lyko, 2018). TET1 and TET3 have bene demonstrated to interact with their genomic targets through direct binding of their respective CXXC domains to DNA (Rasmussen & Helin, 2016). In contrast to the other TET paralogues, the structure of TET2 does not contain any known DNA-binding domains. However, TET2 has been shown to bind tissue-specific transcription factors such as early B-cell factor 1 (EBF1) (Guilhamon et al., 2013) and WT1 (Rampal et al., 2014). TET1 mutant mice have been found to be viable, fertile and grossly normal (Dawlaty et al., 2011). Similarly, TET2 mutant mice are carried to term and appear grossly normal. However, Approximately 1/3 of Tet2−/− and 8% of Tet2+/− mice died within 1 year of age because of the development of myeloid malignancies, suggesting that TET2 functions as a tumour suppressor (Li et al., 2011a). Homozygous mutation of TET3 in mice led to neonatal lethality (Gu et al., 2011).

As a chemically distinct epigenetic mark, 5hmC could constitute a recognition site for specific binding proteins. However, the different kinds of modifications cannot be distinguished by many commonly used sodium bisulphite-based methods of detection (Huang et al., 2010). Iterative oxidation of 5hmC generates 5-formylcytosine (5fC) and 5-carboxylcytosine (5caC), targets of BER, which excises the modified C and incises an unmodified C. This may then remain unmethylated, unless targeted by DNMTs (Rasmussen & Helin, 2016) (Figure 1.11).

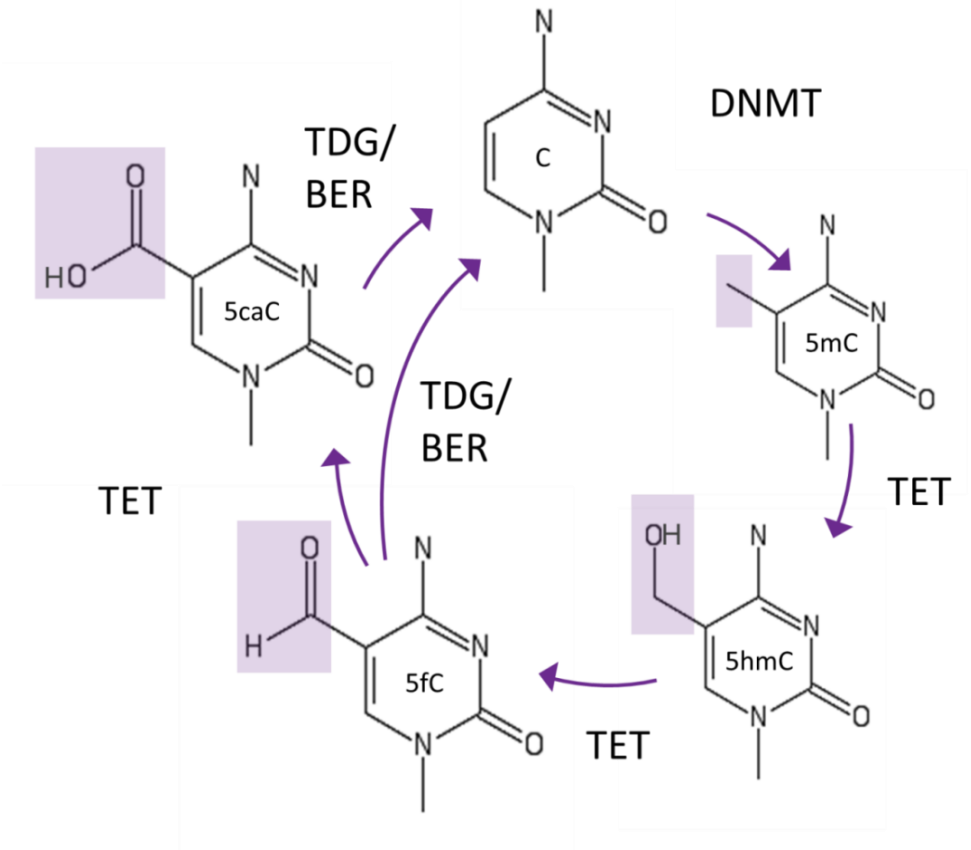

Figure 1.11: Modification of cytosine by DNA methyltransferases (DNMTs) and ten-eleven translocation (TET) proteins

Cytosine (C) is modified to 5-methylcytosine (5mC) by DNA methyltransferases (DNMTs), which can be oxidized to 5-hydroxymethylcytosine (5hmC), 5-formylcytosine (5fC) and 5-carboxylcytosine (5caC) in an iterative manner by ten-eleven translocation (TET) proteins. Unmethylated C is restored passively during DNA replication. Alternatively, 5fC or 5caC can be excised by thymine DNA glycosylase (TDG) to generate an abasic site as part of base excision repair (BER) pathway, leading to restoration of unmethylated cytosine.

1.5 DNA methylation in ageing and photoageing of the skin

Longevity and healthy ageing are among the most complex phenotypes studied to date. The heritability of age at death in adulthood has only a modest heritable component, approximately 30% (Cournil & Kirkwood, 2001). The importance of non-genetic factors is elegantly illustrated by the caste differentiation of honeybees (*Apis mellifera*). Young female larvae to become the long-lived queens are continuously fed large amounts of royal jelly, while larvae to become the short-lived worker bees are switched to a less complex diet of honey and pollen, called worker jelly (Colhoun & Smith, 1960). Metabolism and growth of royal jelly-fed larvae is accelerated; this is accompanied by alterations in transcriptional profiles underscored by changes in DNAm (Drewell et al., 2014). Interestingly, DNMT3 knockdown in honey bees also leads to differentiation of larvae into a queen-like phenotype (Kucharski et al., 2008). This suggests that dietary and other lifestyle factors, through gene-environment interactions and modulation of epigenetic networks, influence lifespan and healthy ageing.

1.5.1 Trends in DNA methylation in human ageing

A perturbed epigenome represents an attractive mechanism for understanding the phenotypic changes associated with human ageing. The fidelity of DNAm maintenance is not 100%; therefore, errors lead to epigenetic drift, an important hallmark of ageing (Teschendorff et al., 2013b). This is demonstrated by studies of monozygotic twins. In early life, monozygtoic twins are epigenetically indistinguishable; however, significant divergence is observed in the overall levels and distribution of 5mC in older individuals (Fraga et al., 2005; Tan et al., 2016). Furthermore, age-predicting algorithms have been developed that utilise DNAm levels at specific genetic loci (Bocklandt et al., 2011; Hannum et al., 2013; Koch & Wagner, 2011; Garagnani et al., 2012; Bekaert et al., 2015; Horvath, 2013; Horvath et al., 2018). These loci predictably “tick” with age, a process distinct from epigenetic drift. Epigenetic age estimators have been shown to out-perform other age-predicting algorithms, for example, telomere length, and transcriptomic and proteomic predictors (Jylhävä et al., 2017). Epigenetic age can be accelerated by endogenous or exogenous

factors, meaning it may represent a prognostic marker of ageing progression (reviewed in Horvath & Raj, 2018).

Studies probing the methylation status of specific CpG sites across the genome suggest that these "predictable" changes in DNAm occur in a context-dependent manner. Specifically, global levels of DNAm decrease in almost all tissues that have been examined, occurring in regions termed partially methylated domains (PMDs) that are characterised by: i) localisation to the nuclear lamina (lamina-associated domains [LADs]); ii) low gene density; iii) low CpG density, and; iv) late replication timing (Zhou et al., 2018). Furthermore, loss of methylation is enhanced by CpG sites flanked by an 'A' or a 'T' base; CpG sites meeting these criteria have been termed 'solo WCGWs' by Zhou and colleagues (2018) and have been shown to undergo preferential hypomethylation in almost all healthy tissue types. By contrast, DNAm sites within promoter-associated CpG islands tend to gain methylation with age (Day et al., 2013; Maegawa et al., 2010; Teschendorff et al., 2010). As ageing is the most important risk factor for cancer, gene-specific hypermethylation may represent a molecular link between these processes. Indeed, hypermethylation of tumour suppressor genes represents an extremely consistent marker of carcinogenesis.

A caveat of some ageing studies is that changes in DNAm in heterogeneous tissues may partly reflect alterations in cell type composition. Indeed, blood, arguably the most conveniently accessible source of DNA for study, may be confounded by a skew in the relative proportion of myeloid to lymphoid cells that occurs with age (Houseman et al., 2012; Teschendorff et al., 2009). However, ageing-related DNAm changes are also detected in more homogeneous cell populations, such as hematopoietic stem cells (Beerman et al., 2013).

1.5.2 Intrinsic ageing changes in the skin DNA methylome

The skin is an ideal model to study age-associated changes in the epigenome. For one, it is tolerant to sampling by relatively non-invasive techniques, such as suction blister induction (liberating only the epidermis from the skin) or full-thickness punch biopsy (Zuber, 2002; Hajime et al., 1990). Furthermore, the separated epidermis and dermis

are constituted of a high degree of cellular homogeneity and undergoes well-known phenotypic changes with age and upon exposure to exogenous factors, such as UVR (section 1.3.3), circumventing a number of issues related to changes in cell type composition. However, careful disentanglement of what represents an intrinsically- or extrinsically-driven change is important for understanding the consequences of their acquisition, and how these changes may be prevented, or even reversed.

Grönniger et al. (2010) have generated DNAm profiles of suction blister roofs and enzymatically separated epidermis and dermis from full-thickness punch biopsies (utilising dispase to cleave DEJ-specific type IV collagen) obtained from the forearm and inner arm of two distinct age groups. A significant shift towards hypermethylation was identified in aged skin, which was more prominent in the epidermal than the dermal compartment. The majority of differentially methylated probes (DMPs) localised within CpG islands; however, as the authors note, this early study, utilising Illumina Infinium arrays limited to 27,578 CpG sites, was biased to detect DNAm within CpG islands. Therefore, changes in DNAm, occurring in distal regulatory elements and gene-poor regions, may not have been apparent using this technology. Nonetheless, the authors performed deep bisulphite sequencing of three candidate genes in intrinsically-aged skin, confirming and expanding the number of hypermethylated sites associated with regions overlapping the promoters of *TET2,* dimethylarginine dimethylaminohydrolase 2 (*DDAH2)* and SEC31-like 2 (*SEC31L2*). Hypermethylation of the TET2 gene promoter in ageing skin may be of particular relevance to the dysregulation of the epigenetic landscape, as it catalyses multiple steps of 5mC oxidation, facilitating DNA demethylation (section 1.4.3.1). Widely recognised as a tumour-suppressor gene, TET2 deletion in mice has been shown to be sufficient to cause myeloid malignancies (Li et al., 2011b).

Murine studies have indicated a down-regulation of the epigenetic enzymes DNMT3a, DNMT3B and TET2 with a concomitant reduction in global methylation levels in the skin of aged mice (Qian and Xu, 2014). When the mRNA levels of DNMTs (Grönniger et al., 2010; Raddatz et al., 2013) and TETs (Raddatz et al., 2013) were examined in

human skin, no significant reduction was identified, although sample sizes have been limited and there appeared to be a slight trend of their reduction in aged skin.

Raddatz et al. (2013) used whole-genome bisulphite sequencing, but provided information only for single pools of five young and aged epidermal samples, taken from the photoexposed forearm. The pooling of samples made statistically robust analysis difficult. Another study generated DNAm profiles of more than 100 epidermal samples from female subjects of a wide age range, using Illumina infinium 450K arrays (Bormann et al., 2016). This study identified discontinuous changes in DNAm that co-occurred with the onset of menopause. However, this study again used the forearm as the site of sampling. Such studies are confounded by the superimposition of intrinsic-related and sun-exposure related differences.

Ageing studies in the skin have identified a greater number of hypermethylated CpG sites in intrinsically-aged photoprotected skin than hypomethylated sites (Vandiver et al., 2015; Grönniger et al., 2010). However, Zhou *et al*. (2018) have shown that when solo WCGWs (section 1.5.1) in the intrinsically-aged upper inner arm DNAm profiles generated by Vandiver were analysed separately, they were found to be significantly hypomethylated in these regions. This suggests that while global decay of 5mC does not occur, these regions lose methylation as is observed in other ageing tissues. However, the degree of promoter-associated hypermethylation may be a greater feature of ageing skin, while hypomethylation is a greater feature of other ageing tissues. This may be a result of the more direct exposure with the outside environment.

1.5.3 Changes associated with exposure to UV radiation

A comparison of the forearm and the upper inner arm in the Grönniger *et al*. (2010) study identified a greater propensity for hypomethylation of the photoexposed forearm. Again, the authors noted that the number of DMPs was greater in the epidermis than the dermis. A loss of methylation was also recapitulated in a comparison of forearm and the more photoprotected upper inner arm of young and aged donors, utilising 450K arrays, which found large blocks of hypomethylation that

were enriched in transcriptionally silent chromatin that heavily interact with the nuclear lamina, termed LADs, and large organised chromatin K9-modifications (LOCKs) (Vandiver et al., 2015). These studies provide excellent evidence of an epigenetic component of the skin response to UVR. However, it is important to consider that epigenetic differences exist between different anatomical sites (Koch & Wagner, 2011). Genome-wide DNAm profiles of fibroblasts isolated from different breast, abdomen, arm, leg, ear and eyelid demonstrated differences between bodysites. A number of DNAm differences were aligned within the four *HOX* clusters, encoding a family of transcription factors that regulate early developmental morphogenetic processes. These differences were identified following three passages in culture, suggesting that the epigenome possesses and maintains a memory of anatomical site of origin (Koch et al., 2011). Whether other skin-resident cells, such as the keratinocytes, melanocyte and others, possess an epigenetic memory of their anatomical site of origin has not been investigated. Vandiver et al. (2015) and Grönniger et al. (2010) account for anatomical differences in their comparison by ascribing changes between the young photoexposed and photoprotected skin as "anatomical" differences, and the additional sites changing between these body sites in the aged group as "photoexposure" differences, due to the added number of years of photoexposure incurred. However, an age range of 18-30 years of age for young donors may falsely ascribe some UVR-related changes, occurring in the first three decades of life, as anatomical differences, making it difficult to ascertain the earliest markers of photoexposure. Furthermore, the upper inner arm may not represent a completely non-photoexposed site, and may therefore not provide an adequate control baseline for these studies.

In contrast to these *in vivo* studies, Lahtz et al. (2013) exposed normal human epidermal keratinocytes (NHEKs) chronically to UVB radiation and assessed DNAm using a methylated CGI recovery assay, reporting that UVR did not induce changes in DNAm in the regions assayed. Given other studies have predominantly identified non-CGI changes in methylation as the main characteristic of UVR exposure *in vivo* (Vandiver et al., 2015), the CGI-focussed analysis could explain the few number of DNAm changes identified. Therefore, this study does not sufficiently answer the

question of whether NHEKs undergo changes in DNAm as have been shown in chronically photoexposed skin.

Studies to date highlight that, while photoexposure may accelerate some features of skin ageing occurring with the passage of time, it is associated with its own pattern of epigenetic aberrations. There remains an open question as to what the earliest changes upon UVR exposure are, and whether sub-erythemal levels of UVR are capable of eliciting these changes.

1.6 Project Hypothesis and Aims

The overarching hypothesis to be addressed in this thesis is that ageing and photoexposure alter DNAm patterns in the skin, with the consequence of impaired skin function. Furthermore, that young and aged skin will respond differently to the same level of UVR exposure.

1.6.1 Aims

The first aim of this project is to determine whether DNMTs and TETs are expressed in the skin, and the compartments in which they are found (Chapter 3: Characterisation of DNA methylation machinery). This may give an indication of whether changes in DNAm patterns are an active process, or simply an erosion that occurs over time.

The second aim is to identify a time and dose-regimen of UVR that can be delivered in an in-vivo human study to elicit changes in DNAm and gene expression (section 4.3 Pilot Study: investigating UVR dose and time regimens in young skin). This will be in the form of a small pilot study, recruiting five young (≤30 years of age) and healthy individuals and exposing the buttock to incremental doses of UVR (40% and 80% of MED) for different numbers of days (5 and 10 days).

The third aim is to extend the observations made in the pilot study to a larger cohort study, expanding the number of young volunteers and recruiting to an additional aged group (≥65 years of age; section 4.4 Follow-up Study: investigating UVR challenge in young and aged skin). This will enable identification of a differential DNAm and gene expression response to UVR challenge that occurs as a function of age.

The final aim is to identify whether DNAm changes that occur with increasing age in the skin are implicated in any differential response to UVR challenge that occurs as a function of age (Chapter 5: The interaction of the ageing DNA methylome and UV radiation challenge).

Chapter 2: Materials and Methods

2.1 Human volunteer studies

2.1.1 Research ethics

All studies were conducted in accordance with the Declaration of Helsinki 1964 (revised Fortaleza, 2013). Ethical approval was granted by the University of Manchester Research Ethics Committee (reference: 16112; see appendix 1). Study participants were identified through poster advertisements and using a volunteer database held at the Dermatopharmcaology Unit (DPU) at Salford Royal NHS Foundation Trust. All volunteers were assessed against inclusion and exclusion criteria (see Appendix 1D; study protocol) and gave written informed consent prior to taking part in these studies.

2.1.2 Pilot study design

Five volunteers were recruited with Fitzpatrick skin phototype II-III between the ages of 18 and 30. The MED of each participant was determined (section 2.1.4.2) before undergoing a 5 and 10 day course of UVR of four 6 mm areas of the buttock at doses 40% and 80% of MED. UVR was applied daily (excluding weekends), such that the 10 day regimen began on a Tuesday, with the 5-day regimen beginning the following Tuesday (see appendix 1D for detailed study timetable). Following a recovery period of 24 (±2) hours, the four sites, together with an unirradiated control site, were biopsied (section 2.1.4.3). Samples were quadrisected and, for molecular analysis, epidermis and dermis were enzymatically separated (section 2.1.4.4), and only epidermis was used. RNA extraction was performed for Lexogen Quantseq 3' mRNA sequencing (section 2.3); DNA extraction for analysis of DNAm using the Infinium EPIC array (section 2.4) and histological analyses (section 2.5).

2.1.3 Follow-up study design

Volunteers with fitzpatrick skin phototype II to III were recruited within two age ranges: 18 to 30 years and ≥65 years (subsequently referred to as "young" and "aged,"

respectively). The MED was determined for each participant (section 2.1.4.2). Next commenced a 5-day course of UVR using 80% of MED applied to the buttock. A two-day break occurred over the weekend, between doses 4 and 5 of UVR. Following a recovery period of 24-hours, the irradiated site was biopsied together with an adjacent unirradiated control (section 2.1.4.3). Each biopsy was quadrisected, giving sufficient material for RNA extraction for Lexogen Quantseq 3' mRNA sequencing (section 2.3); DNA extraction for analysis of DNAm using the Illumina Infinium EPIC array (section 2.4) and histological analyses (section 2.5). For molecular analysis, epidermis and dermis were enzymatically separated (section 2.1.4.4) and only epidermis was used. This workflow is shown diagrammatically in Figure 2.1.

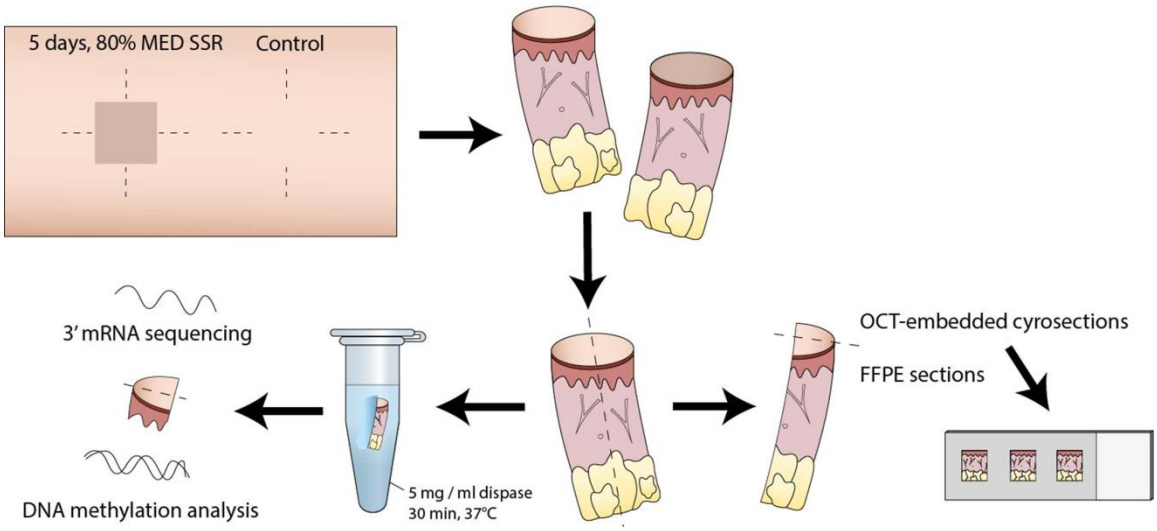

Figure 2.1: Study design and experimental workflow of the follow-up study.

Eighty percent MED was applied daily for 5 days (excluding weekends) to buttock of aged and young individuals. Twenty-four hours later, the irradiated site was biopsied together with an adjacent unirradiated control. Each biopsy was further dissected to allow epigenetic, transcriptomic and histological features of skin response to UVR to be investigated. One quarter of each biopsy was embedded in optimal cutting temperature (OCT) compound for cryostat sectioning and one quarter was formalin-fixed and paraffin-embedded (FFPE) for microtome sectioning. For molecular analysis, epidermis and dermis were enzymatically separated using 5 mg ml^{-1} dispase solution for 30 minutes at 37°C. The epidermis was further bisected, giving sufficient tissue for DNAm analysis and 3' mRNA sequencing.

2.1.4 Clinical procedures

2.1.4.1 *In vivo* UV radiation exposure

UV radiation was delivered by a Multiport® Solar Simulator (Solar Light; PA, USA) model number 601. The solar simulator and its related equipment are shown in Figure 2.2. For this work, the combined UVA+B mode was used (Figure 2.3); the output closely simulates the UV spectrum of the sun. The output is directed through six 8 mm square ports, the irradiance of which can be controlled independently. A data-logging radiometer with a biologically weighted erythema UVR sensor was used to measure spectral irradiance (μW cm^{-2}). Time of irradiation (in seconds) for a particular dose of UVR (mJ cm^{-2}) was calculated using equation (1).

(1)

$$Time\ (seconds) = \frac{Dose\ (mJ\ cm^{-2})}{Irradiance\ (\ mW\ cm^{-2})}$$

Prior to use, the system was allowed to warm for at least 10 minutes. A flexible articulation arm was used to guide placement of the solar simulator ports onto the buttock, and an adhesive safety pad maintained contact between the skin and solar simulator ports throughout.

Figure 2.2: Solar Light Multiport® Solar Simulator system.

The system consists of (A) a xenon arc lamp and (B) six liquid light guides, each 50 cm long, which direct light through six independently controlled 8 mm square ports. (C) A biologically-weighted erythema UVR sensor is (D) used to measure the spectral output of each port using (E) a connected radiometer.

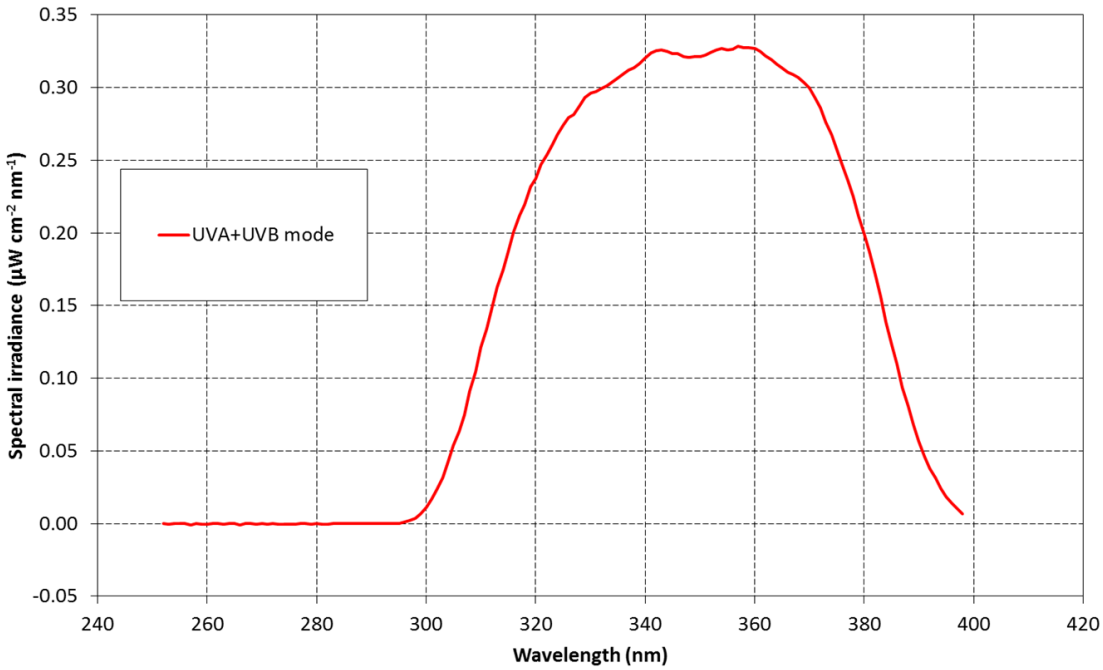

Figure 2.3: Spectral output of the Multiport® solar simulator in UVA+B mode.

Courtesy of Dr Donald Allen (Medical Physics; Salford Royal NHS Foundation Trust).

2.1.4.2 Minimal erythema dose testing

To establish the dose of UVR to administer, a small area of the lower back was irradiated using two applications of the full complement of the Multiport® Solar Simulator ports, delivering a 12-point dose series from 80 to 2 mJ cm^{-2}. The doses of UVR used have previously been shown to encompass the minimal erythema dose (MED; the minimum dose of UVR that results in just perceivable skin reddening) of individuals with Fitzpatrick skin phototype II to III (Barnadas et al., 2014). The skin was examined 24 (±2) hours post-exposure and subsequent exposures were always lower than the MED to avoid burning.

2.1.4.3 Full-thickness skin punch biopsy

Full-thickness skin biopsies were taken by trained nursing staff (Gill Aarons and Jean Bastrilles) at the DPU using a 6 mm punch under local anaesthetic (Figure 2.4). Where visible adipose tissue (hypodermis) was present, this was trimmed. Each biopsy was quadrisected and stored appropriately.

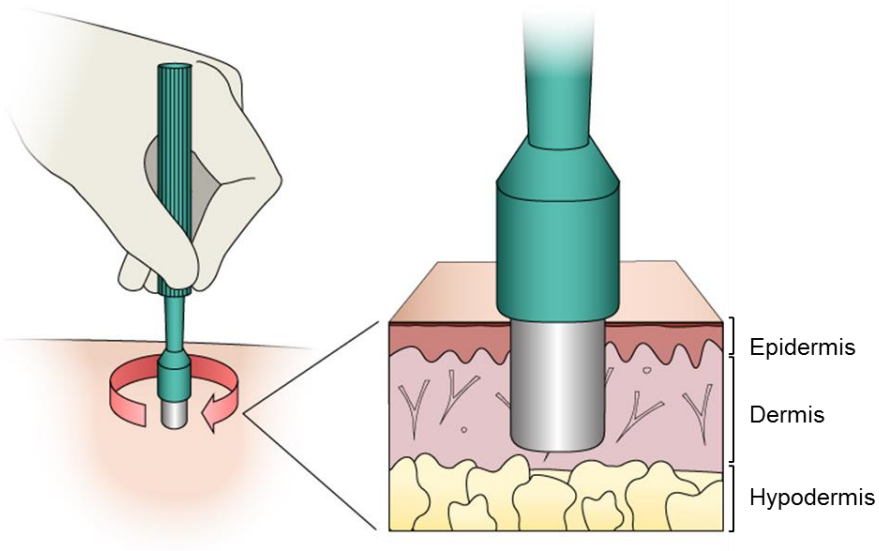

Figure 2.4: The skin layers sampled by full-thickness punch biopsy of the skin.
A punch biopsy is pressed firmly against the skin and rotated several times. Surgical scissors and tweezers are used to excise the biopsy. The punch samples both the epidermis and dermis, and in some individuals may sample the superficial layer of the hypodermis

2.1.4.4 Enzymatic separation of skin tissue layers

For molecular analyses, biopsies were subjected to epidermal-dermal separation using the enzyme dispase. Briefly, either freshly excised or snap frozen portions of each biopsy were washed in metallic-free phosphate buffered saline (PBS), and incubated in 5 mg ml^{-1} dispase II (Sigma-Aldrich; Missouri, USA) in metallic-free PBS at 37°C for up to 45 minutes. Fine forceps were used to peel apart the two layers of the skin, and the

epidermis and dermis were either processed immediately or stored appropriately for downstream applications.

2.2 Other tissue sources

Additional tissue specimens used in chapter 3 for histological analyses were acquired via The University of Manchester Skin Health Biobank (MSHB). This biobank has been approved by the North West 5 Research Committee (reference 09/H1010/10). In total, four different tissue specimens were utilised. These were from white Caucasian female donors, mean age 50.75 ± 8.65 years.

2.3 Lexogen Quantseq 3' mRNA sequencing

2.3.1 RNA extraction from skin biopsies

The pilot study utilised biopsies that had been snap-frozen following biopsy. These were incubated overnight in RNAlater ICE (Thermo Fisher Scientific; Massachusetts, USA) at -20 °C to stabilise RNA and inhibit RNases. Samples were then thawed to allow mechanical separation of the epidermis and dermis using fine forceps and scalpel. In the follow-up study, enzymatic epidermal separation was performed on freshly excised biopsies as described (section 2.1.4.4) and stored in RNAlater before extraction was performed using the RNeasy plus universal kit (Qiagen; Hilden, Germany).

The RNeasy plus universal kit uses QIAzol lysis reagent, which contains phenol and guanidine thiocyanate to facilitate RNA extraction from difficult to lyse tissues and inhibit RNases. Briefly, the RNAlater treated tissue was homogenised on ice in 900 µl QIAzol using an Ultra-Turrax T10 Basic homogeniser (IKA® Werke GmbH & Co. KG.; Staufen, Germany) fitted with a dispersing element (IKA® Werke GmbH & Co. KG) for three bursts of 45 seconds. Homogenates were incubated at room temperature for five minutes to promote dissociation of nucleoprotein complexes, before addition of 180 µl of chloroform. Then, centrifugation at 12,000 x g for 15 minutes at 4°C separated the aqueous and organic phases. RNA partitions to the upper aqueous phase, DNA to the interphase, and proteins to the lower, organic phase. RNA is

precipitated from the aqueous phase by addition of one volume of ethanol. Samples were then transferred to an RNeasy spin column and the bound RNA was washed as per kit instructions in order to remove any contaminating phenol. Elution was performed using 30 µl RNAse-free water, which was applied to the spin column twice to increase the concentration of the eluted RNA. Concentration was determined using a Qubit 4 Fluorometer (Thermo Fisher Scientific). RNA integrity was determined using an Agilent 2200 TapeStation (Agilent Technologies; California, USA). The RNA Integrity Number (RIN) values were all ≥8, indicative of high quality RNA. Samples were stored at −80°C until use.

2.3.2 Library preparation

The Quantseq 3′ mRNA-Seq Library Prep kit (Lexogen GmbH; Vienna, Austria) generates highly strand-specific sequencing libraries close to the 3′ end of polyadenylated RNA. As such, one fragment per transcript is generated, which results in accurate quantification of gene expression. It represents an efficient and cost-effective alternative to microarrays and conventional RNA-sequencing methodologies. A Quantseq 3′ mRNA-Sequencing library for each sample was generated in-house following manufacturer recommendations (pilot study; section 2.1.2), or by Lexogen GmbH (follow-up study; section 2.1.3). In brief, 25 ng RNA was reverse transcribed, initiated by oligo-dT priming. Second strand synthesis was then initiated by random priming, in a manner that DNA polymerase stops at the next hybridised random primer, so that only the fragment closest to the 3′ end is extended. Libraries were amplified for 18 cycles of polymerase chain reaction (PCR), at which point standard nucleotide barcodes were incorporated to allow multiplex sequencing. Next, libraries were size-selected using magnetic beads. Equimolar amounts of each library were then pooled.

2.3.3 Sequencing of Quantseq 3′ mRNA libraries

Libraries were denatured ahead of sequencing using standard Illumina (California, USA) protocols, except 2.2 pM of the denatured libraries were loaded as

recommended by Lexogen GmbH. Seventy-five bp single read sequencing was performed on the pooled library at Unilever R&D using the NextSeq500 system (Illumina). FastQ generation and quality control was performed using the BaseSpace Sequence Hub. For the pilot study, 581 million reads were generated. For the follow-up study, 163 million reads were generated. Data was uploaded to the Bluebee platform (Bluebee Holding B.V.; Rijswijk, the Netherlands), which performed merging of reads from multiple lanes, read trimming and alignment of the reads to the reference human genome (hg19) using STAR aligner (Dobin et al., 2013).

2.3.4 Data analysis using *limma*

The R package *limma* was used to determine differentially expressed genes (DEGs) (Ritchie et al., 2015). Read counts were filtered by expression levels, such that only genes that remained that had a raw read count ≥10 in any one sample, and ≥15 across all samples. In the pilot study, this reduced the starting read matrix from 60,204 ensembl IDs to 16,126 genes. In the follow-up study (which was a compilation of both studies), this reduced the read matrix from 60,199 to 15,865 IDs. The raw read counts were then normalised using the *limma voom* function. A linear model was fitted to the *voom*-normalised counts and empirical Bayes moderated t-statistics computed for each gene. The function *duplicateCorrelation* was used to estimate correlations due to donor, which allowed comparisons between aged and young skin to be made while accounting for donor differences. Samples from the pilot study and follow-up study were combined, while correcting for batch effects in the model matrix. The DEGs were determined as those with a p-adjusted value of ≤0.05 following correction for multiple testing using the Benjamini Hochberg false discovery rate (FDR) method (Benjamini & Hochberg, 1995).

The *limma* approach allows modelling of correlations that exist in the experimental framework (e.g. repeated measures), instead of merely a series of pair-wise comparisons that may miss these trends. Most importantly, the package allows analysis of both RNA-seq and microarray data with very similar pipelines, offering consistency for multiomic studies as performed in this thesis.

2.3.4.1 Testing sets of genes: genesettest and ROAST

Gene set tests lend statistical power to differential gene expression analyses, especially in relating expression patterns across different technologies (for example, integrating gene expression quantification and DNA methylation analyses). The *limma* functions genesettest and ROAST were utilised to test the differential expression of a group of genes as a unit.

The genesettest function is a mean rank gene set test, which tests the hypothesis that a test set of genes is more highly ranked by a user-defined test statistic (in this thesis, the computed t-statistics were used) than randomly permuted genes within the data set (Ritchie et al., 2015).

The ROAST function is a rotational gene set testing method specifically for linear models (Wu et al., 2010). Unlike other gene set test methods that randomly permute genes under the assumption of gene independence (including the *limma* function genesettest), ROAST instead rotates sample labels within the constraints of the linear model.

2.3.4.2 Gene pathway analyses

Further to determination of DEGs, the g:Profiler web server was used to perform functional enrichment analysis (Raudvere et al., 2019). This platform uses a hypergeometric test to measure the significance of a functional term in an input gene list. The data sources used in this thesis were KEGG (Kanehisa et al., 2019), regulatory motif matches from TRANSFAC (Matys, 2006) and GO biological process (Ashburner et al., 2000).

2.3.5 Reanalysis of Choi et al. (2010)

A dataset generated by Choi et al. (2010) using Agilent whole human genome oligo microarrays examined the different transcriptional response of the skin of six individuals to a daily, two-week regimen of UVA, UVB or solar-simulating radiation (SSR; 95% UVA and 5% UVB). Microarray data was downloaded from Gene Expression

Omnibus (GEO; accession number: GSE21429) and subjected to DEG analysis using *Limma* as described previously (section 2.3.4). A list of DEGs was generated for samples exposed to SSR versus their respective unirradiated controls, for comparison to datasets generated as part of this thesis.

2.4 DNA methylation analysis

2.4.1 DNA extraction

A portion of each biopsy was snap frozen in liquid nitrogen for DNA extraction. Biopsies were thawed on ice before epidermis and dermis were separated as described previously (section 2.1.4.4). Extraction of DNA was then performed for the epidermal layer using the DNeasy blood & tissue kit (Qiagen). Briefly, tissues were incubated with proteinase k in buffer ATL at 56°C for 16 hours. Buffer AL and ethanol were added to the samples, which were transferred to spin columns for wash steps and final elution in 100 µl of buffer AE. The eluted DNA was quantified using a Qubit flourometer and visualised by ethidium agarose gel electrophoresis to confirm the quality of the extracted DNA. All samples appeared as tight bands with light smearing, indicative of high quality DNA free of impurities and RNA contamination (Figure 2.5).

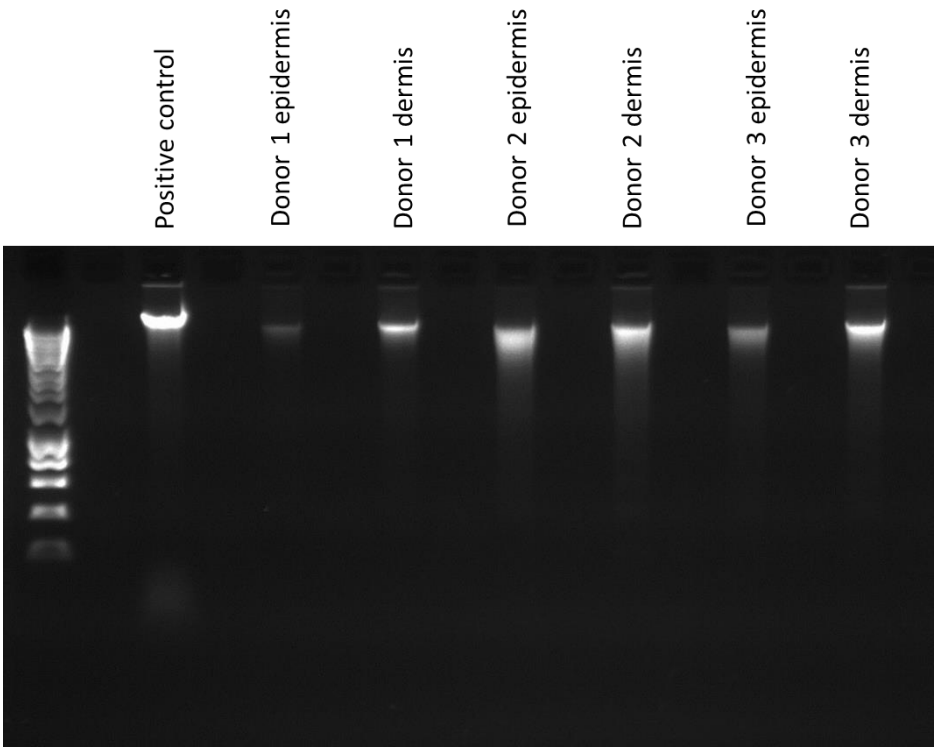

Figure 2.5: Quality assessment of extracted DNA using ethidium agarose gel electrophoresis.

Representative image showing DNA extracted from epidermis and dermis of 3 biopsies, showing tight bands with light smearing. Lack of low molecular weight bands suggested samples were free of impurities and RNA contamination.

2.4.2 Infinium MethylationEPIC BeadChip array

Extracted DNA was sent to NXT-Dx (Ghent, Belgium) for DNAm analysis using the Infinium MethylationEPIC BeadChip (Illumina). Samples were randomised across the different arrays, such that donors were kept on the same chip and no more than two of any one condition was run on the same chip. The array utilises bisulphite conversion with direct, array-based capture and scoring of more than 850,000 query sites across the genome. Treatment of DNA with bisulphite is a commonly employed technique that facilitates DNAm analyses. Under acidic conditions, bisulphite ions ($HSO3^-$) deaminate unmethylated C to uracil (U), while 5mC and 5hmC exhibit low reactivity and remain unchanged. Bisulphite-treated DNA is subjected to whole-genome

amplification that uniformly increases the amount of DNA in the absence of significant amplification bias where U (unmethylated cytosine) is replaced with T.

The chip comprises arrays of two different types: the first (type I), contain two probes corresponding to the 'methylated' or 'unmethylated' state of each query DNAm site (Figure 2.6A). The 3' terminus of each probe is complementary to either C (methylated state) or T (unmethylated state). Type I assays rely on the assumption that DNAm is regionally correlated within the 50 bp span of the probe. The Infinium type II assays comprise only one probe for each DNAm site (Figure 2.6B). In this instance, the 3' terminus of the probe is complementary to the base directly upstream of the query DNAm site. The captured DNA undergoes single-base extension that results in the addition of a labelled G or A base, complementary to either C (methylated state) or T (unmethylated state) that is then measured using a laser to excite the fluorophore of the single-base extension product. This feature enables DNAm status to be assessed independently of neighbouring DNAm sites, unlike Infinium I assays.

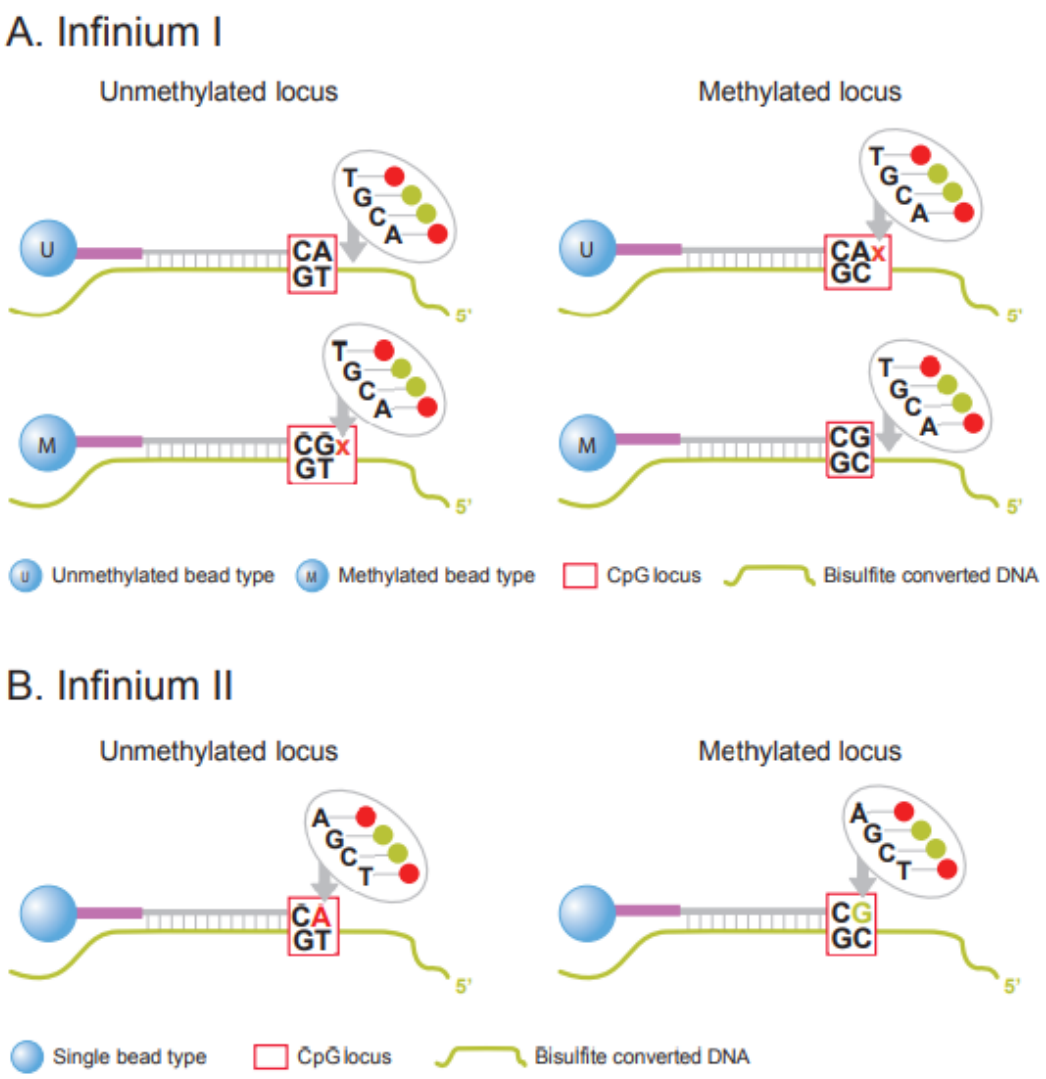

Figure 2.6: Infinium type I and II assay designs.

Both assay types distinguish methylated and unmethylated DNAm sites by selective deamination of unmethylated cytosine (C) to uracil, which is subsequently replaced with thymine (T) during the process of whole-genome amplification. (A) Type I assays comprise a probe for both the methylated and unmethylated version of each query DNAm site. (B) Type II assays comprise only one type of probe that undergoes single base extension with a fluorescently-tagged base when bisulphite-treated DNA binds. Either adenine (A; unmethylated locus) or guanine (G; methylated locus) is added. Figure taken from Illumina (2015).

2.4.2.1 Determining beta-values

The *Chip Analysis Methylation Pipeline* (ChAMP) (Tian et al., 2017) and *minfi* (Aryee et al., 2014) packages were implemented in R, using the raw IDAT files supplied by NXT-Dx. The starting 865, 918 probes were filtered to 741,402 probes using the following criteria:

- Probes with detection p-value < 0.01 (removed 3,403 probes);
- Probes with <3 beads in at least 5% of samples (removed 4,272 probes);
- non-CpG probes (removed 2,984 probes);
- SNP-associated probes (removed 97,127 probes);
- multi-hit probes (removed 11 probes);
- X and Y chromosome probe sets (removed 16,719 probes).

Specifically, SNP-associated probes are automatically removed from the data matrix by the ChAMP filter toolset, based on a list generated specifically for 450K and EPIC arrays (Zhou et al., 2017).

Signal intensities are used to generate beta-values (β), a measure of the DNAm level of each queried site on the chip using the equation (2) where *yi,methylated* and *yi,unmethylated* are the intensities measured by the methylated and unmethylated probes, respectively. The constant offset, α, is applied to the denominator to regularise β when the signal intensity of both methylated and unmethylated probes is low. β are between zero and one, where a value of zero indicates that all copies of that DNAm site in the sample were unmethylated, whereas a value of one indicates that all copies of the site were methylated.

(2)

$$\text{-}Beta_i = \frac{\max(y_i, methylated)}{\max(y_i, unmethylated) + \max(y_i, methylated) + \alpha}$$

2.4.2.2 Adjustment for type II probe bias and batch effects

The presence of both type I and type II probes on the array, which are characterised by altered β distributions and dynamic range, introduces statistical bias. A beta-mixture quantile (BMIQ) normalisation method was implemented to adjust β of type II design probes into a statistical distribution similar to type I probes (Teschendorff et al., 2013a) (Figure 2.7).

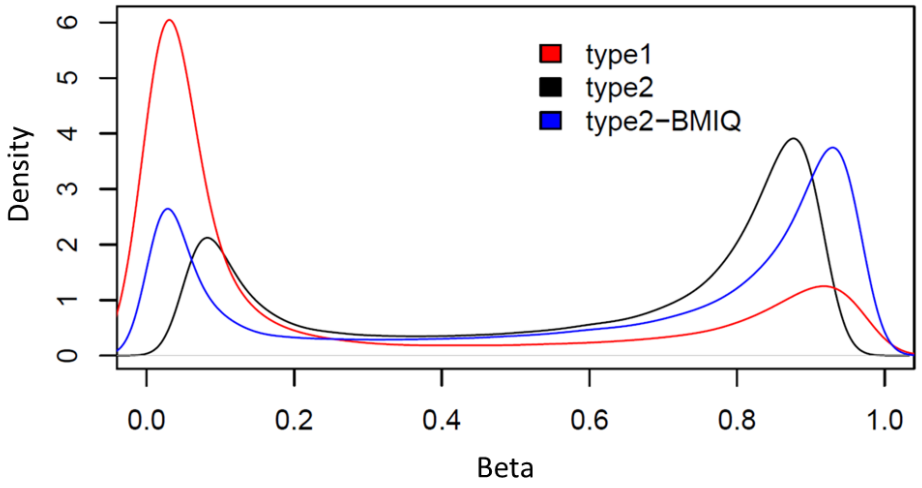

Figure 2.7: Density of type I and type II design probes as measured by Infinium MethylationEPIC BeadChip array before and after BMIQ normalisation.
Representative density plot from one sample showing redistribution of the beta value type II probes following normalisation using beta-mixture quantile (BMIQ) method. Red: type I; black, unnormalised type II; blue: normalised type II.

Following normalisation, singular value decomposition was performed to assess the effect of chip-to-chip variation. As significant differences were present, the *ComBat* package in R was used to correct for these effects, without removing biologically-relevant differences between sample groups (Johnson et al., 2007) (Figure 2.8).

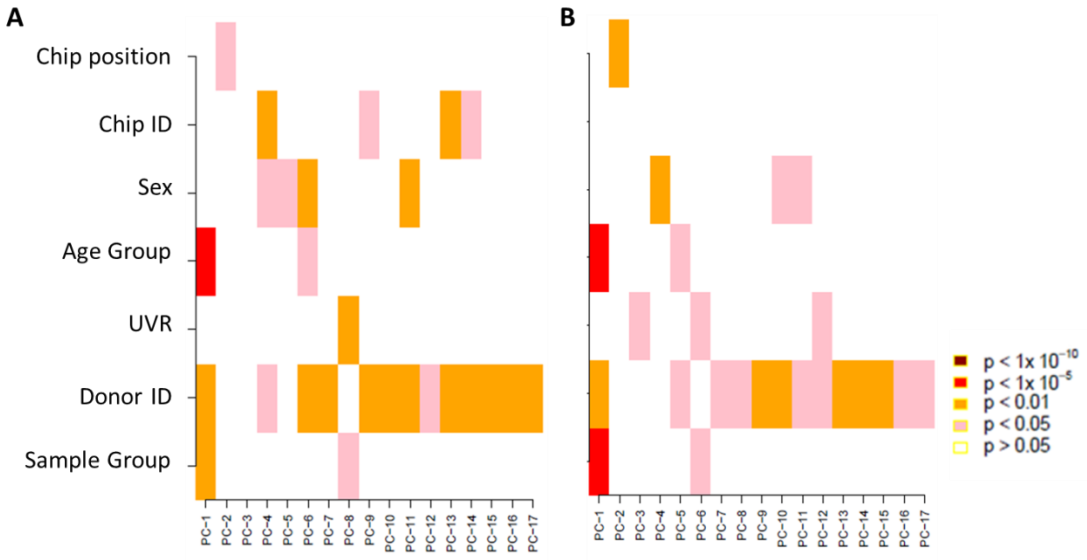

Figure 2.8: Singular value decomposition analysis identified significant batch effect between chip IDs.

(A) Singular value decomposition (SVD) identified chip-to-chip differences as a significant source of variation within the dataset. (B) SVD performed following *ComBat* showed no significant differences due to chip ID without removing biological differences due to age, sex and UV radiation (UVR) exposure. Abbreviations: PC, principal component. Dark red, $p < 1x10^{-10}$; red, $p < 1x10^{-5}$; orange, $p < 0.01$; pink, $p < 0.05$; white, $p > 0.05$.

2.4.2.3 M-value transformation

β were recalculated as m-values, as shown in the equation (3) (Du et al., 2010). The transformation mitigates some of the statistical problems of the β-value (namely, limited value range and strongly bimodal distribution). As such, M-values were used for subsequent statistical analyses, and realigned with β to aid biological interpretability (i.e. 0, unmethylated; 1, methylated) (Bock, 2012).

(3)

$$M_i = log_2\left(\frac{\max(y_{i,}methylated) + \alpha}{\max(y_i, unmethylated) + \alpha}\right)$$

2.4.2.4 Identification of differentially methylated probes

A linear model was fitted to the M-value data matrix using *limma,* as described previously (section 2.3.4). Significant DMPs were identified as those with p-adjusted ≤0.05 following correction for multiple testing using the Benjamini Hochberg FDR method and a change in β (Δβ) of ≥5%.

2.4.2.5 Identification of differentially methylated regions

The *DMRcate* package was used to identify differentially methylated regions (DMRs) between phenotypes (Peters et al., 2015). *DMRcate* uses the square of the moderated t statistic for each CpG site as determined by *limma* and smoothes this metric over a defined bandwidth using a Gaussian kernel to identify regions where multiple DNAm sites are undergoing a coordinated change in DNAm. The standard bandwidth (λ) of 1,000 bp was used as per author recommendations (Peters et al., 2015).

2.4.2.6 Reanalysis of Vandiver et al. (2015) dataset

Vandiver et al. (2015) generated epigenome-wide DNAm profiles of epidermis from the chronically photoexposed forearm and more photoprotected upper inner arm of young and aged volunteers using Infinium 450K arrays. Briefly, β were downloaded from GEO (accession number: GSE52980) and pre-processed as described previously (section 2.4.2). *Limma* was used as described previously to generate DMPs changing between the two age groups (intrinsic ageing DMPs) and between all photoprotected and photoexposed samples (Photoexposure DMPs). These lists were compared to datasets generated as part of this thesis.

2.5 Histological analyses

2.5.1 Tissue preparation

Following biopsy, or acquisition from the MSHB, tissue was fixed by immersion in 10% neutral buffered formalin (Sigma-Aldrich) for 24 hours. Samples were briefly washed in PBS and transferred into 70% ethanol, until processing overnight in a Citadel 2000 (Thermo Fisher Scientific). Samples were paraffin-embedded using plastic histology cassettes at a HistoCentre 2 embedding station (Thermo Fisher Scientific). Formalin-fixed paraffin-embedded (FFPE) tissue blocks were then mounted onto a HM 330 microtome (Microm; Bicester, UK) and cut into 6 µm sections. Sections were collected on Superfrost® Plus microscope slides (Thermo Fisher Scientific) and baked overnight at 37°C to ensure sections had adhered to the slides. Slides were then stored at room temperature until use.

Prior to staining, slides were heated to 65°C for 30 minutes to melt paraffin. Sections were then cleared in two changes of xylene for 10 minutes each, and rehydrated through graded alcohol series of two changes of 100% industrial methylated spirit (IMS), and one change of 90% and 70% IMS for two minutes each. Slides were then rinsed briefly in ddH_2O before use in the histological analyses outlined in the following sections.

2.5.2 Histochemical techniques

2.5.2.1 Warthin-Starry detection of melanin

A recent comparison of histological methods to detect melanin found the Warthin-Starry (WS) stain outperforms the commonplace Fontana-Masson stain in both sensitivity and specificity when compared with electron microscopy methods (Joly-Tonetti et al., 2016). The WS procedure was performed with low pH modification (Warkel et al., 1980). Tissue sections were de-paraffinised and rehydrated as described previously (section 2.5.1). Developing solution was prepared immediately before use comprising silver nitrate, 0.4%; gelatine, 2.6%; and hydroquinone, 0.04% (all Sigma-Aldrich). Slides were incubated with developing solution, and the argyrophil reaction

was allowed to occur for 90 seconds at 54°C before quenching with hot running tap water. Slides were dehydrated in graded alcohol series (70%, 90% and two changes of 100% IMS for two minutes each), cleared in xylene (two changes for 10 minutes each) and mounted using DPX slide mounting medium (Sigma-Aldrich). Quantification of the WS stain concerned the epidermal percentage occupied by melanin pigment (Figure 2.9) as described by Joly-Tonetti et al. (2016).

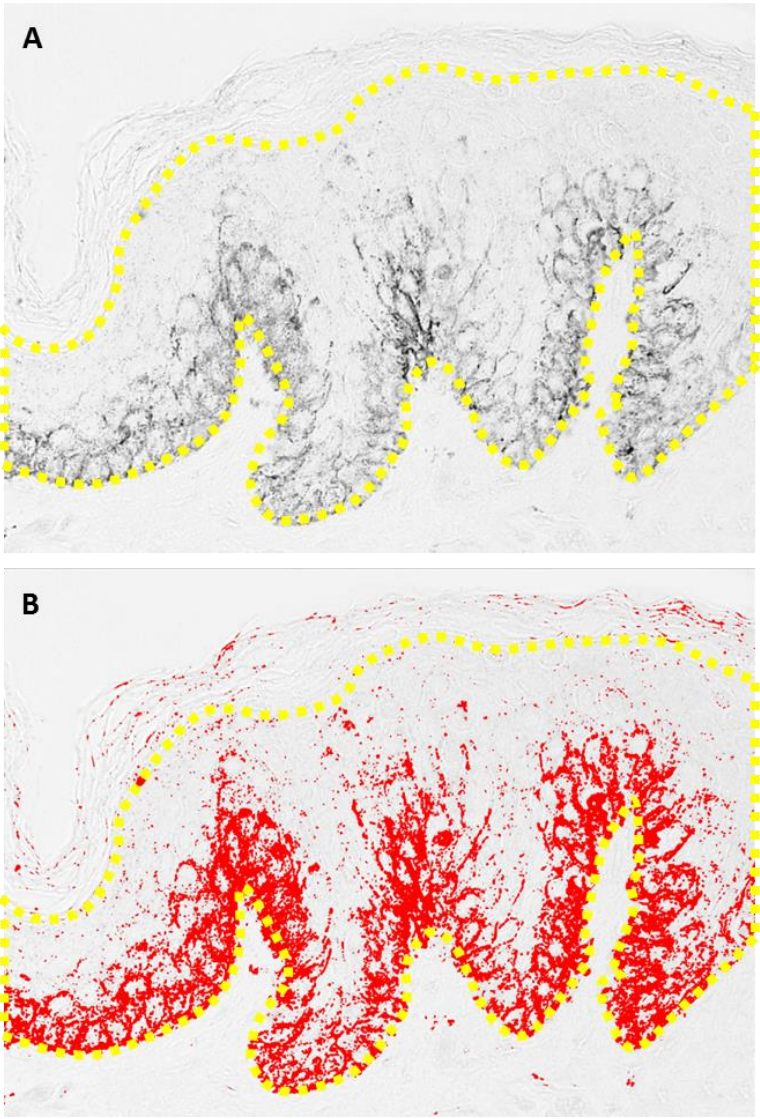

Figure 2.9: Image quantification of the Warthin-Starry histochemical stain.

(A) Images were opened in ImageJ and converted to greyscale. The epidermis was highlighted using the free-hand selection tool as indicated by the dashed yellow line (excluding *stratum corneum* and dermal regions). (B) The images were thresholded (red) and percentage of the red area of the total epidermal area was calculated.

2.5.3 Immunological staining techniques

Immunohistochemistry (IHC) is a powerful research tool used to localise specific antigens *in situ* based on antigen-antibody interactions. Immune-reactive products are visualised using a secondary antibody targeted to the first, typically labelled with either a fluorescent dye (such as fluorescein isothiocyanate [FITC], Texas Red or cy5) or an enzyme that produces a chromogenic product from its substrate (such as peroxidase, alkaline phosphatase or glucose oxidase). The different techniques offer different advantages: chromogenic detection can in general be more sensitive, and produces a photostable coloured precipitate that enables archiving of slides for many years. Fluorescence-based approaches can produce much higher resolution images suitable for subcellular protein localisation, and are generally considered easier to quantify due to the capacity to split different fluorescence signals. Both techniques are used in this thesis. The primary and secondary antibodies used and their experimental conditions are detailed in Table 2.1

The secondary antibodies and kits used were the ImmPRESS™ kit, the ABC kit, and a horse anti-mouse biotinylated secondary antibody coupled with a streptavidin-conjugated Texas Red fluorophore (all Vector Laboratories). The latter two protocols utilise avidin, a basic glycoprotein which has a high affinity for the small water-soluble vitamin, biotin. Biotin can be conjugated to a number of different biological molecules, including antibodies and proteins, which allow formation of large macromolecule complexes where the detected signal is amplified.

Table 2.1: Conditions used for immunofluorescence and immunohistochemistry in tissue.

Antibody	Company code	Dilution	Epitode retrieval	Wash buffer	Peroxide block	Permeabilisation	DNA Denaturation	Secondary antibody	Blocking
Anti-DNMT1	Abcam ab13537	1:25	Citrate buffer	TBS-T	-	1% Triton X-100 (10 minutes)	-	Horse anti-mouse biotinylated Streptavidin Texas red	10% NHS
Anti-DNMT3A	Abcam ab13888	1:50	Citrate buffer	TBS-T	0.6% H2O2 in methanol	Triton X-100 (10 minutes)	-	ABC kit	10% NHS + 3% BSA
Anti-DNMT3B	Abcam ab13604	1:100	Citrate buffer	TBS-T	-	Triton X-100 (10 minutes)	-	Biotin-streptavidin texas red	10% NHS + 3% BSA
Anti-TET1	GeneTex GT1462	1:50	Citrate buffer	TBS-T	-	Triton X-100 (10 minutes)	-	Horse anti-mouse biotinylated Streptavidin Texas red	2.5% NHS
Anti-8-OHdG	JaICA N45.1	1:200	Citrate buffer	TBS	0.6% H2O2 in methanol	-	70mM NaOH in 70% ethanol (3 minutes)	ImmPRESS anti-mouse	2.5% NHS
Anti-CPD	Cosmo Bio CAC-NM-DND-001	1:2,000	Trypsin	TBS	-	-	70mM NaOH in 70% ethanol (4 minutes)	ImmPRESS anti-mouse	2.5% NHS

Abbreviations: DNMT, DNA methyltransferase; TET, ten-eleven translocation; 8-OHdG, 8-hydroxy-2' –deoxyguanosine; cpd, cyclobutane pyrimidine dimer; NHS, normal horse serum; NHS, normal hose serum; NaOH, sodium hydroxide.

2.5.3.1 DNMT and TET Immunofluorescence and immunohistochemistry

Sections were de-paraffinised as described previously and treated as per the conditions outlined in Table 2.1. All incubations were performed at room temperature, unless otherwise stated. Briefly, heat-induced epitope retrieval (HIER) was performed using boiling citrate buffer (10 mM citric acid [pH 6.0] and 0.1% TWEEN® 20 [both Sigma-Aldrich]) for 20 minutes. Sections were cooled for approximately 20 minutes before permeabilisation using Triton™ X-100 (Sigma-Aldrich) in Tris-buffered saline (TBS) for 10 minutes. Non-specific binding was inhibited by incubation for one hour with appropriate blocking agent (normal horse serum [NHS; Vector Laboratories; California, USA] with or without bovine serum albumin [BSA; Sigma-Aldrich] diluted in TBS). Blocked sections were incubated with primary antibodies in antibody diluent (Agilent), overnight at 4°C. The following day, sections were incubated with 10 μg ml^{-1} of a horse anti-mouse biotinylated antibody (Vector Laboratories, CA, USA) for 30 minutes in TBS. A Texas Red® Streptavidin conjugate (Vector Laboratories) was applied to each section at a concentration of 5 μg ml^{-1} in TBS for one hour. Nuclei were counterstained for two minutes with 0.5 μg ml^{-1} of the fluorescent DNA stain 4',6-diamidino-2-phenylindole (DAPI; Thermo Fisher Scientific). All wash steps were performed in three changes of TBS with 0.05% TWEEN® 20 for 5 minutes each, with a final wash in distilled water. Sections were left to air dry in the dark before mounting with Prolong® Gold antifade mountant (Thermo Fisher Scientific). Slides were stored at 4°C until images were acquired, within one week of staining.

Chromogenic imunohistochemistry was performed for DNMT3a. Briefly, sections were treated as for immunofluorescence with the addition of a peroxidase blocking step, consisting of 0.6% H_2O_2 in methanol (both Sigma-Aldrich) for 30 minutes. Following overnight incubation with primary antibody, the ABC Kit was instead used (Vector Laboratories). The ABC reagent was applied for 30 minutes. Then, Immunoreactivity was visualised using SG® chromogen (Vector Laboratories) followed by counterstaining in nuclear fast red (Vector Laboratories) and rinsing in tap water. Sections were dehydrated, cleared and mounted as described for other histochemical stains (section 2.5.2.1).

Immunofluorescence of DNMTs and TETs was comparable to that obtained in FFPE human testis tissue sections (AMSBIO; Abingdon, UK). The testes are an ideal positive control tissue due to an abundance of literature regarding DNMT and TET expression in this tissue (Xu et al., 2015; Ni et al., 2016) and is recommended by the antibody supplier (Abcam; Cambridge, UK).

2.5.3.1.1 Antibody specificity

All primary antibodies used in this thesis were extensively reviewed and have previously been validated for western blot, immunoprecipitation, immunohistochemistry, flow cytometry and chromatin immunoprecipitation. Specifically, the manufacturer-supplied data sheet indicates that in western blot of whole cell lysate from HCT116 cells, the anti-DNMT1 detects a single band of approximately ~180 kDa, corresponding to the molecular weight of DNMT1 protein. Detection of the band is reduced in cell lysates of the same cell line following DNMT1 knockout.

In a similar manner, western blot analysis reported by the manufacturer using the DNMT3A antibody used in this thesis of 293 cell lysate revealed strong immunolabelling of a 120 ~kDa band in DNMT3A-transfected cells, but not DNMT3B-transfected cells. This demonstrates the relative specificity of this antibody for DNMT3A over other, similar DNMTs. Furthermore, the provided example immunocytoflourescence images reveal intense nuclear staining and diffuse cytoplasmic staining, as observed in the staining in this thesis.

The DNMT3B antibody used in this work has been demonstrated to detect a ~97 kDa band by western blot analysis of HeLa and A549 cell lysate, corresponding to the expected molecular weight of DNMT3B whole-length protein. This antibody also detects several lower molecular weight bands, which may represent different isoforms.

Finally, the TET1 antibody was demonstrated by the manufacturer to detect a ~235 kDa band by western blot anaylsis in 293T cells. Knockdown of TET1 by siRNA in the same cell line demonstrated a reduction in the intensity of the detected band.

2.5.3.2 8-hydroxy-2'–deoxyguanosine (8-OHdG) immunohistochemistry

Tissue sections were treated as described previously, using the conditions outlined in Table 2.1. Following an overnight incubation with primary antibody at 4°C, the ImmPRESS™ kit was used. Sections were incubated for 30 minutes with ImmPRESS reagent, which contains micropolymers of horseradish peroxidase conjugated to an anti-mouse 2° antibody. Sections were then incubated with ImmPACT™ SG (Vector Laboratories), a horseradish peroxidase substrate, until staining had developed. Nuclei were counterstained with nuclear fast red; sections were dehydrated, cleared and mounted with DPX mountant as described previously. Immunopositive cells were counted manually on images that were blinded for UVR treatment and age group (Figure 2.10).

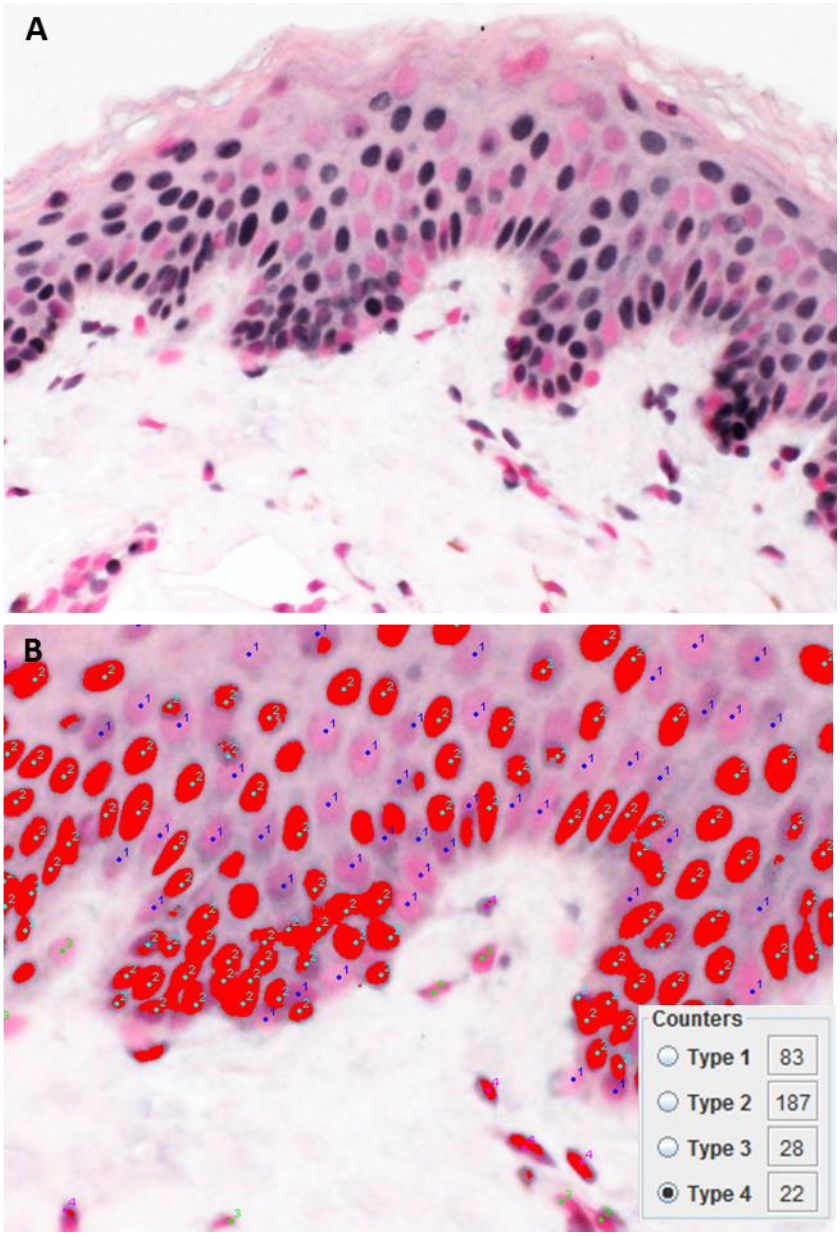

Figure 2.10: Image quantification of 8-hydroxy-2'–deoxyguanosine (8-OHdG) immunohistochemistry.

(A) Images were opened in ImageJ. (B) A threshold (red) was applied to highlight intense immunopositive cells to aid reproducible counting between images. (B, inset) The number of cells above threshold were counted and expressed as percentage of total number of cells, counted separately for the epidermal and dermal compartment. Representative image from a 23-year-old individual following 5 days of sub-erythemal UVR exposures.

2.5.3.3 Cyclobutane pyrimidine dimer (CPD) immunohistochemistry

Staining for CPDs was performed only to confirm their absence; a positive control was used in each staining run. This was a skin biopsy irradiated with 80 mj cm^{-2} (8x standard erythemal dose [SED]), known to produce a severe erythemal response and a high degree of CPD staining.

2.5.4 Microscopy

Images were captured using an Olympus BX53 upright microscope (Olympus; Tokyo, Japan) using a DP73 camera (Olympus) through the cellSens software package (Olympus). For chromogenic and histochemical techniques, images were captured under bright field microscopy. For immunofluorescence experiments, specific band pass filter sets for DAPI, FITC and Texas Red were used to prevent bleed through from one channel to the next using the same microscope. Images were then processed using ImageJ (http://rsb.info.nih.gov/ij).

2.6 Primary cell culture of normal human epidermal keratinocytes

NHEKs isolated from epidermis of juvenile foreskin were purchased from Promocell. Cells were maintained in 12 ml keratinocyte basal medium 2 (supplemented with 0.004 ml bovine pituitary extract, 0.125 ng epidermal growth factor 5 µg insulin, 0.33 µg hydrocortisone, 0.39 µg epinephrine, 10 µg transferrin and 0.06mM calcium chloride [$CaCl_2$] per ml of culture medium) in a 75 cm^2 vented cell culture flask (Corning Costar, Tewksbury, USA). Cells were kept in an incubator with a humidified atmosphere of 5% CO_2- 95% air at 37°C. Medium was replaced every second day, and cells were sub-cultured once 80-90% confluency was reached. Briefly, after removal of the medium the cells were washed with 10 ml PBS without Ca^{2+} and magnesium (Gibco, Paisley, UK). Cells were detached using the DetachKit (Promocell) using a 0.04% trypsin (v/v) and 0.03% ethylenediaminetetraacetic acid (EDTA; v/v) solution. A trypsin neutralising solution was applied and cells were collected in a centrifuge tube. Cells were centrifuged for three minutes at 220 g and the supernatant discarded. Cells were then

resuspended in growth medium and used to seed other culture vessels at a density of 5,000 cells per cm^2. For all experiments, cells of passages two to five were used.

2.6.1 Immunofluorescence of DNMTs and TETs in normal human epidermal keratinocytes

Cells were seeded onto Nunc® Lab-Tek® Chamber Slides™ (Sigma-Aldrich). Cells were grown for 48 hours before fixation by immersion in 4% paraformaldehyde (Sigma-Aldrich) for 10 minutes. Immunofluorescence for DNMTs and TETs was performed essentially as described previously (section 2.5.3.1), with minor adjustments. Cells were permeabilised using 0.1% Triton™ X-100 30 minutes. Non-specific staining was blocked using 5% NHS. DNMT1 (1:100), DNMT3A (1:200), DNMT3B (1:200) and TET1 (1:200) antibodies were applied overnight at 4°C. Then, the same protocol as described previously was followed utilising a horse anti-mouse biotinylated secondary antibody and streptavidin Texas Red flourophore (section 2.5.3.1).

2.6.2 Calcium differentiation of normal human epidermal keratinocytes

Cells were seeded on Thincert™ cell culture inserts with a pore size of 0.4 µm (Greiner Bio-one; Stonehouse, UK) in 12-well culture plates (Corning Costar). Growth medium was added to the plate and the insert. At 100% confluency, $CaCl_2$ was added to the growth medium (1.8 mM) or fresh medium without the addition of high Ca^{2+} was added. Seventy-two hours later, cells were collected using the DetachKit as described previously. Cell pellets were then stored at -80°C until use.

2.6.3 RNA extraction from cells

RNA extraction from cells was performed using the RNeasy Mini Kit (Qiagen). Cell pellets were lysed using the kit-supplied buffer RLT with the addition of β-mercaptoethanol (Sigma-Aldrich; 10 µl of 14.3 M β-mercaptoethanol per ml of buffer

RLT). The cell lysate was further homogenised by passing through a 20-gauge (0.9 mm) needle attached to a RNase-free syringe five times. One volume of 70% ethanol was added to the homogenized lysate, before transferring to a kit-supplied spin column. Both RNA extraction kits used in this thesis then follow the same protocol, as described previously (section 2.3.1)

2.6.4 Reverse transcription quantitative polymerase chain reaction

First strand complementary DNA (cDNA) synthesis was performed using the GoScript™ Reverse Transcription System (Promega; Wisconsin, USA) on a GeneAmp® PCR System 2700 (Applied Biosystems; California, USA). Reverse transcription quantitative polymerase chain reaction (RT-qPCR) was performed to assess mRNA expression using TaqMan® gene expression assays supplied by Applied Biosystems for DNMT1 (Hs00945875_m1), DNMT3a (Hs01027162_m1), DNMT3B (Hs00171876_m1), DNMT3L (Hs01081364_m1), TET1 (Hs00286756_m1), TET2 (Hs00325999_m1), TET3 (Hs00379125_m1) and peptidylprolyl isomerase A (PPIA; Hs99999904_m1) as the endogenous control. All PCR amplifications were performed in 96 well plates. Each reaction well contained a total volume of 20 µl consisting of: 10 µl of TaqMan® universal PCR master mix (Applied Biosystems), 1 µl 20 × TaqMan® gene expression assay, 4 µl RNase-free water and 5 µl cDNA template. Triplicates per sample on each plate were performed and non-cDNA controls included for each gene. Reactions were performed on a StepOnePlus™ Real-Time PCR System (Applied Biosystems). The qPCR cycle was as follows: 95°C for 1 second and 60°C for 20 seconds. Fold changes in gene expression, relative to a control sample and normalised against the endogenous control, were determined using the comparative CT method of quantification (Schmittgen & Livak, 2008).

2.7 Statistical analysis

Data displayed represents the average of 3 images per tissue section and 3 tissue sections per biopsy (a total of 9 images per donor and condition). The different stains

were analysed as detailed in the previous sections. Statistical analyses were performed using GraphPad Prism 7 software. Data presented here was analysed using an unpaired Student's T-test, a paired Student's T-test, a one-sample T-test or a one-way analysis of variance (ANOVA) followed by Tukey's post-test to determine if differences were significant. Significance values are indicated with, *$p < 0.05$, **$p < 0.01$, ***$p < 0.001$, ****$p< 0.0001$. All graphs show mean values and error bars show ± standard error of the mean (SEM).

Chapter 3: Characterisation of DNA methylation machinery

3.1 Introduction

DNA methyltransferases are a family of conserved DNA-modifying enzymes underpinning the most archetypal example of epigenetic programming, the methylation of DNA bases. The canonical DNMTs, which catalyse the transfer of a methyl group from SAM to the fifth carbon position of C, are DNMT1, DNMT3A and DNMT3B. There are three TET paralogues, TET1, TET2 and TET3, which antagonise the function of the DNMTs by catalysing the oxidation of the methyl group to promote the reversal of DNAm (Lyko, 2018). The expression of DNMT1 in skin has been shown in two studies with conflicting expression patterns. In the first, Sen *et al*. (2010) demonstrated DNMT1 immunereactivity was restricted to a small subset of mitotic basal keratinocytes, in-keeping with its role in DNAm maintenance post-replication. However, another study demonstrated DNMT1 expression throughout the epidermis (Yamada et al., 2019). Therefore, the specific expression pattern remains unresolved. Furthermore, to our knowledge, a comprehensive characterisation of the other DNMTs and TETs has not yet been performed in the skin.

In this study, the expression and localisation of the DNAm machinery in human skin specimens obtained from the MSHB (see section 2.2 for donor details) was assessed using commercially available antibodies towards the three canonical DNMT family members (DNMT1, DNMT3A and DNMT3B) and the TET family member TET1. Due to the aforementioned differences in the expression patterns of DNMT1 in the skin (Sen et al., 2010; Yamada et al., 2019), a widely characterised *in vitro* culture model of NHEK differentiation was utilised to confirm the observed expression patterns. Grown in basal keratinocyte medium, NHEKs exhibit properties of the basal layer of the epidermis. They retain the ability to divide, and show low levels of differentiation markers, such as involucrin (Tu et al., 1999). Upon switching into a high Ca^{2+} concentration medium ('Ca^{2+} switch'), NHEKs grow larger, exit the cell cycle and exhibit morphological changes that are consistent with their differentiation in the epidermis *in vivo* (Yuspa et al., 1989; Lee et al., 1998).

3.2 Objectives

The aim of this chapter is identify the expression patterns of DNMTs and TET family proteins in the skin. The specific objectives are as follows:

1) Optimise immunohistochemical and immunofluorescence methodologies to detect DNMTs and TETs in the skin using commercially available antibodies (section 2.5.3.1). This will utilise archival histological specimens obtained from the MSHB (*n*=4, section 2.2);
2) Recapitulate staining patterns observed in the *stratum basale* of the skin using NHEKs maintained in basal keratinocyte media (section 2.6.1);
3) Use NHEK *in-vitro* differentiation model (Ca^{2+} switch; section 2.6.2) to investigate DNMT and TET expression dynamics upon commitment of keratinocytes to terminally differentiate using RT-qPCR (section 2.6.4).

3.3 Results

3.3.1 DNMT1 expression is mainly confined to cells within the basal layer of the epidermis and diffuse cells in the dermis

Firstly, to resolve differences in the expression pattern of DNMT1 reported in the literature (Sen et al., 2010, Yamata et al., 2019), immunofluorescence analysis of DNMT1 was examined. This revealed immunoreactivity was chiefly identified within the basal layer of the epidermis, with some expression in the outer differentiated layers, but this was at a much lower level (Figure 3.1). High power visualisation demonstrated foci that overlaid with DAPI, indicating nuclear localisation and targeting of specific genetic loci. The number of foci was the densest in a subset of cells within the basal layer, while immunoreactivity elsewhere presented with only a moderate number of foci, suggestive of a reduced expression (Figure 3.1B). A number of cells in the basal layer had no immunoreactivity, suggesting that expression is not constitutive and there is differential regulation within this layer and the whole epidermis. DNMT1 was also observed in the dermis in spindle-like cells, suggestive of fibroblasts, as well as spherical cells, suggestive of an activated fibroblast phenotype, especially as these cells appeared to cluster together (Lo et al., 2015) (Figure 3.1C).

In the cell model, NHEKs maintained in basal medium showed a high number of DNMT1+ cells (Figure 3.1D), consistent with a cellular phenotype akin to the basal layer of the epidermis. The immunereactivity was again apparent as nuclear foci. Upon Ca^{2+} switch, the amount of DNMT1 mRNA was significantly decreased ($p \leq 0.01$, Figure 3.1E), which, recapitulates the expression of DNMT1 as observed in the differentiated layers of the epidermis of whole skin sections (Figure 3.1A).

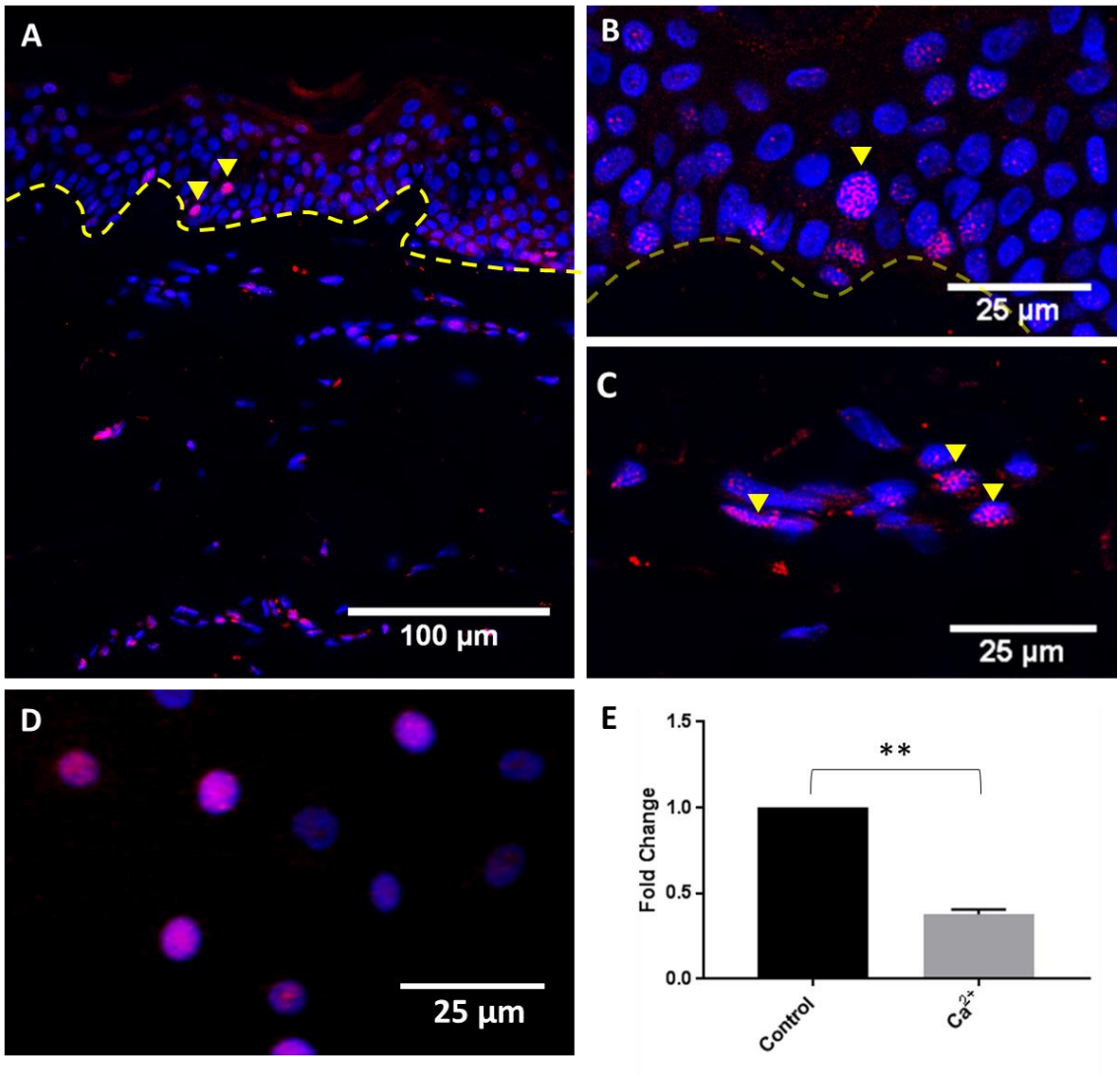

Figure 3.1: DNMT1 expression in human abdominal skin and NHEKs

Human abdominal skin sections were immunolabelled for DNMT1 (red) and counterstained with DAPI (blue). (A) Gross skin localisation is shown together with high power images of (B) epidermis and (C) dermis. Yellow arrows indicate examples of positively stained cells. Dashed line indicates the DEJ. Scale bars are indicated in each panel. Images are representative of *n*=4 individuals. (D) Normal human epidermal keratinocytes (NHEKs) were immunolabelled for DNMT1. (E) qRT-PCR for DNMT1 in NHEKs maintained for 72-hours post-confluency in basal medium (control) and with addition of 1.8 mM $CaCl_2$. Data is represented as mean ± SEM for *n*=3 NHEK donors. Fold change was calculated relative to control cells with samples normalised to PPIA. A one sample T-test was performed relative to 1, where ** $p \leq 0.01$.

3.3.2 DNMT3A shows differential expression across the epidermal layers

The DNMT3A antibody used was not amenable to use in fluorescence microscopy and therefore chromogenic immunohistochemistry was utilised. Here, DNMT3A expression was altered between the different epidermal layers (Figure 3.2). Within the basal layer of the epidermis, staining was localised mainly to the cytoplasm with small nuclear foci. Cytoplasmic immunoreactivity was not as prominent in the upper differentiated layers, showing reduced intensity. However, the upper layers of the epidermis retained focal nuclear immunoreactivity (Figure 3.2B).

The dermal compartment showed high background due to non-specific staining of the connective tissue, possibly due to using a chromogenic staining technique. Although darkly staining nuclei can be observed across the dermis (Figure 3.2C), the number of positive cells, and the subcellular localisation of DNMT3A, could not be adequately determined. Vascular structures demonstrated cytoplasmic staining in the outer cells of the vessel wall. By contrast, the inner cell layers of the blood vessel showed reduced cytoplasmic but strong nuclear staining, which was akin to the pattern observed in the stratification of the epidermis.

As observed with DNMT1 immunolabelling of NHEKs maintained in basal medium, DNMT3A expression demonstrated a staining pattern akin to the basal layer of the epidermis, characterised by diffuse immunoreactivity throughout the cytoplasm and bright focal points within the nucleus (Figure 3.2D). This again suggests that immunofluorescence techniques have captured the precise loci-specific targeting of these enzymes. Upon the addition of high concentration of Ca^{2+} to the medium, there is a trend suggestive of a decrease in DNMT3A mRNA (Figure 3.2E; $p = 0.10$).

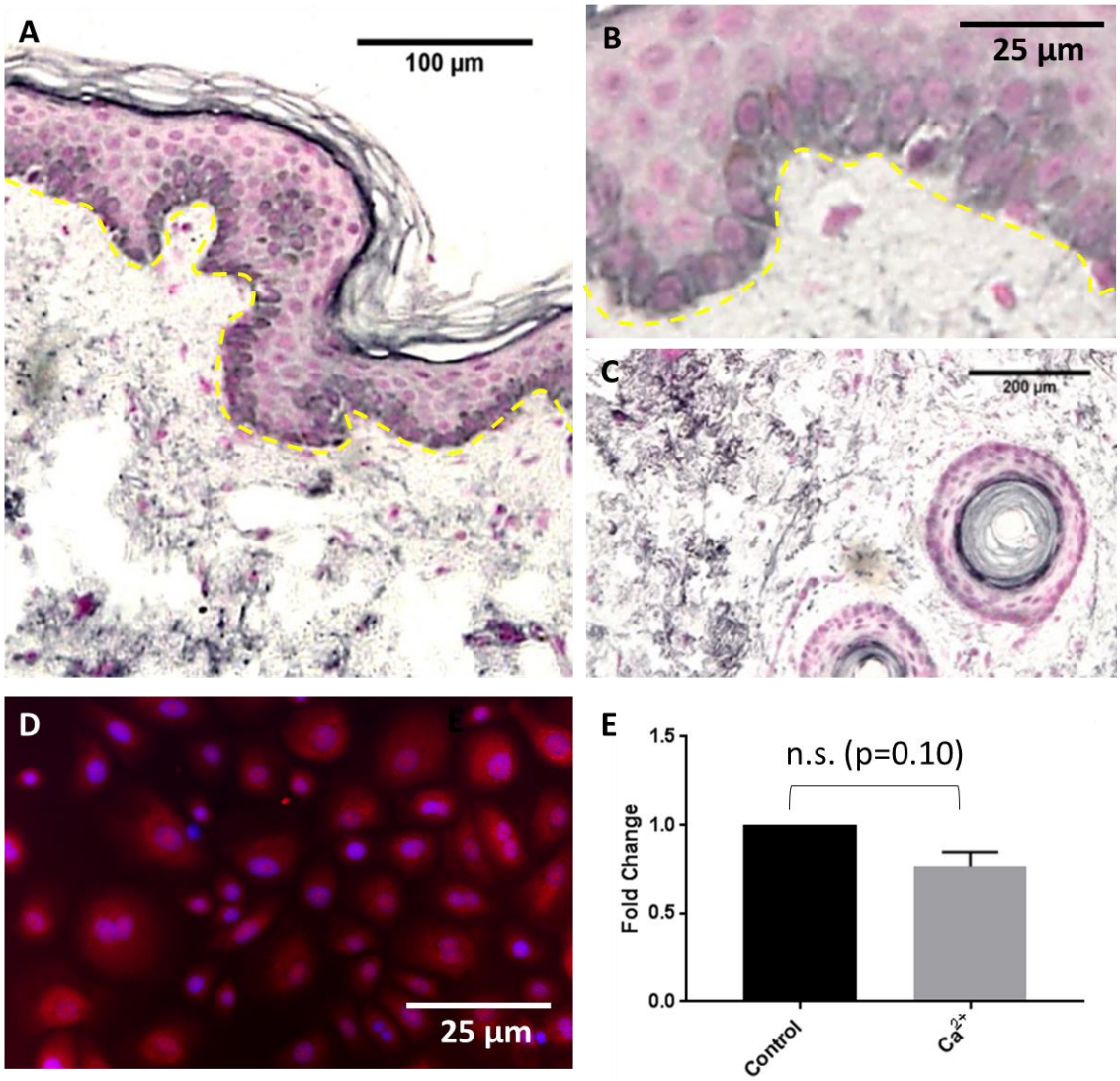

Figure 3.2 DNMT3A expression in human abdominal skin and NHEKs

Human abdominal skin sections were immunolabelled for DNMT3A (black) and counterstained with nuclear fast red (pink). (A) Gross skin localisation is shown together with high power images of (B) epidermal and (C) dermal positive cells. Dashed line indicates the DEJ. Scale bars are indicated in each panel. Images are representative of *n*=4 individuals. (D) NHEKs were maintained in basal medium and immunolabelled for DNMT3A (red) and counterstained with DAPI (blue). (E) qRT-PCR for DNMT3A in NHEKs maintained for 72-hours post-confluency in basal medium (control) and with addition of 1.8 mM $CaCl_2$. Data is represented as mean ± SEM for *n*=3 NHEK donors. Fold change was calculated relative to control cells with samples normalised to PPIA. A one sample T-test was performed relative to 1. Abbreviations: not significant, n.s.

3.3.3 DNMT3B is expressed ubiquitously across the epidermis

Analysis of DNMT3B expression demonstrated immunoreactivity across all layers of the epidermis, localised predominantly in the nucleus (Figure 3.3A). immunereactivity demonstrated small foci, as with previous DNMTs in the skin (Figure 3.3B). Non-specific staining of the *stratum corneum* was also seen that was not reduced upon increased blocking agent or time. Within the dermal compartment, sparse immunopositive cells were observed (Figure 3.3C). These appeared to contain a lesser number of nuclear foci than their epidermal counterparts.

The undifferentiated NHEKs grown in basal medium demonstrated a staining pattern that was, again, comparable to the basal layer of the epidermis (Figure 3.3D). The cells were a heterogeneous population, whereby some cells expressed extremely high levels of DNMT3B while others showed no expression. Upon induction to differentiate, the mRNA levels of DNMT3B were significantly reduced ($p \leq 0.05$; Figure 3.3D).

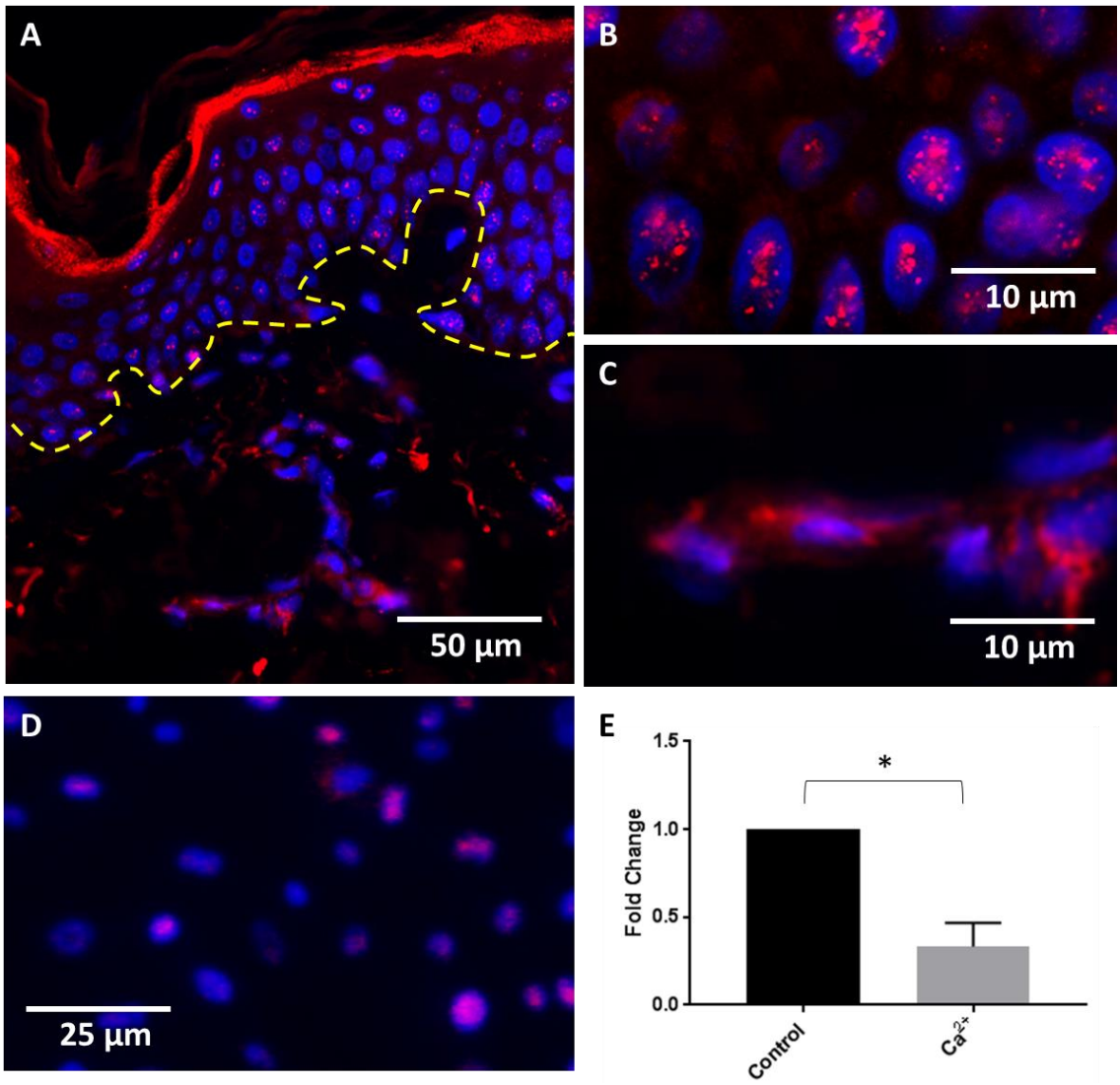

Figure 3.3: DNMT3B expression in human abdominal skin and NHEKs

Human abdominal skin sections were immunolabelled for DNMT3B (red) and counterstained with DAPI (blue). (A) Gross skin localisation is shown together with high power images of (B) epidermal (C) dermal positive cells. Dashed line indicates the DEJ. Scale bars are indicated in each panel. Images are representative of *n*=4 individuals (D) Normal human epidermal keratinocytes (NHEKs) were maintained in basal medium and immune-labelled as described. (E) qRT-PCR for DNMT3B in NHEKs maintained for 72-hours post-confluency in basal medium (control) and with addition of 1.8 mM $CaCl_2$. Data is represented as mean ± SEM for *n*=3 NHEK donors. Fold change was calculated relative to control cells with samples normalised to PPIA. A one sample T-test was performed relative to 1, *$p \leq 0.05$.

3.3.4 DNMT3L is not expressed by normal human epidermal keratinocytes

DNMT3L could not be detected by RT-qPCR in basal medium-maintained NHEKs or those induced to differentiate by addition of high Ca^{2+}, and therefore the presence of protein in the skin was not assessed as part of this work.

3.3.5 TET1 is expressed in the epidermis and sparsely throughout the dermis

Immunofluorescence to visualise TET1 demonstrated its presence in the nuclear compartment with ubiquitous expression across all layers of the epidermis (Figure 3.4A-B), and positive staining of cells in the dermis (Figure 3.4C). As with other epigenetic markers tested in this work, TET1 formed small foci, suggesting its recruitment to specific genomic loci. Immunofluorescence of NHEKs grown in basal medium revealed ubiquitous expression of TET1 in the nucleus. However, the amount of immunereactivity in each cell was variable (Figure 3.4D). The RT-qPCR analysis of TET1 mRNA in NHEKs switched to high Ca^{2+} showed that TET1 expression was not significantly altered upon differentiation, although there was a slight trend to a reduction (Figure 3.4E).

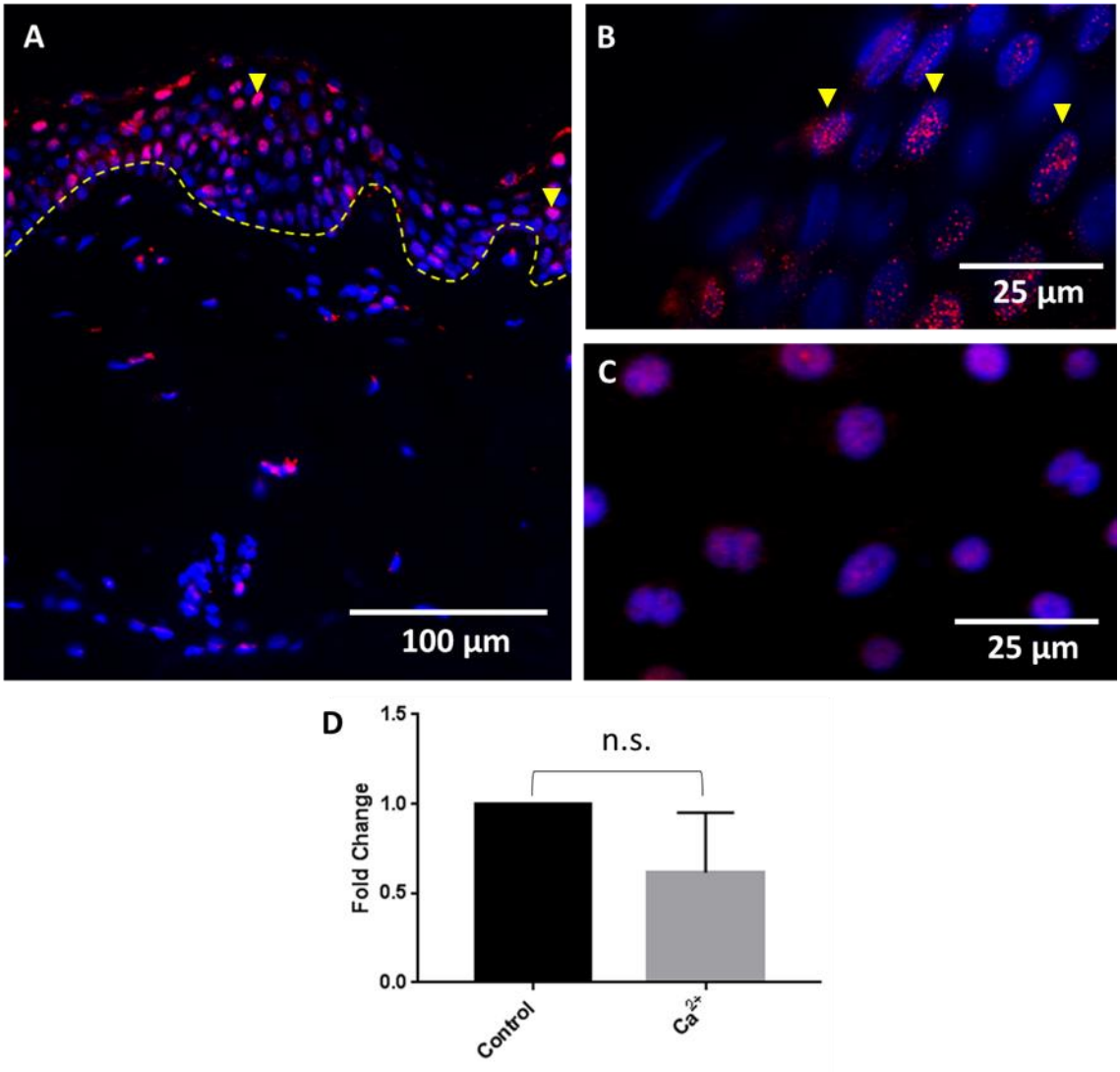

Figure 3.4: TET1 expression in human abdominal skin and NHEKs

Human abdominal skin sections were immunolabelled for TET1 (red) and counterstained with DAPI (blue). (A) Gross skin localisation is shown together with high power images of (B) epidermal positive cells. Yellow arrows indicate examples of positively stained cells. Dashed line indicates the DEJ. Scale bars are indicated in each panel. Images are representative of *n*=4 individuals. (C) Normal human epidermal keratinocytes (NHEKs) were maintained in basal medium and immune-labelled as described. (D) qRT-PCR for TET1 in NHEKs maintained for 72-hours post-confluency in basal medium (control) and with addition of 1.8 mM $CaCl_2$. Data is represented as mean ± SEM for *n*=3 NHEK donors. Fold change was calculated relative to control cells with samples normalised to PPIA. A one sample T-test was performed relative to 1. Abbreviations: n.s., not significant

Immunoreactivity for TET family members TET2 and TET3 produced unreliable staining patterns in the skin, demonstrating considerable inter- and intra-individual variation in localisation and presenting with high levels of non-specific background staining. Therefore, they were not followed up further using immunohistochemical techniques, but were analysed using RT-qPCR in the Ca^{2+} differentiation of NHEKs (Figure 3.5). The mean expression of TET2 (Figure 3.5A) and TET3 (Figure 3.5B) were both increased in expression upon induction of NHEKs to terminally differentiate. However, inter-individual variation between NHEK donors was high and the increase in expression did not reach statistical significance. By contrast, involucrin, which acted as a control to monitor the progression of terminal differentiation, was significantly increased at the mRNA level upon addition of high Ca^{2+} concentration to the medium ($p \leq 0.05$; Figure 3.5C).

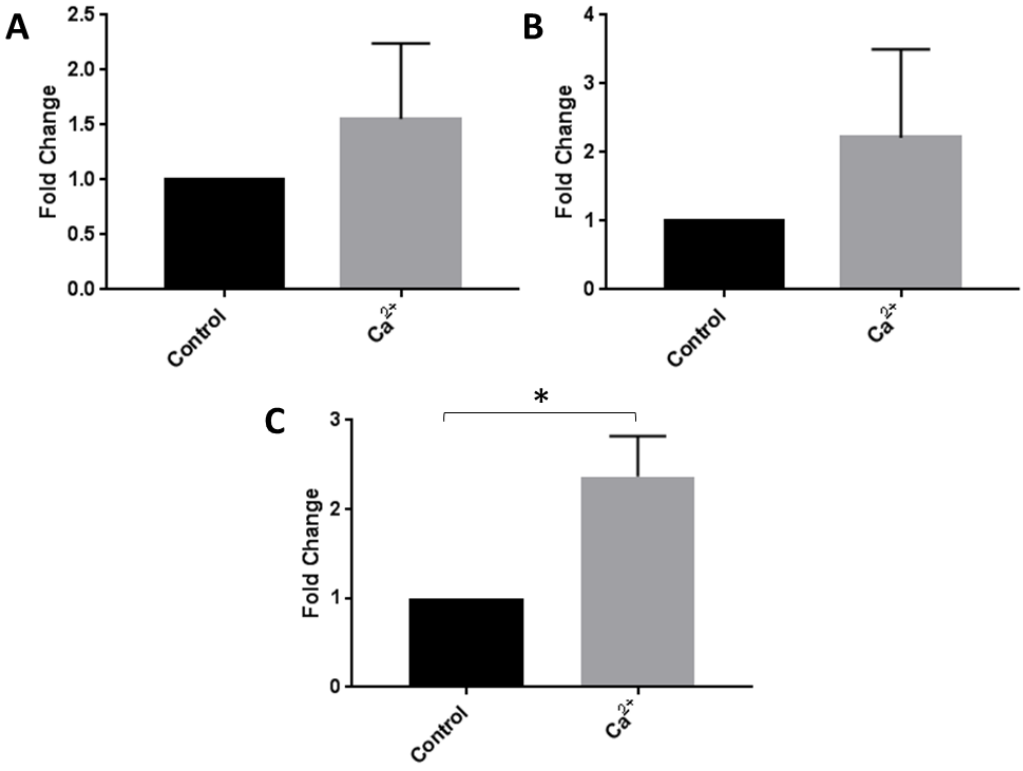

Figure 3.5: Expression of TET2, TET3 and the differentiation marker involucrin in normal human epidermal keratinocytes induced to differentiate.

Normal human epidermal keratinocytes (NHEKs) were maintained for 72-hours post-confluency in basal medium (control) and with addition of 1.8 mM $CaCl_2$. RT-qPCR for (A) TET2, (B) TET3 and (C) Involucrin is shown. Data is represented as mean ± SEM for *n*=3 NHEK donors. Fold change was calculated relative to control cells with samples normalised to PPIA. A one sample T-test was performed relative to 1, *$p \leq 0.05$.

3.4 Discussion

The first aim of this study was to visualise the localisation of enzymes key to maintaining and establishing new DNAm patterns in the skin. Immunohistochemical analyses were successfully performed for DNMT1, DNMT3A, DNMT3B and TET1, while DNMT3L, TET2 and TET3 were examined only at the mRNA level in NHEKs. As discrepancies exist in the literature regarding the localisation of DNMT1 in the skin, the mRNA levels of these enzymes were also analysed in cultured NHEKs that allowed modelling of keratinocyte differentiation *in vitro,* to confirm the observed localisation of DNAm machinery as shown in the skin.

The distribution of DNMT1 observed in this study was consistent with previous analysis by Sen et al. (2010), with DNMT1 identified chiefly in the nuclei of a number of cells residing in the *stratum basale*. Interestingly, a time-course of Ca^{2+}-switched NHEKs was also performed by Sen *et al*., demonstrating a gradual time-dependent loss of DNMT1 mRNA at 24-hours post-Ca^{2+} switch (approximately 50% reduction) and 72-hours (approximately 90% reduction), which is in agreement with the approximately 60% reduction seen in this work (Figure 3.1E). DNMT1 protein, however, was completely eliminated by 24-hours as shown by western blotting (Sen et al., 2010). This may suggest that DNMT1 protein is targeted for degradation upon commitment of NHEKs to terminally differentiate, and highlights the possible role of post-translational events in the regulation of DNMT1 protein levels. Punctate expression of DNMT1 in the *stratum basale* is in agreement with its functional role: DNMT1 displays a preference for hemimethylated substrates, and is therefore the proposed maintenance methyltransferase, known to localise to replication foci during S phase of the cell cycle (Zhang et al., 2011; Liu et al., 1998). The staining presented in this thesis also evidenced diffuse immunoreactivity in the outer differentiated layers of the epidermis that was not readily observed in the work by Sen *et al*., but that was much lower than that observed in the *stratum basale*. Expression in the outer layers of the epidermis may represent its lesser reported role in *de novo* methylation, as the cells of the outer layers of the epidermis do not undergo replication and therefore do not require DNMT1-mediated maintenance of DNAm (Jeltsch & Jurkowska, 2014).

By contrast, DNMT3 (A and B) act as *de novo* DNA methyltransferases that establish DNAm. However, they also appear important for the stable inheritance of some DNAm marks, evidenced by progressive loss of DNAm in various repeats and single-copy genes upon ablation in embryonic stem cells (Chen et al., 2003). The *DNMT3A* genomic locus contains two genes, *DNMT3A1* and *DNMT3A2*. The significance of the expression of different isoforms of DNMT3A is indicated by their different genomic localisation: green fluorescent protein (GFP)-tagged DNMT3A1 and GFP-DNMT3A2 transfected NIH3T3 cells show an almost opposing genomic localisation of the two isoforms (Chen et al., 2002a). *DNMT3A1* is postulated to have a housekeeping role, due to its ubiquitous expression and association with heterochromatic regions. By contrast, *DNMT3A2*, displays a preference for euchromatic regions and is highly expressed in embryonic stem cells. Therefore, DNMT3A2 may be more important to *de novo* methylation than its full-length isoform.

The transcript encoding *DNMT3A2* is initiated from a downstream promoter located in the sixth intron of *DNMT3A* (Chen et al., 2002b). The *DNMT3A2* isoform in humans consequently lacks the N-terminal 223 amino acid residues of the full-length DNMT3A. These N-terminal residues appear essential for the exclusive nuclear localisation of DNMT3A1, as fractionation and western blotting experiments by Chen *et al*. (Chen et al., 2002b) showed a significant proportion of *DNMT3A2*, but not *DNMT3A1*, localised to the cytoplasm in embryonic stem cells. The target epitope for the DNMT3A antibody used in this work lies towards the C terminus (between amino acids 705 to 908) of the protein. Therefore, the antibody should theoretically recognise both major isoforms of DNMT3A. The observed differential localisation of DNMT3A across the different epidermal layers may reflect a change in expression of DNMT3A isoforms, with DNMT3A2 predominantly expressed in the basal layer (exhibiting both cytoplasmic and nuclear immunoreactivity) with a transition to DNMT3A1 upon commitment to terminally differentiate (nuclear immunoreactivity only). The NHEK differentiation model employed in this work recapitulates the observed cytoplasmic and nuclear staining of the basal layer of the epidermis.

The RT-qPCR analysis further showed a decrease in mRNA expression of DNMT3A upon induction to differentiate, although this did not reach the significance threshold of $p < 0.05$. The probed sequence covered the junction of exons 12 and 13, meaning both isoforms would contribute to the amount of DNMT3A mRNA quantified. Specific quantification of the full-length transcript (DNMT3A1) could be achieved by targeting a sequence between exons 1-6, which are lacking in the DNMT3A2 transcript. If levels of DNMT3A1 remained the same upon differentiation, this would confirm that it is levels of DNMT3A2 mRNA that are changing upon differentiation. As DNMT3A1 and DNMT3A2 are homologous in all other exons, specific targeting of DNMT3A2 would not be possible by RT-qPCR or immunohistological techniques. Western blotting of protein lysates from undifferentiated and differentiated keratinocytes would indicate a semi-quantifiable shift in the isoform of DNMT3A protein present due to the presence of multiple bands of different molecular weights.

Over 30 different isoforms of DNMT3B have been identified (Ostler et al., 2007; Xie et al., 1999; Wang et al., 2006; Gopalakrishnan et al., 2009). The full-length isoform (DNMT3B1) and a shorter isoform lacking amino acids coded for by exon 11 (DNMT3B2) have been shown experimentally to possess catalytic activity (Aoki, 2001; Okano et al., 1999). Other isoforms are presumed to lack catalytic activity due to splicing of exons 22 and 23. However, they may act as methylation regulators, akin to the known role of DNMT3L, another non-catalytic DNA methyltransferase (Chédin et al., 2002). Expression of DNMT3B isoforms appears to be developmentally regulated, with DNMT3B1 and DNMT3B6 expressed in embryonic stem cells, and DNMT3B2 and DNMT3B3 isoforms expressed in a restricted manner in somatic tissues (Weisenberger et al., 2004; Chen et al., 2002b). Whether there is differential expression of the different isoforms in the skin upon commitment of the cell to terminally differentiate cannot be determined using the immunohistochemical technique developed in this work. However, this could again be investigated using isoform-specific RT-qPCR targeting alternate exon junctions. Furthermore, western blotting could indicate the molecular weight of the different isoforms present in the skin.

DNMT activity can be modulated by a number of molecular interactions. For example, DNMT3L is a truncated version of DNMT3 that lacks a portion of the catalytic domain and is not an active methyltransferase. However, it is an important cofactor for the enzymatic activity of other DNMT3s (Kareta et al., 2006). In this study, DNMT3L was not detectable by RT-qPCR in NHEKs, and so its protein expression was not investigated in the skin. Raddatz *et al*. (2013) showed by RNA-sequencing that DNMTL transcripts represented <0.1 fragments per kilobase of transcript per million mapped reads (FPKM). This independently confirms the absence, or extremely low expression, of DNMT3L in the skin. The FPKM values for other DNMTs demonstrated that DNAm machinery is expressed to low levels in the skin (all DNMTs and TETs ≤18.8 FPKM) as compared to, for example, epidermal keratins (382.1 [*KRT15*] to 26,232.1 [*KRT10*] FPKM).

The work completed here indicates that while DNMTs appear to be decreased upon traversing through the more terminally differentiated layers of the epidermis, the TETs may inversely be upregulated. This may highlight the importance of DNAm in mediating terminal differentiation of keratinocytes. Since the finding by Tahiliani *et al*. (2009) that TET family proteins are capable of oxidising 5mC to 5hmC, a putative mechanism for the promotion of active demethylation of CpG sites has developed. All TET proteins function in the prevention of hypermethylation of the genome, a finding dramatically illustrated in CGIs, where TET depletion results in prolific hypermethylation (Putiri et al., 2014). Furthermore, loss of TET expression has been reported in numerous cancers including skin, lung and breast, which is suggestive of a critical role in DNAm maintenance (Kudo et al., 2012; Yang et al., 2013). The genomic loci targeted by TET family proteins shows considerable overlap, with TET1 reportedly maintaining the most sites. TET1 displays greater activity at high density CGIs, while TET2 is more actively involved at low density CGIs (Putiri et al., 2014). Interestingly, the NHEK differentiation model indicated no significant changes in mRNA expression of any of the TET proteins (1 to 3). However, there was a trend suggesting TET2 and TET3 could be upregulated almost two-fold upon differentiation. An early study identified that differentiation of keratinocytes in culture decreased the percentage of methylated cytosines, from approximately 3.1% in undifferentiated cells to 1.4% in

differentiated cells (Veres et al., 1989). This fits with the trend of TET2 and 3 mRNA upregulation in our differentiated NHEK model, as this would enhance oxidation of 5mC to 5hmC and its eventual removal by TDG of the BER complex, leading to global losses in DNAm as observed by Veres *et al*. (1989).

A limitation of this study is that the surgical discards of abdoplasty were used. The patient details indicate an average age of 52.6 years ± 11 years, while the keratinocytes used were isolated from the foreskin of juvenile donors. Childhood development and the ageing process may have a confounding effect on the staining patterns observed if differences in DNAm machinery occur in different life stages. Therefore, DNMT and TET expression should be examined in a sample cohort with specific inclusion and exclusion criteria in which age, health status and other factors can be adequately controlled. This may explain why differences in DNMT3B were detectable upon differentiation of NHEKs in culture, but not in the different layers of the epidermis *in situ.*

Overall, this chapter has demonstrated specific expression in different compartments of the skin, and subcellularly, of enzymatic machinery important for DNAm maintenance and establishment.

Chapter 4: Divergent epigenetic effects upon UV radiation challenge in aged and young skin

4.1 Introduction

The epidermis is an ideal tissue in which to study age-related and environmental-related epigenetic changes as it undergoes well-characterised histological and phenotypic changes with increasing age (Farage et al., 2013) and upon acute (D'Orazio et al., 2013) and chronic UVR exposure (Langton et al., 2010). There has been considerable interest in how environmental factors modulate the establishment and maintenance of epigenetic modifications, allowing an organism to respond to its environment through changes in gene expression and phenotype (Mirbahai & Chipman, 2014). Since DNAm is maintained throughout mitotic cell division (Wigler et al., 1981; Almouzni & Cedar, 2016), changes in DNAm, affecting the basal keratinocytes and other skin-resident cells, will persist and may play a role in skin cancer risk (Fu et al., 2017; Liao et al., 2011) and how the skin photoages upon chronic UVR exposure (Vandiver et al., 2015).

Accumulating evidence advocates a key role of DNAm in the skin response to UVR exposure. These studies, comparing DNAm in skin of different ages, and from photoexposed and photoprotected body sites, highlight that photoexposure is associated with its own pattern of epigenetic perturbations divergent to that of intrinsic ageing-related processes (Vandiver et al., 2015; Raddatz et al., 2013). However, it is difficult to dissect which changes are exclusively associated with UVR exposure, as opposed to those related to intrinsic ageing- or body site. Questions therefore remain as to what the earliest changes upon UVR exposure are, and if sub-erythemal levels of UVR are capable of eliciting these changes. In this study, small regions of the buttock are exposed to repetitive, sub-erythemal doses of UVR to recapitulate the early DNAm changes in chronically photoexposed skin, while maintaining an unirradiated internal control that eliminates anatomical and intrinsic ageing related differences.

4.2 Objectives

The hypothesis to be addressed in this chapter is that repeated sub-erythemal UVR challenge will have a measureable effect on DNAm and gene expression within the epidermal compartment of the skin. Furthermore, that young and aged skin will have a differing response to UVR challenge, as measured by these parameters. The specific objectives are as follows:

1. To identify a UVR exposure regimen (trailing 40% or 80% MED, for 5 or 10 days) that produces measureable changes in DNAm and gene expression in an *in vivo* pilot study of 5 young individuals (*n*=5, ≤30 years of age; section 2.1.2). Biopsies will be quadrisected to allow multiple analyses to be performed: DNAm analysis will utilise the Illumina Infinium MethylationEPIC BeadChip array (section 2.4.2) and changes in gene expression will be measured by Lexogen Quantseq 3' mRNA sequencing (section 2.3). The resulting data will be subjected to a linear regression model and DMPs (section 2.4.2.4) and DEGs (section 2.3.4) identified, respectively. Histological markers of UVR exposure will also be analysed to confirm the effects of UVR exposure, including 8-OHdG (section 2.5.3.2) and CPD (section 2.5.3.3) immunohistochemistry, and the WS histochemical stain for melanin (section 2.5.2.1).

2. To use the UVR exposure regimen identified in objective 1, increasing the number of young individuals recruited and including an older cohort (≥65 years of age, section 2.1.3). The DNAm and gene expression analysis will be repeated as previously described and the response to UVR compared between the age groups. Pathway analysis will also be performed (section 2.3.4.2).

4.3 Pilot Study: investigating UVR dose and time regimens in young skin

4.3.1 Sub-erythemal UV radiation alters histological damage markers in a pilot study of five young individuals

An *in vivo* pilot study was performed to investigate how a five- and 10-day course of sub-erythemal (40% and 80% MED) UVR exposure affects DNAm and transcription in the skin of a young cohort (n=5, ages 18-30). The two main adaptive defence mechanisms of the skin to UVR damage are the stimulation of melanin synthesis and thickening of the epidermis. Therefore, the skin was assessed histologically so as to confirm a response to the level of UVR applied. The WS procedure was performed as per section 2.5.2.1. The amount of melanin present increased in a time- and dose-dependent manner. The greatest amount of melanin was present following 10-days of daily irradiation using 80% of MED ($P < 0.001$; Figure 4.1). Due to correction of p-values for multiple tests, other comparisons were not significant.

DNA damage following UVR challenge was investigated. While cyclobutane pyrimidine dimers were not detected, oxidative DNA damage was detected in the form of 8-oh-dG. The percentage of 8-OHdG-positive cells was increased in all samples exposed to UVR (Figure 4.2). Interestingly, the highest levels of 8-OHdG were observed at the lower UVR dose of 40% MED, following 10- and 5-days of UVR exposure (both $p < 0.05$; Figure 4.2).

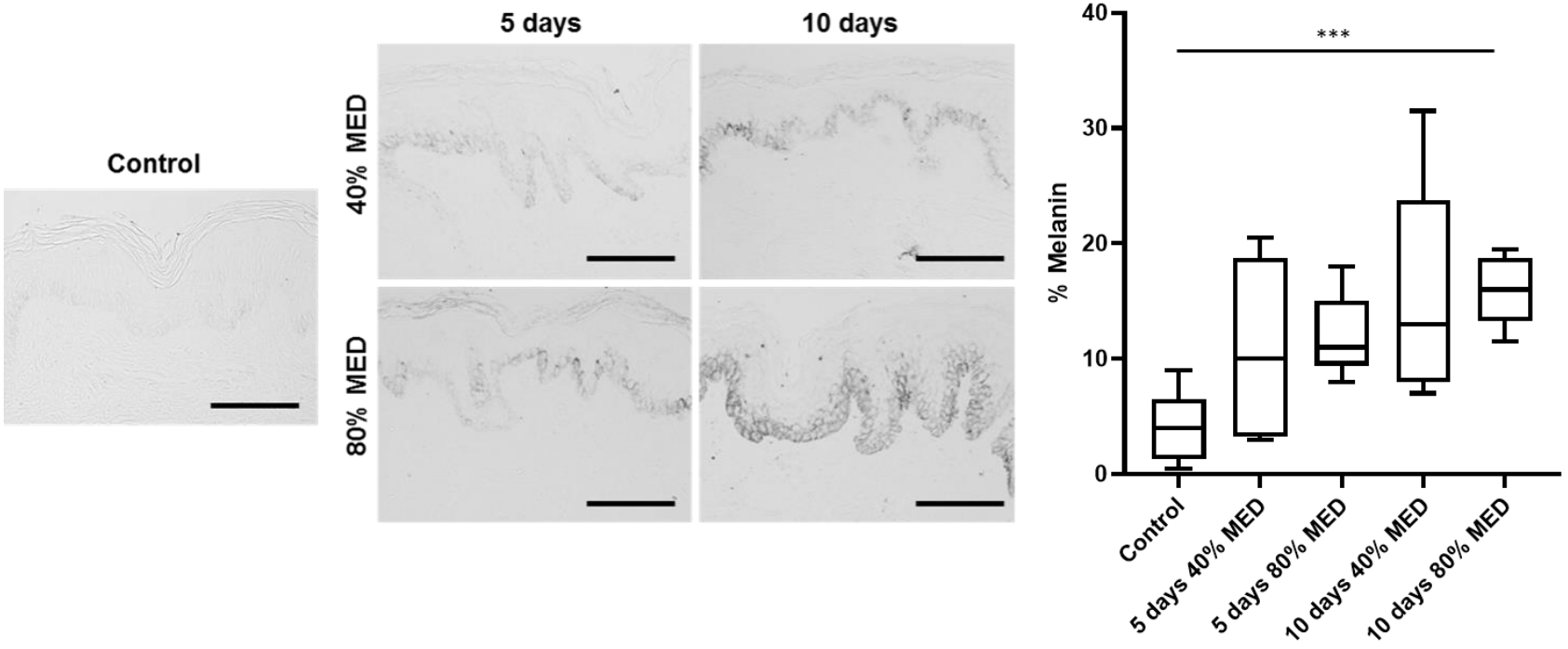

Figure 4.1: Warthin-Starry detection of melanin in a pilot study of 5 young individuals following different regimens of sub-erythemal UVR challenge.

Quantification represents stained area as a percentage of the epidermal area. Scale bars = 100 µM. All measurements represent the average per group for n=5 donors, 3 tissue sections per donor and 3 fields of view per section (total = 9 images per donor). Box plots indicate the median, interquartile range and min and max values. Asterisks indicate level of significance, where P <0.001, ***.

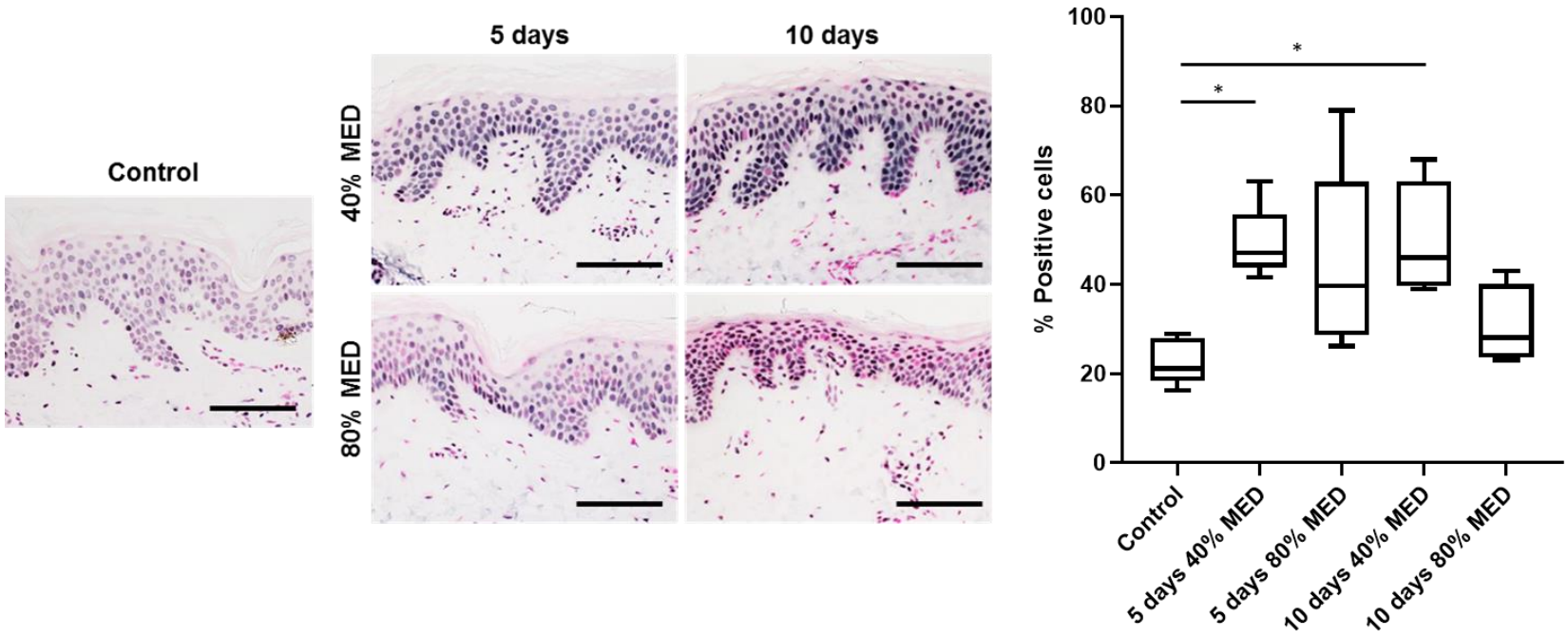

Figure 4.2: Immunohistochemical staining 8-OHdG in a pilot study of 5 young individuals following different regimens of sub-erythemal UVR challenge.

Quantification represents the number of immune-positive cells given as a percentage of the total number of epidermal cells. Scale bars = 100 µM. All measurements represent the average per group for n=5 donors, 3 tissue sections per donor and 3 fields of view per section (total = 9 images). Box plots indicate the median, interquartile range and min and max values. Asterisks indicate level of significance, where $P < 0.05$, *.

4.3.2 Different UVR-exposure regimens were all suggestive of a similar epigenetic response

DNAm profiles were generated for all donors and conditions using the infinium EPIC array, with the exception of 80% MED for 10 days for donor 1. This was due to the donor developing an erythema response to the UVR regimen. The PCA revealed clustering dominated by donor differences (Figure 4.3). In particular, sex differences created two distinct clusters along principal component 1 (PC1; Figure 4.3), with the green and purple data points corresponding to males and other colours the female study participants.

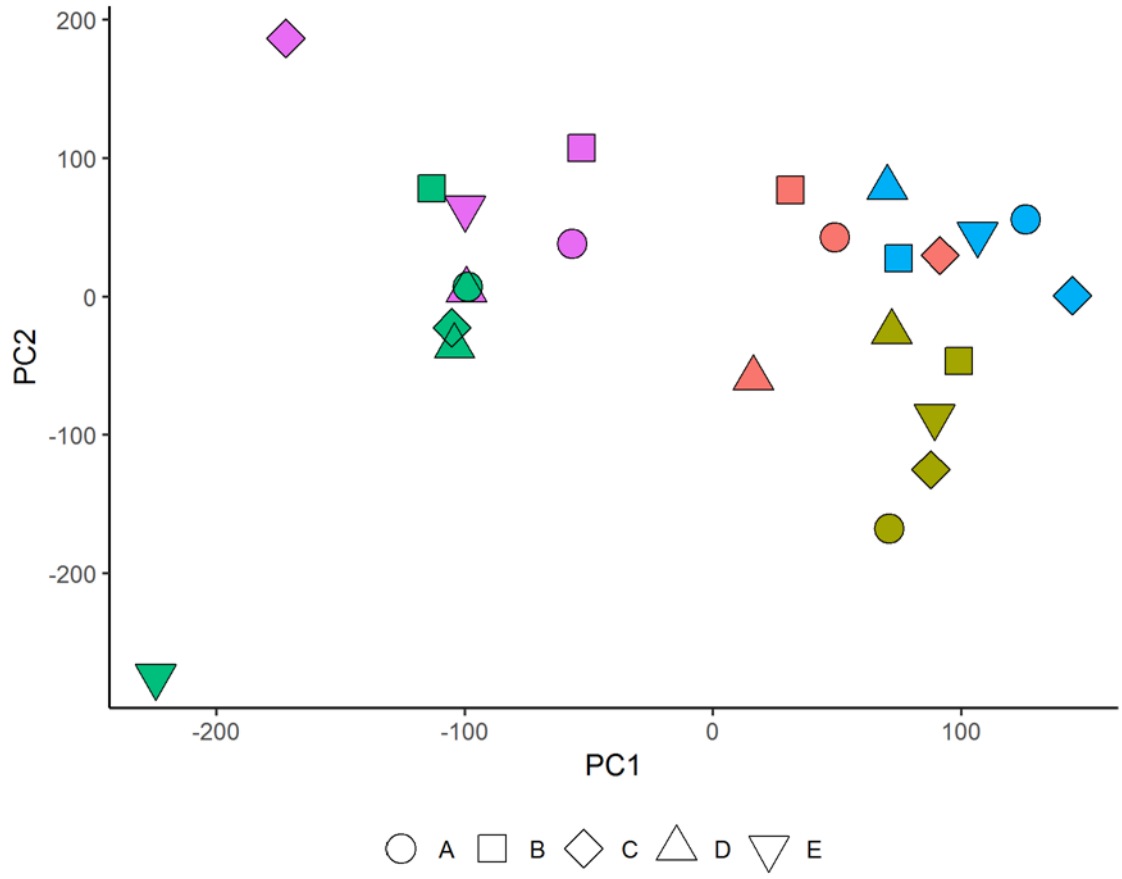

Figure 4.3: Principal component analysis of DNA methylation profiles in a pilot study of 5 young individuals following different regimens of sub-erythemal UVR challenge

DNA methylation profiles were generated following different doses (40% and 80% minimal erythemal dose; MED) and numbers of days (5 and 10 days) of UVR challenge. A, control; B, 5-days of 40% MED; C, 5-days of 80% MED; D, 10-days of 40% MED; E, 10-days of 80% MED.

In order to increase the statistical power of the DMP analysis, a linear regression model was performed that pooled all of the UV irradiated samples versus unirradiated control to identify DMPs associated with UVR. Next, the two doses of UVR (40% and 80% MED) at the 5-day time point were pooled, versus unirradiated control to identify DMPs associated with 5-days of UVR. Finally, the same pooled analysis of doses was performed at the 10-day time point versus unirradiated control. The 10-days analysis returned the greatest number of probes with an unadjusted p-value of <0.05 (3,440 probes), followed by the 5-day analysis (2,901 probes) and the UVR analysis (2,302 probes) (Table 4.1). However, the DMPs may be subtle as they do not appear to be significant after FDR adjustment of p-values.

Of the DMPs identified following 5- and 10-days of UVR challenge, 807 were differentially methylated in the same direction at both time points, a significantly greater number than expected by chance (Odds ratio = 61.6, $p < 1 \times 10^{-99}$) (Figure 4.4). This adds confidence to these DMPs as real effects of UVR exposure, as they repeat in two independently irradiated samples of skin. Furthermore, the non-overlapping DMPs after five (2,094 DMPs) and 10-days (2,633 DMPs) of UVR may represent acute and chronically-persistent changes in DNAm, respectively. However, this would need to be verified in a greater number of individuals.

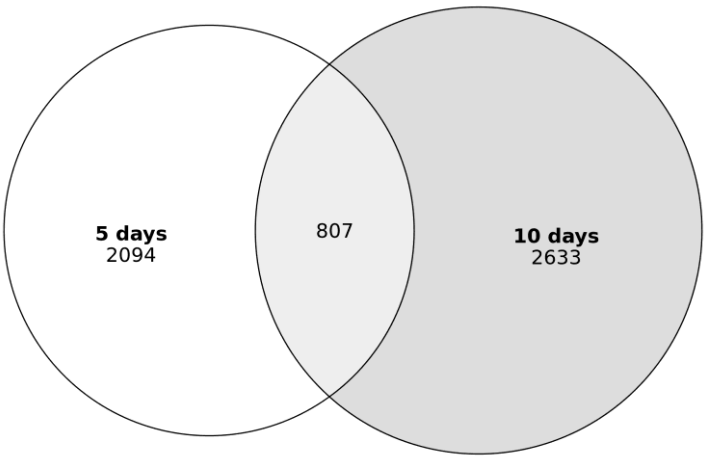

Figure 4.4: Number of overlapping differentially methylated probes following 5 and 10-days of sub-erythemal UVR challenge.

Following determination of differentially methylated probes at each time-point, the lists of probes was examined for their overlap.

To establish whether these DMPs are consistent with UVR associated changes as identified in the literature, this study was compared to those identified between the forearm and the upper inner arm by Vandiver *et al*. (2015). Following a reanalysis of the Vandiver *et al*. (2015) data set (section 2.4.2.6), DMPs in the sub-erythemal UVR regimens examined in our study produced significantly overlapping results (Table 4.1). The greatest number of overlapping probes was observed for the 10-days of sub-erythemal UVR analysis versus unirradiated control (odds ratio = 2.5, p value = 4.846×10^{-98}), although the other comparisons also showed a similar and significant enrichment in the number of overlapping probes (all UVR-exposed samples, 336 DMPs, odds ratio = 2.5, p =1.179×10^{-68}; 5-days, odds ratio = 2.5, p value = 1.510×10^{-88};Table 4.1). Due to the different arrays used (450K versus EPIC arrays), >50% of the DMPs identified were not queried in the Vandiver *et al*. (2015) dataset (Table 4.1; row 3), and therefore the overlap is likely to be an underestimate.

Table 4.1: Number of differentially methylated probes following different regimens of sub-erythemal UVR exposure and their overlap with Vandiver *et al.* (2015).

	Total UV	**5 days**	**10 days**
Differentially methylated probes (unadjusted p ≤0.05)	2,302	2,901	3,440
Number measured on 450K	872	1,146	1,320
Overlap with Vandiver	336	479	545
Odds ratio	2.5	2.5	2.5
P-value of overlap	1.179×10^{-68}	1.510×10^{-88}	4.846×10^{-98}

The number of differentially methylated probes detected on the earlier 450K generation of array was determined to enable comparison with the Vandiver *et al*. (2015) dataset. The significance of the overlap between the two studies was determined using Fisher's test.

4.3.3 Transcriptional response to UVR challenge was robust

In comparison to the only subtle differences in DNAm detected, a robust transcriptional response was observed, as determined by Quantseq 3' mRNA sequencing. One sample provided insufficient amounts of RNA and was not included (donor two, 5-days of 40% MED). The same linear modelling approach was used to determine differential gene expression following sub-erythemal UVR challenge using 40% and 80% of MED daily for 5 and 10-days (Table 4.2). The transcriptional response with the highest number of DEGs identified was observed following 80% of MED applied daily for 5-days, which identified 671 DEGs.

These changes were compared with those identified in a reanalysis of transcriptional profiles following 10-days of similar levels of UVR, generated in Choi *et al*. (2010). This analysis found 392 significantly DEGs with SSR in the Choi *et al*. dataset. The greatest number of genes found to overlap was with our 5 days with 80% of MED analysis, identifying 29 overlapping genes (odds ratio = 1.5, p = 0.014) (Table 4.2). The genes in this overlapping list were enriched in the KEGG pathways "melanogenesis" (four genes, $p = 1.055 \times 10^{-4}$) and "tyrosine metabolism" (three genes, $p = 2.869 \times 10^{-4}$), which are known pathways activated upon UVR exposure (Brenner & Hearing, 2008) and thus adds additional validation that the UVR protocol employed could detect key transcriptional changes. Although representing only a small number of genes, the statistically strongest overlap in this comparison was with our 10 day analyses, particularly the 80% dose, which represented the closest experimental protocol as the Choi *et al*. (2010) study (9 genes, odds ratio = 28.4, $p = 2.848 \times 10^{-13}$).

Table 4.2: Differentially expressed genes following sub-erythemal UVR challenge using 40% and 80% of MED applied daily for 5 and 10 days

Days	All	5 days			10 days		
Dose	**All**	**Both**	**40% MED**	**80% MED**	**Both**	**40% MED**	**80% MED**
Adjusted p < 0.05	123	56	0	671	11	7	10
Adjusted p < 0.1	433	305	0	1,650	32	7	12
Measured in Choi *et al*.	102	51		594	9	7	10
Overlap	15	6		29	7	6	9
ODDs ratio	3.7	3.7		1.5	24.6	27.1	28.4
P value	8.875×10^{-05}	0.005		0.014	1.033×10^{-09}	6.622×10^{-09}	2.848×10^{-13}

Differentially expressed genes in this dataset for each UVR exposure regimen were compared to genes identified by Choi *et al*. (2010). As this additional dataset utilised Agilent whole human genome oligo microarrays, it was necessary to reduce the RNA-sequencing dataset to the probeset included on this array. Then, the significance of the overlap between the two studies was determined using Fisher's test.

4.4 Follow-up Study: investigating UVR challenge in young and aged skin

4.4.1 Aged skin was suggestive of a lower tolerance for UVR

Having identified that a significant number of DMPs occurred consistently at both time-points and doses of UVR trialled, a follow-up study was performed in a larger cohort, comparing changes in the skin of young and aged volunteers exposed *in vivo* to 80% of MED for five days. In total, DNAm profiles of 29 subjects were included in this analysis. As shown in the CONSORT diagram (Figure 4.5), 24 individuals participated in the follow-up study and an additional five individuals from the pilot study were included in the analysis. The young cohort consisted of 17 participants with a mean (± standard deviation [SD]) age of 22.67 (± 3.2) years and comprising of 11 females (64.71%) and 6 males (35.29%; Table 4.3). The aged cohort consisted of 12 individuals with a mean (± SD) age of 70.67 (± 5.5) years. This group consisted of 7 females (58.33%) and 5 males (41.67%). These sex differences were not significantly different between the age cohorts, as determined by chi-squared test (χ^2 = 0.121, p = 0.728; Table 4.3). The mean (± SD) MED of the young cohort was 24.42 (± 4.0) mJ cm^{-2}, which was higher than that of the aged cohort, of 21.82 (± 6.0) mJ cm^{-2}. However, this reduction was suggestive only of a trend (T-test, p = 0.071).

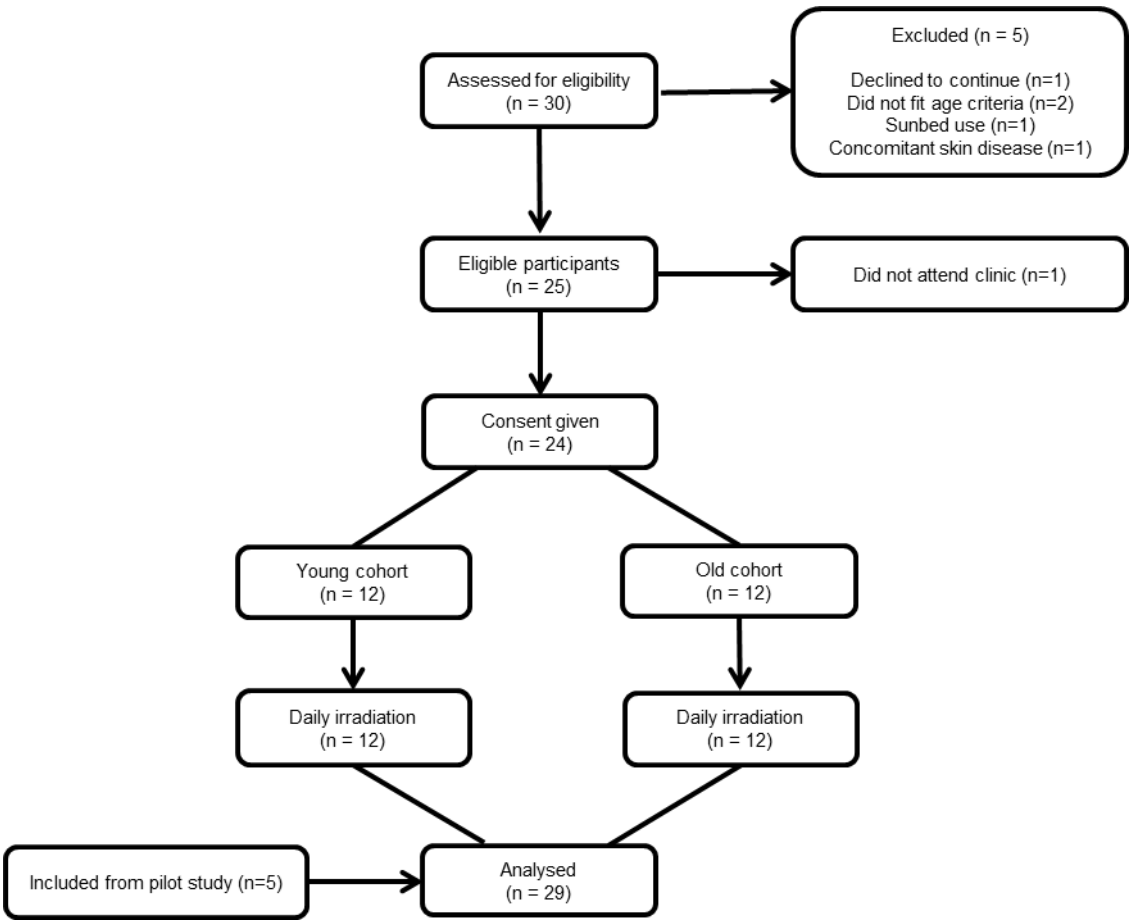

Figure 4.5: Study CONSORT diagram.

Thirty contacts were made and individuals were screened for eligibility. One individual declined to continue, two did not fit age criteria, one was excluded for use of sunbed, and one disclosed concomittant skin disease. Of the eligible 25 individuals, one failed to attend clinic with no reason given. The remaining 24 individuals gave written informed consent to participate in the study and formed a young cohort (n=12, 18-30 years) and an aged cohort (n=12, ≥65 years). All participants giving consent completed the study. Samples collected from an additional 5 young individuals from a pilot study were included in the analysis (total young, *n*=17; total aged *n*=12).

Table 4.3: Comparison of the characteristics of the young and aged group

Group	Number of participants	Sex (*n, %*)		Minimal erythema dose ($\bar{x} \pm SD$)	Age ($\bar{x} \pm SD$)
		Male	Female		
Young	17	6 (35.29)	11 (64.71)	24.42 ± 4.0	22.67 ± 3.2
Aged	12	5 (41.67)	7 (58.33)	21.82 ± 6.0	70.67 ± 5.5
***p* value**		0.728†		0.071‡	1.167×10^{-18} ‡

† χ^2 test, ‡ Unpaired Student's T-test

4.4.2 DNA methylation changes are associated with both intrinsic ageing and daily UVR challenge of the skin

4.4.2.1 Principal component analysis demonstrated clustering by age and UVR in epidermal DNAm profiles

DNAm profiles were generated using the Infinium MethylationEPIC BeadChip. Using the whole DNAm dataset (758,057 probes), PCA was performed prior to statistical modelling, to gain an indication of the genome-scale differences present. Almost 40% of the variation within the dataset was accounted for by the first three PCs (Figure 4.6A). PC1 and PC2 showed two clusters indicating batch differences between the pilot and follow-up study (PC1; Figure 4.6B) and clustering of young and aged samples readily apparent along the y-axis (PC2; Figure 4.6B). PC3 identified slight separation of the daily UVR-exposed skin from unirradiated control skin along the Y-axis (PC3; Figure 4.6B) although this only accounted for 5.859 % of the variance between samples.

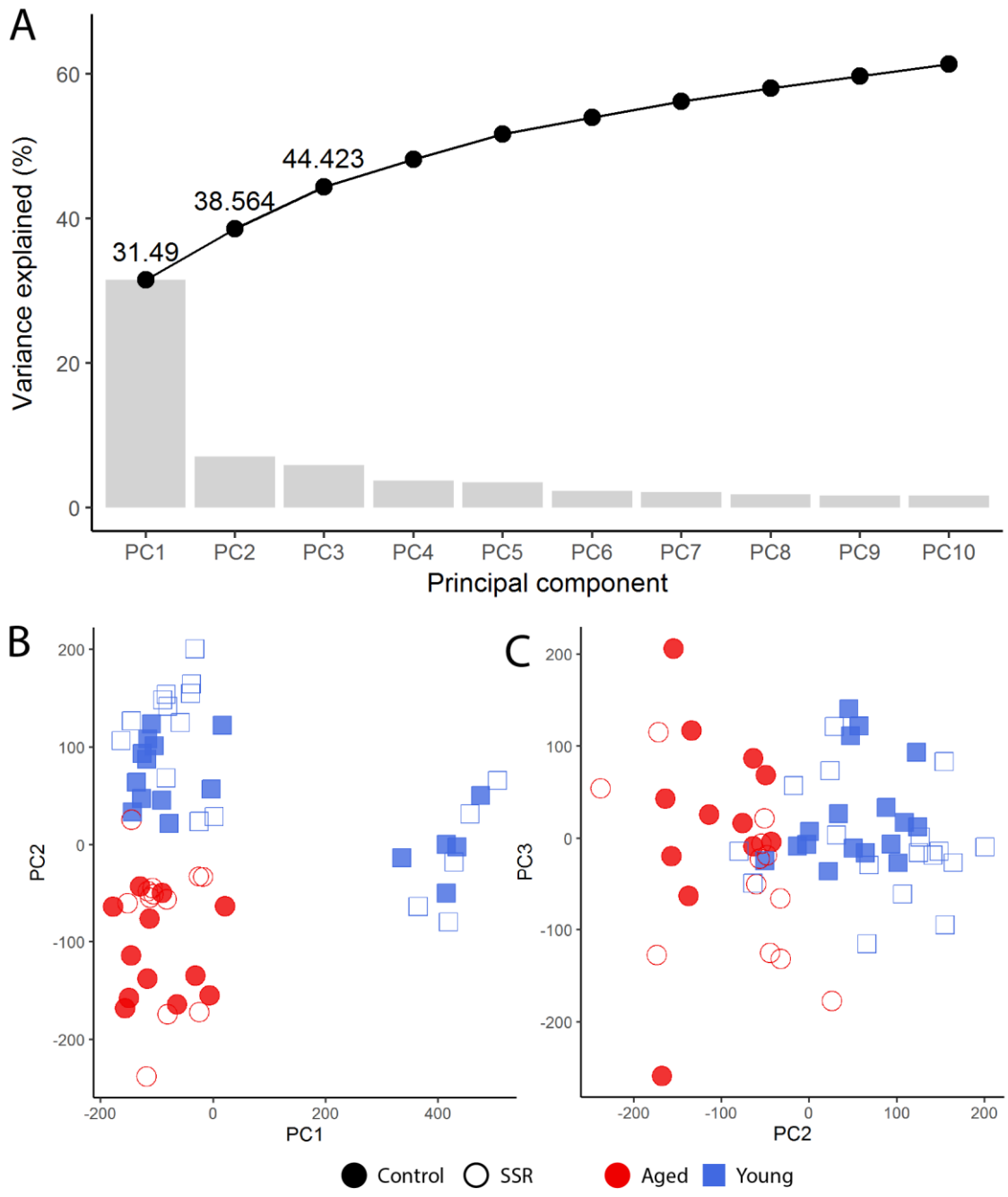

Figure 4.6: Principal component analysis of DNA mehtylation profiles in young aged skin following daily UVR challenge

The DNAm state at 758,057 CpG sites in aged and young skin exposed and unexposed to 5 suberythemal doses of UVR were used to perform principal component analysis (PCA). (A) Cumulative plot showing each PC. To determine biological or technical sources of variation (B) PC1 and PC2 or (C) PC2 and PC3 were plotted. Aged, red; young, blue; control, filled shapes; SSR, open shapes.

4.4.2.2 Differentially methylated CpG sites are skewed towards a loss of methylation

A linear regression model was fitted to the dataset and empirical Bayes moderated t-statistics for each probe were computed. In the young group, no DMPs were identified following UVR challenge that met the stringent FDR filter applied. However, in aged skin, 366 DMPs were identified following UVR exposure (Table 4.4). Of these, the majority were loss of DNAm at a ratio of 15:1. In a combined analysis where the age groups were pooled 1,704 DMPs were identified following UVR challenge. Again, most of these were a loss of DNAm, at a ratio of 30:1 (Table 4.4).

Unsupervised hierarchical clustering of UVR and control samples successfully sorted more than 80% of the samples based on the 1,704 DMPs identified (Figure 4.7). In some instances, where the irradiated sample clustered falsely with the unirradiated control samples, the study participant's two samples clustered together. This may suggest that the donor has not responded as strongly as others to the UVR challenge, or that their baseline unirradiated control had a higher level of UVR exposure previously. These analyses were repeated following removal of the 5 samples generated in the pilot study, to allow investigation in a dataset with equal *n* number and no batch effect. The trends identified were repeated in this analysis (appendix II).

Table 4.4: Number of differentially methylated probes following repeated sub-erythemal exposure to UVR in young and aged skin

	Age group		
	Young	**Aged**	**Young and aged**
n	17	12	29
Hypermethylated sites #	0	23	55
Hypomethylated sites #	0	343	1,649
Ratio Hyper:hypo	-	15:1	30:1

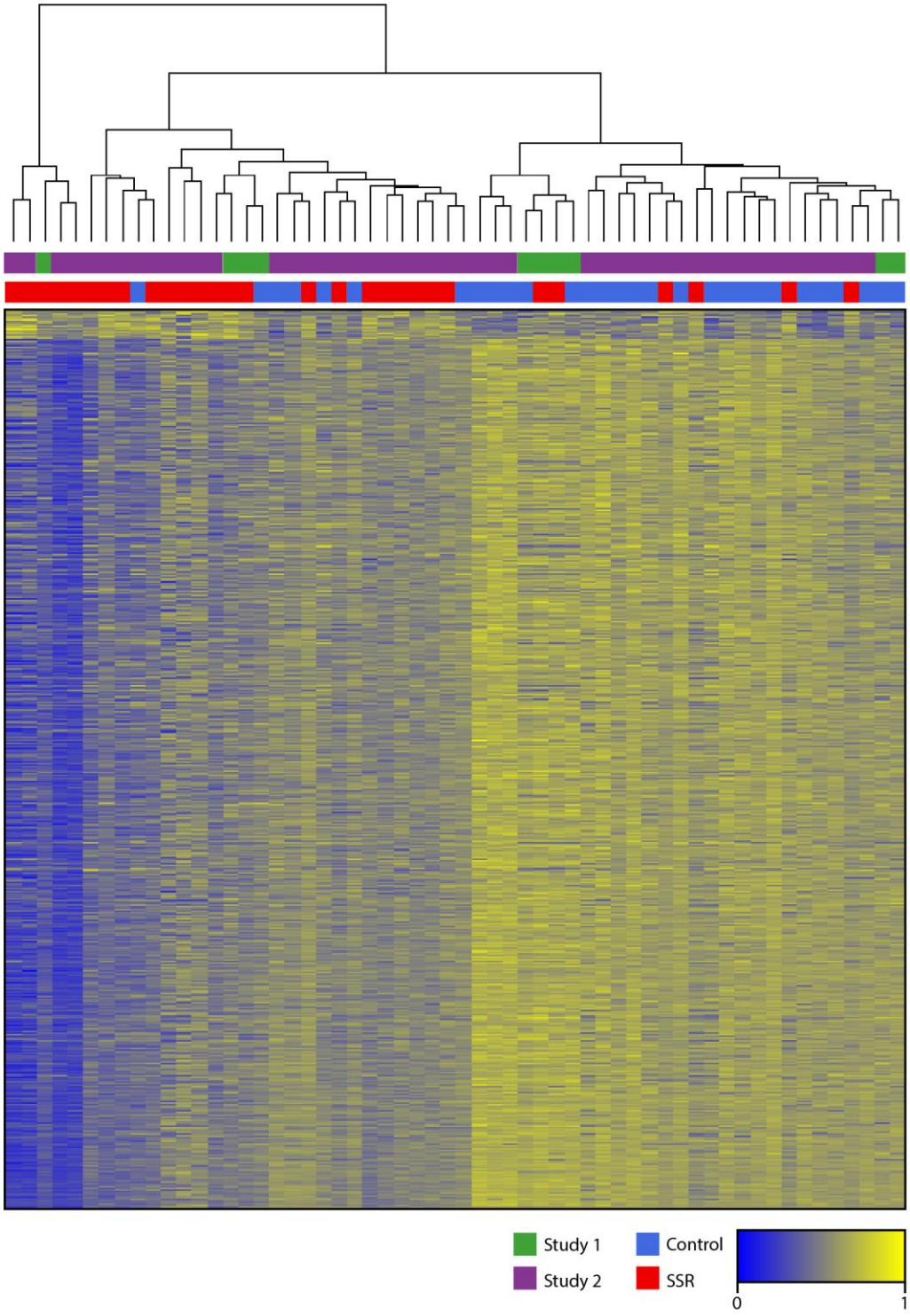

Figure 4.7: Unsupervised hierarchical clustering of 1,704 differentially methylated probes identified following 5 days of sub-erythemal UVR challenge.

Irradiated or unirradiated control skin is indicated by the red and green blocks (red, SSR; blue, control). Each row represents a differentially methylated probe, where a beta value of 1 (methylated) is indicated by yellow and a value of 0 (unmethylated) is indicated by blue as per the key. Samples are represented by columns.

4.4.2.3 Greater degree of change in methylation in aged skin than young skin following UVR challenge

In the DMP analysis, changes were observed following UVR challenge in the aged cohort that reached significance following FDR adjustment of p-values, but not in the young cohort. Yet, pooling the age groups identified changes following UVR challenge that were significant. Collectively, these comparisons suggested that consistent changes occurred in both age cohorts, but the magnitude of DNAm change may have been greater in the aged group, which elevated these DMPs above the FDR-adjusted significance threshold in aged skin in the age-stratified model but not young skin.

To interrogate this further, Δβ of 1,704 DMPs identified following UVR challenge in the pooled age group analysis were compared in young and aged skin in a violin plot (Figure 4.8). The Δβ of hypomethylated probes was a mean of two percent lower in aged skin than young (paired Student's T-test, $p \leq 2x10^{-29}$), suggesting that aged skin loses DNAm to a greater amount following UVR challenge than young skin.

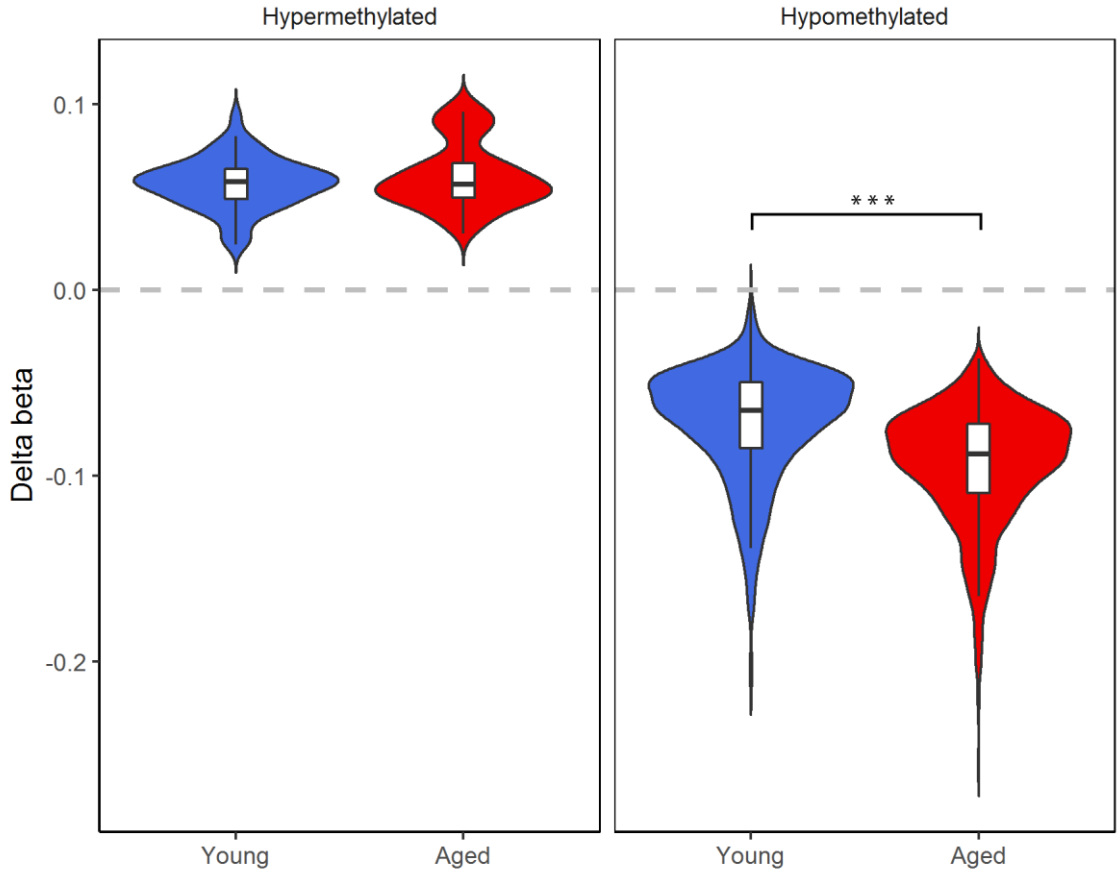

Figure 4.8: Delta beta values of 1,704 DMPs following UVR challenge in young and aged skin.

Violin plot of 1,704 differentially methylated sites identified following UVR challenge. The change in beta value for the young and aged group were determined. Left: hypermethylated probes (*n*=55); right: hypomethylated probes (*n*=1,649). Statistical significance was determined using a paired Student's T-test. ***, p <0.001.

4.4.2.4 DNA methylation age is accelerated in aged but not young skin following UVR challenge

To further assess perturbations in DNAm following UVR exposure, an 'age-predicting' algorithm was applied (Horvath et al., 2018), which uses DNAm level at 391 CpG sites to calculate a DNAm age. Using this algorithm, the DNAm profiles of participants in this study was highly correlated with actual age of the donors in both unirradiated and UVR irradiated epidermis (R^2 = 0.933 and 0.948, respectively; Figure 4.9). Comparison of

unirradiated control and UVR-exposed tissue suggested a trend of an acceleration of DNAm age in the aged (T-test; p = 0.08) but not the young cohort.

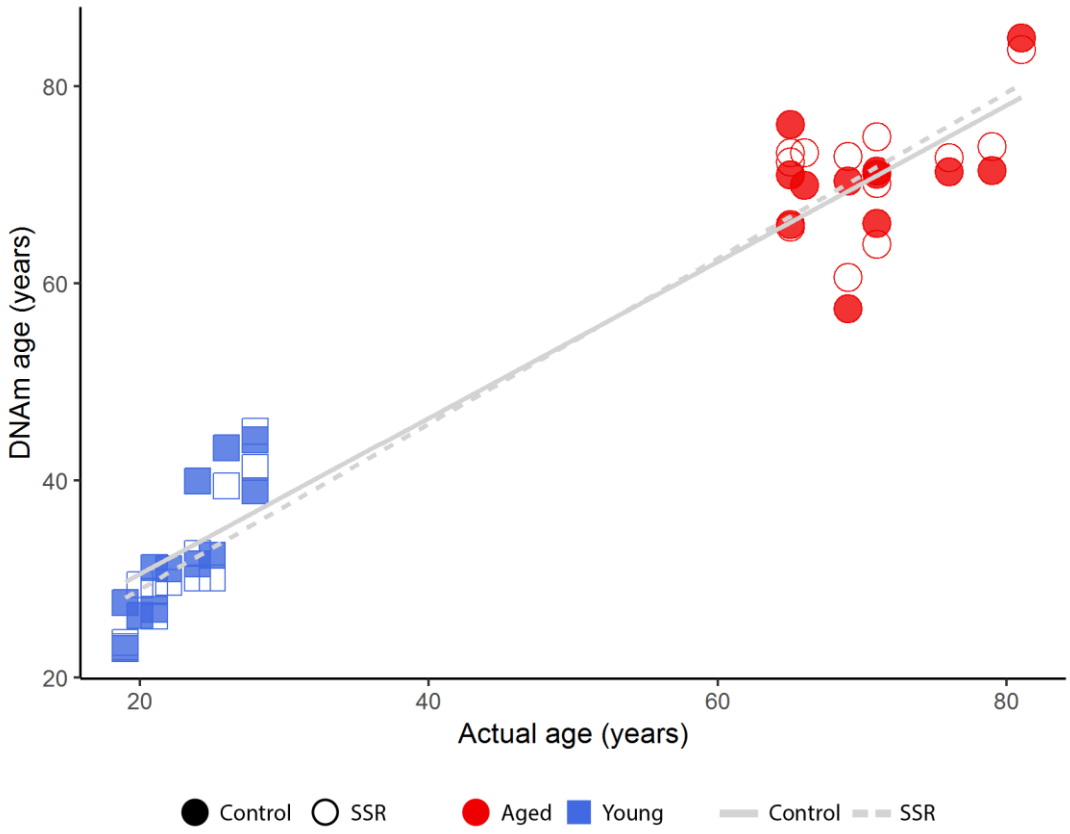

Figure 4.9: DNA methylation age of UVR-challenged and unniraidated control skin in the aged and young cohort as determined by Horvath skin and blood clock.

Methylation levels of 391 CpG sites defined by the Horvath skin and blood clock were used to determine DNA methylation age of UVR-challenged and unirradiated control skin in young and aged volunteers as compared to age of donor. Aged, red; young, blue; control, filled shapes; SSR, open shapes; solid line, trend-line for unirradiated control samples; dashed line, trend-line for SSR-irradiated samples.

4.4.2.5 Changes in methylation occur preferentially in gene-poor open seas following UVR challenge

The genomic distribution of CpG sites found to be differentially methylated following sub-erythemal UVR exposure were also investigated (Figure 4.10). Hypermethylated

CpG sites were significantly underrepresented in CpG islands (Fisher's test; $p < 0.01$, OR = 0.17) and enriched in open seas (Fisher's test; $p < 0.01$, OR = 2.21). Sites found to be hypomethylated were also underrepresented in CpG islands and shores (Fisher's test; both $p < 0.001$, OR = 0.03 and 0.36) and were even more heavily enriched in open sea (Fisher's test, $p < 0.001$, OR = 5.14). There was no significant enrichment or underrepresentation in other genomic regions.

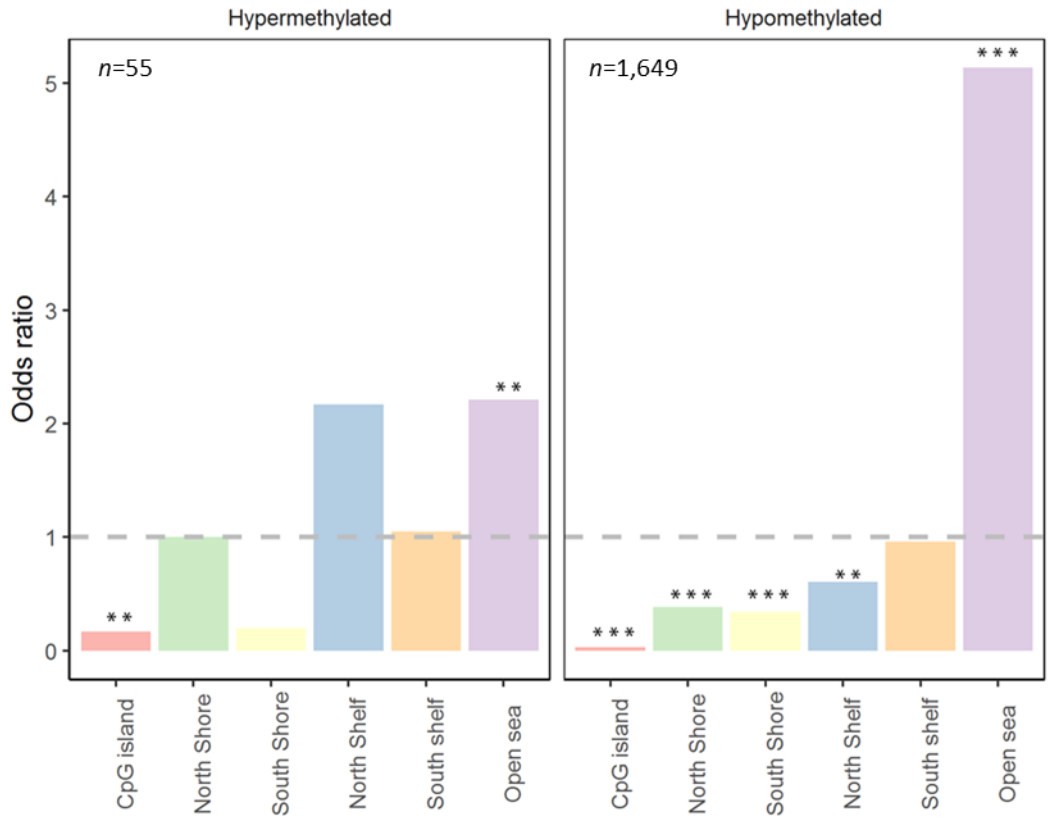

Figure 4.10: Genomic distribution of differentially methylated CpG sites in skin exposed to UVR

Fisher's exact test odds ratios of differentially methylated CpG sites falling within discrete genomic regions as compared to the total distribution of CpG sites on the Infinium MethylationEPIC BeadChip array. Differential methylation is subdivided into hypermethylated and hypomethylated changes.

4.4.3 Young skin mounted a greater transcriptomic response following UVR challenge

Next, the transcriptomic changes in young and aged skin following UVR challenge were investigated. Principal component analysis of all 15,862 mRNAs identified by 3' mRNA sequencing was performed (Figure 4.11), identifying major sources of variation related to study number (principal component 1: left hand side, follow-up study; right hand side, pilot study). Principal component 3 captured the variation associated with both age and UVR challenge (Figure 4.11B, Y-axis).

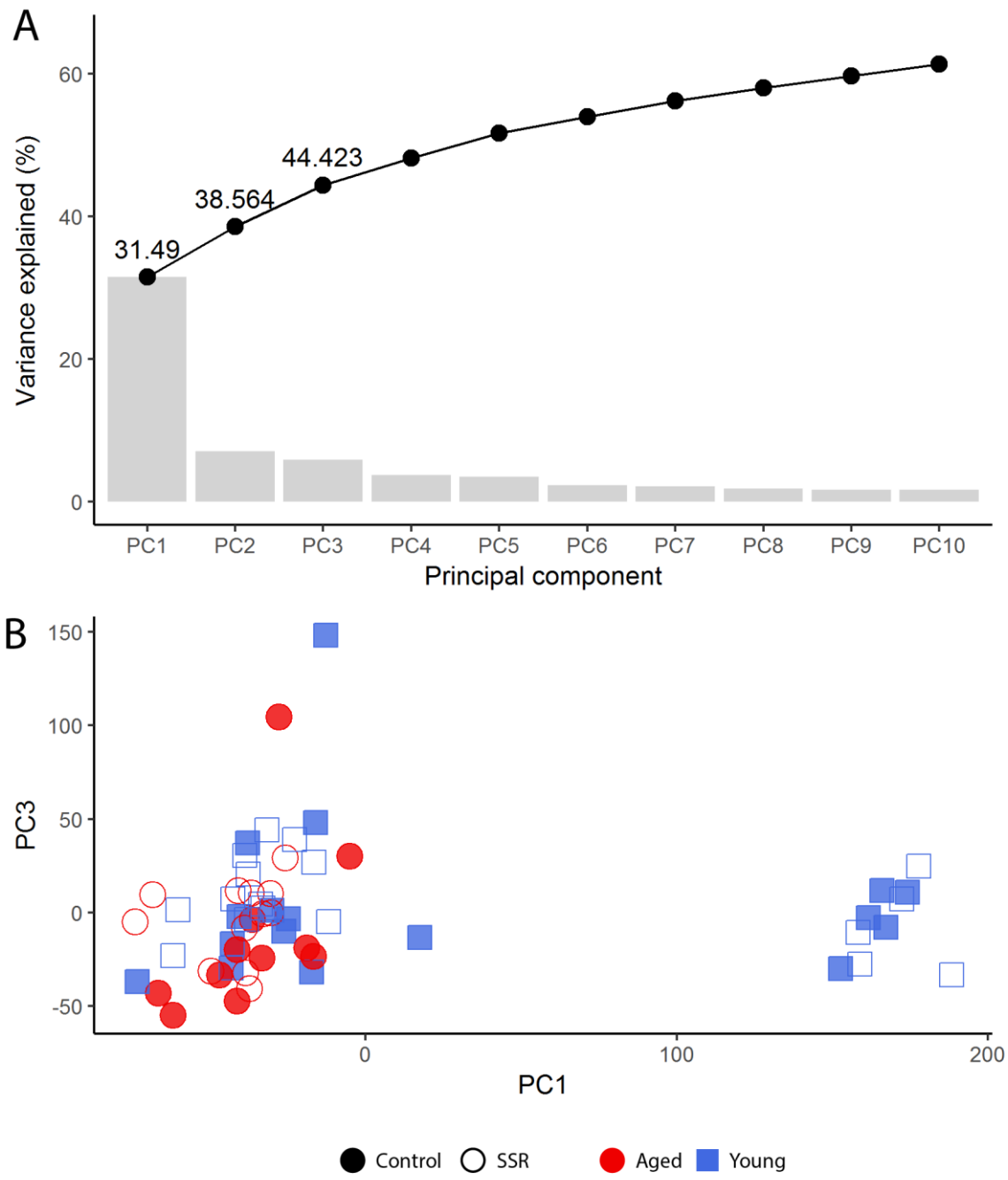

Figure 4.11: Principal component analysis of transcripts identified by 3' mRNA sequencing.

(A) Cumulative plot of the first 10 principal components. Labels indicate the cumulative percentage of variance explained by the first three components. (B) Principal components 1 and 3 stratify samples by study number and age, respectively. Aged, red; young, blue; control, filled shapes; SSR, open shapes. Abbreviations: PC, principal component.

Differential expression was determined; both young and aged skin showed a transcriptomic response to UVR challenge (Table 4.5). Young skin showed a considerable number of changes in gene expression, equating to 286 genes. Aged skin showed a dampened number of DEGs; however, the *n* number of this group was lower than the young, which could explain the observed differences in number of DEGs. For this reason, differential gene expression was also determined without donors from study 1 included, resulting in a dataset with equal *n* number and no batch effect. This analysis demonstrated a repetition in the trends observed (appendix II).

A pooled analysis was also performed in which aged and young donors were combined and DEGs following UVR challenge were determined. In this way, a greater number of DEGs were identified that showed consistent changes in both age groups, amounting to 1,050 DEGs (Table 4.5). Of these analyses, there was substantial overlap in the identified DEGs (see Venn diagram, appendix III). Unsupervised hierarchical clustering of samples based on the 1,050 genes undergoing differential expression following UVR challenge successfully sorted 70% of the samples into UVR challenged or unirradiated control groups (Figure 4.12). The non-sorted samples represent those from the pilot study, which again indicated the presence of a batch effect. In addition, samples from the follow-up study that sorted incorrectly were paired with their respective control sample, indicating there were also donor differences present that out-weighed the response of these individuals to UVR challenge.

Table 4.5: Differentially expressed genes identified following UVR challenge in young and in aged skin

	Age group		
	Young	**Aged**	**Young and aged**
n	17	12	29
Upregulated #	177	32	608
Downregulated #	109	44	442

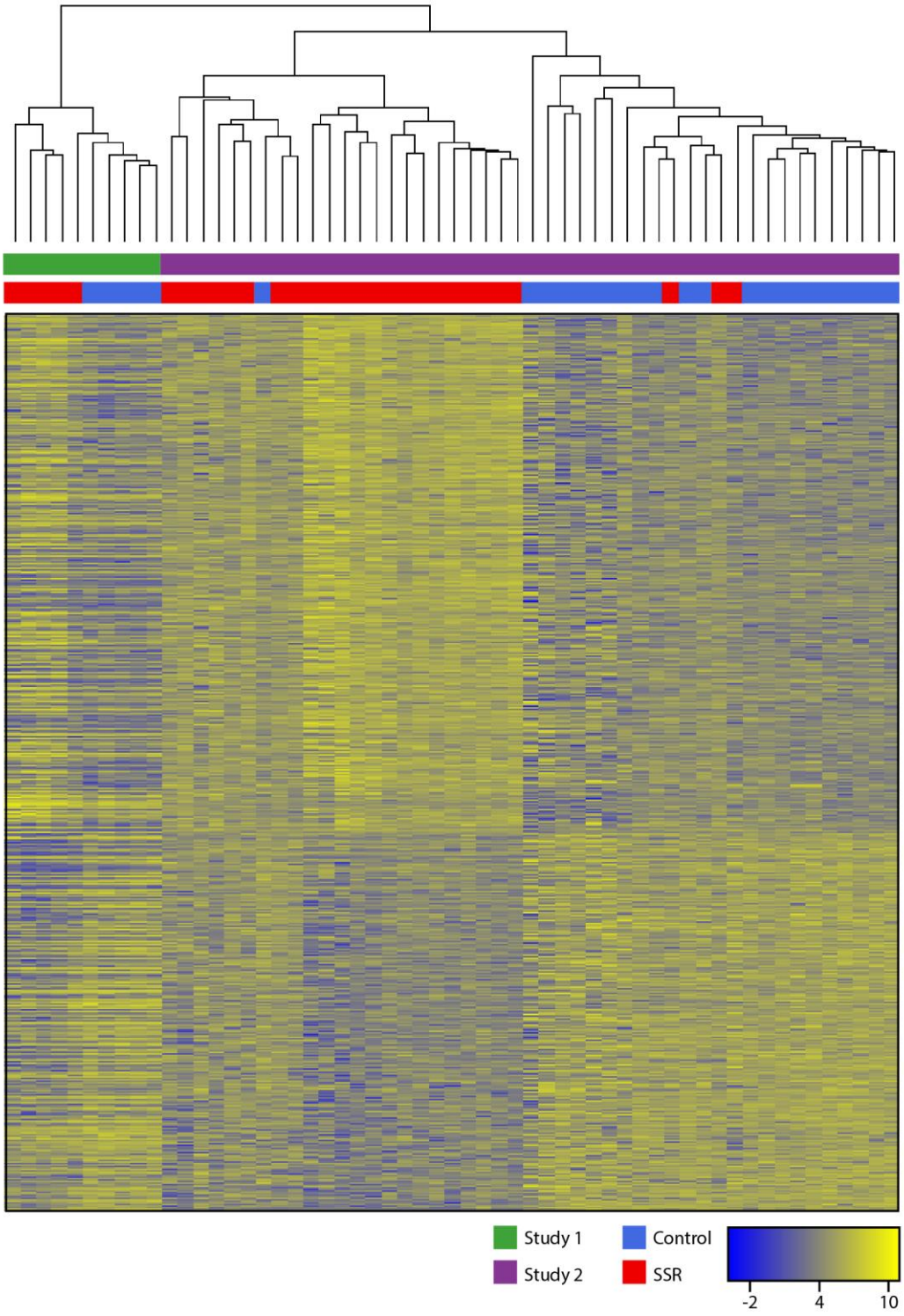

Figure 4.12: Unsupervised hierarchical clustering of 1,050 differentially expressed genes identified following 5 days of sub-erythemal UVR challenge.

irradiated and uniraidated controls are indicated by the red and blue blocks (red, SSR; blue, control). Each row represents a differentially expressed gene expressed in log of counts per million (logCPM) where a high epxression is indicated by yellow and low expresison by blue as per the key. Samples are represented by columns.

4.4.3.1 Differentially expressed genes are overrepresented in GO terms associated with cell cycle and repair while aged skin shows reduced representation

Young and aged skin showed substantial differences in the number of DEGs identified following UVR challenge, which was suggestive of a dampened transcriptional response in aged skin. The top 500 genes by significance value in the different age groups following UVR challenge were annotated with GO terms. In comparison to young skin challenged with UVR, the aged group displayed fewer terms, and substantially higher p-values, consistent with fewer genes supporting the terms. In young skin challenged with UVR, the GO terms identified were related to the cell cycle, p53-mediated damage response and pigmentation (Figure 4.13)

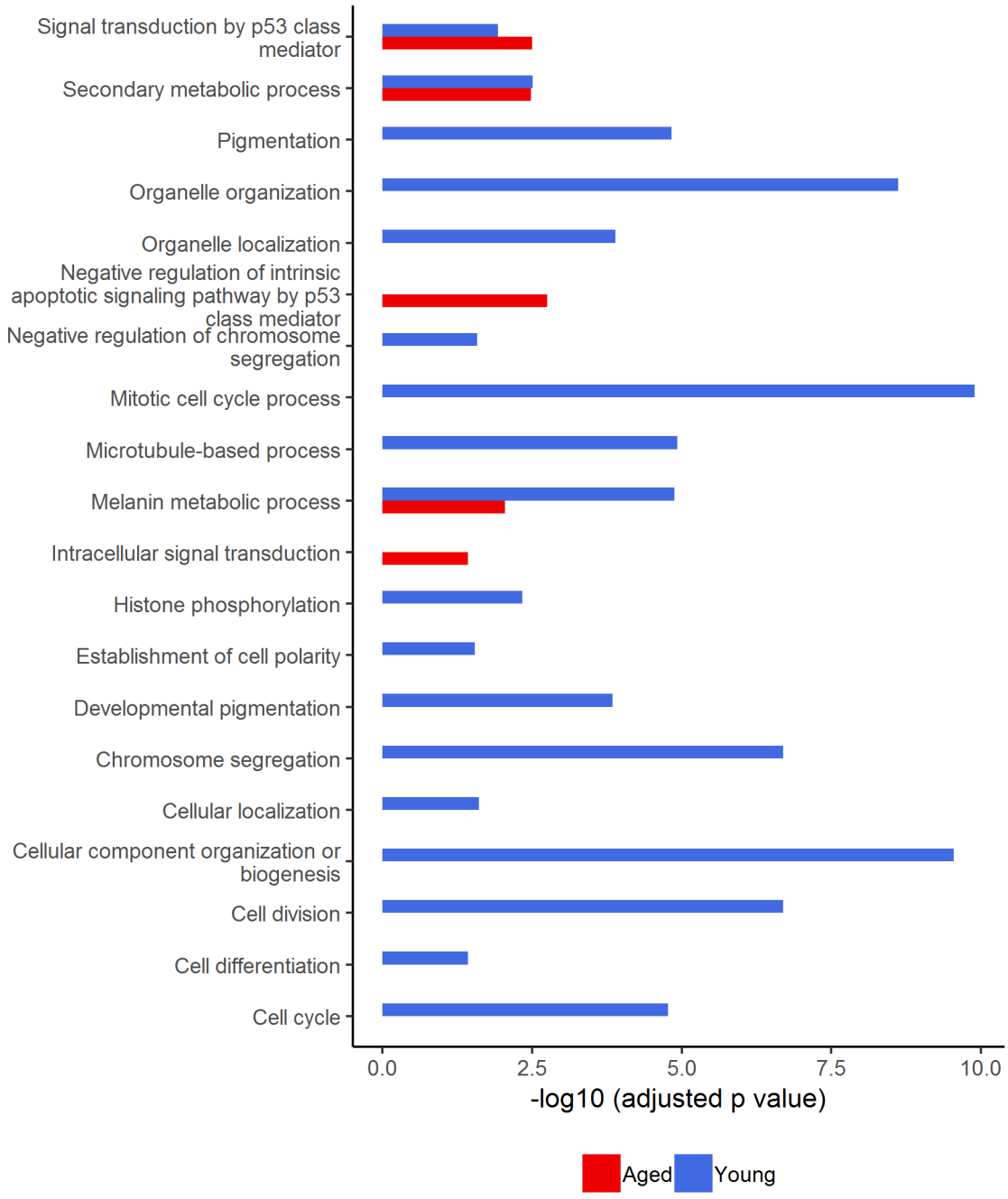

Figure 4.13: Differences in GO term enrichment in the response of young and aged skin to UVR challenge.

The 500 most significantly differentially expressed genes identified in each age group following UVR challenge were annotated with GO terms using GprofileR. The negative log10 p values of overrepresented terms are shown. Red, aged; blue, young.

4.4.3.2 Gene-regulatory effects of differentially methylated sites in distal regulatory elements can be predicted using an independent dataset

As DNAm changes occurred preferentially in open seas (Figure 4.10), which are often many kb away from a transcriptional start site of a gene, it is difficult to infer the effect of changes in DNAm upon gene transcription. To investigate the connectivity between distant DNAm sites and gene expression, an independent dataset was used –Bormann *et al.* (2016) – in which DNAm and matched RNA transcriptional profiles were generated.

Of 1,704 DMPs identified using the EPIC array in our study following UVR challenge, only 327 were measured on the previous 450K array used in the Bormann *et al*. (2016) study. Pairwise Spearman correlation coefficients were generated between these 327 DNAm sites and all of the potential gene targets for which donor-matched expression levels had been determined. Where the correlation exceeded ≥0.5 or ≤-0.5 in this independent dataset, the gene was assessed in our 3' mRNA sequencing for differential expression following UVR challenge. There were 1,224 mRNAs, detected in both Bormann and our 3' mRNA sequencing, that were within this cut-off. These genes were overrepresented in the list of DEGs determined following UVR challenge (159 genes, odds ratio = 1.7, $p = 1.314 \times 10^{-11}$), suggesting that changes in DNAm may be occurring in distal regulatory sites, and impacting upon gene expression many kb away.

4.5 Discussion

There are three major findings of this study: first, that sub-erythemal UVR challenge (40% or 80% MED) applied daily for 5- or 10-days was sufficient to induce changes in DNAm and gene expression in the epidermis. Secondly, that the changes in DNAm in the young and aged cohorts are consistent; however, the number and magnitude is greater in the epidermis of aged individuals. Finally, alternative transcriptional pathways are activated in young and aged epidermis following UVR challenge. These findings will now be discussed in greater detail.

The UVR exposure regimens trialled in five young individuals identified only subtle changes in DNAm, which nonetheless overlapped significantly with those identified in a reanalysis of DMPs between the forearm and upper inner arm in the Vandiver *et al*. (2015) dataset. Often, several thousand DNAm sites are queried in epigenome-wide studies. As such, the severity of correcting for this many statistical tests may not detect subtle changes in DNAm amongst small sample sizes. Therefore, this pilot study may have been underpowered.

Therefore, DNAm changes were investigated in a larger cohort study, comparing changes in the epidermis of young and aged volunteers to UVR challenge. While in the pilot study the failure to identify DMPs using a FDR cut-off of five percent was hypothesised to be due to the small sample size used, strong DNAm changes were also not detected within the young cohort in the follow-up study in response to UVR challenge. However, DMPs were detected in the aged cohort following UVR challenge, and in an analysis that pooled the two age groups together. That DNAm changes could be identified in the aged cohort but not the young in the age-stratified model was a surprising result for several reasons. Firstly, the aged cohort was of a lower *n* number than the young. Secondly, the average MED of the aged cohort was lower than that of the young, although this was suggestive only of a trend (T-test; $p = 0.08$). This meant that the aged cohort received an average dose of UVR that was 3 mJ cm^{-2} lower than that of the young cohort. Indeed, studies as early as the 1980's identified an increase in sun sensitivity as a feature of ageing skin, exemplified by a decrease in the dose of UVR eliciting erythema (the MED) (Amblard et al., 1982). Therefore, giving a dose of

UVR tailored to each person was an extremely important aspect of the study design, rather than a fixed dose for all volunteers, which may have meant the aged cohort experienced more severe damage in regard to, for example, oxidative stress and DNA damage. This may, in turn, have confounded the observed differences in DNAm.

The analyses that pooled the two age groups together was suggestive of there being DMPs that were common between young and aged skin upon UVR challenge, but that the magnitude of change at these DNAm sites was greater in the aged group, pushing these sites over the significance threshold in the age-stratified analyses of this group but not in the young. Indeed, our analyses revealed that of the DMPs in the combined age comparison, the hypomethylated probes exhibited a significantly greater reduction in DNAm in the aged epidermis than the young, by a mean of two percent (section 4.4.2.3). This suggests that aberrations do not accumulate linearly over a lifetime, but that aged skin is inhibited in its ability to protect its epigenome from UVR challenge and acquires these changes abruptly upon UVR challenge. To our knowledge, this represents the first study to identify a significantly divergent epigenetic and transcriptional effect in the skin occurring as a function of age.

A similar observation has been made in a study investigating the contribution DNAm differences in ageing to cardiovascular disease (Xiao et al., 2018). Both sexes were shown to acquire DNAm changes steadily before 30 to 40 years of age. At 290 DNAm sites, females continued to acquire only small changes in DNAm with increasing age, while males experienced an abrupt acquisition of DNAm changes that occurred in middle age. Further examination of reported lifestyle differences between males and females supports the notion of environmental stressors contributing to these differences: of the 290 DMPs accelerated in acquisition in middle aged men versus women, 70 and 51 DMPs were also different in a study of drinkers and non-drinkers (Philibert et al., 2014) and smokers and non-smokers (Dogan et al., 2014), respectively. Well-documented lifestyle differences between the sexes are recognised to contribute to the development of cardiovascular disease an average of 7 to 10 years earlier in males (Valkonen & Van Poppel, 2004; Maas & Appelman, 2010). While this cardiovascular disease study focussed primarily on the sexual dimorphic acquisition of

DNAm changes, the sudden acquisition of DNAm differences in middle age is reminiscent of the changes that occurred in aged but not young skin upon UVR challenge, adding weight to the hypothesis that the effect of a lifetime of environmental stressors is brought to bear in later life.

The DMPs identified following UVR challenge were heavily skewed towards a loss of DNAm (at a ratio of 30:1 hypomethylated sites for every hypermethylated site identified), that recapitulated findings by Vandiver *et al*. (2015), of large blocks of hypomethylation in the chronically photoexposed forearm which overlapped those identified in cancerous tissue, and later shown in aged tissue (Zhou et al., 2018). Hypomethylation has been shown in around half of the genome, in PMDs characterised by low gene density, low GC-density, late replication timing and localisation at the nuclear lamina (Bergman & Cedar, 2013; Quante & Bird, 2016). While the mechanisms that lead to hypomethylation remain poorly understood, a number of hypotheses have been presented. For one, the maintenance methyltransferase, DNMT1, has been shown to methylate sites less efficiently in CG-poor regions, while the presence of methylated CpG sites in close proximity allosterically increases its activity in CG-dense regions (Hermann et al., 2004).

Furthermore, it is hypothesised that the replication of these regions late in S phase leaves little time to re-establish DNAm patterns (Zhou et al., 2018). Therefore, hypomethylation may act as a mitotic clock that measures the rate of cellular division (Zhou et al., 2018). Given that UVR leads to hyperproliferation of the epidermis sun-exposure could accelerate this clock, which reflects an increase in the cell proliferation markers Ki-67 and proliferating cell nuclear antigen-(El-Abaseri et al., 2006).

It is also possible that lower levels of DNMTs in aged skin, coupled with the aforementioned mechanisms, would lead to an increased loss of DNAm in these regions. This would need to be confirmed by examining the protein levels of the DNMTs in aged and young skin, which would be possible using immunofluorescence staining for these proteins in the tissue collected in this study. In addition to aberrations in the levels and activity of DNMTs, loss of DNAm could be due to alterations in the availability of the methyl donor, SAM. As the regions undergoing

hypomethylation are late-replicating, it is tempting to assume that the methyl donor, SAM, becomes depleted, and its product, SAH, becomes elevated. It has previously been shown that a decreased ratio of SAM/SAH in the cell leads to inhibition of DNA methyltransferase activity (Garcea et al., 1989). It could be that aged cells are unable to restore the ratio of SAM:SAH as efficiently as young cells.

Furthermore, SAM, which is biosynthesised during one carbon metabolism (Figure 4.14), may be affected by the availability of intermediates in the folate and methionine cycles. *In vitro* data have demonstrated that human plasma exposed to UVA radiation has a reduced folate concentration (Branda & Eaton, 1978). In addition, 5-methyltetrahydrofolate, the main circulatory form of folate, is degraded by UVB (Steindal et al., 2006), and is sensitive to oxidation by UVR exposure-derived ROS (Tam et al., 2009). Fair-skinned individuals undergoing photochemotherapy also displayed low serum folate concentrations, giving early evidence of folate depletion occurring *in vivo* (Branda & Eaton, 1978). Another study found serum folate is sensitive to seasonal fluctuations of solar UVR; significantly lower levels of serum folate are observed in the summer months, when UVR levels are at their highest (Valencia-Vera et al., 2019). Given that the epidermis is an avascular structure, receiving nourishment from vessels in the underlying dermis, the inefficient delivery of micronutrients such as folate, and its potential degradation upon UVR exposure, suggests that serum folate deficiencies would be equal, if not exacerbated, in the epidermis of UVR-exposed skin. While there is currently a dearth of information regarding one-carbon metabolism reactions in skin, determining the degree of folate depletion in skin cells may, in part, explain the propensity of photoexposed skin to be globally depleted of DNAm.

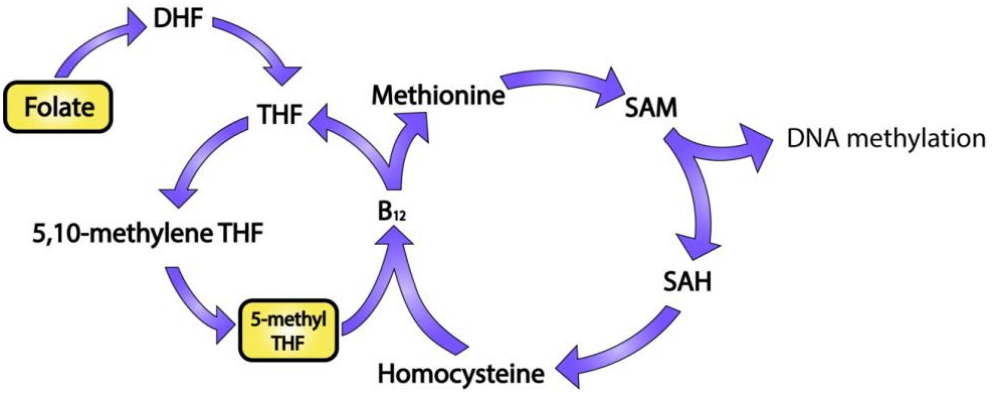

Figure 4.14: One-carbon metabolism and its photosensitive intermediates.
DNA methyltransferases utilise S-adenosyl methionine as a methyl donor, forming S-adenosylhomocysteine (SAH). SAH is enzymatically converted to homocysteine, which can be remethylated, forming methionine, using a methyl group from 5-methyltetrahydrofolate (5-methyl THF) and utilising vitamin B12 as cofactor. Experimental and *in vivo* evidence suggests folate and 5-methyl THF are sensitive to photodegradation (see text for details).

DNA hypomethylation has long been proposed to allow the aberrant expression and transposition of retroelements, which cause chromosomal aberrations at the point of insertion. Tumors with greater amounts of hypomethylation had more LINE-1 insertions, in 8 of 9 cancer types analysed (Zhou et al., 2018), showing a concurrent enrichment of LINE-1 breakpoints in the hypomethylated region (Zhou et al., 2018; Lee et al., 2012). Although this evidence is only correlative in nature, it serves as a potential connection between DNAm-related photoexposure and a process directly linked to cancer initiation by transposition of retroelements in the genome.

In addition to the DNAm changes observed in the epidermis following UVR challenge, substantial changes in transcription were observed. In the pilot study, a time-dependent increase in the number of DMPs identified was observed, with the greatest number observed at 10-days of UVR. Contrarily to this observation, the greatest transcriptional response occurred at 5-days of UVR challenge. This suggests that the main transcriptional response to UVR challenge is not controlled by DNAm, but

possibly by signalling pathways that lead to rapid changes in gene transcription (El-Abaseri et al., 2006). The lower number of genes identified in our 10 day analysis could suggest that the skin has become 'tolerant' to the level of UVR exposure delivered.

Human skin has developed two main defence mechanisms to guard against the damaging effects of UVR: epidermal thickening and an increase in pigmentation. The ability to adjust melanin content of epidermal cells after UV exposure is based on the individual's melanogenic potential. 'Tanning' is readily apparent two to three days after UVR exposure, resulting from an increase in the number and activity of functional melanocytes, and increased synthesis and transfer of melanosomes (Brenner & Hearing, 2008). UVB-induced tanning is photoprotective (estimated sun protective factor of 3). The WS analysis highlights that melanin deposition is increased in a dose and time-dependent manner, acting to protect against subsequent UVR exposure. As the higher dose of UVR (80% MED) induced a greater increase in melanogenesis, it may be that the UVR is dispersed to a greater extent as compared to the lower dose, leading to less damage (as confirmed by the number of 8-OHdG positive cells) and therefore less of a signal to induce transcriptional changes. Similarly, the amount of melanin is greater at 10 days versus 5 days, which may prevent the skin from responding to subsequent exposure in the 10 day time-point as compared to 5 days.

These observations could in-part explain the few transcriptional changes identified in our study as compared to Choi *et al*. (2010). The statistically strongest overlap in this comparison was with our 10 day analyses, particularly the 80% dose, which represents the closest experimental protocol as the Choi *et al*. (2010) study. However, a lower number of DEGs were identified in our 10 day analyses. This may be due to the UVR regimen used. Choi *et al*. (2010) used a low dose of UVR for the first five days of UVR exposure, increasing the dose in the second week from 40% to 60% MED, which likely posed a continuous challenge to the skin.

The follow-up study, recruiting young and aged individuals, confirmed the strong transcriptional response in young individuals, which occurred at 5-days of UVR challenge in the pilot study. Interestingly, more DEGs were identified in young skin following UVR challenge as compared to the aged group, which was confirmed in a

comparison using equal *n* number in the two groups (appendix II). This further supports the notion that DNAm is not the major causative factor in eliciting changes in gene expression, as the young group exhibited reduced amount of DNAm changes but a greater amount of DEG. What drives the divergent transcriptional response in young and aged skin has not previously been investigated. It is possible that changes in DNAm in the aged epidermis that occur during the natural course of intrinsic ageing may partly explain the observed differences in transcription following UVR challenge. Therefore, the next chapter will explore differences in the unirradiated baseline DNAm profiles of these two age groups.

Chapter 5: The interaction of the ageing DNA methylome and UV radiation challenge

5.1 Introduction

The over-arching aim of this thesis is to assess the interaction of intrinsically-aged skin and its response to UVR challenge. Epigenetic changes in intrinsic ageing have been reported extensively in almost all tissues (Zhou et al., 2018). Two mechanisms have been identified: the first, accumulation of DNAm noise (Tan et al., 2016; Fraga et al., 2005) and, second, predictable and site-specific DNAm changes (Bocklandt et al., 2011; Hannum et al., 2013; Koch & Wagner, 2011; Garagnani et al., 2012; Bekaert et al., 2015; Horvath, 2013; Horvath et al., 2018). The latter represents a promising molecular marker that is affected by endogenous or exogenous factors, meaning it may represent a prognostic marker of biological ageing (reviewed in Horvath & Raj, 2018).

Ageing-associated changes in DNAm have also been investigated in the skin. Other studies have compared DNAm using bisulphite sequencing (Raddatz et al., 2013) and 450K arrays (Bormann et al., 2016), using samples obtained from the forearm, leading to confounding by photoexposure-related changes. The photoprotected upper inner arm from different ages have also been compared, using Illumina Infinium 27K (Grönniger et al., 2010) and 450K arrays (Vandiver et al., 2015). Without the confounding effect of photoexposure, these studies provided early evidence of a trend towards hypermethylation in aged skin, occurring in both the epidermal and dermal compartment.

The study reported herein, to our knowledge, represents the highest genomic coverage EWAS from non-pooled samples. Furthermore, samples in this study were exclusively collected from the photoprotected buttock, meaning differences identified are not confounded by photoexposure. It is possible that DNAm changes in intrinsically-aged skin impair phenotypic plasticity, preventing adequate adaptation to the environment. However, experimental evidence of this has remained elusive. The epigenetic response of these same individuals to UVR challenge was explored in

chapter 4, and it would benefit these analyses to understand the differences in the baseline epigenetics of the two age cohorts.

5.2 Objectives

The hypothesis to be investigated in this chapter is that aged skin accumulates epigenetic abnormalities at the level of the DNA methylome and transcriptome. Furthermore, that these changes inhibit the phenotypic plasticity of the skin, partially explaining divergent response to UVR challenge across age cohorts observed in chapter 4. The specific objectives are as follows:

1. To utilise the DNAm profiles generated in chapter 4 to identify DMPs (section 2.4.2.4) and DMRs (section 2.4.2.5) related to intrinsic ageing of the skin, by comparing the young and aged groups.

2. To identify gene expression changes (section 2.3.4) that occur in the skin due to intrinsic ageing, as for DNAm in objective 1.

3. To use gene set testing methodologies (section 2.3.4.1) to address whether changes in DNAm occurring across CpG islands and/or shores (identified in objective 1) collectively alter gene expression in intrinsically-aged skin (identified in objective 2). Then, to identify top candidate DNAm-linked changes in expression using Spearman correlation analyses. Of the identified genes, perform pathway analyses (section 2.3.4.2) to identify collections of genes affected by both DNAm and mRNA level alterations.

4. Finally, a key objective of this chapter is to address whether DMRs identified in objective 1, which arise due to intrinsic ageing of the skin, subsequently impact the transcriptional response to UVR challenge that was found to be different between the age groups in chapter 4. This will utilise gene set testing methodologies as described previously.

5.3 Results

5.3.1 DNA methylation changes are a major feature of intrinsic skin ageing

DNAm profiles were subjected to principal component analysis in the previous chapter (section 4.4.2.1), which demonstrated clear clustering of the young and aged cohort (PC2; Figure 4.6B). As PCs 1 and 2 showed no observable separation of samples based on the sub-erythemal UVR exposure, these samples were included in the following intrinsic ageing analyses to add power to the statistical model.

5.3.1.1 Intrinsic ageing-related DNA methylation changes are skewed towards hypermethylation

A linear regression model identified 48,114 DMPs between age groups (Table 5.1). There was a skew towards hypermethylation (ratio of 1.11:1 hypermethylated: hypomethylated sites). The same model was re-run in the absence of the additional 5 volunteers' DNAm profiles generated in the pilot study to ensure batch variation was not affecting the result. As in the previous analysis, a slight trend of hypermethylation was observed. (Appendix II). Unsupervised hierarchical clustering using these DMPs successfully sorted age groups (Figure 5.1).

Table 5.1: Number of significantly different methylation sites in intrinsic ageing

Group	**Young**	**Aged**
n	17	12
Hypermethylated sites #	24,913	
Hypomethylated sites #	22,421	
Ratio Hyper:hypo	1.11:1	

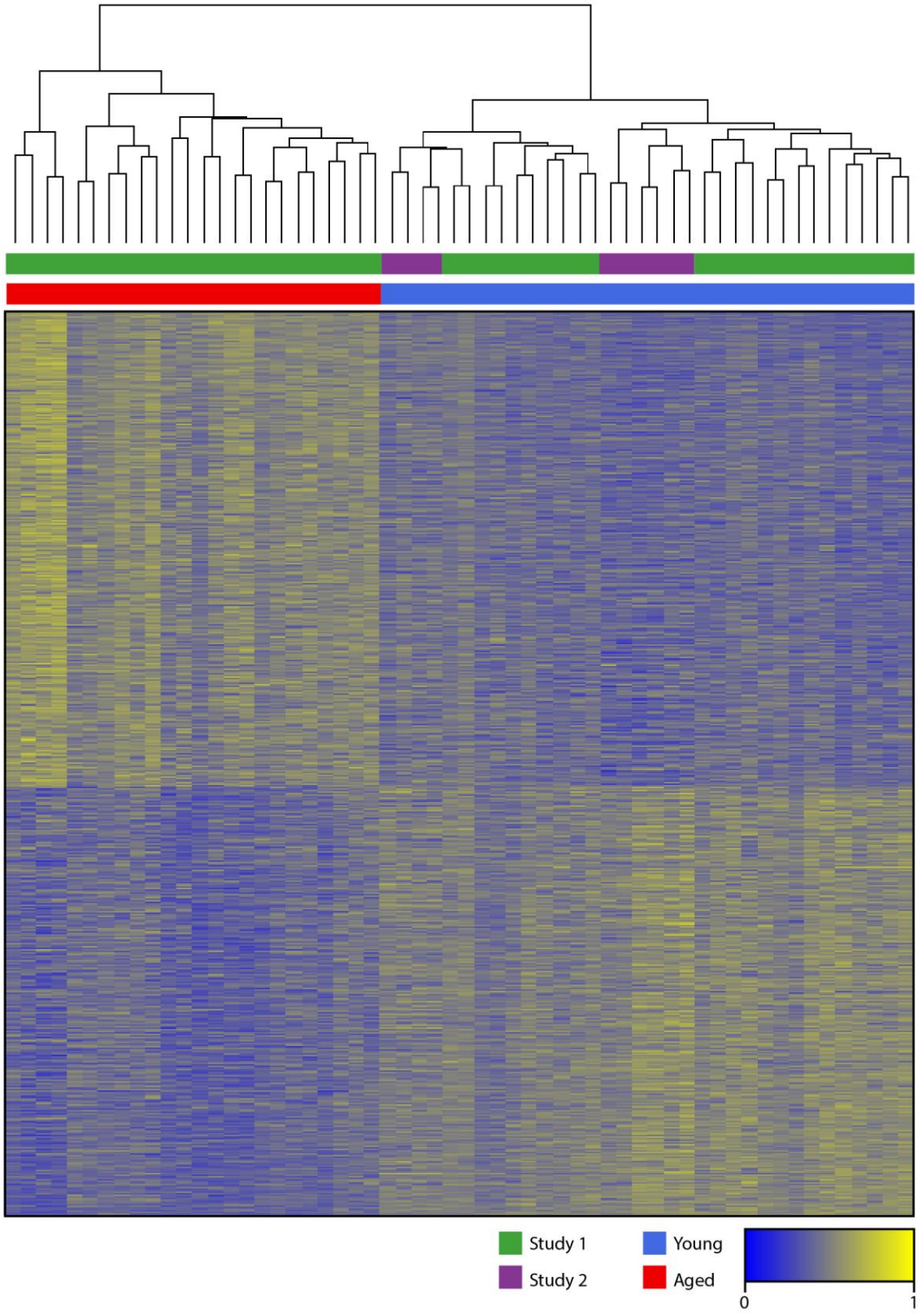

Figure 5.1: Unsupervised hierarchical clustering of 48,114 DMPs between age groups. Age group is indicated by the blocks (young, blue; aged, red). Study number is also indicated (study 1, green; study 2, purple). Each row represents a DMP as per the key (methylated, yellow; unmethylated, blue). Samples are represented by each column.

5.3.1.2 Age-associated differentially methylated sites are enriched in discrete genomic regions

The genomic location of CpG sites has a major role in determining their function. The genomic distribution of the DMPs identified between age groups were assessed, distinguishing between CpG islands, shores (the 2,000 bp regions flanking CpG islands), shelves (the 2,000 flanking the shore) and isolated CpG sites (open seas; CpG sites >4,000 kb from a CpG island) (Figure 5.2). As compared to the distribution of CpG sites queried on the EPIC array, DNAm sites found to be hypermethylated with age were enriched in both the north and south shores ($p < 0.001$, odds ratios [ORs] = 1.23 and 1.21, respectively) and were impoverished at islands ($p < 0.01$, OR = 0.96), north and south shelves ($p < 0.001$, ORs = 0.78 and 0.85, respectively) and open seas ($p < 0.001$, OR = 0.94). Sites hypomethylated with age were enriched in open seas ($p < 0.001$, OR = 1.31), both north and south shores ($p < 0.001$, ORs = 1.43 and 1.5, respectively) and shelves ($p < 0.001$, ORs = 1.34 and 1.24, respectively).

A feature of ageing tissues is large-scale loss of DNAm in regions collectively labelled PMDs (section 1.5.1). These are late-replicating regions that have been shown to overlap with the nuclear lamina. The hypomethylated probes in the intrinsically-aged comparison, however, were not significantly enriched in LADs as determined ina fibroblast cell line (Guelen et al., 2008). In fact, they were underrepresented in these regions (OR= 0.735, p value= 2.2×10^{-16}). This could be an artefact of using a fibroblast cell. However, *in vivo* studies have shown enrichment of hypomethylated sites in LADs, albeit only in the photoexposed epidermis of aged study participants and not photoprotected epidermis (Vandiver et al., 2015). Another study identified so-called "solo WCGWs" (Zhou et al., 2018), representing a series of CpGs flanked by either an A or T on each side, which have been shown to undergo preferential hypomethylation in almost all healthy tissue types, suggesting that the local sequence context may impact LAD demethylation. Of these sites covered on the epic array (26,733), of 22,421 hypomethylated sites in ageing, 1,652 were overlapping. This overlap was highly significant (OR= 2.254, p value= 2.2×10^{-16}).

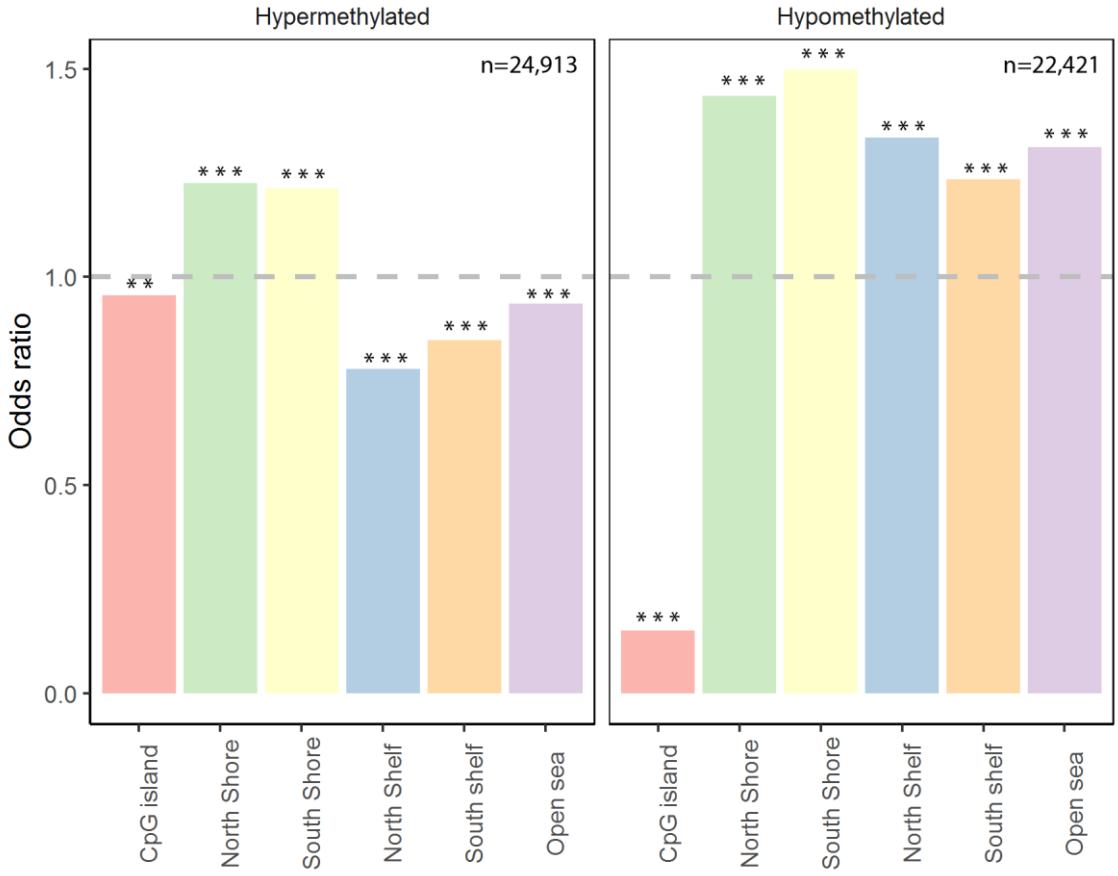

Figure 5.2: Genomic annotation of 47,334 DMPs with age in the CpG island, shore, shelf and open sea context.

Odds ratios were determined by Fisher's exact test for 24,913 hypermethylated DNAm sites and 22,421 hypomethylated sites (B). The dashed line indicates an odds ratio of 1 (no enrichment). Asterisks indicate level of significance, where P < 0.05, *; P < 0.01, **, P <0.001, ***.

5.3.1.3 Differentially methylated regions were abundant in intrinsically-aged skin

DMRs, which comprise coordinated changes in DNAm across multiple, consecutive sites, could represent regions involved in gene transcriptional regulation more so than singular DMPs. Using the DMRcate method (section 2.4.2.5), 15,069 regions, encapsulating at least 2 CpG sites, exhibited a ≥5% increase in DNAm in aged skin (Table 5.2). A frequency histogram of the number of DMRs and the number of DNAm sites they contain is shown in Figure 5.3, demonstrating that there were more than

twice as many hypermethylated DMRs that contained a higher number of DNAm sites (≥20 CpG sites) than hypomethylated DMRs. The identified DMRs were sorted by adjusted P-values, as determined using Stouffer's method (Riley et al., 1949; Peters et al., 2015). The top three DMRs overlapped with the CpG island and/or shore of ZIC1, FOXG1 and NEFM (Figure 5.4).

Table 5.2: The number of DMRs identified between age groups

Group	**Young**	**Aged**
n	17	12
Hypermethylated regions #	7,842	
Hypomethylated regions #	7,227	
Ratio Hyper:hypo	1.08:1	

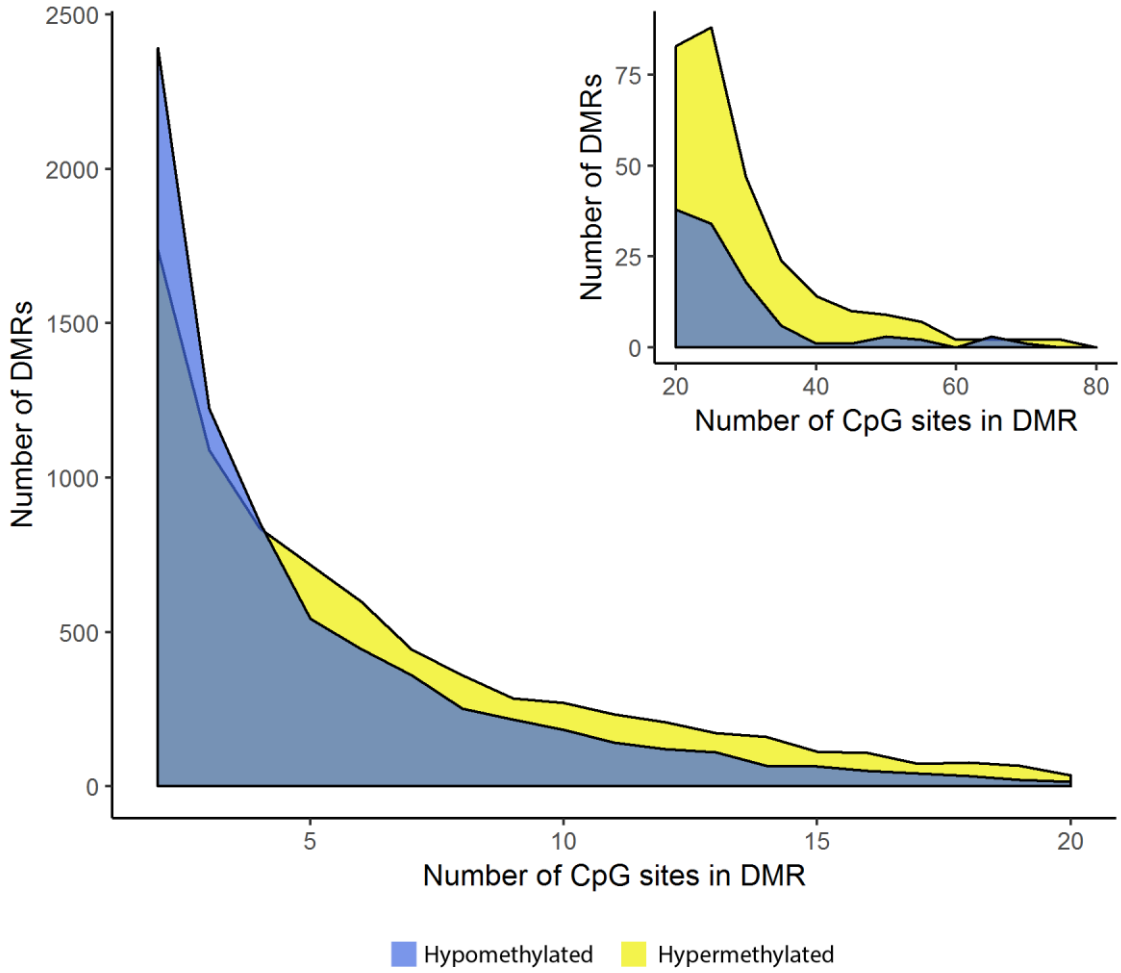

Figure 5.3: Number of DNAm sites in the identified DMRs between young and aged groups.

Smoothed frequency histogram showing the number of hypomethylated (blue) and hypermethylated (yellow) DMRs and the number of DNAm sites involved. Inset shows DMRs with high numbers of involved CpG sites, shown on separate axes to aid visualisation.

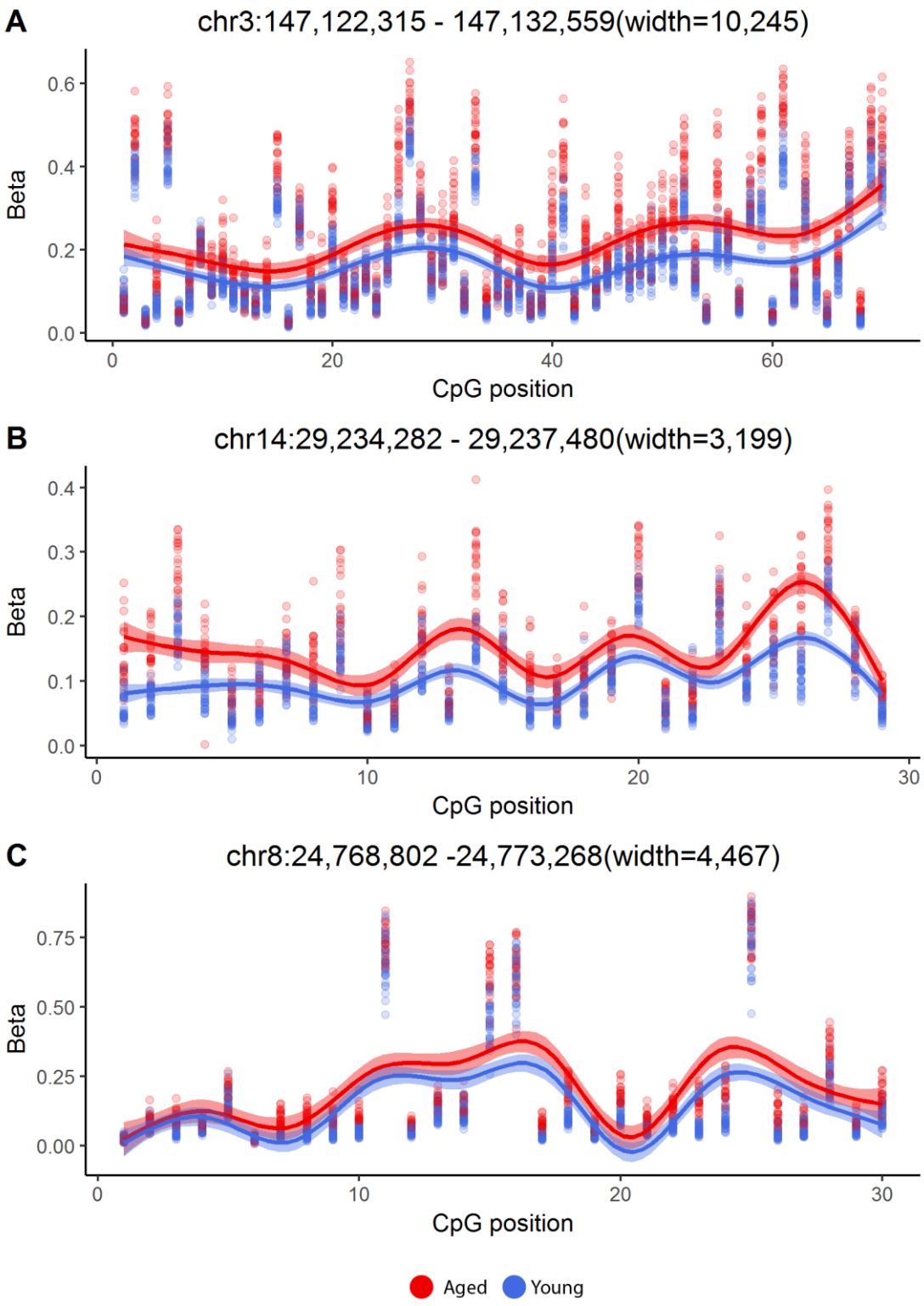

Figure 5.4: The top 3 significant DMRS between age groups.

DMRs were identified using the DMRcate method and were ranked by Stouffer. Shown are (A) ZIC1, (B) FOXG1 and (C) NEFM. The X-axis indicates the position of a CpG site within the DMR. Chromosome and genomic coordinates of the DMR are indicated above each plot.

5.3.2 The intrinsically-aged skin transcriptome is relatively stable

Whether transcriptional differences were also present between the age groups was also investigated within the 3' mRNA sequencing dataset, which was introduced in chapter 4 (section 4.4.3). In the previous chapter, PCA of the transcriptional profiles of young and aged individuals, irradiated and unirradiated with UV, was performed (section 4.4.2). Principal component 3 captured the variation associated with both age and UVR challenge, whereby aged samples clustered lower on the Y-axis than their young counterparts (Figure 4.6B).

The DEGs between the age groups were determined using *Limma*. In this analysis, only 29 DEGs were identified (10 upregulated, 19 downregulated), which demonstrated the relative stability of the intrinsically-aged skin transcriptome (Table 5.3). Of the other DEGs, 3 represented uncharacterised novel transcripts whose function remains unknown. As previously stated, the analysis reported included study participants recruited to a larger follow-up study, and five donors that participated in the pilot study. To ensure the batch effect was adequately controlled in the linear model, the model was re-run in the absence of transcriptional profiles from donors in the pilot study. As expected, the reduction in *n* number resulted in detection of fewer DEGs. However, the number and the genes identified were similar (appendix II).

The 29 identified changes in expression were used to perform unsupervised hierarchical clustering. This analysis identified two main groups including 24 of the young samples (inclusive of control and UVR challenge; Figure 5.5, left side) and a second major group inclusive of all of the aged samples, interspersed with a fewer number of young samples (Figure 5.5, right side).

Table 5.3: Number of differentially expressed genes between age groups

Group	**Young**	**Aged**
n	17	12
Upregulated #	10	
Downregulated #	19	

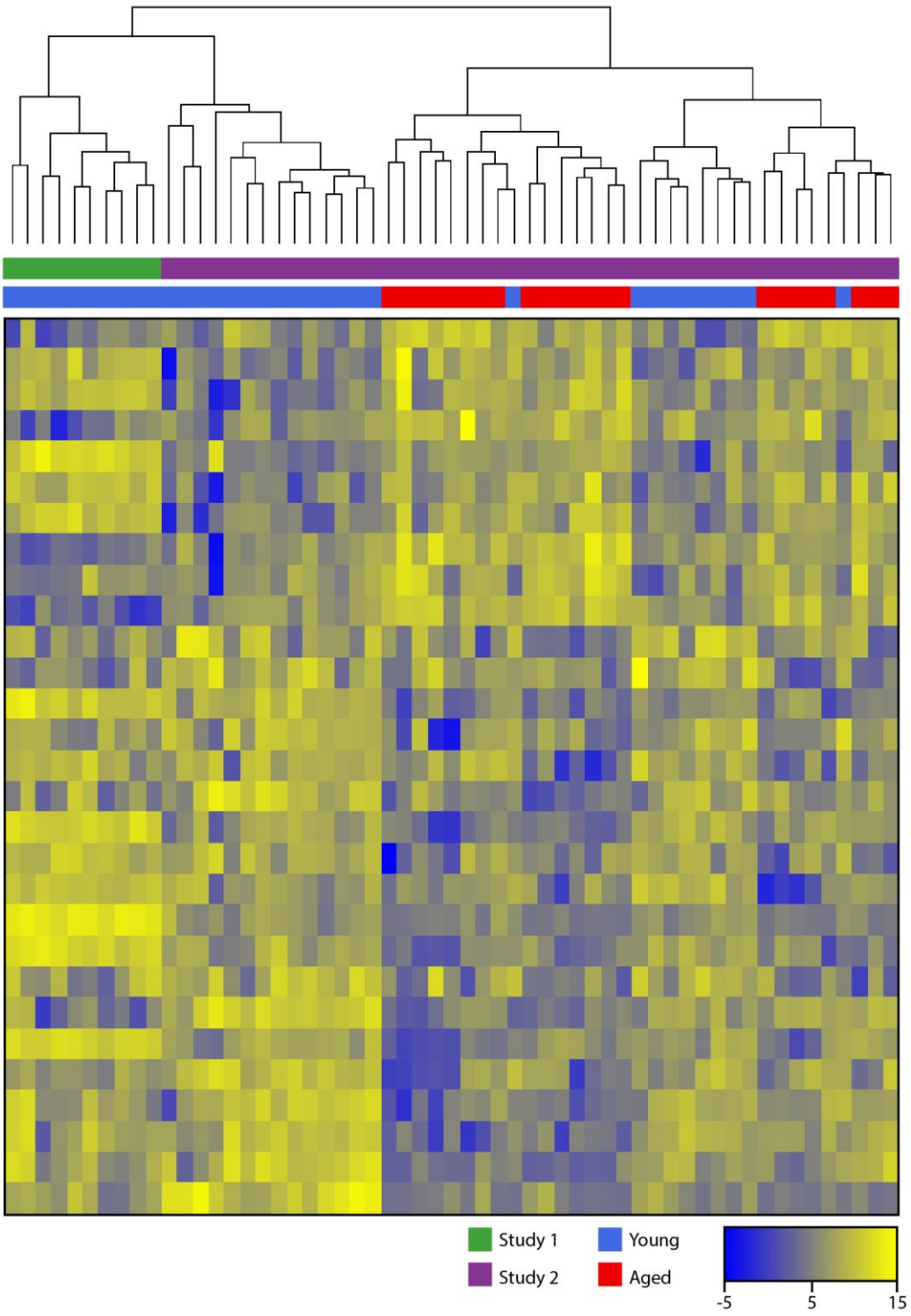

Figure 5.5: Unsupervised hierarchical clustering of 29 differentially expressed genes identified between age groups.

Samples are represented by the columns, with age group indicated (young, blue; aged, red). Study number is also indicated (study 1, green; study 2, purple). Each row represents a differentially expressed gene coloured by logCPM (counts per million; high expression, yellow; low expression, blue).

5.3.3 Differential DNA methylation is significantly linked to gene expression in intrinsically-aged epidermis

The DEG analysis revealed very few changes in gene expression between age groups. This could suggest that either the current study is under-powered to detect such changes, or that the skin transcriptome is relatively stable over a lifetime. Yet having observed extensive changes in DNAm within intrinsically-aged skin, their effect on gene expression was further investigated.

The DMRs identified in intrinsically-aged skin overlapped a CGI or shore ±2,000 bp from 5,408 genes' transcriptional start sites. Of these 5,408 genes, 3,159 were identified in the RNA-sequencing performed. The *Limma* function *geneSetTest* was used to determine whether these genes with an associated hypermethylated or hypomethylated DMR were collectively upregulated, downregulated or a mixed mode of regulation was observed, as compared to randomly permuted genes in the dataset (Table 5.4). Genes associated with hypermethylated DMRs in intrinsically-aged skin were found to be significantly down-regulated ($p = 2.457 \times 10^{-15}$). The actively changing proportion of genes was significant, 17.76% ($p = 0.017$). Mixed regulation of genes associated with hypermethylated DMRs in intrinsically-aged skin was even more significant (8.004×10^{-18}), with the active proportion of genes being 25.62% ($p = 0.039$). However, upregulation of genes associated with hypermethylated DMRs in intrinsically-aged skin was not significant using the *geneSetTest* function and the active proportion of these genes was also not significant.

Genes associated with hypomethylated DMRs were also examined: these genes were significantly down-regulated ($p \leq 0.01$), and mixed regulation was even more significant ($p = 2.168 \times 10^{-9}$) by *geneSetTest*. There was no significant proportion of genes up, down or mix-regulated in the non-competitive test, although there was a trend of up-regulation and mixed-regulation ($p = 0.127$ and $= 0.117$, respectively).

The analyses combining both the hypermethylated and hypomethylated DMRs in intrinsically-aged skin was even more convincing, with significantly greater down-regulation and mixed-regulation of genes than randomly permuted genes in the dataset (p value $\leq 1.019 \times 10^{-13}$ and 3.994×10^{-26}, respectively). Collectively, this

suggests that significant regulation of associated genes is achieved through differential methylation of CGIs and shores, yet direction of regulation (whether up- or down-regulated), does not always support the notion of increased methylation equating to downregulation of the associated gene.

Table 5.4: Results of genesettest and roast to determine association of differentially methylated regions (DMRs) with the mRNA expression of nearby gene

				mRNA regulation		
				Downregulated	**Upregulated**	**Mixed-regulated**
DMR	**Hypermethylated**	**Gene set test**	**p value**	2.457×10^{-15}	1	8.004×10^{-18}
		Roast	**Active proportion**	0.178	0.079	0.256
			p value	0.017	0.983	0.039
	Hypomethylated	**Gene set test**	**p value**	0.010	0.990	2.168×10^{-9}
		Roast	**Active proportion**	0.092	0.136	0.228
			p value	0.873	0.127	0.117
	All	**Gene set test**	**p value**	1.019×10^{-13}	1	3.994×10^{-26}
		Roast	**Active proportion**	0.129	0.111	0.240
			p value	0.306	0.693	0.076

Differentially methylated regions between the young and aged cohort were identified and annotated to genes with a transcriptional start site within ± 2,000 bp. The genesettest and roast function within *limma* were used to test whether differential methylation was associated with downregulation, upregulation or mixed regulation of the annotated genes as a group.

5.3.3.1 DNA methylation in intrinsically-aged skin drives changes in the expression of genes enriched in metabolism, stemness and cancer pathways

In order to determine the top candidate genes undergoing purported epigenetic regulation in our dataset, Spearman correlation coefficients were generated between these 3,159 mRNA transcripts associated with a DMR in intirniscally-aged skin, and the maximally changing CpG site within that DMR. There were 651 significantly correlated changes. Of these, 425 were negatively correlated (i.e. methylation associated with lower gene expression) and 226 were positively correlated (i.e. methylation associated with higher gene expression). Figure 5.7 exemplifies the correlation achieved for 6 selected genes, IRX6, H19, SPON2, DPYSL3, DCUN1D3 and MSRB3 which had the highest T-statistic within the intrinsic ageing DEG analysis.

The 651 significantly correlated genes were further subjected to gprofileR analysis and the KEGG pathways in which they were enriched were determined. The downregulated genes were associated with “Metabolic pathways” (33 genes, adjusted p value ≤ 0.039), and up-regulated genes were associated with “Basal cell carcinoma” (8 genes, adjusted p value < 0.003), “Hippo signalling pathway” (12 genes, adjusted p value < 0.004), “Pathways in cancer” (23 genes, adjusted p value < 0.02), “Notch signalling pathway” (6 genes, adjusted p value < 0.029), “Signalling pathways regulating pluripotency of stem cells” (10 genes, adjusted p value < 0.035) (Figure 5.6).

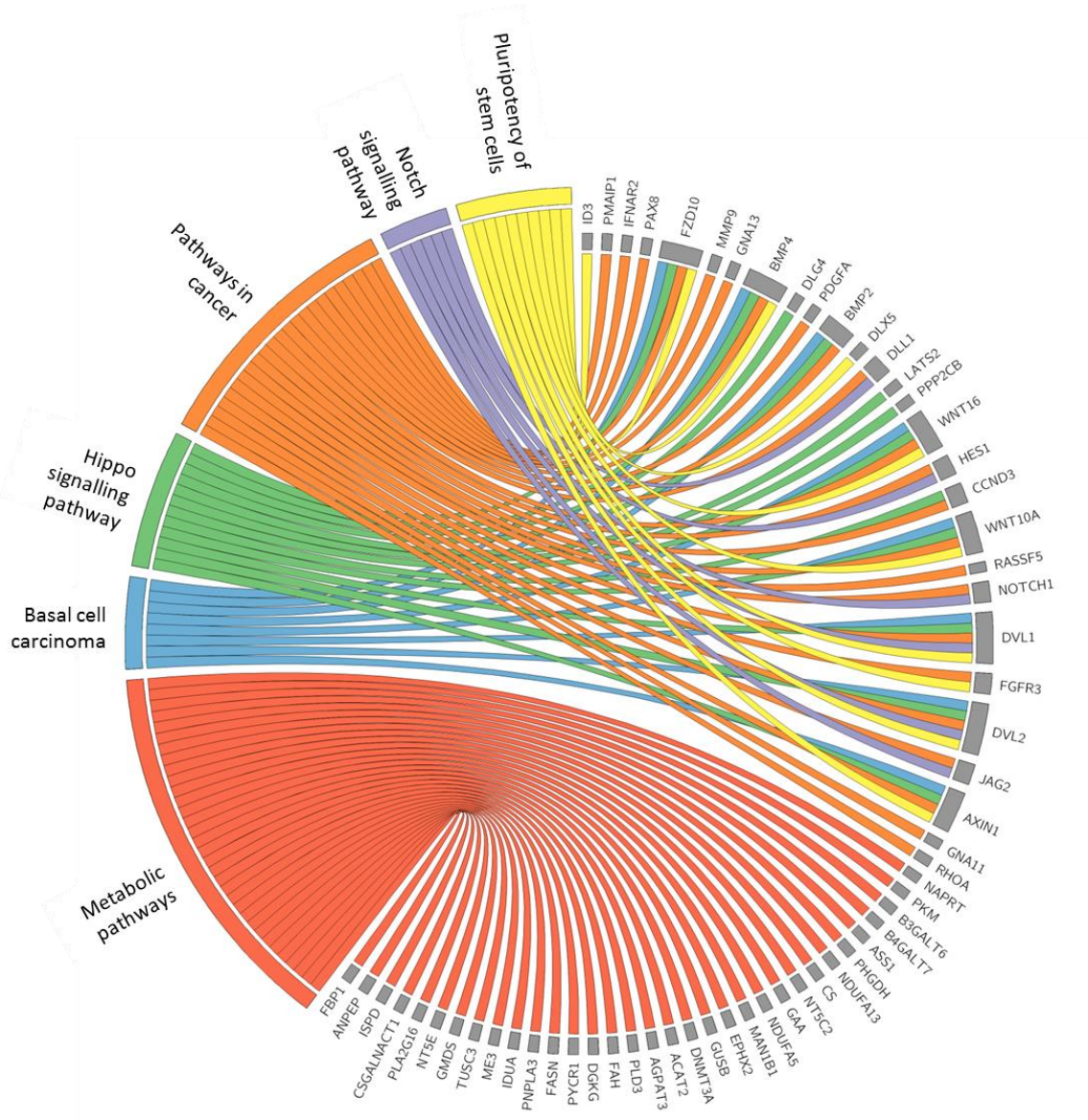

Figure 5.6: Circos plot showing pathway enrichment for genes showing differential methylation and altered transcription in intrinsically-aged skin.

651 genes identified as having significantly correlated DMRs and transcripts in intrinsic ageing were subjected to pathway analysis using GprofileR. Genes are ordered by log2-fold-change in a clockwise manner, whereby up-regulated genes are shown at the top and down-regulated genes are towards the bottom. Ribbons connect genes to the KEGG pathway showing over-enrichment

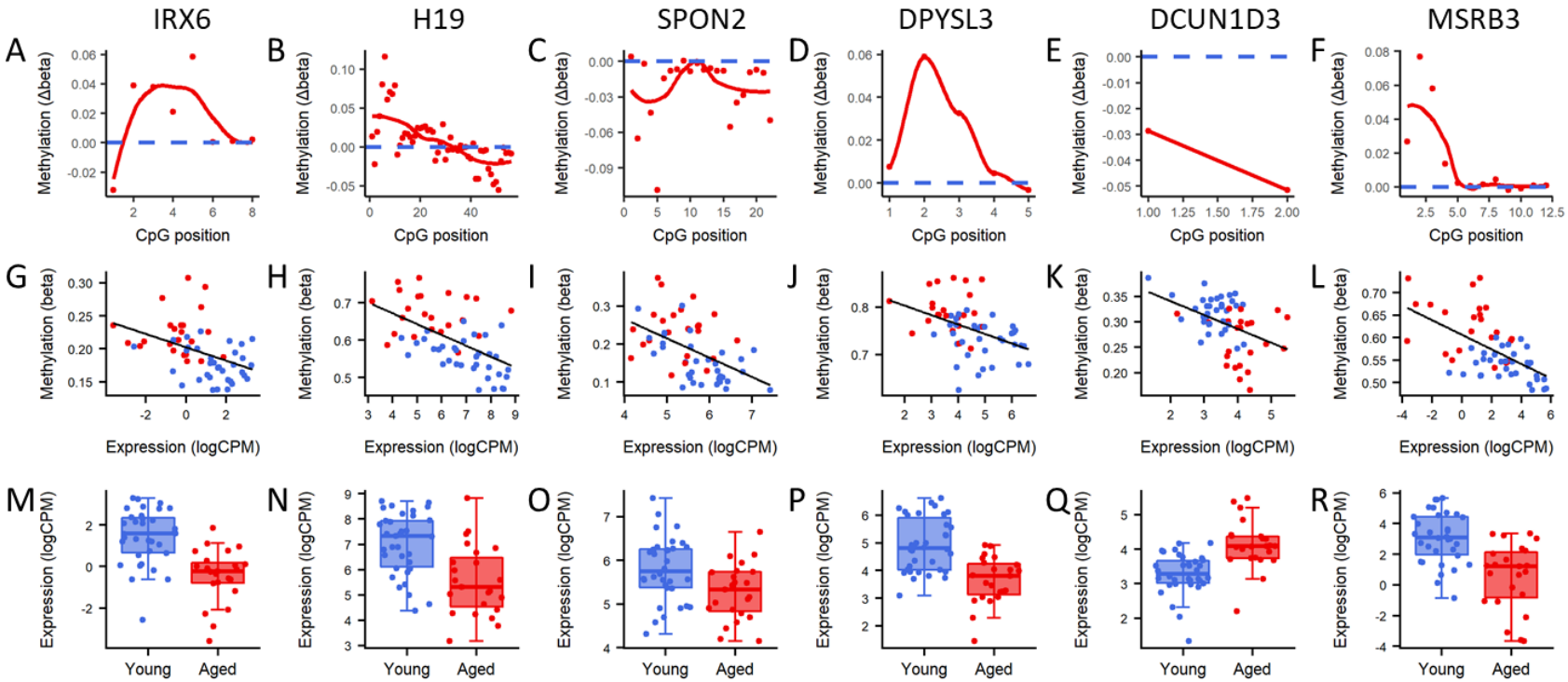

Figure 5.7: Correlation of differentially methylated regions (DMRs) with expression levels of the associated genes.

Shown are six example genes: IRX6, H19, SPON2, DPYSL3, DCUN1D3 and MSRB3. Differentially methylated regions (DMRs) identified using the DMRcate method overlapping a CpG island ±2,000 base pairs of their transcriptional start site (A-F). The CpG with the largest absolute beta fold change associated with the DMR correlates with expression level of the nearby gene (G-L). The identified genes undergo changes in gene expression between age groups (M-R).

5.3.3.1.1 Transcription factor consensus sequence enrichment

As DNAm within gene regulatory regions is typically associated with gene silencing, the 226 positive correlations between DMRs and gene expression in intrinsically-aged skin were surprising. Of this 226, 99 of these genes exhibited an increase in expression in intrinsically-aged skin. It was hypothesised that these 99 genes may share common transcription factor binding motifs, as a recent study identified a number of transcription factors that were insensitive to methylated DNA, or enhanced by it (Yin et al., 2017). GprofileR was used to identify significantly overrepresented sequences within these 99 genes (Figure 5.8). The most significantly enriched motifs were consensus sequences for Myc-associated zinc finger protein (MAZ), Churchill (CHURC1) and Sp1.

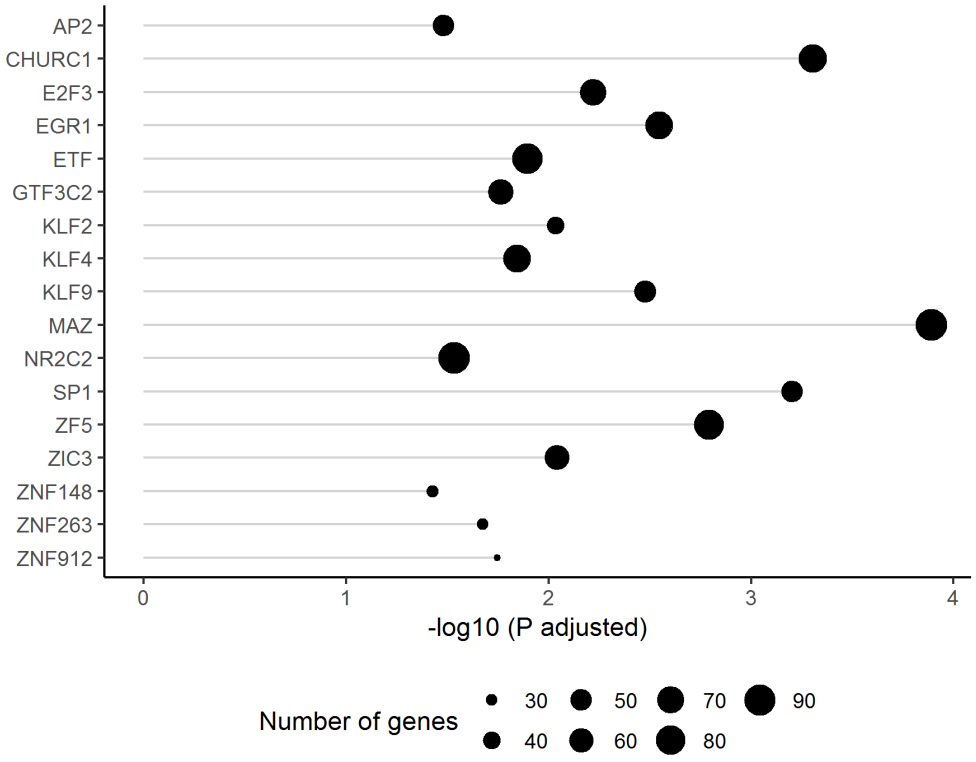

Figure 5.8: Transcription factor enrichment in genes hypermethylated and up-regulated as determined by GprofileR analysis.

Shown are transcription factors with recognition motifs enriched in the 99 genes shown to be hypermethylated and up-regulated in intrinsically-aged skin. The length of the bar indicates the –log10 adjusted p-value for that transcription factor, and circle size indicates the number of genes to which they may bind.

5.3.4 The aged DNA methylome disposes skin to respond poorly to UVR challenge

In the previous chapter, aged skin was shown to have a dampened transcriptional response following UVR challenge that was characterised by failure to activate key UV-responsive pathways.

It was hypothesises that transcripts that change in young skin following UVR challenge, but were dampened in their response in aged skin, are a result of DNAm changes that occur with increasing age. Genes that were associated with a DMR in intrinsically-aged skin were found to be significantly less transcriptionally up-regulated following UVR challenge in aged skin compared to young as compared to randomly permuted genes ($p = 1.055 \times 10^{-14}$). However, they were not additionally down-regulated in aged skin upon UVR challenge ($p = 1$). The top five candidate genes in this analysis are shown in Table 5.5. This suggests that the aged DNA methylome predisposes skin to respond poorly to UVR challenges by inhibiting activation of key UVR-response genes in skin.

Table 5.5: Top five differentially methylated genes in intrinsically-aged skin showing differences in regulation in young and aged skin following UVR challenge

Gene	Description	logFC†
EMILIN3	elastin microfibril interfacer 3	-2.908
KRT86	keratin 86	-2.110
COMP	cartilage oligomeric matrix protein	-2.092
MSRB3	methionine sulfoxide reductase B3	-2.088
LGR5	leucine rich repeat containing G protein-coupled receptor 5	-1.907

† log fold-change of the differences between young UVR exposure and aged UVR exposure transcriptional response

1.1 Discussion

Modification of the epigenome in ageing has been shown to be genomic context-dependent and linked with DNA replication dynamics (Shipony et al., 2014; Zhou et al., 2018). In the studies reported in this thesis, hypomethylated DMPs in intrinsically-aged skin were enriched in shores and open sea regions, and were overrepresented in a list of so-called WCGW sites (Zhou et al., 2018). A depletion of methyl marks at solo WCGW sites has been shown to occur in PMDs in almost all healthy tissue types (Zhou et al., 2018). Furthermore, WCGW DNAm loss was shown to begin during foetal development and accumulates throughout life, representing a purported 'mitotic clock' that measures the rate of cellular division.

In contrast to other tissue types, this and other studies have identified a greater number of hypermethylated DMPs in intrinsically-aged skin (Vandiver et al., 2015; Raddatz et al., 2013) than hypomethylated sites, at odds with other tissues. Of hypermethylated CpG sites, enrichment was observed in CpG island shores while islands showed an odds ratio close to 1 (Figure 5.2). CpG island shores are regions of intermediate CpG density in the regions flanking the CpG island, shown to be hypervariable across a multitude of phenotypes, in comparison to methylation levels at their respective CpG island, and correlate more strongly with gene expression (Irizarry et al., 2009; Doi et al., 2009). In this study, 651 DMRs were significantly correlated to the expression level of the nearby gene using Spearman correlation analysis, demonstrating a connection between aberrant DNAm and a functional role in gene expression regulation in intrinsically-aged skin.

Of the many hundreds of genes identified in this correlation analysis, a number represented interesting roles in mediation of ROS levels. Oxidative stress occurs when ROS exceed the capacity of protective anti-oxidant systems, leading to oxidative attack on cellular structures, such as DNA (de Jager et al., 2017). Oxidation-modified forms of proteins also accumulate during ageing (Davalli et al., 2016). The susceptibility of amino acids to oxidation by ROS varies greatly; however, the sulphur-containing amino acid methionine is readily oxidised by ROS, resulting in a diastereomeric mixture of methionine-R-sulfoxide and methionine-S-sulfoxide residues (Lourenço dos Santos et

al., 2018). Mammalian cells express two families of methionine-sulfoxide-reductases capable of repairing these lesions: a single MsrA enzyme, specific for the reduction of the S-form of methionine sulfoxide, and three MsrB enzymes (1–3) specific to the R-form (Moskovitz et al., 2002). Msr is thought to be an important scavenger of ROS, as cyclic oxidation and reduction of methionine indirectly protects cells against oxidative stress (Levine et al., 1999). In this study, the nearby CpG island and/or shore of the MSRB3 gene was found to be hypermethylated in intrinsically-aged skin, which was highly and significantly correlated with RNA transcript levels (Figure 5.7). MsrB3 has two isoforms, MsrB3A and MsrB3B, which are targeted to the endoplasmic reticulum (ER) and mitochondria, respectively (Kim, 2003). One study found that overexpression of human ER-type MsrB in *Drosophila* and the mammalian cell-line A549 increased resistance to oxidative stress, while depletion led to decreased cell viability(Kwak et al., 2012), suggesting that MsrB3 protects from ER-mediated stress. Future work should address whether MSRB3 protein is depleted in intrinsically-aged skin, as suggested by its decrease in mRNA expression. The further analysis performed in this chapter that integrates DNAm in intrinsically-aged skin with the dampened transcriptional response observed in chapter 5, demonstrated the differential upregulation between young and aged skin exposed to UVR. Reintroduction of the MSRB3 mRNA into a cellular model may lessen the burden of increased ROS levels observed in ageing cells, especially upon exposure to UVR, with possible beneficial impact on the ageing phenotype by enhancing protein repair and indirect ROS scavenging.

Another gene whose CpG island and/or shore were found to be hypermethylated in intrinsically-aged skin was Iroquois Homeobox 6 (IRX6), a member of the Iroquois homeobox gene family of transcription factors. The mRNA expression of IRX6 was negatively correlated with CpG island methylation levels in this study, suggesting that, together with its target genes, it may be important in intrinsic skin ageing. While the function of IRX6 is poorly defined, the wider gene family is involved in embryonic patterning, morphogenesis, growth and differentiation (Hu et al., 2018). Interestingly, the Human Protein Atlas suggests that IRX6 is localised to the mitochondria in human embryonic kidney (HEK) 293 cells, while in in the human melanoma cell line SK-MEL-

30, IRX6 immunoreactivity is more pronounced in the nucleus with some mitochondrial co-localisation (Thul et al., 2017). In skin sections labelled with the same antibody, immunoreactivity appears in all layers of the epidermis, showing clear nuclear exclusion (Uhlén et al., 2015) and, possibly, demonstrating a staining pattern suggestive of mitochondrial-localisation as seen in HEK 293 cells. In humans, mitochondrial DNA comprises approximately 16,600 base pairs that encode 37 genes: 2 rRNAs, 22 tRNAs and 13 protein-coding genes involved in the generation of ATP (Anderson et al., 1981). Nuclear transcription factors have been detected in mammalian mitochondria as early as the 1990's (Reviewed in Leigh-Brown et al., 2010), including STAT3 (Wegrzyn et al., 2009), oestrogen receptors (Yang et al., 2004), myocyte enhancer factor 2D (She et al., 2011), p53 (Caelles et al., 1994; Marchenko et al., 2002), p43 (Wrutniak et al., 1995), NF-κB (Cogswell et al., 2003), cAMP-responsive element binding protein (CREB) (Cammarota et al., 1999) and FoxO3A (Caballero-Caballero et al., 2013; Celestini et al., 2018). It is possible that IRX6 represents a previously untested transcriptional regulator of the mitochondrial genome. Given that its mRNA is reduced in intrinsically-aged skin in this study, it may contribute to mitochondrial dysfunction, leading to increased ROS, as seen with increasing age.

The 651 genes correlated changes in CpG island and/or shore methylation and mRNA expression were significantly over-represented in a number of KEGG pathways. The pathway "Signalling pathways regulating pluripotency of stem cells" was significantly over-represented in the DMR:gene correlated changes in intrinsically-aged skin. The genes involved in this pathway were HRAS, OTX1, MEIS1, TCF3, WNT16, FGFR3, ID3, DVL2, WNT10A, AXIN1, FZD10, DVL1, BMP4 and DLX5, which showed an up-regulation at the mRNA level in intrinsically-aged skin. A study by Sun *et al*. (2014) profiled young and old murine hematopoietic stem cells, observing multi-omic dysregulation of stem cell function that coalesced in enhancement of stem cell identity and self-renewal, and repressed differentiation. These observations in murine hematopoietic stem cells support those identified in this study, which mirror phenotypic stem cell behaviour *in vivo* (Ermolaeva et al., 2018). For example, in aged skin, the epidermis is markedly thinner, which could reflect an increase in stemness and a subsequent reduction in the

propensity of epidermal stem cells to divide, as driven by the changes in DNAm identified in this study.

More than half of the identified methylation: expression interactions represented a significant negative correlation (425 negatively correlated and 226 positively correlated), which fits with the dogma of methylation representing a block to transcriptional machinery. A recent study, utilising a methylation-sensitive protocol, determined the binding of many of the major classes of transcription factors. While binding of bHLH, bZIP, and ETS was inhibited by methylated CpG sequence within their recognition motifs, a number of transcription factors were found to be insensitive to methylation, and transcription factors such as homeodomain, POU, and NFAT even preferred to bind methylated DNA CpG sequence (Yin et al., 2017).

These data warrant an assessment of the transcription factors associated with a positive correlation for their ability to bind methylated sequences. However, as only the maximally changing CpG site within the DMR has been correlated with gene expression, it may be that the maximally changing site is not sufficiently connected to the transcription factor consensus sequence to impact binding or recognition. A possible way of ameliorating this would be to extract methylation levels of CpG sites that fall within transcription factor consensus sequences and specifically interrogating these levels. Given that the EPIC array used for this work does not measure all CpG sites contained within the genome (Zhou et al., 2017), it is possible that adequate genomic coverage is not achieved using an array-based approach for this analysis. An alternative technology may be whole-genome bisulphite sequencing, or transcription factor chip-seq, to determine the specific effect of DNAm obscuration of transcription factor binding sites.

The impact of intrinsically-driven skin ageing on the DNA methylome is immense. Whether the changes in DNAm identified in this study correlate with changes in protein levels is an open question. To address this, a portion of each skin biopsy taken was prepared for histological analysis; an avenue for future work could be to correlate the multiomic changes identified in this chapter to changes in protein abundance.

Elastin microfibril interface-located protein (EMILINs) and multimerins are a family of structurally related ECM glycoproteins with a range of functions in tissues enriched in elastic fibres (Colombatti et al., 2012). Most elastic fibres consist of an amorphous core of cross-linked elastin surrounded by a peripheral mantle of microfibrils; in the aorta, it is where these components are in close contact that EMILINs are immunolabelled (Bressan et al., 1993). In other tissues, EMILIN was found in structures lacking amorphous elastin, including the oxytalan fibres (fibrillin-rich microfibrils) of the ciliary zonule (Bressan et al., 1993) and DEJ of skin (Corallo et al., 2017; Schiavinato et al., 2016). The work outlined in this thesis identified EMILIN3 (also called multimerin 1) as differentially methylated in intrinsically-aged skin. Upon UVR challenge, EMILIN3 mRNA is less up-regulated in aged skin following UVR challenge than young skin. The consequences of this could be further investigated using immunofluorescence labelling of EMILIN3 protein in skin. Corrallo *et al*. (Corallo et al., 2017) showed a restricted distribution of EMILIN3 in post-natal mouse skin. Specifically, at P0, EMILIN3 immuno-positivity co-localised with fibrillin-1, decorating the candelabra-like fibrillin-rich structures that extend from the DEJ into the papillary dermis. By P72, EMILIN3 deposition had tapered, demonstrating restricted expression to the hair follicle bulge region (Corallo et al., 2017). While EMILIN3 may therefore be dispensable in the post-natal skin of the mouse, whether this is recapitulated in human skin, or whether protein levels change following skin challenges, has not been determined. The DEJ is a site of extensive remodelling in chronically photoexposed skin. Early work in this laboratory identified a reduction and reorganisation of fibrillin-positive fibres in close proximity to the DEJ following chronic sun exposure (Watson et al., 1999). Whether restoration of EMILIN3 impacts these candelabra-like structures, or promotes their reformation following UVR exposure, could be an avenue for further exploration. Indeed, levels of another EMILIN family member, EMILIN1, has been shown to regulates biogenesis of oxytalan fibres in periodontal ligament fibroblast culture (Nakatomi et al., 2011).

Chapter 6: Discussion

6.1 Summary of results

The studies presented herein collectively demonstrate the importance of DNAm in mediating the phenotypic manifestations of ageing and chronic photoexposure in the skin.

Chapter 3 demonstrated specific expression of enzymatic machinery important for DNAm maintenance and establishment in the different compartments of the skin. Immunohistochemical analyses were successfully performed for DNMT1, DNMT3A, DNMT3B and TET1, while DNMT3L, TET2 and TET3 were examined only at the mRNA level. The above enzymes were also analysed in NHEKs that were maintained in basal or high $Ca2^{+}$-differentiating medium. This allowed modelling of keratinocyte differentiation *in vitro* confirming the localisation of DNAm machinery consistent with that shown in the skin. Whilst the expression levels of DNMTs decreased as the cells transversed through the suprabasal layers of the epidermis, these studies also suggested that TETs were inversely upregulated, thus highlighting the importance of DNAm in mediating epidermal homeostasis.

There has been considerable interest in how environmental factors, such as UVR exposure, modulate the establishment and maintenance of DNAm within the skin. A number of limitations met by other studies investigating DNAm changes in photoexposed skin have been negated in this study. Specifically, two previous studies comparing the epidermis of the photoexposed forearm across a wide age spectrum (Raddatz et al., 2013; Bormann et al., 2016) were confounded by the superimposition of intrinsic ageing and photoexposure-related differences. Other studies have made important insights by disentangling these confounding factors through the comparison of photoexposed and photoprotected body sites of individuals of different ages (Vandiver et al., 2015; Grönniger et al., 2010). However, epigenetic differences have been identified between distinct anatomical sites (Koch et al., 2011). Vandiver *et al.* (2015) and Grönniger *et al*. (2010) account for anatomical differences by ascribing changes between body sites in young individuals (<30 years of age) as “anatomical.”

The additional sites changing between anatomical sites in older individuals were ascribed as “photoexposure.” However, this falsely ascribes some of the earliest DNAm changes of photoexposure, occurring in the first three decades of life, as anatomical differences. In the studies reported herein, a controlled regimen of UVR was applied within the clinic to the photoprotected buttock. The repetitive, sub-erythemal doses of UVR applied simulated levels of radiation experienced, for example, on an average day in Manchester. By obtaining biopsies of adjacent irradiated and non-irradiated skin, anatomical and intrinsic ageing related differences were effectively controlled.

A pilot study of five young individuals found that sub-erythemal UVR challenge (40% or 80% MED) applied daily for 5 or 10 days, induced changes in DNAm and gene expression in the epidermis. Although these DNAm changes were subtle, the most significantly changing DMPs overlapped with those in the chronically-photoexposed forearm, identified in a reanalysis of the Vandiver *et al.* (2015) study.

A follow-up study was performed comparing changes in the skin of young and aged volunteers exposed *in vivo* to 80% of MED for five days. There are four major findings of this study. First, highly significant DMPs were detected in the aged cohort following UVR challenge, and in an analysis that pooled the two age groups together. However, in an analysis that examined only the young individuals, statistically robust DMPs were again not detected upon UVR challenge, despite the substantial increase in sample size. Of the DMPs identified by the analyses that pooled the two age groups, hypomethylated probes exhibited a significantly greater change in DNAm in the aged epidermis than the young. This suggests that aberrations do not accumulate linearly over a lifetime, but that aged skin is inhibited in its ability to protect its epigenome and acquires these changes abruptly upon UVR challenge (Figure 6.1).

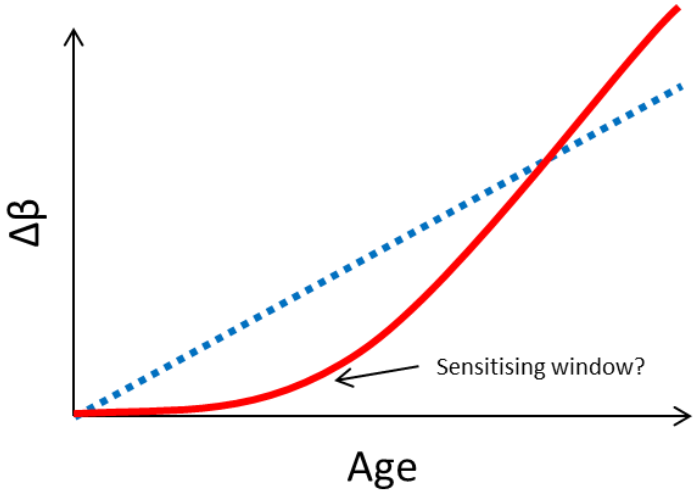

Figure 6.1: Linear acquisition of DNA methylation changes or sensitisation in ageing?
The blue line indicates the acquisition of time-dependent DNA methylation (DNAm) changes that is the current assumption (Δβ). The solid red line indicates the acquisition of DNAm changes as supported by studies in this thesis: the sudden and abrupt acquisition of DNAm changes in more elderly individuals, while young age prevents the acquisition of these changes until a 'sensitising window' is reached, possibly at ≥65 years of age or earlier.

Secondly, the DMPs identified following UVR challenge were heavily skewed towards a loss of DNAm at a ratio of 30:1 hypomethylated sites for every hypermethylated site identified. Furthermore, these DMPs were overrepresented in open seas. In chapter 5, the intrinsic ageing-related differences (with no UVR challenge) between these two age cohorts were also examined. This comparison identified a slight skew towards hypermethylation, with DMPs overrepresented in CGI shores. Collectively, these comparisons highlight that UVR challenge and intrinsic ageing are associated with their own, divergent, global patterns of DNAm perturbations.

The third finding was enabled by the generation of both DNAm profiles and donor-matched transcriptome data. This enabled the identification of genes with age-related changes in DNAm correlating with gene expression. These genes were enriched in "Metabolic pathways," "Basal cell carcinoma," "Hippo signalling pathway," "Pathways in cancer," "Notch signalling pathway" and "Signalling pathways regulating pluripotency of stem cells."

The final key finding of this thesis is that the transcriptional response in aged skin challenged with UVR is dampened when compared to young skin (Table 4.5). This was characterised by a failure to activate key UV-responsive pathways, including melanin biosynthesis and mitotic cell cycle processes (Figure 4.13). The mRNAs driving this divergent age-dependent response to UVR challenge were ranked. Those mRNAs whose gene was differentially methylated in intrinsically-aged skin were significantly more highly ranked in this list than expected by chance. This was shown to be due to reduced upregulation of these genes in aged skin (following UVR challenge) as opposed to reduced downregulation of these genes. These data suggests that the aged DNA methylome predisposes skin to respond poorly to UVR challenges by inhibiting activation of key UVR-response genes in skin (Figure 6.2).

In conclusion, the integration of DNAm changes in intrinsically-aged skin and upon UVR challenge, and the differential transcriptional regulation in the two aged groups has identified the epigenetic determinants of optimal skin response to UVR.

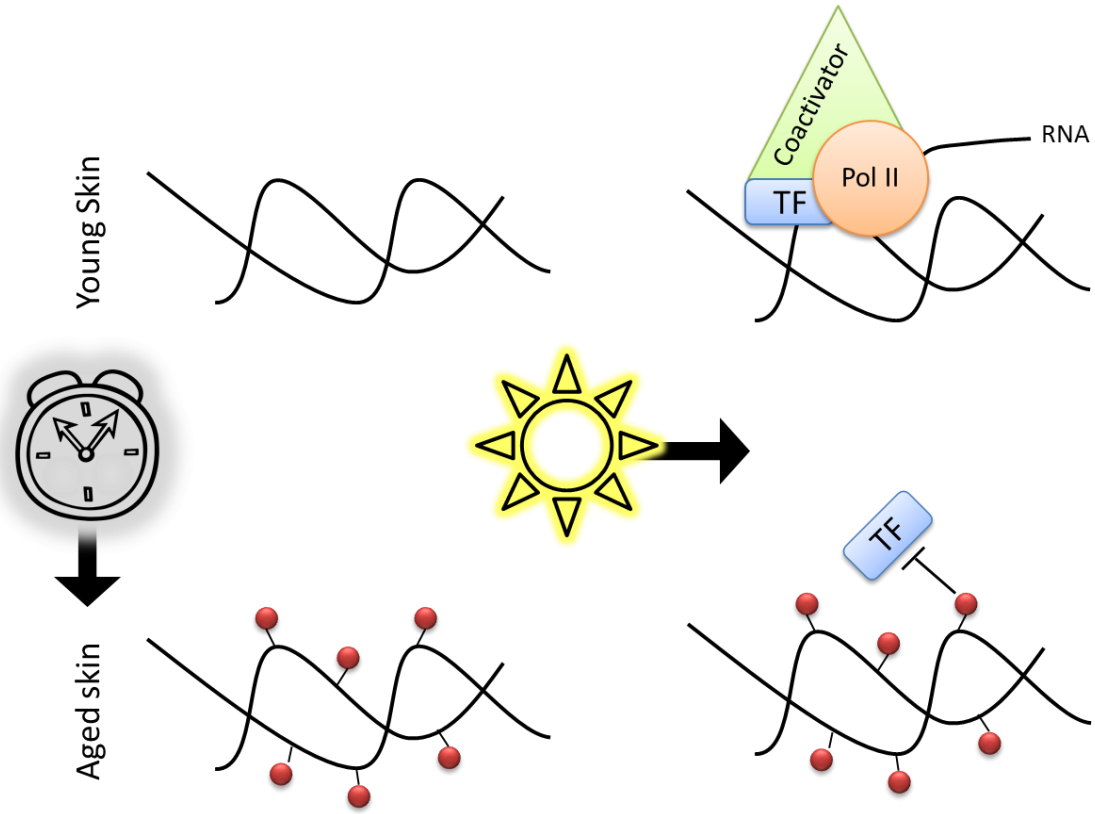

Figure 6.2: The interaction of intrinsically-driven DNA methylation changes and the skin response to UV radiation challenge

In young skin, CpG islands and shores of genes important for the UVR response are unmethylated and permissive to expression. In aged skin, these DNA regions become progressively methylated. These genes may not be constitutively expressed in unchallenged skin. However, upon challenge of the skin with UVR, in young skin transcription of relevant genes is activated. In aged skin the presence of methyl marks inhibits the transcription of the gene, by, for example, obscuring the recognition site of transcription factors. This inhibits the appropriate response of aged skin to UVR challenge. Red circles represent methylated DNA.

6.2 Future perspectives

Whilst the work presented herein has contributed to the understanding of DNAm in intrinsic skin ageing and its response to UVR, many questions remain that are pertinent to the translation of DNAm research into strategies to improve skin health in an ageing population.

6.2.1 Question 1: What DNAm changes are functionally important in skin ageing?

6.2.1.1 (Epi) genome editing

A major hurdle associated with determining the role of DNAm changes in the ageing skin phenotype is to identify whether these modifications are causative in altered gene expression or are merely correlative. Using CRISPR-Cas9 to target DNMT or TET fusion proteins to specific locations in the genome has allowed targeted DNAm editing in cell lines (Liu et al., 2016). For example, demethylation of the *BDNF* promoter IV by dCas9-TET1 was shown to induce BDNF expression in post-mitotic neurons (Liu et al., 2016). Using this technology, it may be possible to directly demethylate gene promoters' and CGI shores hypermethylated in intrinsically-aged skin in isolated keratinocytes from aged donors, and determine transcriptional changes.

6.2.1.2 'Big data trifecta' – integration of the epigenome, transcriptome and proteome

To further address this research question, the DNAm and 3' mRNA correlations could be validated using additional protein analyses. Immunofluorescence of tissue sections, while providing valuable information in regards to tissue and subcellular localisation, is an extremely low-throughput methodology. Furthermore, high quality antibodies are not always available. Liquid chromatography-mass spectrometry (LC-MS/MS) analysis has recently been used to identify age-associated differences in photoexposed and photoprotected skin (Newton et al., 2019). A number of pathways identified in this LC-MS/MS study were also identified in this thesis (e.g. metabolism and ROS scavenging).

An aptamer-based proteomic platform has also recently been developed called SOMAscan (SomaLogic, Boulder, CO). This platform utilises much smaller volumes of biologic material, with an enhanced dynamic range, than traditional LC-MS/MS approaches (Billing et al., 2017). Regardless of the methodology used, matched biological samples analysed by a trifecta of DNAm, mRNA and proteomic analyses would represent an incredibly rich source of information to answer pertinent questions related to ageing and photoexposure of the skin.

6.2.2 Question 2: What drives DNAm in intrinsically-aged and photoexposed skin?

Photoexposure is often described as an acceleration of the ageing process. However, the epigenome-wide study performed in this thesis has highlighted that these two processes are divergent in the DNAm changes with which they are associated. Age-dependent dysregulation was observed as hypermethylation of gene-associated CGI shores, while UVR challenge induced hypomethylation of open seas. It is an open question as to what drives the different pattern of DNAm perturbations that are induced.

6.2.2.1 Alterations in DNMT and TET expression

In chapter 5, it was demonstrated that DNMT3A was associated with a DMR in intrinsically aged skin, which was negatively correlated with its mRNA levels (Figure 5.6). Establishing how the DNMTs and TETs are dysregulated in intrinsically-aged and photoexposed skin may shed light on the DNAm changes that occur. Any analysis should be performed with the view to distinguish between the isoforms of these enzymes. This is demonstrated by studies of the ageing hippocampus. Neuronal activity induces the expression of DNMT3A2, and hippocampal levels of this isoform determine cognitive ability in both young adult and aged mice (Sanchez-Mut & Gräff, 2015; Feng et al., 2010; Oliveira et al., 2012). Ageing has been associated with a decrease in hippocampal DNMT3A1 and DNMT3A2 mRNA (Oliveira et al., 2012). This elegant study by Oliveira *et al*. (2012) demonstrated that specific restoration of

DNMT3A2 in aged mice reversed memory deficits, whilst its knockdown in young mice impaired memory formation. This highlights that differential regulation of DNMT isoforms may play a role in the ageing-associated acquisition of DNAm.

As discussed in chapter 3, different isoforms target different regions of the genome and likely influence different DNAm patterns. Chen *et al*. (Chen et al., 2002b) show opposing genomic localisation of GFP-tagged DNMT3A isoforms in transfected NIH3T3 cells. The shorter-length isoform, DNMT3A2 localised to DAPI 'dark spots' that are associated with heterochromatin regions. If DNMT3A2 is downregulated in aged skin as in the ageing hippocampus, this may partly explain the loss of methylation enriched in solo WCGWs (Zhou et al., 2018) in heterochromatin regions in intrinsically-aged skin. Furthermore, loss of DNMT3A2 in intrinsically-aged skin may contribute to the greater loss of methylation observed upon UVR exposure in this age group (Figure 4.8).

6.2.2.2 One-carbon metabolism and replenishment of SAM

Potential mechanisms explaining the loss of DNAm upon UVR challenge were discussed in chapter 4. Specifically, the availability of folate and one-carbon metabolites may play a role through inhibition of the production of the methyl donor SAM (Mentch & Locasale, 2016). Whilst folate and key derivatives are sensitive to photodegradation by UVR (Tam et al., 2009; Valencia-Vera et al., 2019), vitamin D is produced endogenously in the skin upon UVB exposure (Holick, 2017). The greatest determinant of vitamin D production is pigmentation, as melanin competes with vitamin D precursors to absorb UVB radiation (Fajuyigbe & Young, 2016). The vitamin D–folate paradigm proposes that skin pigmentation evolved as a balancing mechanism to maintain levels of these vitamins that are key to human health (Jones et al., 2018; Jablonski & Chaplin, 2017; Branda & Eaton, 1978), although others oppose this theory (Elias & Williams, 2018).

Even though one-carbon metabolism is quintessentially important in ageing and age-associated diseases (Suh et al., 2016), the health effects of one-carbon metabolism are not well-understood. In addition to identifying the extent of photodegradation of the key intermediates in one-carbon metabolism, the enzymatic machinery involved

should be examined in young and aged skin, and interrogated functionally in keratinocytes derived from young and aged individuals. One study has previously identified an age-specific effect of folate deplete, replete and supplemented feeds on the rat colon. A folate-deplete diet may resemble the molecular environment of the epidermis upon photoexposure. In this study, colonic folate levels were significantly lower in the aged rats in each feeding group. Uracil misincorporation into the DNA was also used as molecular read-out of the effect of folate depletion. Folate deficiency slows thymidylate synthesis from deoxyuridylate, resulting in an imbalance in deoxyribonucleotides that leads to excessive uracil misincorporation into the DNA. The aged rats had approximately 50% more uracil incorporated into their colonic DNA, even when fed a diet considered to meet metabolic needs ("replete" feed). However, folate supplementation four times this amount ("supplemented" feed) was effective in eliminating evidence of inadequate folate status in aged as it is in young rats. Collectively, this suggests that aged rats are more susceptible to folate depletion and require more dietary folate than considered "replete" in young rats.

These prospects raise additional problems in the skin: the epidermis is an avascular structure dependent on the vasculature of the underlying dermis for delivery of nutrients. In ageing skin, the vasculature is impeded, compounding the problem of nutrient delivery. This raises the question of whether topically applied folate is a better source of one-carbon units than oral supplementation. Indeed, trials of topically applied folate have produced positive results in skin parameters, including firmness (Fischer et al., 2011), although no study has examined the effect of topically applied folate on either uracil misincorporation or DNAm.

6.2.3 Question 3: Are changes in DNAm recapitulated in the dermis of the skin and smaller cell populations?

The studies in this thesis examined, principally, the effects of intrinsic ageing and UVR exposure on the epidermis. Measurement of bulk tissue is not amenable to detect changes occurring in smaller cell populations, such as the melanocytes, Merkel and Langerhans cells. These cell populations may be more amenable to study following

expansion in culture, to increase the number of cells available for study. Another approach could utilise single-cell DNAm profiling (reviewed in Karemaker & Vermeulen, 2018).

Furthermore, the underlying dermis is the thickest of the skin layers, differing from the epidermis in both its structure and function. This layer houses an array of fibroblasts with diverse potential to secrete extracellular matrix that provides skin with tensile strength and elastic properties, which are compromised in ageing. Longwave UV radiation (UVA) penetrates the dermis of the skin, and the changes in DNAm that occur in this deeper skin layer have not adequately been addressed previously. By understanding the critical role of DNAm across all layers of the skin, this would enable the development of novel strategies that maintain skin health and appearance in an ageing population.

References

Adams, J.C. & Watt, F.M. (1989). Fibronectin inhibits the terminal differentiation of human keratinocytes. *Nature*. 340 (6231). p.pp. 307–309.

Allan, J., Harborne, N., Rau, D.C. & Gould, H. (1982). Participation of core histone 'tails' in the stabilization of the chromatin solenoid. *Journal of Cell Biology*. 93 (2). p.pp. 285–297.

Allfrey, V.G., Faulkner, R. & Mirsky, A.E. (1964). Acetylation and methylation of histones and their possible role in the regulation of RNA synthesis. *Proceedings of the National Academy of Sciences of the United States of America*. [Online]. 51 (5). p.pp. 786–94. Available from: http://www.ncbi.nlm.nih.gov/pubmed/14172992. [Accessed: 28 July 2019].

Allis, C.D. & Jenuwein, T. (2016). The molecular hallmarks of epigenetic control. *Nature Reviews Genetics*. [Online]. 17 (8). p.pp. 487–500. Available from: http://dx.doi.org/10.1038/nrg.2016.59.

Almouzni, G. & Cedar, H. (2016). Maintenance of epigenetic information. *Cold Spring Harbor Perspectives in Biology*. 8 (5).

Amblard, P., Beani, J., Gautron, R., Reymond, J. & Doyon, B. (1982). Statistical study of individual variations in sunburn sensitivity in 303 volunteers without photodermatosis. *Archives of Dermatological Research*. 274 (3–4). p.pp. 195–206.

Anderson, S., Bankier, A.T., Barrell, B.G., De Bruijn, M.H.L., Coulson, A.R., Drouin, J., Eperon, I.C., Nierlich, D.P., Roe, B.A., Sanger, F., Schreier, P.H., Smith, A.J.H., Staden, R. & Young, I.G. (1981). Sequence and organization of the human mitochondrial genome. *Nature*. 290 (5806). p.pp. 457–465.

Andrews, A.J. & Luger, K. (2011). Nucleosome Structure(s) and Stability: Variations on a Theme. *Annual Review of Biophysics*. [Online]. 40 (1). p.pp. 99–117. Available from: http://www.annualreviews.org/doi/10.1146/annurev-biophys-042910-155329.

Aoki, A. (2001). Enzymatic properties of de novo-type mouse DNA (cytosine-5) methyltransferases. *Nucleic Acids Research*. 29 (17). p.pp. 3506–3512.

Aryee, M.J., Jaffe, A.E., Corrada-Bravo, H., Ladd-Acosta, C., Feinberg, A.P., Hansen, K.D. & Irizarry, R.A. (2014). Minfi: a flexible and comprehensive Bioconductor package for the analysis of Infinium DNA methylation microarrays. *Bioinformatics (Oxford, England)*. [Online]. 30 (10). p.pp. 1363–9. Available from: http://www.ncbi.nlm.nih.gov/pubmed/24478339. [Accessed: 10 February 2019].

Ashburner, M., Ball, C.A., Blake, J.A., Botstein, D., Butler, H., Cherry, J.M., Davis, A.P., Dolinski, K., Dwight, S.S., Eppig, J.T., Harris, M.A., Hill, D.P., Issel-Tarver, L., Kasarskis, A., Lewis, S., Matese, J.C., Richardson, J.E., Ringwald, M., Rubin, G.M. &

Sherlock, G. (2000). Gene ontology: Tool for the unification of biology. *Nature Genetics*.

Bannister, A.J. & Kouzarides, T. (2011). Regulation of chromatin by histone modifications. *Cell research*. [Online]. 21 (3). p.pp. 381–95. Available from: http://www.ncbi.nlm.nih.gov/pubmed/21321607. [Accessed: 7 April 2018].

Barnadas, M.A., Pérez Ferriols, A., Lorente, J., de Cabo, X., Lecha, M., Gardeazábal, J., Rodríguez Granados, M.T., Aguilera, P., Aguilera, J., Martínez-Lozano, J.A., Sola, Y., de Argila, D., Giménez-Arnau, A., de Gálvez Aranda, M.V., Utrillas, M.P. & Carrrascosa, J.M. (2014). Determination of Minimal Erythema Dose and Anomalous Reactions to UVA Radiation by Skin Phototype. *Actas Dermo-Sifiliográficas (English Edition)*. 105 (8). p.pp. 780–788.

Basset-Seguin, N., Moles, J.-P., Mils, V., Dereure, O. & Guilhou, J.-J. (1994). TP53 Tumor Suppressor Gene and Skin Carcinogenesis. *Journal of Investigative Dermatology*. [Online]. 103 (Suppl 5). p.pp. 102–106. Available from: http://www.nature.com/doifinder/10.1111/1523-1747.ep12399372. [Accessed: 1 August 2019].

Basu, A.K. (2018). DNA damage, mutagenesis and cancer. *International Journal of Molecular Sciences*. 19 (4).

Beerman, I., Bock, C., Garrison, B.S., Smith, Z.D., Gu, H., Meissner, A. & Rossi, D.J. (2013). Proliferation-dependent alterations of the DNA methylation landscape underlie hematopoietic stem cell aging. *Cell Stem Cell*. 12 (4). p.pp. 413–425.

Bekaert, B., Kamalandua, A., Zapico, S.C., Van De Voorde, W. & Decorte, R. (2015). Improved age determination of blood and teeth samples using a selected set of DNA methylation markers. *Epigenetics*. 10 (10). p.pp. 922–930.

Benjamin, C.L. & Ananthaswamy, H.N. (2007). p53 and the pathogenesis of skin cancer. *Toxicology and Applied Pharmacology*. 224 (3) p.pp. 241–248.

Benjamini, Y. & Hochberg, Y. (1995). Controlling the False Discovery Rate: A Practical and Powerful Approach to Multiple Testing. *Journal of the Royal Statistical Society: Series B (Methodological)*. 57 (1). p.pp. 289–300.

Bergman, Y. & Cedar, H. (2013). DNA methylation dynamics in health and disease. *Nature Structural and Molecular Biology*. 20 (3). p.pp. 274–281.

Bickenbach, J.R., Vormwald-Dogan, V., Bachor, C., Bleuel, K., Schnapp, G. & Boukamp, P. (1998). Telomerase is not an epidermal stem cell marker and is downregulated by calcium. *Journal of Investigative Dermatology*. 20 (3). p.pp. 274–281.

Billing, A.M., Ben Hamidane, H., Bhagwat, A.M., Cotton, R.J., Dib, S.S., Kumar, P., Hayat, S., Goswami, N., Suhre, K., Rafii, A. & Graumann, J. (2017). Complementarity of SOMAscan to LC-MS/MS and RNA-seq for quantitative profiling of human embryonic and mesenchymal stem cells. *Journal of Proteomics*. 150. p.pp. 86–97.

Bock, C. (2012). Analysing and interpreting DNA methylation data. *Nature Reviews Genetics*. [Online]. 13 (10). p.pp. 705–719. Available from: http://www.nature.com/articles/nrg3273. [Accessed: 20 February 2019].

Bocklandt, S., Lin, W., Sehl, M.E., Sánchez, F.J., Sinsheimer, J.S., Horvath, S. & Vilain, E. (2011). Epigenetic predictor of age. *PLoS ONE*. 6 (6).

Böhmdorfer, G. & Wierzbicki, A.T. (2015). Control of Chromatin Structure by Long Noncoding RNA. *Trends in Cell Biology*. 25 (10) p.pp. 623–632.

Bormann, F., Rodríguez-Paredes, M., Hagemann, S., Manchanda, H., Kristof, B., Gutekunst, J., Raddatz, G., Haas, R., Terstegen, L., Wenck, H., Kaderali, L., Winnefeld, M. & Lyko, F. (2016). Reduced DNA methylation patterning and transcriptional connectivity define human skin aging. *Aging Cell*. [Online]. 15 (3). p.pp. 563–571. Available from: http://doi.wiley.com/10.1111/acel.12470. [Accessed: 17 January 2019].

Van Den Bossche, K., Naeyaert, J.M. & Lambert, J. (2006). The quest for the mechanism of melanin transfer. *Traffic*. 7 (7) p.pp. 769–778.

Brait, M. & Sidransky, D. (2011). Cancer epigenetics: above and beyond. *Toxicology mechanisms and methods*. [Online]. 21 (4). p.pp. 275–88. Available from: http://www.ncbi.nlm.nih.gov/pubmed/21495866. [Accessed: 9 April 2018].

Branchet, M.C., Boisnic, S., Frances, C. & Robert, A.M. (1990). Skin thickness changes in normal aging skin. *Gerontology*. 36 (4). p.pp. 28–35.

Branda, R.F. & Eaton, J.W. (1978). Skin color and nutrient photolysis: an evolutionary hypothesis. *Science (New York, N.Y.)*. [Online]. 201 (4356). p.pp. 625–6. Available from: http://www.ncbi.nlm.nih.gov/pubmed/675247. [Accessed: 17 January 2019].

Brenner, M. & Hearing, V.J. (2008). The protective role of melanin against UV damage in human skin. *Photochemistry and Photobiology*. 84 (3) p.pp. 539–549.

Bressan, G.M., Daga-Gordini, D., Colombatti, A., Castellani, I., Marigo, V. & Volpin, D. (1993). Emilin, a component of elastic fibers preferentially located at the elastin-microfibrils interface. *Journal of Cell Biology*. 121 (1). p.pp. 201–212.

Bruls, W.A.G., Slaper, H., Van Der Leun, J.C. & Berrens, L. (1984). Transmission of human epidermis and stratum corneum as a function of thickness in the ultraviolet and visible wavelengths. *Photochemistry and Photobiology*. 40 (4). p.pp. 485–494.

Buckingham, E.M. & Klingelhutz, A.J. (2011). The role of telomeres in the ageing of human skin. *Experimental Dermatology*. 20 (4). p.pp. 297–302.

Bulat, V., Situm, M., Dediol, I., Ljubicić, I. & Bradić, L. (2011). The mechanisms of action of phototherapy in the treatment of the most common dermatoses. *Collegium*

antropologicum. [Online]. 35 (Suppl 2). p.pp. 147–151. Available from: http://www.ncbi.nlm.nih.gov/pubmed/22220423.

Busam, K.J. (2010). *Dermatopathology*. 1st Ed. Saunders.

Byvoet, P., Shepherd, G.R., Hardin, J.M. & Noland, B.J. (1972). The distribution and turnover of labeled methyl groups in histone fractions of cultured mammalian cells. *Archives of biochemistry and biophysics*. [Online]. 148 (2). p.pp. 558–567. Available from: http://www.ncbi.nlm.nih.gov/pubmed/5063076. [Accessed: 8 April 2018].

Caballero-Caballero, A., Engel, T., Martinez-Villarreal, J., Sanz-Rodriguez, A., Chang, P., Dunleavy, M., Mooney, C.M., Jimenez-Mateos, E.M., Schindler, C.K. & Henshall, D.C. (2013). Mitochondrial localization of the Forkhead box class O transcription factor FOXO3a in brain. *Journal of Neurochemistry*. 124 (6). p.pp. 749–756.

Cadet, J. & Davies, K.J.A. (2017). Oxidative DNA damage & repair: An introduction. *Free Radical Biology and Medicine*. 107 p.pp. 2–12.

Cadet, J. & Douki, T. (2018). Formation of UV-induced DNA damage contributing to skin cancer development. *Photochemical and Photobiological Sciences*. 17 (12) p.pp. 1816–1841.

Cadet, J. & Richard Wagner, J. (2013). DNA base damage by reactive oxygen species, oxidizing agents, and UV radiation. *Cold Spring Harbor Perspectives in Biology*. 5 (2).

Caelles, C., Helmberg, A. & Karin, M. (1994). p53-Dependent apoptosis in the absence of transcriptional activation of p53-target genes. *Nature*. 370 (6486). p.pp. 220–223.

Cammarota, M., Paratcha, G., Bevilaqua, L.R.M., De Stein, M.L., Lopez, M., Pellegrino De Iraldi, A., Izquierdo, I. & Medina, J.H. (1999). Cyclic AMP-responsive element binding protein in brain mitochondria. *Journal of Neurochemistry*. 72 (6). p.pp. 2272–2277.

Celestini, V., Tezil, T., Russo, L., Fasano, C., Sanese, P., Forte, G., Peserico, A., Lepore Signorile, M., Longo, G., De Rasmo, D., Signorile, A., Gadaleta, R.M., Scialpi, N., Terao, M., Garattini, E., Cocco, T., Villani, G., Moschetta, A., Grossi, V. & Simone, C. (2018). Uncoupling FoxO3A mitochondrial and nuclear functions in cancer cells undergoing metabolic stress and chemotherapy article. *Cell Death and Disease*. 9 (2). p.p. 231.

Chandler, S., Cossins, J., Lury, J. & Wells, G. (1996). Macrophage metalloelastase degrades matrix and myelin proteins and processes a tumour necrosis factor-α fusion protein. *Biochemical and Biophysical Research Communications*. 228 (2). p.pp. 421–429.

Chédin, F., Lieber, M.R. & Hsieh, C.L. (2002). The DNA methyltransferase-like protein

DNMT3L stimulates de novo methylation by Dnmt3a. *Proceedings of the National Academy of Sciences of the United States of America*. 99 (26). p.pp. 16916–16921.

Chen, T., Ueda, Y., Dodge, J.E., Wang, Z. & Li, E. (2003). Establishment and Maintenance of Genomic Methylation Patterns in Mouse Embryonic Stem Cells by Dnmt3a and Dnmt3b. *Molecular and Cellular Biology*. 23 (16). p.pp. 5594–5605.

Chen, T., Ueda, Y., Xie, S. & Li, E. (2002a). A Novel Dnmt3a Isoform Produced from an Alternative Promoter Localizes to Euchromatin and Its Expression Correlates with Active *de Novo* Methylation. *Journal of Biological Chemistry*. [Online]. 277 (41). p.pp. 38746–38754. Available from: http://www.ncbi.nlm.nih.gov/pubmed/12138111. [Accessed: 15 August 2019].

Chen, T., Ueda, Y., Xie, S. & Li, E. (2002b). A Novel Dnmt3a Isoform Produced from an Alternative Promoter Localizes to Euchromatin and Its Expression Correlates with Active *de Novo* Methylation. *Journal of Biological Chemistry*. 277 (41). p.pp. 38746–38754.

Chien, A.L., Suh, J., Cesar, S.S.A., Fischer, A.H., Cheng, N., Poon, F., Rainer, B., Leung, S., Martin, J., Okoye, G.A. & Kang, S. (2016). Pigmentation in African American skin decreases with skin aging. *Journal of the American Academy of Dermatology*. 75 (4). p.pp. 782–787.

Chikakane, K. & Takahashi, H. (1995). Measurement of skin pH and its significance in cutaneous diseases. *Clinics in Dermatology*. 13 (4). p.pp. 299–306.

Choi, E.H., Man, M.Q., Xu, P., Xin, S., Liu, Z., Crumrine, D.A., Jiang, Y.J., Fluhr, J.W., Feingold, K.R., Elias, P.M. & Mauro, T.M. (2007). Stratum corneum acidification is impaired in moderately aged human and murine skin. *Journal of Investigative Dermatology*. 127 (12). p.pp. 2847–2856.

Choi, W., Miyamura, Y., Wolber, R., Smuda, C., Reinhold, W., Liu, H., Kolbe, L. & Hearing, V.J. (2010). Regulation of human skin pigmentation in situ by repetitive UV exposure: molecular characterization of responses to UVA and/or UVB. *The Journal of Investigative Dermatology*. [Online]. 130 (6). p.pp. 1685–96. Available from: http://www.ncbi.nlm.nih.gov/pubmed/20147966. [Accessed: 7 April 2018].

Ciarletta, P. & Ben Amar, M. (2012). Papillary networks in the dermal-epidermal junction of skin: A biomechanical model. *Mechanics Research Communications*. 42. p.pp. 68–76.

Cogswell, P.C., Kashatus, D.F., Keifer, J. a, Guttridge, D.C., Reuther, J.Y., Bristow, C., Roy, S., Nicholson, D.W. & Baldwin, A.S. (2003). NF-kappa B and I kappa B alpha are found in the mitochondria. Evidence for regulation of mitochondrial gene expression by NF-kappa B. *The Journal of Biological Chemistry*. [Online]. 278 (5). p.pp. 2963–2968. Available from: http://www.ncbi.nlm.nih.gov/pubmed/12433922.

Cole, M.A., Quan, T., Voorhees, J.J. & Fisher, G.J. (2018). Extracellular matrix regulation

of fibroblast function: redefining our perspective on skin aging. *Journal of Cell Communication and Signaling*. 12 (1) p.pp. 35–43.

Colhoun, E.H. & Smith, M. V. (1960). Neurohormonal properties of royal jelly. *Nature*. 188 (4753). p.pp. 854–855.

Colombatti, A., Spessotto, P., Doliana, R., Mongiat, M., Bressan, G.M. & Esposito, G. (2012). The EMILIN/multimerin family. *Frontiers in Immunology*. 2 (93).

Contet-Audonneau, J.L., Jeanmaire, C. & Pauly, G. (1999). A histological study of human wrinkle structures: Comparison between sun-exposed areas of the face, with or without wrinkles, and sun-protected areas. *British Journal of Dermatology*. 140 (6). p.pp. 1038–1047.

Corallo, D., Schiavinato, A., Bizzotto, D., Milanetto, M., Guljelmovic, M., Keene, D.R., Sengle, G., Braghetta, P. & Bonaldo, P. (2017). EMILIN3, an extracellular matrix molecule with restricted distribution in skin. *Experimental Dermatology*. 26 (5) p.pp. 435–438.

Cournil, A. & Kirkwood, T. (2001). If you would live long, choose your parents well. *Trends in Genetics*. 17 (5). p.pp. 233–235.

Cui, C.Y. & Schlessinger, D. (2015). Eccrine sweat gland development and sweat secretion. *Experimental Dermatology*. 24 (9). p.pp. 644–650.

Cui, R., Widlund, H.R., Feige, E., Lin, J.Y., Wilensky, D.L., Igras, V.E., D'Orazio, J., Fung, C.Y., Schanbacher, C.F., Granter, S.R. & Fisher, D.E. (2007). Central Role of p53 in the Suntan Response and Pathologic Hyperpigmentation. *Cell*. 128 (5). p.pp. 853–864.

D'Alba, L. & Shawkey, M.D. (2019). Melanosomes: Biogenesis, properties, and evolution of an ancient organelle. *Physiological Reviews*. 99 (1) p.pp. 1–19.

D'Orazio, J., Jarrett, S., Amaro-Ortiz, A. & Scott, T. (2013). UV radiation and the skin. *International Journal of Molecular Sciences*. 14 (6) p.pp. 12222–12248.

D'Orazio, J.A., Nobuhisa, T., Cui, R., Arya, M., Spry, M., Wakamatsu, K., Igras, V., Kunisada, T., Granter, S.R., Nishimura, E.K., Ito, S. & Fisher, D.E. (2006). Topical drug rescue strategy and skin protection based on the role of Mc1r in UV-induced tanning. *Nature*. 443 (7109). p.pp. 340–344.

Daly, C.H. & Odland, G.F. (1979). Age-related changes in the mechanical properties of human skin. *Journal of Investigative Dermatology*. 73 (1). p.pp. 84–87.

Davalli, P., Mitic, T., Caporali, A., Lauriola, A. & D'Arca, D. (2016). ROS, Cell Senescence, and Novel Molecular Mechanisms in Aging and Age-Related Diseases. *Oxidative Medicine and Cellular Longevity*. 2016. p.pp. 1–18.

Dawlaty, M.M., Ganz, K., Powell, B.E., Hu, Y.C., Markoulaki, S., Cheng, A.W., Gao, Q.,

Kim, J., Choi, S.W., Page, D.C. & Jaenisch, R. (2011). Tet1 is dispensable for maintaining pluripotency and its loss is compatible with embryonic and postnatal development. *Cell Stem Cell*.

Day, K., Waite, L.L., Thalacker-Mercer, A., West, A., Bamman, M.M., Brooks, J.D., Myers, R.M. & Absher, D. (2013). Differential DNA methylation with age displays both common and dynamic features across human tissues that are influenced by CpG landscape. *Genome Biology*. 14 (9).

Deaton, A.M. & Bird, A. (2011). CpG islands and the regulation of transcription. *Genes & Development*. [Online]. 25 (10). p.pp. 1010–1022. Available from: http://www.ncbi.nlm.nih.gov/pubmed/21576262. [Accessed: 8 April 2018].

DeLuca, H.F. (2004). Overview of general physiologic features and functions of vitamin D. *The American Journal of Cinical Nutrition*. 80 (Suppl 6). p.pp. 1689–1696.

Dobin, A., Davis, C.A., Schlesinger, F., Drenkow, J., Zaleski, C., Jha, S., Batut, P., Chaisson, M. & Gingeras, T.R. (2013). STAR: Ultrafast universal RNA-seq aligner. *Bioinformatics*. 29 (1). p.pp. 15–21.

Dogan, M. V., Shields, B., Cutrona, C., Gao, L., Gibbons, F.X., Simons, R., Monick, M., Brody, G.H., Tan, K., Beach, S.R.H. & Philibert, R.A. (2014). The effect of smoking on DNA methylation of peripheral blood mononuclear cells from African American women. *BMC Genomics*. 15 (1).

Doi, A., Park, I.H., Wen, B., Murakami, P., Aryee, M.J., Irizarry, R., Herb, B., Ladd-Acosta, C., Rho, J., Loewer, S., Miller, J., Schlaeger, T., Daley, G.Q. & Feinberg, A.P. (2009). Differential methylation of tissue-and cancer-specific CpG island shores distinguishes human induced pluripotent stem cells, embryonic stem cells and fibroblasts. *Nature Genetics*. 41 (12). p.pp. 1350–1353.

Drewell, R.A., Bush, E.C., Remnant, E.J., Wong, G.T., Beeler, S.M., Stringham, J.L., Lim, J. & Oldroyd, B.P. (2014). The dynamic DNA methylation cycle from egg to sperm in the honey bee Apis mellifera. *Development (Cambridge)*. 141 (13). p.pp. 2702–2711.

Du, P., Zhang, X., Huang, C.-C., Jafari, N., Kibbe, W.A., Hou, L. & Lin, S.M. (2010). Comparison of Beta-value and M-value methods for quantifying methylation levels by microarray analysis. *BMC Bioinformatics*. [Online]. 11 (1). p.p. 587. Available from: https://bmcbioinformatics.biomedcentral.com/articles/10.1186/1471-2105-11-587. [Accessed: 20 February 2019].

Egger, G., Liang, G., Aparicio, A. & Jones, P.A. (2004). Epigenetics in human disease and prospects for epigenetic therapy. *Nature*. 429 (6990) p.pp. 457–463.

Eklund, A.G., Altshuler, S.L., Altshuler, P.C., Chow, J.C., Hidy, G.M., Lloyd, A.C., Prather, M.J., Watson, J.G., Zalzal, P., Andersen, S.O., Halberstadt, M.L. & Borgford-Parnell, N. (2013). Stratospheric ozone, global warming, and the principle of unintended

consequences--an ongoing science and policy success story. *Journal of the Air and Waste Management Association*. 63 (6). p.pp. 607–647.

El-Abaseri, T.B., Putta, S. & Hansen, L.A. (2006). Ultraviolet irradiation induces keratinocyte proliferation and epidermal hyperplasia through the activation of the epidermal growth factor receptor. *Carcinogenesis*. 27 (2). p.pp. 225–231.

Elias, P.M. & Williams, M.L. (2018). Comment on: The Vitamin D⁻Folate Hypothesis as an Evolutionary Model for Skin Pigmentation: An Update and Integration of Current Ideas. *Nutrients*. [Online]. 10 (11). Available from: http://www.ncbi.nlm.nih.gov/pubmed/30441753. [Accessed: 10 September 2019].

Ermolaeva, M., Neri, F., Ori, A. & Rudolph, K.L. (2018). Cellular and epigenetic drivers of stem cell ageing. *Nature Reviews Molecular Cell Biology*. 19 (9) p.pp. 594–610.

Fajuyigbe, D. & Young, A.R. (2016). The impact of skin colour on human photobiological responses. *Pigment Cell and Melanoma Research*. 29 (6) p.pp. 607–618.

Farage, M.A., Miller, K.W., Elsner, P. & Maibach, H.I. (2013). Characteristics of the Aging Skin. *Advances in Wound Care*. [Online]. 2 (1). p.pp. 5–10. Available from: http://www.liebertpub.com/doi/10.1089/wound.2011.0356.

Farage, M.A., Miller, K.W., Elsner, P. & Maibach, H.I. (2008). Intrinsic and extrinsic factors in skin ageing: A review. *International Journal of Cosmetic Science*. 30 (2). p.pp. 87–95.

Feng, J., Zhou, Y., Campbell, S.L., Le, T., Li, E., Sweatt, J.D., Silva, A.J. & Fan, G. (2010). Dnmt1 and Dnmt3a maintain DNA methylation and regulate synaptic function in adult forebrain neurons. *Nature Neuroscience*. 13 (4). p.pp. 423–430.

Fischer, F., Achterberg, V., März, A., Puschmann, S., Rahn, C.D., Lutz, V., Krüger, A., Schwengler, H., Jaspers, S., Koop, U., Blatt, T., Wenck, H. & Gallinat, S. (2011). Folic acid and creatine improve the firmness of human skin in vivo. *Journal of Cosmetic Dermatology*.

Fisher, G.J., Datta, S.C., Talwar, H.S., Wang, Z.Q., Varani, J., Kang, S. & Voorhees, J.J. (1996). Molecular basis of sun-induced premature skin ageing and retinoid antagonism. *Nature*. 379 (6563). p.pp. 335–339.

Fitzpatrick, T.B. (1988). The Validity and Practicality of Sun-Reactive Skin Types I Through VI. *Archives of Dermatology*. 124 (6). p.pp. 869–871.

Fitzpatrick, T.B. & Breathnach, A.S. (1963). The epidermal melanin unit system. *Dermatologische Wochenschrift*. [Online]. 147. p.pp. 481–489. Available from: http://www.ncbi.nlm.nih.gov/pubmed/14172128. [Accessed: 24 July 2019].

Fletcher, T.M. & Hansen, J.C. (1995). Core histone tail domains mediate

oligonucleosome folding and nucleosomal DNA organization through distinct molecular mechanisms. *Journal of Biological Chemistry*. 270 (43). p.pp. 25359–25362.

Fraga, M.F., Ballestar, E., Paz, M.F., Ropero, S., Setien, F., Ballestar, M.L., Heine-Suñer, D., Cigudosa, J.C., Urioste, M., Benitez, J., Boix-Chornet, M., Sanchez-Aguilera, A., Ling, C., Carlsson, E., Poulsen, P., Vaag, A., Stephan, Z., Spector, T.D., Wu, Y.-Z., Plass, C. & Esteller, M. (2005). Epigenetic differences arise during the lifetime of monozygotic twins. *Proceedings of the National Academy of Sciences of the United States of America*. [Online]. 102 (30). p.pp. 10604–9. Available from: http://www.ncbi.nlm.nih.gov/pubmed/16009939. [Accessed: 8 April 2018].

Fu, S., Wu, H., Zhang, H., Lian, C.G. & Lu, Q. (2017). DNA methylation/hydroxymethylation in melanoma. *Oncotarget*. 8 (44). p.pp. 78163–78173.

Fuchs, E. (2016). Epithelial Skin Biology: Three Decades of Developmental Biology, a Hundred Questions Answered and a Thousand New Ones to Address. *Current Topics in Developmental Biology*. [Online]. 116. p.pp. 357–374. Available from: https://www.sciencedirect.com/science/article/abs/pii/S0070215315001994. [Accessed: 31 July 2019].

Garagnani, P., Bacalini, M.G., Pirazzini, C., Gori, D., Giuliani, C., Mari, D., Di Blasio, A.M., Gentilini, D., Vitale, G., Collino, S., Rezzi, S., Castellani, G., Capri, M., Salvioli, S. & Franceschi, C. (2012). Methylation of ELOVL2 gene as a new epigenetic marker of age. *Aging Cell*. 11 (6). p.pp. 1132–1134.

Garcea, R., Daino, L., Pascale, R., Simile, M.M., Puddu, M., Ruggiu, M.E., Seddaiu, M.A., Satta, G., Sequenza, M.J. & Feo, F. (1989). Protooncogene methylation and expression in regenerating liver and preneoplastic liver nodules induced in the rat by diethylnitrosamine: Effects of variations of s-adenosylmethionine: S-adenosylhomocysteine ratio. *Carcinogenesis*. 10 (7). p.pp. 1183–1192.

Garcia-Ramirez, M., Dong, F. & Ausio, J. (1992). Role of the histone 'Tails' in the folding of oligonucleosomes depleted of histone H1. *Journal of Biological Chemistry*. 267 (27). p.pp. 19587–19595.

Gershey, E.L., Haslett, G.W., Vidali, G. & Allfrey, V.G. (1969). Chemical studies of histone methylation. Evidence for the occurrence of 3-methylhistidine in avian erythrocyte histone fractions. *Journal of Biological Chemistry*. 244 (18). p.pp. 4871–4877.

Ghadially, R., Brown, B.E., Sequeira-Martin, S.M., Feingold, K.R. & Elias, P.M. (1995). The aged epidermal permeability barrier. Structural, functional, and lipid biochemical abnormalities in humans and a senescent murine model. *Journal of Clinical Investigation*. 95 (5). p.pp. 2281–2290.

Gilaberte, Y., Prieto-Torres, L., Pastushenko, I. & Juarranz, Á. (2016). Anatomy and Function of the Skin. In: *Nanoscience in Dermatology*. [Online]. Academic Press,

pp. 1–14. Available from: https://www.sciencedirect.com/science/article/pii/B978012802926800001X#bib1. [Accessed: 31 July 2019].

Gioia, M., Monaco, S., Van Den Steen, P.E., Sbardella, D., Grasso, G., Marini, S., Overall, C.M., Opdenakker, G. & Coletta, M. (2009). The Collagen Binding Domain of Gelatinase A Modulates Degradation of Collagen IV by Gelatinase B. *Journal of Molecular Biology*. 386 (2). p.pp. 419–434.

Gopalakrishnan, S., Van Emburgh, B.O., Shan, J., Su, Z., Fields, C.R., Vieweg, J., Hamazaki, T., Schwartz, P.H., Terada, N. & Robertson, K.D. (2009). A novel DNMT3B splice variant expressed in tumor and pluripotent cells modulates genomic DNA methylation patterns and displays altered DNA binding. *Molecular Cancer Research*. 7 (10). p.pp. 1622–1634.

Greer, E.L. & Shi, Y. (2012). Histone methylation: a dynamic mark in health, disease and inheritance. *Nature Reviews Genetics*. [Online]. 13 (5). p.pp. 343–357. Available from: http://www.ncbi.nlm.nih.gov/pubmed/22473383. [Accessed: 8 April 2018].

Greider, C.W. & Blackburn, E.H. (1989). A telomeric sequence in the RNA of Tetrahymena telomerase required for telomere repeat synthesis. *Nature*. 337. p.pp. 331–337.

Grönniger, E., Weber, B., Heil, O., Peters, N., Stäb, F., Wenck, H., Korn, B., Winnefeld, M. & Lyko, F. (2010). Aging and Chronic Sun Exposure Cause Distinct Epigenetic Changes in Human Skin. *PLoS Genetics*. [Online]. 6 (5). Available from: http://dx.plos.org/10.1371/journal.pgen.1000971. [Accessed: 12 September 2017].

Grove, G.L. & Kligman, A.M. (1983). Age-associated changes in human epidermal cell renewal. *Journals of Gerontology*. 38 (2). p.pp. 137–142.

Gu, T.P., Guo, F., Yang, H., Wu, H.P., Xu, G.F., Liu, W., Xie, Z.G., Shi, L., He, X., Jin, S.G., Iqbal, K., Shi, Y.G., Deng, Z., Szabó, P.E., Pfeifer, G.P., Li, J. & Xu, G.L. (2011). The role of Tet3 DNA dioxygenase in epigenetic reprogramming by oocytes. *Nature*.

Gu, X., Nylander, E., Coates, P.J., Fahraeus, R. & Nylander, K. (2015). Correlation between Reversal of DNA Methylation and Clinical Symptoms in Psoriatic Epidermis Following Narrow-Band UVB Phototherapy. *The Journal of Investigative Dermatology*. 135 (8). p.pp. 2077–2083.

Guelen, L., Pagie, L., Brasset, E., Meuleman, W., Faza, M.B., Talhout, W., Eussen, B.H., De Klein, A., Wessels, L., De Laat, W. & Van Steensel, B. (2008). Domain organization of human chromosomes revealed by mapping of nuclear lamina interactions. *Nature*. 453 (7197). p.pp. 948–951.

Guilhamon, P., Eskandarpour, M., Halai, D., Wilson, G.A., Feber, A., Teschendorff, A.E., Gomez, V., Hergovich, A., Tirabosco, R., Fernanda Amary, M., Baumhoer, D., Jundt, G., Ross, M.T., Flanagan, A.M. & Beck, S. (2013). Meta-analysis of IDH-

mutant cancers identifies EBF1 as an interaction partner for TET2. *Nature Communications*.

Gunin, A.G., Kornilova, N.K., Vasilieva, O. V. & Petrov, V. V. (2011). Age-related changes in proliferation, the numbers of mast cells, eosinophils, and cd45-positive cells in human dermis. *Journals of Gerontology - Series A Biological Sciences and Medical Sciences*. 66 (4). p.pp. 385–392.

Gunn, D.A., Rexbye, H., Griffiths, C.E.M., Murray, P.G., Fereday, A., Catt, S.D., Tomlin, C.C., Strongitharm, B.H., Perrett, D.I., Catt, M., Mayes, A.E., Messenger, A.G., Green, M.R., van der Ouderaa, F., Vaupel, J.W. & Christensen, K. (2009). Why some women look young for their age. *PLoS ONE*. 4 (12).

Hajime, M., Katsuyuki, S., Takako, K., Takaaki, I., Yukio, K. & Seichiro, S. (1990). Treatment of Vitiligo with Epidermal Grafting Using the Suction Blister. *skin research*. 32 (5). p.pp. 694–697.

Hannum, G., Guinney, J., Zhao, L., Zhang, L., Hughes, G., Sadda, S.V., Klotzle, B., Bibikova, M., Fan, J.B., Gao, Y., Deconde, R., Chen, M., Rajapakse, I., Friend, S., Ideker, T. & Zhang, K. (2013). Genome-wide Methylation Profiles Reveal Quantitative Views of Human Aging Rates. *Molecular Cell*. 49 (2). p.pp. 359–367.

Harman, D. (1956). Aging: a theory based on free radical and radiation chemistry. *Journal of gerontology*. 11 (3). p.pp. 298–300.

Has, C. (2018). Peeling Skin Disorders: A Paradigm for Skin Desquamation. *Journal of Investigative Dermatology*. 138 (8). p.pp. 1689–1691.

Hebbes, T.R., Clayton, A.L., Thorne, A.W. & Crane-Robinson, C. (1994). Core histone hyperacetylation co-maps with generalized DNase I sensitivity in the chicken beta-globin chromosomal domain. *The EMBO journal*. [Online]. 13 (8). p.pp. 1823–30. Available from: http://www.ncbi.nlm.nih.gov/pubmed/8168481. [Accessed: 8 April 2018].

Hergeth, S.P. & Schneider, R. (2015). The H1 linker histones: multifunctional proteins beyond the nucleosomal core particle. *EMBO reports*. 16 (11). p.pp. 1439–1453.

Hermann, A., Goyal, R. & Jeltsch, A. (2004). The Dnmt1 DNA-(cytosine-C5)-methyltransferase methylates DNA processively with high preference for hemimethylated target sites. *Journal of Biological Chemistry*. 279 (46). p.pp. 48350–48359.

Hinz, J.M. & Czaja, W. (2015). Facilitation of base excision repair by chromatin remodeling. *DNA Repair*. 36 p.pp. 91–97.

Holick, M.F. (2017). *Ultraviolet B Radiation: The Vitamin D Connection*. 996. p.pp. 137–154.

Holliday, R. & Pugh, J.E. (1975). DNA modification mechanisms and gene activity during

development. *Science*. [Online]. 187 (4173). p.pp. 226–232. Available from: http://www.ncbi.nlm.nih.gov/pubmed/1111098. [Accessed: 28 July 2019].

Horvath, S. (2013). DNA methylation age of human tissues and cell types. *Genome Biology*. 14 (10).

Horvath, S., Oshima, J., Martin, G.M., Lu, A.T., Quach, A., Cohen, H., Felton, S., Matsuyama, M., Lowe, D., Kabacik, S., Wilson, J.G., Reiner, A.P., Maierhofer, A., Flunkert, J., Aviv, A., Hou, L., Baccarelli, A.A., Li, Y., Stewart, J.D., Whitsel, E.A., Ferrucci, L., Matsuyama, S. & Raj, K. (2018). Epigenetic clock for skin and blood cells applied to Hutchinson Gilford Progeria Syndrome and <i>ex vivo</i> studies. *Aging*. [Online]. 10 (7). p.pp. 1758–1775. Available from: http://www.ncbi.nlm.nih.gov/pubmed/30048243. [Accessed: 14 March 2019].

Horvath, S. & Raj, K. (2018). DNA methylation-based biomarkers and the epigenetic clock theory of ageing. *Nature Reviews Genetics*. 19 (6) p.pp. 371–384.

Hu, W., Xin, Y., Zhang, L., Hu, J., Sun, Y. & Zhao, Y. (2018). Iroquois homeodomain transcription factors in ventricular conduction system and arrhythmia. *International Journal of Medical Sciences*. 15 (8). p.pp. 808–815.

Huang, Y., Pastor, W.A., Shen, Y., Tahiliani, M., Liu, D.R. & Rao, A. (2010). The behaviour of 5-hydroxymethylcytosine in bisulfite sequencing. *PLoS ONE*. 5 (1).

Ikenhata, H. & Ono, T. (2011). The Mechanisms of UV Mutagenesis. *Journal of Radiation Research*. [Online]. 52 (2). p.pp. 115–125. Available from: https://academic.oup.com/jrr/article-lookup/doi/10.1269/jrr.10175.

Illumina (2015). Illumina Methylation BeadChips Achieve Breadth of Coverage Using 2 Infinium Chemistries. *Illumina Inc.* p.pp. 2–5.

Ioshikhes, I.P. & Zhang, M.Q. (2000). Large-scale human promoter mapping using CpG islands. *Nature Genetics*. 26 (1). p.pp. 61–63.

Irizarry, R.A., Ladd-Acosta, C., Wen, B., Wu, Z., Montano, C., Onyango, P., Cui, H., Gabo, K., Rongione, M., Webster, M., Ji, H., Potash, J., Sabunciyan, S., Feinberg, A.P. & Genet Author manuscript, N. (2009). Genome-wide methylation analysis of human colon cancer reveals similar hypo-and hypermethylation at conserved tissue-specific CpG island shores HHS Public Access Author manuscript. *Nat Genet*. [Online]. 41 (2). p.pp. 178–186. Available from: http://www.nature.com/authors/editorial_policies/license.html#terms.

Jablonski, N.G. & Chaplin, G. (2017). The colours of humanity: The evolution of pigmentation in the human lineage. *Philosophical Transactions of the Royal Society B: Biological Sciences*. 372 (1724).

de Jager, T.L., Cockrell, A.E. & Du Plessis, S.S. (2017). Ultraviolet Light Induced Generation of Reactive Oxygen Species. *Advances in Experimental Medicine and Biology*. [Online]. 996. p.pp. 15–23. Available from:

http://link.springer.com/10.1007/978-3-319-56017-5_2. [Accessed: 14 January 2019].

Jeltsch, A. & Jurkowska, R.Z. (2014). New concepts in DNA methylation. *Trends in Biochemical Sciences*. 39 (7) p.pp. 310–318.

Jensen, J.M., Förl, M., Winoto-Morbach, S., Seite, S., Schunk, M., Proksch, E. & Schütze, S. (2005). Acid and neutral sphingomyelinase, ceramide synthase, and acid ceramidase activities in cutaneous aging. *Experimental Dermatology*. 14 (8). p.pp. 609–618.

Jin, B. & Robertson, K.D. (2013). DNA methyltransferases, DNA damage repair, and cancer. *Advances in Experimental Medicine and Biology*. 754. p.pp. 3–29.

Jjingo, D., Conley, A.B., Yi, S. V., Lunyak, V. V. & Jordan, I.K. (2012). On the presence and role of human gene-body DNA methylation. *Oncotarget*. [Online]. 3 (4). p.pp. 462–74. Available from: http://www.ncbi.nlm.nih.gov/pubmed/22577155. [Accessed: 28 July 2019].

Jobe, E.M., McQuate, A.L. & Zhao, X. (2012). Crosstalk among epigenetic pathways regulates neurogenesis. *Frontiers in Neuroscience*. 6 (59).

Johnson, W.E., Li, C. & Rabinovic, A. (2007). Adjusting batch effects in microarray expression data using empirical Bayes methods. *Biostatistics*. [Online]. 8 (1). p.pp. 118–127. Available from: http://www.ncbi.nlm.nih.gov/pubmed/16632515. [Accessed: 6 February 2019].

Joly-Tonetti, N., Wibawa, J.I.D., Bell, M. & Tobin, D. (2016). Melanin fate in the human epidermis: a reassessment of how best to detect and analyse histologically. *Experimental Dermatology*. 25 (7) p.pp. 501–504.

Jones, P., Lucock, M., Veysey, M. & Beckett, E. (2018). The vitamin D–folate hypothesis as an evolutionary model for skin pigmentation: An update and integration of current ideas. *Nutrients*. 10 (5). p.p. 554.

Jylhävä, J., Pedersen, N.L. & Hägg, S. (2017). Biological Age Predictors. *EBioMedicine*. 21. p.pp. 29–36.

Kaidbey, K.H., Agin, P.P., Sayre, R.M. & Kligman, A.M. (1979). Photoprotection by melanin—a comparison of black and Caucasian skin. *Journal of the American Academy of Dermatology*. 1 (3). p.pp. 249–260.

Kanehisa, M., Sato, Y., Furumichi, M., Morishima, K. & Tanabe, M. (2019). New approach for understanding genome variations in KEGG. *Nucleic Acids Research*.

Karemaker, I.D. & Vermeulen, M. (2018). Single-Cell DNA Methylation Profiling: Technologies and Biological Applications. *Trends in Biotechnology*. 36 (9) p.pp. 952–965.

Kareta, M.S., Botello, Z.M., Ennis, J.J., Chou, C. & Chédin, F. (2006). Reconstitution and Mechanism of the Stimulation of *de Novo* Methylation by Human DNMT3L. *Journal of Biological Chemistry*. [Online]. 281 (36). p.pp. 25893–25902. Available from: http://www.ncbi.nlm.nih.gov/pubmed/16829525. [Accessed: 28 July 2019].

Kim, H.-Y. (2003). Methionine Sulfoxide Reduction in Mammals: Characterization of Methionine-R-Sulfoxide Reductases. *Molecular Biology of the Cell*. 15 (3). p.pp. 1055–1064.

Kim, M. & Costello, J. (2017). DNA methylation: an epigenetic mark of cellular memory. *Experimental & Molecular Medicine*. [Online]. 49 (4). Available from: http://www.nature.com/articles/emm201710. [Accessed: 17 January 2019].

Koch, C.M., Suschek, C. V., Lin, Q., Bork, S., Goergens, M., Joussen, S., Pallua, N., Ho, A.D., Zenke, M. & Wagner, W. (2011). Specific Age-Associated DNA Methylation Changes in Human Dermal Fibroblasts. *PLoS ONE*. [Online]. 6 (2). Available from: https://dx.plos.org/10.1371/journal.pone.0016679. [Accessed: 24 March 2019].

Koch, C.M. & Wagner, W. (2011). Epigenetic-aging-signature to determine age in different tissues. *Aging*. 3 (10). p.pp. 1018–1027.

Koivunen, P. & Laukka, T. (2018). The TET enzymes. *Cellular and Molecular Life Sciences*. [Online]. 75 (8). p.pp. 1339–1348. Available from: http://www.ncbi.nlm.nih.gov/pubmed/29184981. [Accessed: 28 July 2019].

Kucharski, R., Maleszka, J., Foret, S. & Maleszka, R. (2008). Nutritional control of reproductive status in honeybees via DNA methylation. *Science*. 319 (5871). p.pp. 1827–1830.

Kudo, Y., Tateishi, K., Yamamoto, K., Yamamoto, S., Asaoka, Y., Ijichi, H., Nagae, G., Yoshida, H., Aburatani, H. & Koike, K. (2012). Loss of 5-hydroxymethylcytosine is accompanied with malignant cellular transformation. *Cancer Science*. 103 (4). p.pp. 670–676.

Kwak, G.H., Lim, D.H., Han, J.Y., Lee, Y.S. & Kim, H.Y. (2012). Methionine sulfoxide reductase B3 protects from endoplasmic reticulum stress in Drosophila and in mammalian cells. *Biochemical and Biophysical Research Communications*. 420 (1). p.pp. 130–135.

Lahtz, C., Kim, S.-I., Bates, S.E., Li, A.X., Wu, X. & Pfeifer, G.P. (2013). UVB irradiation does not directly induce detectable changes of DNA methylation in human keratinocytes. *F1000Research*. [Online]. 2. p.p. 45. Available from: http://www.ncbi.nlm.nih.gov/pubmed/24555035. [Accessed: 8 April 2018].

Lambers, H., Piessens, S., Bloem, A., Pronk, H. & Finkel, P. (2006). Natural skin surface pH is on average below 5, which is beneficial for its resident flora. *International Journal of Cosmetic Science*. 28 (5). p.pp. 359–370.

Langton, A.K., Alessi, S., Hann, M., Chien, A.L.L., Kang, S., Griffiths, C.E.M. & Watson,

R.E.B. (2019a). Aging in Skin of Color: Disruption to Elastic Fiber Organization Is Detrimental to Skin's Biomechanical Function. *Journal of Investigative Dermatology*. 139 (4). p.pp. 779–788.

Langton, A.K., Graham, H.K., Griffiths, C.E.M. & Watson, R.E.B. (2019b). Ageing significantly impacts the biomechanical function and structural composition of skin. *Experimental Dermatology*. 28 (8). p.pp. 981–984.

Langton, A.K., Graham, H.K., McConnell, J.C., Sherratt, M.J., Griffiths, C.E.M. & Watson, R.E.B. (2017). Organization of the dermal matrix impacts the biomechanical properties of skin. *British Journal of Dermatology*. 177 (3). p.pp. 818–827.

Langton, A.K., Halai, P., Griffiths, C.E.M., Sherratt, M.J. & Watson, R.E.B. (2016). The impact of intrinsic ageing on the protein composition of the dermal-epidermal junction. *Mechanisms of Ageing and Development*. 156. p.pp. 14–16.

Langton, A.K., Sherratt, M.J., Griffiths, C.E.M. & Watson, R.E.B. (2010). A new wrinkle on old skin: The role of elastic fibres in skin ageing. *International Journal of Cosmetic Science*. 32 (5) p.pp. 330–339.

Laverdet, B., Danigo, A., Girard, D., Magy, L., Demiot, C. & Desmoulière, A. (2015). Skin innervation: Important roles during normal and pathological cutaneous repair. *Histology and Histopathology*. 30 (8). p.pp. 875–892.

Lavker, R.M., Zheng, P. & Dong, G. (1987). Aged skin: A study by light, transmission electron, and scanning electron microscopy. *Journal of Investigative Dermatology*. 88 (Suppl 3). p.pp. 44–51.

Lawlor, K.T. & Kaur, P. (2015). Dermal contributions to human interfollicular epidermal architecture and self-renewal. *International Journal of Molecular Sciences*. 16 (12). p.pp. 28098–28107.

Lee, D.H. & Pfeifer, G.P. (2003). Deamination of 5-methylcytosines within cyclobutane pyrimidine dimers is an important component of UVB mutagenesis. *Journal of Biological Chemistry*. 278 (12). p.pp. 10314–10321.

Lee, E., Iskow, R., Yang, L., Gokcumen, O., Haseley, P., Luquette, L.J., Lohr, J.G., Harris, C.C., Ding, L., Wilson, R.K., Wheeler, D.A., Gibbs, R.A., Kucherlapati, R., Lee, C., Kharchenko, P. V. & Park, P.J. (2012). Landscape of somatic retrotransposition in human cancers. *Science*. 337 (6097). p.pp. 967–971.

Lee, Y.S., Yuspa, S.H. & Dlugosz, A.A. (1998). Differentiation of cultured human epidermal keratinocytes at high cell densities is mediated by endogenous activation of the protein kinase C signaling pathway. *Journal of Investigative Dermatology*. 111 (5). p.pp. 762–766.

Leigh-Brown, S., Enriquez, J.A. & Odom, D.T. (2010). Nuclear transcription factors in mammalian mitochondria. *Genome Biology*. 11 (7).

Lerche, C.M., Philipsen, P.A. & Wulf, H.C. (2017). UVR: sun, lamps, pigmentation and Vitamin D. *Photochemical and Photobiological Sciences*. 16 (3). p.pp. 291–301.

Levine, R.L., Berlett, B.S., Moskovitz, J., Mosoni, L. & Stadtman, E.R. (1999). Methionine residues may protect proteins from critical oxidative damage. *Mechanisms of Ageing and Development*. 107 (3). p.pp. 323–332.

Levy, M.Z., Allsopp, R.C., Futcher, A.B., Greider, C.W. & Harley, C.B. (1992). Telomere end-replication problem and cell aging. *Journal of Molecular Biology*. 225 (4). p.pp. 951–960.

Li, E., Bestor, T.H. & Jaenisch, R. (1992). Targeted mutation of the DNA methyltransferase gene results in embryonic lethality. *Cell*.

Li, Z., Cai, X., Cai, C.L., Wang, J., Zhang, W., Petersen, B.E., Yang, F.C. & Xu, M. (2011a). Deletion of Tet2 in mice leads to dysregulated hematopoietic stem cells and subsequent development of myeloid malignancies. In: *Blood*. 2011.

Li, Z., Cai, X., Cai, C.L., Wang, J., Zhang, W., Petersen, B.E., Yang, F.C. & Xu, M. (2011b). Deletion of Tet2 in mice leads to dysregulated hematopoietic stem cells and subsequent development of myeloid malignancies. *Blood*. 118 (17). p.pp. 4509–4518.

Liao, L.M., Brennan, P., van Bemmel, D.M., Zaridze, D., Matveev, V., Janout, V., Kollarova, H., Bencko, V., Navratilova, M., Szeszenia-Dabrowska, N., Mates, D., Rothman, N., Boffetta, P., Chow, W.H. & Moore, L.E. (2011). Line-1 methylation levels in leukocyte DNA and risk of renal cell cancer. *PLoS ONE*. 6 (11).

Lin, J.Y. & Fisher, D.E. (2007). Melanocyte biology and skin pigmentation. *Nature*. 445 (7130). p.pp. 843–850.

Liu, X.S., Wu, H., Ji, X., Stelzer, Y., Wu, X., Czauderna, S., Shu, J., Dadon, D., Young, R.A. & Jaenisch, R. (2016). Editing DNA Methylation in the Mammalian Genome. *Cell*. 167 (1). p.pp. 233–247.

Liu, Y., Oakeley, E.J., Sun, L. & Jost, J.P. (1998). Multiple domains are involved in the targeting of the mouse DNA methyltransferase to the DNA replication foci. *Nucleic Acids Research*. 26 (4). p.pp. 1038–1045.

Lo, D.D., Hu, M.S., Zimmermann, A.S., Longaker, M.T. & Peter Lorenz, H. (2015). Differences in Foetal, Adult Skin and Mucosal Repair. In: *Stem Cell Biology and Tissue Engineering in Dental Sciences*. [Online]. Academic Press, pp. 691–702. Available from: https://www.sciencedirect.com/science/article/pii/B9780123971579000552. [Accessed: 20 August 2019].

Lourenço dos Santos, S., Petropoulos, I. & Friguet, B. (2018). The Oxidized Protein Repair Enzymes Methionine Sulfoxide Reductases and Their Roles in Protecting against Oxidative Stress, in Ageing and in Regulating Protein Function.

Antioxidants. 7 (12). p.p. 191.

Luger, K., Mäder, a W., Richmond, R.K., Sargent, D.F. & Richmond, T.J. (1997). Crystal structure of the nucleosome core particle at 2.8 A resolution. *Nature*. 389 (6648). p.pp. 251–260.

Lyko, F. (2018). The DNA methyltransferase family: A versatile toolkit for epigenetic regulation. *Nature Reviews Genetics*. 19 (2). p.pp. 81–92.

Maas, A.H.E.M. & Appelman, Y.E.A. (2010). Gender differences in coronary heart disease. *Netherlands Heart Journal*. 18 (12) p.pp. 598–603.

Maegawa, S., Hinkal, G., Kim, H.S., Shen, L., Zhang, L., Zhang, J., Zhang, N., Liang, S., Donehower, L.A. & Issa, J.P.J. (2010). Widespread and tissue specific age-related DNA methylation changes in mice. *Genome Research*. 20 (3). p.pp. 332–340.

Marchenko, N.D., Zaika, A. & Moll, U.M. (2002). Death Signal-induced Localization of p53 Protein to Mitochondria. *Journal of Biological Chemistry*. 275 (21). p.pp. 16202–16212.

Martinez-Fernandez, L., Banyasz, A., Esposito, L., Markovitsi, D. & Improta, R. (2017). UV-induced damage to DNA: Effect of cytosine methylation on pyrimidine dimerization. *Signal Transduction and Targeted Therapy*. 2. p.p. 17021.

Matys, V. (2006). TRANSFAC(R) and its module TRANSCompel(R): transcriptional gene regulation in eukaryotes. *Nucleic Acids Research*.

McGhee, J.D. & Ginder, G.D. (1979). Specific DNA methylation sites in the vicinity of the chicken β-globin genes. *Nature*. [Online]. 280 (5721). p.pp. 419–420. Available from: http://www.ncbi.nlm.nih.gov/pubmed/460418. [Accessed: 28 July 2019].

Mentch, S.J. & Locasale, J.W. (2016). One-carbon metabolism and epigenetics: Understanding the specificity. *Annals of the New York Academy of Sciences*.

Mirbahai, L. & Chipman, J.K. (2014). Epigenetic memory of environmental organisms: A reflection of lifetime stressor exposures. *Mutation Research - Genetic Toxicology and Environmental Mutagenesis*. 764–765. p.pp. 10–17.

Mohammad, H.P. & Baylin, S.B. (2010). Linking cell signaling and the epigenetic machinery. *Nature Biotechnology*. [Online]. 28 (10). p.pp. 1033–1038. Available from: http://www.nature.com/articles/nbt1010-1033. [Accessed: 9 April 2018].

Monaco, S., Sparano, V., Gioia, M., Sbardella, D., Di Pierro, D., Marini, S. & Coletta, M. (2006). Enzymatic processing of collagen IV by MMP-2 (gelatinase A) affects neutrophil migration and it is modulated by extracatalytic domains. *Protein Science*. 15 (12). p.pp. 2805–2815.

Montagna, W. & Carlisle, K. (1979). Structural changes in aging human skin. *Journal of Investigative Dermatology*. 73 (1). p.pp. 47–53.

Moore, L.D., Le, T. & Fan, G. (2013). DNA methylation and its basic function. *Neuropsychopharmacology : official publication of the American College of Neuropsychopharmacology*. [Online]. 38 (1). p.pp. 23–38. Available from: http://www.ncbi.nlm.nih.gov/pubmed/22781841. [Accessed: 28 July 2019].

Moran, S., Arribas, C. & Esteller, M. (2016). Validation of a DNA methylation microarray for 850,000 CpG sites of the human genome enriched in enhancer sequences. *Epigenomics*. 8 (3). p.pp. 389–399.

Moskovitz, J., Jenkins, N.A., Gilbert, D.J., Copeland, N.G., Jursky, F., Weissbach, H. & Brot, N. (2002). Chromosomal localization of the mammalian peptide-methionine sulfoxide reductase gene and its differential expression in various tissues. *Proceedings of the National Academy of Sciences*. 93 (8). p.pp. 3205–3208.

Moyzis, R.K., Buckingham, J.M., Cram, L.S., Dani, M., Deaven, L.L., Jones, M.D., Meyne, J., Ratliff, R.L. & Wu, J.R. (1988). A highly conserved repetitive DNA sequence, (TTAGGG)n, present at the telomeres of human chromosomes. *Proceedings of the National Academy of Sciences*. 85 (18). p.pp. 6622–6626.

Murakami, M., Ohtake, T., Dorschner, R.A., Schittek, B., Garbe, C. & Gallo, R.L. (2002). Cathelicidin anti-microbial peptide expression in sweat, an innate defense system for the skin. *Journal of Investigative Dermatology*. 119 (5). p.pp. 1090–1095.

Murray, K. (1964). The Occurrence of iε-N-Methyl Lysine in Histones. *Biochemistry*. [Online]. 3 (1). p.pp. 10–15. Available from: http://pubs.acs.org/doi/abs/10.1021/bi00889a003. [Accessed: 8 April 2018].

Nakatomi, Y., Tsuruga, E., Nakashima, K., Sawa, Y. & Ishikawa, H. (2011). EMILIN-1 regulates the amount of oxytalan fiber formation in periodontal ligaments in vitro. *Connective Tissue Research*. 52 (1). p.pp. 30–35.

Naylor, E.C., Watson, R.E.B. & Sherratt, M.J. (2011). Molecular aspects of skin ageing. *Maturitas*. [Online]. 69 (3). p.pp. 249–256. Available from: http://linkinghub.elsevier.com/retrieve/pii/S0378512211001496. [Accessed: 26 July 2017].

Neerken, S., Lucassen, G.W., Bisschop, M.A., Lenderink, E. & Nuijs, T. (A. M.. (2004). Characterization of age-related effects in human skin: A comparative study that applies confocal laser scanning microscopy and optical coherence tomography. *Journal of Biomedical Optics*. 9 (2). p.p. 274.

Newton, V.L., Riba-Garcia, I., Griffiths, C.E.M., Rawlings, A. V., Voegeli, R., Unwin, R.D., Sherratt, M.J. & Watson, R.E.B. (2019). Mass spectrometry-based proteomics reveals the distinct nature of the skin proteomes of photoaged compared to intrinsically aged skin. *International Journal of Cosmetic Science*. 41 (2). p.pp. 118–131.

Ni, K., Dansranjavin, T., Rogenhofer, N., Oeztuerk, N., Deuker, J., Bergmann, M., Schuppe, H.C., Wagenlehner, F., Weidner, W., Steger, K. & Schagdarsurengin, U.

(2016). TET enzymes are successively expressed during human spermatogenesis and their expression level is pivotal for male fertility. *Human Reproduction*. 31 (7). p.pp. 1411–1424.

Nonaka, S., Kaidbey, K.H. & Kligman, A.M. (1984). Photoprotective Adaptation: Some Quantitative Aspects. *Archives of Dermatology*. 120 (5). p.pp. 609–612.

Okano, M., Bell, D.W., Haber, D.A. & Li, E. (1999). DNA methyltransferases Dnmt3a and Dnmt3b are essential for de novo methylation and mammalian development. *Cell*. 99 (3). p.pp. 247–257.

Oliveira, A.M.M., Hemstedt, T.J. & Bading, H. (2012). Rescue of aging-associated decline in Dnmt3a2 expression restores cognitive abilities. *Nature Neuroscience*. 15 (8). p.pp. 1111–1113.

Orentreich, D., Leone, A.-S., Arpino, G. & Burack, H. (2001). Sunscreens: practical applications. *Comprehensive Series in Photosciences*. [Online]. 3. p.pp. 535–559. Available from: https://www.sciencedirect.com/science/article/pii/S1568461X01800636. [Accessed: 25 July 2019].

Ortonne, J.P. (1990). Pigmentary changes of the ageing skin. *British Journal of Dermatology*. 122 (Suppl 35). p.pp. 21–28.

Ostler, K.R., Davis, E.M., Payne, S.L., Gosalia, B.B., Expósito-Céspedes, J., Beau, M.M.L. & Godley, L.A. (2007). Cancer cells express aberrant DNMT3B transcripts encoding truncated proteins. *Oncogene*. 26 (38). p.pp. 5553–5563.

Pera, A., Campos, C., López, N., Hassouneh, F., Alonso, C., Tarazona, R. & Solana, R. (2015). Immunosenescence: Implications for response to infection and vaccination in older people. *Maturitas*. 82 (1). p.pp. 50–55.

Peters, T.J., Buckley, M.J., Statham, A.L., Pidsley, R., Samaras, K., V Lord, R., Clark, S.J. & Molloy, P.L. (2015). De novo identification of differentially methylated regions in the human genome. *Epigenetics and Chromatin*. 8 (1).

Philibert, R.A., Penaluna, B., White, T., Shires, S., Gunter, T., Liesveld, J., Erwin, C., Hollenbeck, N. & Osborn, T. (2014). A pilot examination of the genome-wide DNA methylation signatures of subjects entering and exiting short-term alcohol dependence treatment programs. *Epigenetics*. 9 (9). p.pp. 1212–1219.

Pilkington, S.M., Ogden, S., Eaton, L.H., Dearman, R.J., Kimber, I. & Griffiths, C.E.M. (2018). Lower levels of interleukin-1β gene expression are associated with impaired Langerhans' cell migration in aged human skin. *Immunology*. 153 (1). p.pp. 60–70.

Portela, A. & Esteller, M. (2010). Epigenetic modifications and human disease. *Nature Biotechnology*. 28 (10). p.pp. 1057–1068.

Probst, A. V., Dunleavy, E. & Almouzni, G. (2009). Epigenetic inheritance during the cell cycle. *Nature Reviews Molecular Cell Biology*. [Online]. 10 (3). p.pp. 192–206. Available from: http://www.ncbi.nlm.nih.gov/pubmed/19234478. [Accessed: 12 September 2017].

Prost-Squarcioni, C., Fraitag, S., Heller, M. & Boehm, N. (2008). Functional histology of dermis. *Annales de Dermatologie et de Venereologie*. 135 (1).

Putiri, E.L., Tiedemann, R.L., Thompson, J.J., Liu, C., Ho, T., Choi, J.H. & Robertson, K.D. (2014). Distinct and overlapping control of 5-methylcytosine and 5-hydroxymethylcytosine by the TET proteins in human cancer cells. *Genome Biology*. 15 (6).

Quante, T. & Bird, A. (2016). Do short, frequent DNA sequence motifs mould the epigenome? *Nature Reviews Molecular Cell Biology*. 17. p.pp. 257–262.

Raddatz, G., Hagemann, S., Aran, D., Söhle, J., Kulkarni, P.P., Kaderali, L., Hellman, A., Winnefeld, M. & Lyko, F. (2013). Aging is associated with highly defined epigenetic changes in the human epidermis. *Epigenetics & chromatin*. [Online]. 6 (1). p.p. 36. Available from: http://www.ncbi.nlm.nih.gov/pubmed/24279375. [Accessed: 15 April 2018].

Rampal, R., Alkalin, A., Madzo, J., Vasanthakumar, A., Pronier, E., Patel, J., Li, Y., Ahn, J., Abdel-Wahab, O., Shih, A., Lu, C., Ward, P.S., Tsai, J.J., Hricik, T., Tosello, V., Tallman, J.E., Zhao, X., Daniels, D., Dai, Q., Ciminio, L., Aifantis, I., He, C., Fuks, F., Tallman, M.S., Ferrando, A., Nimer, S., Paietta, E., Thompson, C.B., Licht, J.D., Mason, C.E., Godley, L.A., Melnick, A., Figueroa, M.E. & Levine, R.L. (2014). DNA Hydroxymethylation Profiling Reveals that WT1 Mutations Result in Loss of TET2 Function in Acute Myeloid Leukemia. *Cell Reports*.

Rangel-Huerta, E. & Maldonado, E. (2017). Transit-Amplifying Cells in the Fast Lane from Stem Cells towards Differentiation. *Stem Cells International*. 2017.

Rasmussen, K.D. & Helin, K. (2016). Role of TET enzymes in DNA methylation, development, and cancer. *Genes & development*. [Online]. 30 (7). p.pp. 733–50. Available from: http://www.ncbi.nlm.nih.gov/pubmed/27036965. [Accessed: 17 January 2019].

Raudvere, U., Kolberg, L., Kuzmin, I., Arak, T., Adler, P., Peterson, H. & Vilo, J. (2019). g:Profiler: a web server for functional enrichment analysis and conversions of gene lists (2019 update). *Nucleic acids research*.

Ray, P.D., Huang, B.W. & Tsuji, Y. (2012). Reactive oxygen species (ROS) homeostasis and redox regulation in cellular signaling. *Cellular Signalling*. 24 (5). p.pp. 981–990.

Riggs, A.D. (1975). X inactivation, differentiation, and DNA methylation. *Cytogenetic and Genome Research*. [Online]. 14 (1). p.pp. 9–25. Available from: http://www.ncbi.nlm.nih.gov/pubmed/1093816. [Accessed: 28 July 2019].

Riley, J.W., Stouffer, S.A., Suchman, E.A., Devinney, L.C., Star, S.A. & Williams, R.M. (1949). The American Soldier: Adjustment During Army Life. *Am. Sociol. Rev*. 14 (4) p.p. 557.

Ristow, M. & Schmeisser, S. (2011). Extending life span by increasing oxidative stress. *Free Radical Biology and Medicine*. 51 (2). p.pp. 327–336.

Ritchie, M.E., Phipson, B., Wu, D., Hu, Y., Law, C.W., Shi, W. & Smyth, G.K. (2015). limma powers differential expression analyses for RNA-sequencing and microarray studies. *Nucleic acids research*. [Online]. 43 (7). p.p. e47. Available from: http://www.ncbi.nlm.nih.gov/pubmed/25605792. [Accessed: 6 February 2019].

Rittié, L. & Fisher, G.J. (2002). UV-light-induced signal cascades and skin aging. *Ageing Research Reviews*. 1 (4). p.pp. 705–720.

Rodríguez-Paredes, M., Bormann, F., Raddatz, G., Gutekunst, J., Lucena-Porcel, C., Köhler, F., Wurzer, E., Schmidt, K., Gallinat, S., Wenck, H., Röwert-Huber, J., Denisova, E., Feuerbach, L., Park, J., Brors, B., Herpel, E., Nindl, I., Hofmann, T.G., Winnefeld, M. & Lyko, F. (2018). Methylation profiling identifies two subclasses of squamous cell carcinoma related to distinct cells of origin. *Nature Communications*. [Online]. 9 (1). p.p. 577. Available from: http://www.ncbi.nlm.nih.gov/pubmed/29422656. [Accessed: 17 January 2019].

Romani, N., Brunner, P.M. & Stingl, G. (2012). Changing views of the role of langerhans cells. *Journal of Investigative Dermatology*. 132 (3). p.pp. 872–881.

Sanchez-Mut, J. V. & Gräff, J. (2015). Epigenetic alterations in Alzheimer's disease. *Frontiers in Behavioral Neuroscience*. 9. p.p. 347.

Schauber, J. & Gallo, R.L. (2008). Antimicrobial peptides and the skin immune defense system. *Journal of Allergy and Clinical Immunology*. 122 (2). p.pp. 261–266.

Schiavinato, A., Keene, D.R., Wohl, A.P., Corallo, D., Colombatti, A., Wagener, R., Paulsson, M., Bonaldo, P. & Sengle, G. (2016). Targeting of EMILIN-1 and EMILIN-2 to Fibrillin Microfibrils Facilitates their Incorporation into the Extracellular Matrix. *Journal of Investigative Dermatology*. 136 (6). p.pp. 1150–1160.

Schmittgen, T.D. & Livak, K.J. (2008). Analyzing real-time PCR data by the comparative CT method. *Nature Protocols*. 3 (6). p.pp. 1101–1108.

Sellheyer, K. (2003). Pathogenesis of solar elastosis: Synthesis or degradation? *Journal of Cutaneous Pathology*. 30 (2). p.pp. 123–127.

Sen, G.L., Reuter, J.A., Webster, D.E., Zhu, L. & Khavari, P.A. (2010). DNMT1 maintains progenitor function in self-renewing somatic tissue. *Nature*. 463 (7280). p.pp. 563–567.

She, H., Yang, Q., Shepherd, K., Smith, Y., Miller, G., Testa, C. & Mao, Z. (2011). Direct

regulation of complex I by mitochondrial MEF2D is disrupted in a mouse model of Parkinson disease and in human patients. *Journal of Clinical Investigation*. 121 (3). p.pp. 930–940.

Shen, Y., Stanislauskas, M., Li, G., Zheng, D. & Liu, L. (2017). Epigenetic and genetic dissections of UV-induced global gene dysregulation in skin cells through multi-omics analyses. *Scientific reports*. [Online]. 7. p.p. 42646. Available from: http://www.ncbi.nlm.nih.gov/pubmed/28211524. [Accessed: 8 April 2018].

Shipony, Z., Mukamel, Z., Cohen, N.M., Landan, G., Chomsky, E., Zeliger, S.R., Fried, Y.C., Ainbinder, E., Friedman, N. & Tanay, A. (2014). Dynamic and static maintenance of epigenetic memory in pluripotent and somatic cells. *Nature*. 513 (7516). p.pp. 115–119.

Simpson, C.L., Patel, D.M. & Green, K.J. (2011). Deconstructing the skin: Cytoarchitectural determinants of epidermal morphogenesis. *Nature Reviews Molecular Cell Biology*. 12 (9). p.pp. 565–580.

Situm, M., Bulat, V., Majcen, K., Dzapo, A. & Jezovita, J. (2014). Benefits of controlled ultraviolet radiation in the treatment of dermatological diseases. *Collegium antropologicum*. 38 (4). p.pp. 1249–1253.

Smittenaar, C.R., Petersen, K.A., Stewart, K. & Moitt, N. (2016). Cancer incidence and mortality projections in the UK until 2035. *British Journal of Cancer*. [Online]. 115 (9). p.pp. 1147–1155. Available from: http://www.ncbi.nlm.nih.gov/pubmed/27727232. [Accessed: 5 February 2018].

Sotiropoulou, P.A. & Blanpain, C. (2012). Development and homeostasis of the skin epidermis. *Cold Spring Harbor Perspectives in Biology*. 4 (7).

Srinivas, U.S., Tan, B.W.Q., Vellayappan, B.A. & Jeyasekharan, A.D. (2019). ROS and the DNA damage response in cancer [published online ahead of print, December 21, 2018]. *Redox Biology*.

Statista (2019). *Size of the anti-aging market worldwide from 2018 to 2023 (in billion U.S. dollars)*. [Online]. 2019. Available from: https://www.statista.com/statistics/509679/value-of-the-global-anti-aging-market/. [Accessed: 15 September 2019].

Steindal, A.H., Juzeniene, A., Johnsson, A. & Moan, J. (2006). Photodegradation of 5-methyltetrahydrofolate: Biophysical Aspects. *Photochemistry and Photobiology*. [Online]. 82 (6). p.p. 1651. Available from: http://www.ncbi.nlm.nih.gov/pubmed/16879038. [Accessed: 17 January 2019].

Südel, K.M., Venzke, K., Mielke, H., Breitenbach, U., Mundt, C., Jaspers, S., Koop, U., Sauermann, K., Knußmann-Hartig, E., Moll, I., Gercken, G., Young, A.R., Stäb, F., Wenck, H. & Gallinat, S. (2005). Novel Aspects of Intrinsic and Extrinsic Aging of Human Skin: Beneficial Effects of Soy Extract¶. *Photochemistry and Photobiology*. 81 (3). p.pp. 381–587.

Suh, E., Choi, S.-W. & Friso, S. (2016). One-Carbon Metabolism: An Unsung Hero for Healthy Aging. In: *Molecular Basis of Nutrition and Aging*. [Online]. Academic Press, pp. 513–522. Available from: https://www.sciencedirect.com/science/article/pii/B9780128018163000364. [Accessed: 10 September 2019].

Sun, D., Luo, M., Jeong, M., Rodriguez, B., Xia, Z., Hannah, R., Wang, H., Le, T., Faull, K.F., Chen, R., Gu, H., Bock, C., Meissner, A., Göttgens, B., Darlington, G.J., Li, W. & Goodell, M.A. (2014). Epigenomic profiling of young and aged HSCs reveals concerted changes during aging that reinforce self-renewal. *Cell Stem Cell*. 14 (5). p.pp. 673–688.

Tahiliani, M., Koh, K.P., Shen, Y., Pastor, W.A., Bandukwala, H., Brudno, Y., Agarwal, S., Iyer, L.M., Liu, D.R., Aravind, L. & Rao, A. (2009). Conversion of 5-Methylcytosine to 5-Hydroxymethylcytosine in Mammalian DNA by MLL Partner TET1. *Science*. [Online]. 324 (5929). p.pp. 930–935. Available from: http://www.ncbi.nlm.nih.gov/pubmed/19372391. [Accessed: 9 April 2018].

Tam, T.T.T., Juzeniene, A., Steindal, A.H., Iani, V. & Moan, J. (2009). Photodegradation of 5-methyltetrahydrofolate in the presence of Uroporphyrin. *Journal of Photochemistry and Photobiology B: Biology*. [Online]. 94 (3). p.pp. 201–204. Available from: http://www.ncbi.nlm.nih.gov/pubmed/19138530. [Accessed: 17 January 2019].

Tan, Q., Heijmans, B.T., Hjelmborg, J. v. B., Soerensen, M., Christensen, K. & Christiansen, L. (2016). Epigenetic drift in the aging genome: a ten-year follow-up in an elderly twin cohort. *International Journal of Epidemiology*. 45 (4). p.pp. 1146–1158.

Taverna, S.D., Li, H., Ruthenburg, A.J., Allis, C.D. & Patel, D.J. (2007). How chromatin-binding modules interpret histone modifications: lessons from professional pocket pickers. *Nature Structural & Molecular Biology*. [Online]. 14 (11). p.pp. 1025–1040. Available from: http://www.nature.com/doifinder/10.1038/nsmb1338.

Taylor, R.S., Ogoshi, M., Chaffins, M., Ramirez, R.D., Piatyszek, M.A. & Shay, J.W. (1996). Detection of telomerase activity in malignant and nonmalignant skin conditions. *Journal of Investigative Dermatology*. 106 (4). p.pp. 759–765.

Teschendorff, A.E., Marabita, F., Lechner, M., Bartlett, T., Tegner, J., Gomez-Cabrero, D. & Beck, S. (2013a). A beta-mixture quantile normalization method for correcting probe design bias in Illumina Infinium 450 k DNA methylation data. *Bioinformatics*. [Online]. 29 (2). p.pp. 189–196. Available from: http://www.ncbi.nlm.nih.gov/pubmed/23175756. [Accessed: 6 February 2019].

Teschendorff, A.E., Menon, U., Gentry-Maharaj, A., Ramus, S.J., Weisenberger, D.J., Shen, H., Campan, M., Noushmehr, H., Bell, C.G., Maxwell, A.P., Savage, D.A., Mueller-Holzner, E., Marth, C., Kocjan, G., Gayther, S.A., Jones, A., Beck, S., Wagner, W., Laird, P.W., Jacobs, I.J. & Widschwendter, M. (2010). Age-dependent

DNA methylation of genes that are suppressed in stem cells is a hallmark of cancer. *Genome Research*. 20 (4). p.pp. 440–446.

Teschendorff, A.E., West, J. & Beck, S. (2013b). Age-associated epigenetic drift: Implications, and a case of epigenetic thrift? *Human Molecular Genetics*. 22 (R1). p.pp. 7–15.

Thul, P.J., Akesson, L., Wiking, M., Mahdessian, D., Geladaki, A., Ait Blal, H., Alm, T., Asplund, A., Björk, L., Breckels, L.M., Bäckström, A., Danielsson, F., Fagerberg, L., Fall, J., Gatto, L., Gnann, C., Hober, S., Hjelmare, M., Johansson, F., Lee, S., Lindskog, C., Mulder, J., Mulvey, C.M., Nilsson, P., Oksvold, P., Rockberg, J., Schutten, R., Schwenk, J.M., Sivertsson, A., Sjöstedt, E., Skogs, M., Stadler, C., Sullivan, D.P., Tegel, H., Winsnes, C., Zhang, C., Zwahlen, M., Mardinoglu, A., Pontén, F., Von Feilitzen, K., Lilley, K.S., Uhlén, M. & Lundberg, E. (2017). A subcellular map of the human proteome. *Science*. 356 (6340).

Tian, Y., Morris, T.J., Webster, A.P., Yang, Z., Beck, S., Feber, A. & Teschendorff, A.E. (2017). ChAMP: updated methylation analysis pipeline for Illumina BeadChips A. Valencia (ed.). *Bioinformatics*. [Online]. 33 (24). p.pp. 3982–3984. Available from: http://www.ncbi.nlm.nih.gov/pubmed/28961746. [Accessed: 10 February 2019].

Tommasi, S., Denissenko, M.F. & Pfeifer, G.P. (1997). Sunlight induces pyrimidine dimers preferentially at 5-methylcytosine bases. *Cancer Research*. 57 (21). p.pp. 4727–4730.

Tu, C.L., Oda, Y. & Bikle, D.D. (1999). Effects of a calcium receptor activator on the cellular response to calcium in human keratinocytes. *Journal of Investigative Dermatology*. 113 (3). p.pp. 340–345.

Uhlén, M., Fagerberg, L., Hallström, B.M., Lindskog, C., Oksvold, P., Mardinoglu, A., Sivertsson, Å., Kampf, C., Sjöstedt, E., Asplund, A., Olsson, I.M., Edlund, K., Lundberg, E., Navani, S., Szigyarto, C.A.K., Odeberg, J., Djureinovic, D., Takanen, J.O., Hober, S., Alm, T., Edqvist, P.H., Berling, H., Tegel, H., Mulder, J., Rockberg, J., Nilsson, P., Schwenk, J.M., Hamsten, M., Von Feilitzen, K., Forsberg, M., Persson, L., Johansson, F., Zwahlen, M., Von Heijne, G., Nielsen, J. & Pontén, F. (2015). Tissue-based map of the human proteome. *Science*. 347 (6220).

Valencia-Vera, E., Aguilera, J., Cobos, A., Bernabó, J.-L., Pérez-Valero, V. & Herrera-Ceballos, E. (2019). Association between seasonal serum folate levels and ultraviolet radiation. *Journal of Photochemistry and Photobiology B: Biology*. [Online]. 190. p.pp. 66–71. Available from: http://www.ncbi.nlm.nih.gov/pubmed/30502586. [Accessed: 14 January 2019].

Valkonen, T. & Van Poppel, F. (2004). The contribution of smoking to sex differences in life expectancy: Four Nordic countries and The Netherlands 1970–1989. *The European Journal of Public Health*. 7 (3). p.pp. 302–310.

Vandiver, A.R., Irizarry, R.A., Hansen, K.D., Garza, L.A., Runarsson, A., Li, X., Chien, A.L., Wang, T.S., Leung, S.G., Kang, S. & Feinberg, A.P. (2015). Age and sun exposure-

related widespread genomic blocks of hypomethylation in nonmalignant skin. *Genome Biology*. [Online]. 16 (1). p.p. 80. Available from: http://www.ncbi.nlm.nih.gov/pubmed/25886480. [Accessed: 12 September 2017].

Veres, D.A., Wilkins, L., Coble, D.W. & Lyon, S.B. (1989). DNA Methylation and differentiation of human keratinocytes. *Journal of Investigative Dermatology*. 93 (5). p.pp. 687–690.

Waddington, C.H. (2012). The epigenotype, Endeavor, 1942, vol. 1 (pp. 18-20) Reprinted in. *International Journal of Epidemiology*. 41 (1). p.pp. 20–23.

Waddington, C.H. (1957). *The Strategy of the Genes*. 1st Ed. London: Allen & Unwin.

Wang, J., Walsh, G., Liu, D.D., Lee, J.J. & Mao, L. (2006). Expression of ΔDNMT3B variants and its association with promoter methylation of p16 and RASSF1A in primary non-small cell lung cancer. *Cancer Research*. 66 (17). p.pp. 8361–8366.

Warkel, R.L., Luna, L.G. & Helwig, E.B. (1980). A modified Warthin-Starry procedure at low pH for melanin. *American Journal of Clinical Pathology*. 73 (6). p.pp. 812–815.

Watson, R.E.B., Griffiths, C.E.M., Craven, N.M., Shuttleworth, C.A. & Kielty, C.M. (1999). Fibrillin-rich microfibrils are reduced in photoaged skin. Distribution at the dermal-epidermal junction. *Journal of Investigative Dermatology*. 112 (5). p.pp. 782–787.

Watt, F.M. (2002). Role of integrins in regulating epidermal adhesion, growth and differentiation. *EMBO Journal*. 21 (15). p.pp. 3919–3926.

Wegrzyn, J., Potla, R., Chwae, Y.J., Sepuri, N.B.V., Zhang, Q., Koeck, T., Derecka, M., Szczepanek, K., Szelag, M., Gornicka, A., Moh, A., Moghaddas, S., Chen, Q., Bobbili, S., Cichy, J., Dulak, J., Baker, D.P., Wolfman, A., Stuehr, D., Hassan, M.O., Fu, X.Y., Avadhani, N., Drake, J.I., Fawcett, P., Lesnefsky, E.J. & Larner, A.C. (2009). Function of mitochondrial Stat3 in cellular respiration. *Science*. 323 (5915). p.pp. 793–797.

Weisenberger, D.J., Velicescu, M., Cheng, J.C., Gonzales, F.A., Liang, G. & Jones, P.A. (2004). Role of the DNA Methyltransferase Variant DNMT3b3 in DNA Methylation. *Molecular Cancer Research*. 2 (1). p.pp. 62–72.

Wigler, M., Levy, D. & Perucho, M. (1981). The somatic replication of DNA methylation. *Cell*. 24 (1). p.pp. 33–40.

Woo, S.H., Lumpkin, E.A. & Patapoutian, A. (2015). Merkel cells and neurons keep in touch. *Trends in Cell Biology*. 25 (2). p.pp. 74–81.

Wrutniak, C., Cassar-Malek, I., Marchal, S., Rascle, A., Heusser, S., Keller -, J.M., Flechon, J., Dauca, M., Samarut, J., Ghysdael, J. & Cabello, G. (1995). A 43-kDa protein related to c-Erb A α1 is located in the mitochondrial matrix of rat liver.

Journal of Biological Chemistry. 270 (27). p.pp. 16347–16354.

Wu, D., Lim, E., Vaillant, F., Asselin-Labat, M.L., Visvader, J.E. & Smyth, G.K. (2010). ROAST: Rotation gene set tests for complex microarray experiments. *Bioinformatics*.

Xiao, F.H., Chen, X.Q., He, Y.H. & Kong, Q.P. (2018). Accelerated DNA methylation changes in middle-aged men define sexual dimorphism in human lifespans. *Clinical Epigenetics*. 10 (1).

Xie, S., Wang, Z., Okano, M., Nogami, M., Li, Y., He, W.W., Okumura, K. & Li, E. (1999). Cloning, expression and chromosome locations of the human DNMT3 gene family. *Gene*. 236 (1). p.pp. 87–95.

Xu, H.X., Qin, J.Z., Zhang, K.Y. & Zeng, W.X. (2015). Dynamic expression profile of DNA methyltransferases in rat testis development. *Polish Journal of Veterinary Sciences*. 18 (3). p.pp. 549–556.

Yamada, T., Hasegawa, S., Iwata, Y., Arima, M., Kobayashi, T., Numata, S., Nakata, S., Sugiura, K. & Akamatsu, H. (2019). UV irradiation-induced DNA hypomethylation around WNT1 gene: Implications for solar lentigines. *Experimental Dermatology*. 28 (6). p.pp. 723–729.

Yang, H., Liu, Y., Bai, F., Zhang, J.Y., Ma, S.H., Liu, J., Xu, Z.D., Zhu, H.G., Ling, Z.Q., Ye, D., Guan, K.L. & Xiong, Y. (2013). Tumor development is associated with decrease of TET gene expression and 5-methylcytosine hydroxylation. *Oncogene*. 32 (5). p.pp. 663–669.

Yang, S.-H., Liu, R., Perez, E.J., Wen, Y., Stevens, S.M., Valencia, T., Brun-Zinkernagel, A.-M., Prokai, L., Will, Y., Dykens, J., Koulen, P. & Simpkins, J.W. (2004). Mitochondrial localization of estrogen receptor . *Proceedings of the National Academy of Sciences*. 101 (12). p.pp. 4130–4135.

Yang, X.-J. & Seto, E. (2007). HATs and HDACs: from structure, function and regulation to novel strategies for therapy and prevention. *Oncogene*. [Online]. 26 (37). p.pp. 5310–5318. Available from: http://www.nature.com/articles/1210599. [Accessed: 7 April 2018].

Yin, Y., Morgunova, E., Jolma, A., Kaasinen, E., Sahu, B., Khund-Sayeed, S., Das, P.K., Kivioja, T., Dave, K., Zhong, F., Nitta, K.R., Taipale, M., Popov, A., Ginno, P.A., Domcke, S., Yan, J., Schübeler, D., Vinson, C. & Taipale, J. (2017). Impact of cytosine methylation on DNA binding specificities of human transcription factors. *Science*. 356 (6337).

Young, A.R. (1997). Chromophores in human skin. *Physics in Medicine and Biology*. 42 (5). p.pp. 789–802.

Yuspa, S.H., Kilkenny, A.E., Steinert, P.M. & Roop, D.R. (1989). Expression of murine epidermal differentiation markers is tightly regulated by restricted extracellular

calcium concentrations in vitro. *Journal of Cell Biology*. 109 (3). p.pp. 1207–1217.

Zeyer, K.A., Zhang, R.M., Kumra, H., Hassan, A. & Reinhardt, D.P. (2019). The Fibrillin-1 RGD Integrin Binding Site Regulates Gene Expression and Cell Function through microRNAs. *Journal of Molecular Biology*. 431 (2). p.pp. 401–421.

Zhang, J., Gao, Q., Li, P., Liu, X., Jia, Y., Wu, W., Li, J., Dong, S., Koseki, H. & Wong, J. (2011). S phase-dependent interaction with DNMT1 dictates the role of UHRF1 but not UHRF2 in DNA methylation maintenance. *Cell Research*. 21 (12). p.pp. 1723–1739.

Zhang, J., Wang, X., Vikash, V., Ye, Q., Wu, D., Liu, Y. & Dong, W. (2016). ROS and ROS-Mediated Cellular Signaling. *Oxidative Medicine and Cellular Longevity*. 2016. p.p. 4350965.

Zhang, Z. & Michniak-Kohn, B.B. (2012). Tissue engineered human skin equivalents. *Pharmaceutics*. 4 (1). p.pp. 26–41.

Zhou, W., Dinh, H.Q., Ramjan, Z., Weisenberger, D.J., Nicolet, C.M., Shen, H., Laird, P.W. & Berman, B.P. (2018). DNA methylation loss in late-replicating domains is linked to mitotic cell division. *Nature Genetics*. 50 (4). p.pp. 591–602.

Zhou, W., Laird, P.W. & Shen, H. (2017). Comprehensive characterization, annotation and innovative use of Infinium DNA methylation BeadChip probes. *Nucleic acids research*. 45 (4).

Zuber, T.J. (2002). Punch biopsy of the skin. *American Family Physician*. 65 (6) p.pp. 1155–1158.

Appendix I

Epigenetic Determinants of the Optimal Skin Response to UV Radiation

Bethany M Barnes BSc
Rachel E B Watson BSc, PhD
Christopher E M Griffiths BSc, MB ChB, MD, FRCP

Centre for Dermatology Research
The University of Manchester

Dermatophamacology Unit
Salford Royal NHS Foundation Trust

Research Governance Sponsor:
The University of Manchester

31/08/2016
Version 2

Introduction

Ageing skin displays a number of well-defined degenerative changes that includes altered architecture of the dermal matrix, accumulation of DNA damage, variations in gene expression profiles and a higher prevalence of senescent cells [1-4]. The mechanisms through which these changes become established features of aged skin are poorly understood. However, recent advances in technologies to study the epigenome, particularly DNA methylation, have enabled new insights into the cellular control of biological pathways and their dysregulation with increasing age. DNA methylation is a dynamic yet stable epigenetic mark. Monozygotic twins in early life are epigenetically indistinguishable; however, significant divergence is observed in the overall levels and distribution of 5-methylcystosine in older individuals [5]. This indicates that accumulated exposure to internal and environmental stresses (such as ultraviolet [UV] radiation) is likely reflected by variance in DNA methylation patterns that can be propagated during cell division, resulting in permanent maintenance of the acquired phenotype. These differentially methylated regions (DMRs) will therefore pinpoint the genes most affected by repeated exposure to stressors. How such epigenetic changes influence the response of aged skin to new stressor exposure is unclear, but could offer new routes for rejuvenating the skin or preventing the accumulation of damage.

Objective

Although much research has focussed on single, high UV radiation doses (i.e. greater than 3 times the minimal erythema dose [MED]), UV exposure of 0.4x or 0.8x the MED more closely mimics *in vivo* exposure levels for UK nationals, equitable to approximately 20 minutes in the midday sun for individuals with Fitzpatrick type III skin [6]. Multiple low-dose exposures to UV radiation are possibly a greater driver of skin ageing in UK nationals than short, very high doses. This study aims to establish whether repeated challenges of low dose UV radiation will lead to an altered epigenetic status in skin, with the consequence of impaired skin function as observed clinically in ageing.

Study Design

A pilot study (study 1) will be performed in up to 10 healthy volunteers between 18 and 45 years of age. Four sites on the upper buttock will be irradiated with solar simulated radiation (SSR) at doses of 0.4x and 0.8x of the MED. The MED will be determined for each participant within the cohort, as follows: a small area of the lower back will be irradiated with increasing doses of UV radiation, up to doses capable of producing moderate reddening of the skin. Twenty-four hours post-exposure, the minimum dose - which produces just perceivable reddening of the skin - will be determined.

Two 10 ml blood samples may be taken: one prior to commencement of SSR and one following completion of the SSR programme. The test sites will undergo repeated exposures to UV radiation for up to 10 days. Twenty-four hours following the final irradiation, 6 mm diameter skin biopsies will be taken from the exposed sites together with an unirradiated control from the contralateral buttock (five biopsies total). Each participant will therefore provide the following biopsies:

I. Unirradiated control sample;
II. Irradiated sample 0.4x MED (5 day exposure);
III. Irradiated sample 0.8x MED (5 day exposure);
IV. Irradiated sample 0.4x MED (10 day exposure);
V. Irradiated sample 0.8x MED (10 day exposure)

For the follow up study, up to 24 healthy volunteers will be recruited (based on power calculations from data provided by study 1). A 10 ml blood sample may be taken prior to commencement of SSR and one following completion of the SSR programme. Buttock will be irradiated with SSR using the dosage and time scale determined in study 1. Two 6 mm skin biopsies will be taken from the buttock following the irradiation protocol, one from the exposure site and a second from an unirradiated control site.

Study Procedure

Study 1

The study 1 will aim to determine the optimal sub-erythemal dose and time-frame for the detection of genome-wide methylation changes. Following determination of the individual's MED, doses of 0.4x and 0.8x the MED will each be applied to separate sites on the buttock using a solar simulator. Daily irradiation will occur for up to 10 days; no irradiation will take place over weekends, with two additional sites undergoing irradiation with both sub-erythemal doses of SSR for days 6 - 10. An erythema meter and a chromometer will be used to assess the degree of redness and pigmentation, respectively. In addition, a 10 ml whole sample of blood will be drawn prior to irradiation and 24 hr following the final irradiation exposure to test the response of systemic markers of UV exposure.

Irradiation time course:

Day	Mon	Tues	Wed	Thurs	Fri	Sat	Sun
Action	Blood sample taken MED testing	MED Assessment SSR (1)	SSR (2)	SSR (3)	SSR (4)	nil	nil
Day	Mon	Tues	Wed	Thurs	Fri	Sat	Sun
Action	SSR (5)	SSR (6) (1)	SSR (7) (2)	SSR (8) (3)	SSR (9) (4)	nil	nil
Day	Mon	Tues	Wed	Thurs	Fri	Sat	Sun
Action	SSR (10) (5)	Blood sample taken Biopsy	nil	nil	nil	nil	nil

On the eleventh day, five 6 mm biopsies will be taken under 1% lignocaine anaesthesia. Biopsy sites will be sutured with 1x 4/o ethilon® and participants instructed on appropriate wound care. After 7-10 days following the biopsies, participants will be asked to return for suture removal. The biopsies will be bisected and snap frozen in liquid nitrogen at the Dermatopharmacology Unit prior to transportation to facilities at the University of Manchester. Consent from participants to store the

tissue samples under the Human Tissue Act in a designated freezer will be obtained prior to biopsy. Differences in the distribution of methyl marks will be compared between samples, using *Illumina Infinum*® array technology and bioinformatics approaches to compare any DMRs identified. The effects of the most significantly modulated regions may then be determined in the tissue using staining techniques including immunohistochemistry (IHC) and, where antibodies are unavailable, *in situ* hybridisation histochemistry.

Study 2

Up to 24 subjects will be recruited to study 2. Healthy volunteers will be classified into young (18-45 years, n=12) and aged (65 years and over, n=12) groups. A 10 ml blood sample will be taken prior to commencement of the irradiation protocol, and one following its completion. Each volunteer will be subjected to multiple, sub-erythemal doses of UV radiation as determined to be optimal in the pilot study. An erythema meter and chromometer will be used to assess the degree of redness and pigmentation, respectively, prior to each exposure. A total of two 6 mm biopsies will be taken:

i. Unirradiated control sample;
ii. Irradiated sample (dose and time course indicated by study 1).

In conjunction with datasets within Unilever R&D and wider scientific literature, the resulting DMRs will help to elucidate the biological pathways paramount to driving the aged skin phenotype. The following bioinformatic comparisons of DNA methylation patterns will be performed:

i. Unirradiated (control) versus irradiated skin;
ii. Young versus aged in unirradiated skin;
iii. Young versus aged SSR exposure response;
iv. Blood versus tissue.

Participant Recruitment

Initial contact with the research team will be via telephone or email. Potential participants will be asked a short series of questions to determine their suitability for the study based on the inclusion criteria outlined below. Those that are suitable will be provided with the participant information sheet appropriate to study 1 or study 2, and interested individuals will be invited to attend the Dermatopharmacology Unit at Salford Royal Hospital NHS Foundation Trust. During the first visit, participation in the study will be discussed fully and potential participants will have the opportunity to ask questions. Those who remain willing to take part will be recruited to the study. All participants will be asked to read and sign a consent form.

Inclusion Criteria

- White Caucasian (Fitzpatrick skin type I-III);
- Within the cohort age criteria;
- BMI between 18 – 34.9;
- Willing to submit to clinical examination of the buttock;
- Willing to receive UV irradiation on the buttocks;
- Willing to have up to 5x 6mm diameter biopsies from the buttocks;
- Signed, informed consent given.

Exclusion Criteria

- Pregnant or breastfeeding;
- A history of experimental drug use or use of an experimental device in the 30 days prior to entry into the study;
- A history of keloid scars;
- Use of a sunbed in the last 6 months;
- Diabetics;
- Currently taking any anticoagulant medication, anti-platelet medication, taking regular high-dose aspirin (>300 mg daily) or has a history of blood clotting disorders;
- Use of topical or systemic retinoids within the past 6 months and/or 12 months;
- Use of topical or systemic steroids or other drug treatment within the past 2 weeks and/or 6 months;
- Recent tattooing (within 1 month);
- Presenting with a concomitant skin disease;

Ethical Considerations

Application of solar simulated radiation may produce redness and mild irritation akin to sunburn during determination of minimal erythemal dose. The skin biopsies may additionally result in a small, permanent scar, and there is a small risk of infection at the site. Participants will be required to provide written informed consent prior to recruitment onto the study. A Participant Information Sheet detailing the aims and purposes of the study will be provided, and this will be discussed fully with each potential participant, giving them the opportunity to ask questions and fully consider what is involved in the study. A copy of the form is provided for each participant to keep, and includes contact details for out-of-hours care in the unlikely event that this is required. Additionally, participant identity will be anonymised once the biopsies are taken, with only members of the clinical staff having access to the volunteer's identity.

References

1. Watson, R.E.B., et al., *Fibrillin-Rich Microfibrils are Reduced in Photoaged Skin. Distribution at the Dermal-Epidermal Junction*. 1999. **112**(5): p. 782-787.
2. Fisher, G.J., et al., *Collagen Fragmentation Promotes Oxidative Stress and Elevates Matrix Metalloproteinase-1 in Fibroblasts in Aged Human Skin*. The American Journal of Pathology, 2009. **174**(1): p. 101-114.
3. Rijken, F., et al., *Responses of black and white skin to solar-simulating radiation: differences in DNA photodamage, infiltrating neutrophils, proteolytic enzymes induced, keratinocyte activation, and IL-10 expression.* J Invest Dermatol, 2004. **122**(6): p. 1448-55.
4. Waaijer, M.E., et al., *The number of p16INK4a positive cells in human skin reflects biological age*. Aging Cell, 2012. **11**(4): p. 722-5.
5. Fraga, M. F., Ballestar, E., Paz, M. F., Ropero, S., Setien, F., Ballestar, M. L., Heine-Suñer, D., Cigudosa, J. C., Urioste, M., Benitez, J., Boix-Chornet, M., Sanchez-Aguilera, A., Ling, C., Carlsson, E., Poulsen, P., Vaag, A., Stephan, Z., Spector, T. D., Wu, Y.-Z., Plass, C. & Esteller, M. (2005). *Epigenetic differences arise during the lifetime of monozygotic twins*. Proceedings of the National Academy of Sciences of the United States of America, **102**(30), p. 10604-10609.
6. Terushkin, V., et al., *Estimated equivalency of vitamin D production from natural sun exposure versus oral vitamin D supplementation across seasons at two US latitudes.* J Am Acad Dermatol, 2010. **62**(6): p. 3.

Appendix II

Part a: Differentially methylated probes identified in young and aged skin following UVR challenge in dataset with equal *n* number.

	Age group		
	Young	**Aged**	**Young and aged**
n	12	12	24
Hypermethylated sites #	0	0	81
Hypomethylated sites #	0	52	1,520
Ratio Hyper:hypo	-	-	1:19

Part b: Number of differentially expressed genes identified in young and aged skin following UVR challenge in dataset with equal n number.

	Age group		
	Young	**Aged**	**Young and aged**
n	12	12	24
Upregulated #	84	22	511
Downregulated #	47	29	329

Part c: Number of differentially methylated probes identified in intrinsically aged skin versus young in dataset with equal *n* number

Group	**Young**	**Aged**
n	12	12
Hypermethylated sites #	25,091	
Hypomethylated sites #	23,132	

Part b: Number of differentially expressed genes identified in in intrinsically aged skin versus young in dataset with equal *n* number

Group	**Young**	**Aged**
n	12	12
Upregulated #	8	
Downregulated #	14	

Appendix III

Overlap of differentially expressed genes identified following sub-erythemal UVR challenge in the follow-up study. The methodology is summarised in table 4.5 and in-text.